This is to certify that the

dissertation entitled

Further Development and Characterization of the Desorption Ionization Technique, K^+IDS, and Investigation of the Mechanisms of Fragmentation and Ionization of Desorption Ionization Techniques

presented by

Karen Jean Light

has been accepted towards fulfillment of the requirements for

Ph.D. degree in Chemistry

John Allison
Major professor

Date 11/26/90

FURTHER DEVELOPMENT AND CHARACTERIZATION OF THE DESORPTION IONIZATION TECHNIQUE, K^+IDS, AND INVESTIGATION OF THE MECHANISMS OF FRAGMENTATION AND IONIZATION OF DESORPTION IONIZATION TECHNIQUES

By

Karen Jean Light

A DISSERTATION

Submitted to
Michigan State University
in partial fulfillment of the requirements
for the degree of

DOCTOR OF PHILOSOPHY

Department of Chemistry

1990

ABSTRACT

FURTHER DEVELOPMENT AND CHARACTERIZATION OF THE DESORPTION IONIZATION TECHNIQUE, K+IDS, AND INVESTIGATION OF THE MECHANISMS OF FRAGMENTATION AND IONIZATION OF DESORPTION IONIZATION TECHNIQUES

By

Karen Jean Light

Further development and characterization of K^+ ionization of desorbed species, K^+IDS, is performed to gain a better understanding of this desorption ionization technique. K^+IDS utilizes a thermionic emitter material as a source for gas phase K^+ ions and rapid heating of thermally labile compounds to promote desorption of intact analyte molecules and neutral thermal degradation products. K^+ adduct ions are formed when K^+ emission occurs simultaneously with sample desorption. A two-filament probe tip design, which improves the overlap of K^+ emission with sample desorption, is evaluated. The K^+ emitter surface is resistively heated to temperatures in excess of 900°C and the sample filament wire is radiatively heated to temperatures between 100-200°C. Temperature studies of the sample filament wire show the effects of the heating rate and the final temperatures reached by this sample filament wire on the K^+IDS mass spectra. The applicability of the K^+IDS technique is extended to the analysis of cardiac glycosides with both molecular weight and structural information obtainable from the K^+IDS mass spectra. A new nomenclature scheme is proposed that allows for the accurate identification of neutral thermal degradation products and fragment ions produced by desorption ionization techniques, such as K^+IDS. This naming scheme allows the designation of hydrogen shifts, multiple cleavages, and adduct formation observed in the analysis of these cardiac glycosides.

Adaptation of the K^+IDS technique to a double-focusing mass spectrometer is explored to investigate the mass limit of the K^+IDS technique. Modifications to the pre-existing direct chemical ionization probe and power supply of the JEOL HX-110 double-focusing mass spectrometer are made to perform the K^+IDS experiment. Difficulties arise in achieving a fast scan rate that can detect the rapid changes in the K^+IDS mass spectra with the double-focusing instrument.

The FAB mass spectrometric analysis of the cardiac glycosides is performed to gain a better understanding of this desorption ionization technique compared to the K^+IDS technique. A detailed mechanistic study of the FAB mass spectrum of digoxin is described. All information obtained by a double-focusing mass spectrometer, including tandem mass spectrometry and high resolution peak matching, is used to deduce the structural formulas of the fragment ions observed in the FAB mass spectrum and the possible fragmentation pathways.

This thesis is dedicated to my entire family and especially my mother and father whose never-ending love, support and encouragement inspired me to achieve.

ACKNOWLEDGMENTS

I owe much to my mentor John Allison whose support and guidance was always strongest when I needed it most. I really admire and appreciate his dedication to his graduate students and to the development of science. I would also like to thank Dan Bombick and Dan Kassel for introducing me to "K+IDS" and their leadership and support in teaching me the "art" of graduate research.

Then there were the "three stooges" who always seemed to be there with a good laugh or reassuring smile to keep me going through good and bad. Thanks "big brother" for all of our good conversations, hospitality trips, and the good advice (although the last one you were wrong on....I just had to be patient!). To Gary, Kurt and Jason, who brought new life - and partying - to our group, thanks for all the fun times. Someday, Jason, maybe I'll give you another chance to spike one in my face!

The grad school experience would not have been complete without the "flamingo crew". I'll never forget all the good times we shared - the wallpaper party, late night swims, and of course the waterbed to name a few. May our blenders always churn pink. The annual winter ski trips were such a great getaway from all of the horrors of grad school such as the seminars and 2nd year orals. Someday Sabo, maybe the rest of us will figure out just what "we touched on" that evening in wintry north! A special thanks to Kris for being such a good friend and to Judy for being such a good roommate and friend throughout the five-year graduate school experience.

I owe many thanks to all those hard-working "specialists" of the Mass Spectrometry Facility. I will really miss all of you! Thanks Doug for all your confidence in me, Mel for all your assistance in keeping the computer world running, Melinda for all the extras you do, and Bev for all the hard work you do to make us look good! And then there's Mike...who had an uncanny way of brightening up the day. I have no doubt that if it weren't for your...patience?...the HP's would have been history long ago! Thanks for all the extra help in keeping them running. I'm really going to miss being able to bug you when something needs fixing. But I guess Jason can fill in that role! Thanks for all the electronics lessons you gave while fixing the instruments.

And last, but most importantly, I would like to thank Jon for all the confidence, self-assurance, and joy he has brought to my life through all of his love and support. Your ability to make me laugh in the face of despair helped me through many stressful times. You are the best friend I could ever have and I love you for it.

TABLE OF CONTENTS

LIST OF TABLES

LIST OF FIGURES

CHAPTER 1. INTRODUCTION

1. DESORPTION IONIZATION TECHNIQUES

Mass spectrometry, as an analytical tool, has been traditionally used for the analysis of volatile analytes or compounds that are easily derivatized to some volatile species. The common ionization technique for such volatile samples is electron ionization (EI). This ionization technique is well characterized and the mechanisms of ion formation and fragmentation are well documented.[1] Another ionization technique that is commonly used for volatile species is chemical ionization (CI)[2], which is considered to be a softer ionization technique than EI, and provides information about the sample that complements EI results. CI utilizes gas phase reagent ions to ionize the sample in the gas phase via ion/molecule reactions. Adduct ions are often produced with this ionization method that contain the intact molecular species. Little fragmentation is observed with CI relative to EI, hence CI is considered as a soft ionization process. Both EI and CI provide a means of ionizing gas phase species, but do not provide a means of transferring the sample from the condensed phase to the gas phase. This greatly limits the applicability of these techniques to volatile species.

Desorption ionization (DI) techniques circumvent this sample volatility requirement by providing a means of transporting thermally labile compounds from the condensed phase (either solid or liquid) into the gas phase and by providing a means of ionizing the sample. The development of these techniques has greatly expanded the realm of mass spectrometry, especially in the field of biochemistry where most of the compounds of interest are large multifunctional molecules which are thermally labile. There are many desorption ionization techniques currently in use with continual development of new techniques. Field desorption (FD) was one of the first ionization techniques developed for nonvolatile compounds.[3] More recently, plasma desorption (PD)[4], laser desorption (LD)[5], fast atom bombardment (FAB)[6], and liquid secondary ionization mass spectrometry (LSIMS)[7] have been developed as desorption ionization techniques for thermally labile compounds. These DI techniques utilize particle bombardment of the sample to transfer energy to the sample to form gas phase ionic species. For example, LD utilizes photons to bombard the sample, FAB

utilizes fast heavy atoms (Xe or Ar) and LSIMS utilizes ions (Cs^+) for bombardment. The overall idea is the same, but the techniques vary in the amount of energy imparted and the rate at which the energy is deposited into the sample. This difference in energy deposition, coupled to chemical differences, leads to differences in mechanisms of ion formation and fragmentation, and differences in the mass spectra obtained. Also direct insertion techniques such as DEI[8] and DCI[9] have been developed which combine the traditional EI and CI techniques with methods of transferring thermally labile compounds into the gas phase. Ionization techniques also have been developed to combine liquid chromatography with mass spectrometry (LC/MS). Thermospray[10] and continuous flow FAB[11] are among these LC/MS techniques that are gaining much attention. The difficulty in this endeavour is dealing with the large volume of solvent while maintaining the vacuum system for mass spectrometric analysis.

There are many different DI techniques currently in use, all of which have their strengths and weaknesses. None of these techniques is all inclusive or solves all of the mass spectrometric needs for the analysis of thermally labile compounds. FAB and LSIMS, perhaps the most widely used DI techniques, require the use of a liquid matrix, such as glycerol or nitrobenzyl alcohol, to dissolve the sample, control the sampling rate, and aid in ion formation. Due to the presence of this matrix, many ions originate from the matrix which complicate the mass spectra and often interfere with the observation of sample-related ions. This is especially true in the low-mass range where ions from the matrix often dominate the mass spectra and mask analyte ions present. Therefore, mass spectrometry/mass spectrometry (MS/MS) is often necessary to obtain low mass information without interference from the matrix.[12] This technique allows for the parent ion to be selected and only those fragments produced from the selected parent ion are observed in the MS/MS spectrum. LD mass spectrometry has proven to be a very useful technique especially for large biomolecules where much energy is needed to ionize and desorb the intact species with little fragmentation.[13] This technique, however, requires very sophisticated, expensive instrumentation, and much care and experience to keep both the laser and the mass spectrometer operational simultaneously. Because there is no ideal DI technique currently available, this field of mass spectrometry is constantly developing.

The main analytical goal of these DI techniques is to generate gas-phase ions that provide molecular weight and structural information pertaining to the compound of interest. Cationization is a process that may assist in the mass spectrometric determination of molecular weight. Cationization typically produces $[M]A^+$ ions where A is most often an alkali metal cation such as Na^+ or K^+. This adduct ion formation has been utilized with LD, FAB, FD, and LSIMS to aid in molecular weight determination. More recently, cationization has been utilized as a means of obtaining additional structural information. Mallis and Russel reported differences in fragmentation of $[M]H^+$ and $[M]Na^+$ ions of small peptides such as hippuryl-L-histidyl-L-leucine (HHL) when collisionally activated.[14] The Na^+ adduct ions were produced by adding 1 μg of NaCl to the sample. They suggest that the highly polar functional groups commonly present in the thermally labile compounds studied, such as peptides and saccharides, have different H^+ and A^+ ion affinites (where A is an alkali metal such as Li, Na, or K). Thus, the binding sites of H^+ and A^+ may be different and induce different fragmentations with the aid of collisionally activated dissociation. Many other research groups have reported similar advantages of performing collisionally induced dissociation on alkali adduct ions of oligosaccharides[15] and peptides[16] for increased structural information over protonated species. The addition of alkali salts to the sample or matrix is the most common way of producing adduct ions with these DI techniques. The other way of obtaining alkali ions is by their presence as impurities in the sample.

Cationization is not a new concept. Röllgen and coworkers were among the first to recognize the utility of forming adduct ions with alkali metal cations.[17] Their early studies involved formation of Li^+ adducts with volatile and thermally labile compounds. They applied electric fields to solid LiI to produce a large flux of Li^+ ions in the gas phase. They also studied the mechanisms of Na^+ and K^+ adduct ion formation formed by laser desorption.[18] They determined that cationization can be a surface reaction, when alkali salts are in contact with the sample, or adduct ion formation can be a gas phase addition process. To prove this gas phase adduct ion process, Röllgen et al. designed a two-filament probe to spatially separate the alkali ion source (alkali salt) from the sample holder.[19] This design still produced adduct ion formation, suggesting a gas-phase mechanism of alkali ion attachment. Van der Peyl, Haverkamp, and Kistemaker supported this gas phase mechanism of

adduct ion formation with a series of studies performed by LD mass spectrometry.[20] The experimental design insured that the K^+ emitter (obtained commercially) was spatially separated from the sample housing with no line-of-sight between the two components. They observed K^+ attachment to an intact gas-phase sucrose molecule when there was no possibility of the adduct being formed by surface reactions.

Most of the developmental work with DI techniques is in creating alternative methods and trying to increase the mass range rather than in gaining a better understanding of the mechanisms of fragmentation and ion formation involved. The ionization methods which are gaining the most attention and which may revolutionize the role of mass spectrometry in biological research are matrix-assisted laser desorption and electrospray ionization (ESI).[21] It has been demonstrated that both LD[22] and ESI[23] are capable of extending the ionization and molecular weight determinations to compounds with molecular weights greater than 100,000 daltons. Electrospray ionization was first developed by Dole and coworkers to produce gas-phase macroions that were detected in a Faraday cage with the molecular weight determined by stopping potentials.[24] Yamashita and Fenn were among the first researchers to combine ESI with mass spectrometry (ESI-MS) in 1984.[25] By 1988, Fenn and coworkers had gained much attention and interest in their new ionization method with the report of intact multiply charged ions of proteins up to a molecular weight of 40,000 daltons.[26] Since then, much interest and research has been devoted to the development of this technique and increasing the mass limit of ESI-MS. Electrospray ion formation is a two-step process where highly charged droplets are dispersed at pressures approaching atmospheric pressure, followed by droplet evaporation. Briefly, a high electric field is applied to a small flow of liquid from a capillary tube. This electric field results in the formation of highly charged liquid droplets due to the disruption of the liquid surface. The solvent evaporates leaving behind multiply charged analyte molecules. A more detailed explanation of this technique can be found elsewhere.[21]

The desorption ionization technique examined in this dissertation differs from many of the DI techniques discussed above in that the sample is not bombarded by particles to promote vaporization, but instead is heated radiatively (or resistively) to induce desorption of the sample. This DI technique is called K^+IDS, potassium ion ionization of desorbed species, and

was developed at Michigan State University as an economical and simple way of analyzing thermally labile analytes with a quadrupole mass spectrometer.[27] This technique utilizes a thermionic emitter, a material that produces a large flux of ions when heated, and rapid heating of a thermally labile compound to promote desorption of both the intact molecule and neutral products of thermal degradation. The thermionic emitter used produces a large flux of K^+ ions in the gas phase. These K^+ ions attach to the neutral gas-phase species desorbed from the sample to produce K^+ adducts. No matrix is required with this technique. Therefore, all of the ions observed are K^+ adducts representative of the sample. The mass spectra produced are easily interpreted based on one fragmentation mechanism (1,2-elimination). Implementation of this technique to a quadrupole mass spectrometer that is equipped with a direct insertion probe inlet is inexpensive and simple. The further development and characterization of this technique is one of the main goals of this research.

2. K^+IDS THEORY

There are two concepts that are important to the K^+IDS technique. One is the use of thermionic emitters to form gas-phase K^+ ions that are used as reagent ions in a way similar to those used in chemical ionization. The other concept is the use of rapid heating of a thermally labile compound to promote vaporization of the sample with little thermal degradation. When these two processes are combined and occur simultaneously, a K^+IDS mass spectrum can be obtained. The K^+ ions attach to neutral gas-phase species, possibly in a three-body collision process, and are observed as K^+ adducts. This K^+ attachment induces little or no fragmentation and merely samples the neutrals present in the gas phase which are produced by the heating of the sample.

A. PRODUCTION OF GAS-PHASE K^+ IONS

The most important aspect of the K^+IDS technique is the production of a large flux of K^+ ions in the gas phase. This is accomplished with the use of thermionic emitter materials that are patterned after the aluminosilicate mixtures described by Blewett and Jones in 1936.[28] They determined that the mixture Al_2O_3:Li_2O:$2SiO_2$ was the best mixture for producing a large flux of Li^+

ions. The same mixture doped with K_2O instead of Li_2O has proven to be a good source of K^+ ions when the mixture is heated to temperatures between 800 and 1200°C. Extensive discussions of how these materials are capable of emitting metal ions can been found elsewhere.[29] The emission of K^+ ions is dependent primarily on the work function of the surface and the ionization energy of the potassium atom. The work function of the surface is essentially a measure of the electron affinity of the surface. This term is explained and discussed in detail by Bombick.[29]

B. DESORPTION OF THERMALLY LABILE COMPOUNDS

The other concept important to the K^+IDS technique is the transfer of the thermally labile compounds into the gas phase with minimal thermal degradation of the sample. The use of rapid heating to promote desorption of the intact molecule over competitive decomposition reactions of thermally labile compounds was described by Beuhler and coworkers for the mass spectrometric analysis of underivatized peptides.[30] The enhancement of the volatility of a complex thermally labile species due to rapid heating of the sample is based on a kinetic analysis of the competitive decomposition and vaporization processes. This will be explored in more detail later. Low temperatures and slow heating rates will promote more decomposition than high temperatures and fast heating rates, which favor desorption of the intact molecule. If this relationship holds, then the temperature variables and heating rates may provide a means of adjusting and controlling the types of information obtained. The ideal case would be to use heating rates and experimental conditions that allowed for the detection of degradation products early in the analysis followed by desorption of the intact species all within one K^+IDS mass spectrometric analysis. Therefore, both structural and molecular weight information would be obtained and the relationship between the temperature of the surface and the appearance of different adduct ions could be used to deduce information about the structure of the analyte and the relative strengths of the bonds broken to form the various degradation products. This goal is pursued in Chapter 2.

C. EXPERIMENTAL CONSIDERATIONS FOR THE K^+IDS TECHNIQUE.

The K^+IDS technique is performed at Michigan State University on an HP 5985 GC/MS/DS quadrupole mass spectrometer that has a mass range of 10-1000 daltons. A schematic of the ion source and the K^+IDS apparatus are shown in Figure 1.1. A modified direct insertion probe is used to insert the K^+ aluminosilicate bead into the center of the ion source. The tip of this modified probe is shown in Figure 1.2. The K^+ bead filament is made by threading 0.007 inch rhenium wire through a two-holed ceramic (3/64" outer diameter, 0.010" inner diameter) leaving a 1mm loop at the top. This tip is spot-welded to nickel wire leads that are fed through the K^+IDS probe. The aluminosilicate mixture is then applied to the tip of this filament loop to make the K^+ bead in one of two ways. The dry aluminosilicate powder can be melted on a piece of platinum with an oxygen/acetylene torch. The filament loop is dipped into the molten bead material to capture some of the glass onto the wire. Another way to make a K^+ bead is by first making a slurry of the aluminosilicate powder in acetone. A Pasteur pipette is used to transfer this slurry to the wire loop. Then the tip is inserted into a bunsen burner flame to evaporate the solvent and slightly harden the bead surface. The ideal bead, made with either technique, has a thin coating of the aluminosilicate mixture completely covering the bare wire. A bead that is too large takes longer to produce K^+ ions once current is applied to the bead. On the other hand, if the wire is not completely covered, the spectra seem to contain much more noise, possibly due to ionization of gas-phase molecules on the bare, hot wire surface. Once the bead is made, it is conditioned inside the ion source of the mass spectrometer by slowly ramping the current applied to the bead. A current ramp of approximately 1A/min in 0.25A steps from 0A to 3.8A is a good rate for conditioning. A current source is used to provide 0-4A to the K^+ bead in order to heat the thermionic emitter material. Also, a low voltage power supply is used to provide a bias voltage to the tip of the K^+ bead of 0 to +10 V with respect to the CI volume (repeller). A power supply was designed that satisfied both of these requirements at Michigan State University by M. Rabb. A schematic of the electronic design of this power supply is provided in Figure 1.3. The K^+IDS experiment is generally performed with a current of 2.2-3.5 A and a bias voltage of +2 to +4 V. More details of the technique are provided elsewhere.[29]

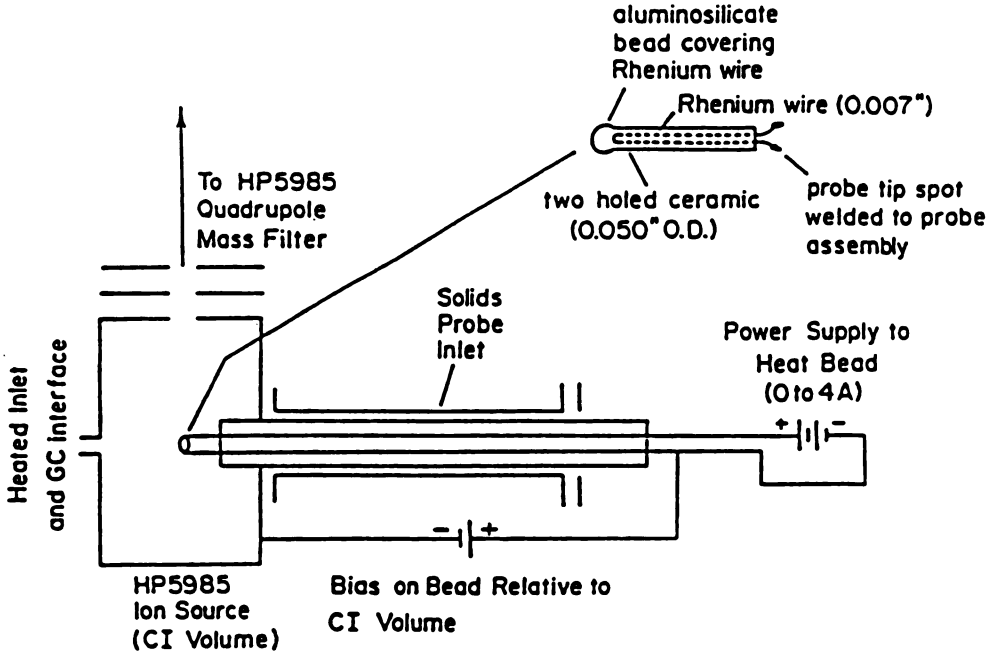

Figure 1.1 Schematic of the ion source of the quadrupole mass spectrometer and the experimental design of the K+IDS experiment.

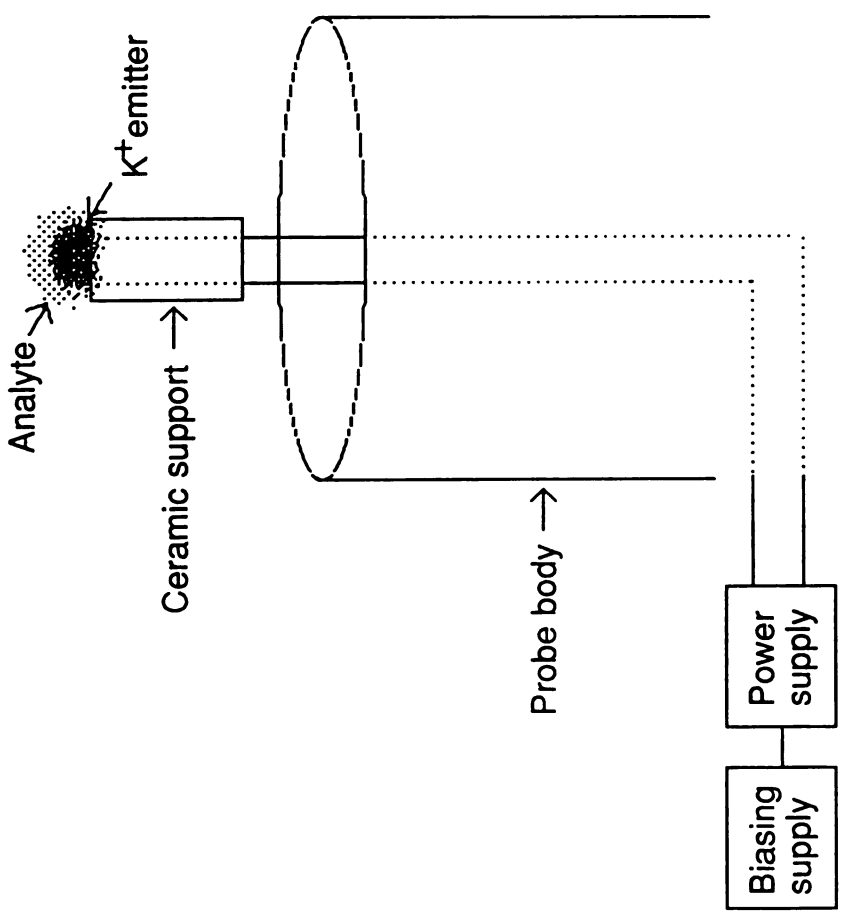

Figure 1.2 Original K^+IDS probe tip design.

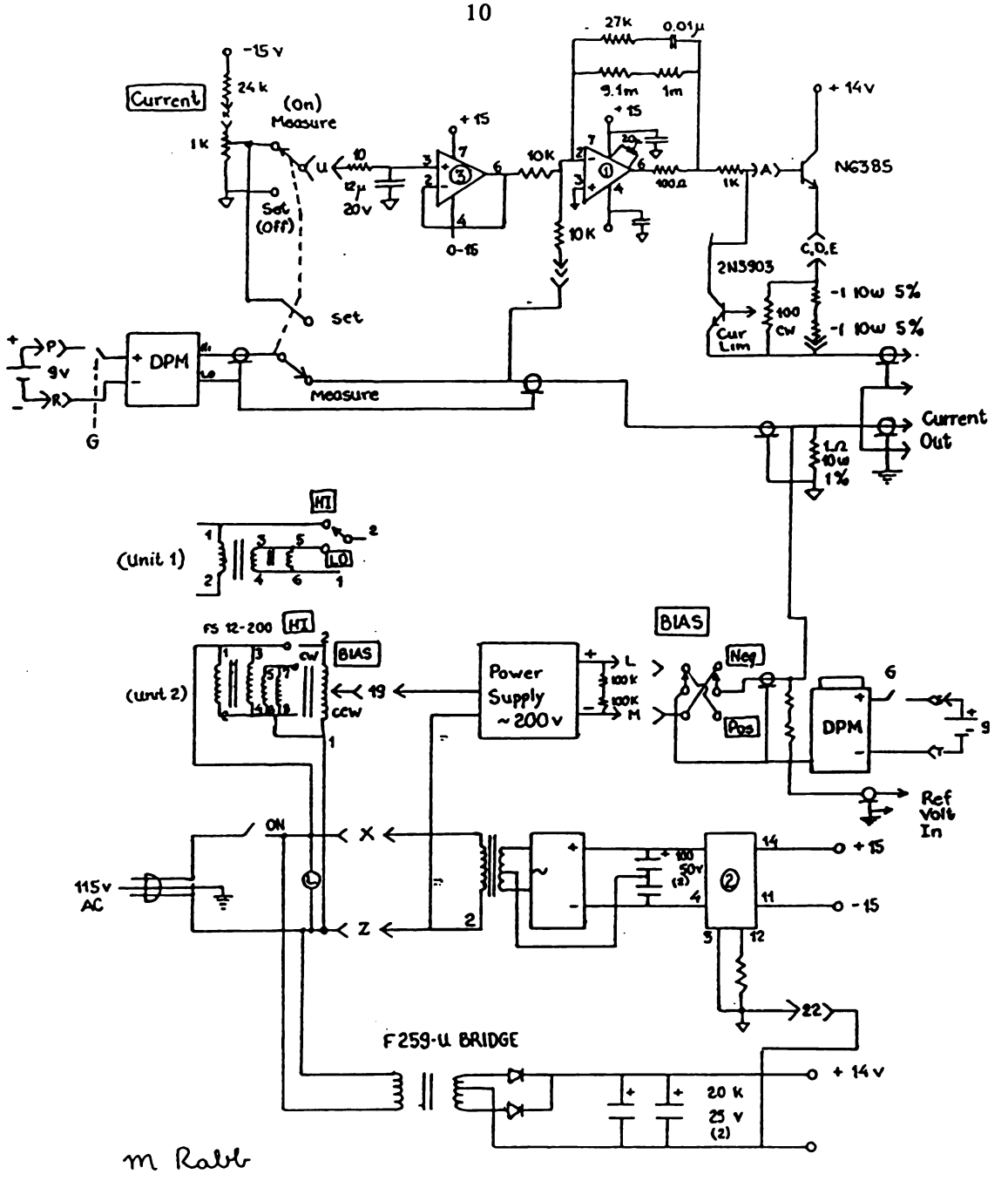

Figure 1.3 Schematic diagram of the electronics for the K+IDS power supply designed and constructed by Marty Rabb.

Calibration of the instrument, particularly the mass axis, is performed in the positive EI mode in the traditional way for GC/MS and/or DIP analyses. PFTBA is introduced into the ion source at a pressure of 2-5 x 10^{-6} torr with the ion source temperature at 150-200°C. The voltages of the focusing lenses and the other variables are adjusted for optimum EI results. The K^+IDS signals are too short-lived to allow for good calibration of the instrument with K^+ adduct ions. Once the instrument has been calibrated (especially the mass axis) in the EI mode, the source is cooled down to room temperature for the K^+IDS experiment. The EI filament is turned off for the K^+IDS experiments by setting the emission current and the electron energy to their lowest possible values. The K^+ emission is monitored with the override tuning program and the focusing lenses and other source variables affecting the ion signal are adjusted for optimum K^+ transmission, introducing only minimal changes in the parameters from the original EI tuning file.

The original K^+IDS experiment or "Classic K^+IDS", which used a single K^+ bead filament, is performed in the following way. (Details of how the technique has changed and how it is currently done will be presented in Chapter 2.) The sample is deposited onto the K^+ bead as either a solution or a slurry in some organic solvent. Acetone is the preferred solvent as it evaporates quickly, however, methanol also is used frequently as many of the samples will not dissolve in acetone. Water as a solvent is avoided whenever possible as it is difficult to evaporate completely and often produces spectra which contain much more noise than those from samples with the other solvents. This phenomenon is not completely understood, but serves as an observation and guideline. Once the sample is deposited onto the K^+ bead and all of the solvent has evaporated, the probe is inserted into the ion source of the mass spectrometer. Data collection is started immediately and then a preset current of approximately 3.0A and a preset bias voltage of approximately +3V is selected. The preset current allows for rapid heating of the emitter. This is in contrast to the temperature (current) ramping procedure commonly used with many other techniques including DCI. This K^+IDS procedure is the original mode of operation with a single filament probe tip. Details on the modifications made to the procedure and probe tip design that are currently employed will be discussed in Chapter 2.

CHAPTER 2. CHARACTERIZATION OF THE K+IDS TECHNIQUE

1. INTRODUCTION

Initial development and characterization of the K+IDS technique by Bombick[29] showed the utility of this technique and the wide applicability to a variety of thermally labile compounds including saccharides, peptides, polymers and steroids. Bombick explored the mechanisms of adduct formation and fragmentation characteristics of the K+IDS technique. The addition of a neutral collision gas produced an increase in adduct formation for small analyte molecules.[29] Under normal K+IDS experimental conditions, Bombick determined that the lower limit of detection for polyphenylether was approximately 500 ng at a signal-to-noise ratio of five. When N_2 was introduced into the ion source as a neutral collision gas to a source pressure of approximately one torr, the detection limit for polyphenylether was lowered to approximately 250 ng at a signal-to-noise ratio of five.[29] This increase in adduct formation with the presence of a collision gas confirms that K^+ adduct formation is a three-body collision process in the gas phase, at least for small analyte molecules. The three-body collision process may not be the only way of stabilizing the excited K^+ adduct ion. Woodin and Beauchamp proved that Li^+ attachment to an analyte molecule produced an excited complex that could be stabilized by the emission of an infrared photon, instead of by a three-body collision.[31] These bimolecular infrared radiative association reactions are assumed to be the dominant stabilization mechanism at very low pressures where the time between collisions exceeds 100 milliseconds. This photon emission process has gained popularity as a possible mechanism for interstellar chemistry, but is not likely to be responsible for the stabilization of the K^+ adduct ions formed in K+IDS. Suppose a thermally labile analyte, A, is desorbed intact into the gas phase as shown in reaction 2.1. A K^+ ion may

$$A_s \rightarrow A_g \qquad 2.1$$

$$A_g + K^+ \rightarrow AK^{+*} \qquad 2.2$$

$$AK^{+*} \rightarrow A_g + K^+ \qquad 2.3$$

attach to this gas-phase neutral with the binding energy of the K^+ ion to the analyte of approximately 20 kcal/mol.[32] This leads to an activated complex, AK^{+*}, as shown in reaction 2.2. This excess energy present in AK^+ can be dissipated in several ways. The energy can be used to dissociate the complex back to A and K^+, reaction 2.3. A collision with a third body or emission of a photon can eliminate some of this excess energy so that dissociation (reaction 2.3) is no longer possible and the adduct is stabilized. If ions only spend approximately 10^{-6} sec in the ion source, the pressure in the source, or in some localized region, needs to be 10^{-2} torr in order to have an average of one collision/ion in 10^{-6}sec.[33] This localized high pressure necessary for the stabilizing third body collision is likely to occur near the K^+ emitter where a large flux of K^+ ions and neutral analyte species are present in the gas phase. Therefore, it is reasonable to assume that the majority of the K^+ adduct formations are due to a three-body collision process.

Bombick also suggested that degradation of the compounds analyzed by K^+IDS appear to follow one simple fragmentation mechanism. This mechanism is a 1,2-elimination mechanism for cleaving a skeletal bond, which produces two neutral products. An example of this mechanism is shown in Figure 2.1 for the thermal degradation of sucrose. The ions observed in the K^+IDS mass spectrum of sucrose are labeled in Figure 2.1. It is very common for saccharides to fragment at the glycosidic bonds when thermally stressed. This characteristic fragmentation of saccharides will be further explored and utilized in Chapter 3. All thermal degradation products observed to date with the K^+IDS technique can be explained by means of this 1,2-elimination mechanism. The most common fragmentations observed with the K^+IDS technique are cleavage of the glycosidic bonds for compounds containing saccharides and dehydration for compounds containing hydroxyl groups.

The concept of "rapid heating" of a thermally labile sample to promote desorption has been studied by Beuhler and coworkers.[30] They described two ways of enhancing the volatility of thermally labile compounds such as underivatized peptides. One way of achieving this volatility enhancement is to use relatively inert surfaces for deposition of the samples. One study has been performed where volatility enhancement has been achieved by depositing peptides, such as thyrotropin releasing hormone (TRH), onto teflon.[34] This inert surface reduces the energy of bonding of the molecules to the surface and thus makes it easier to preferentially break these surface-to-molecule

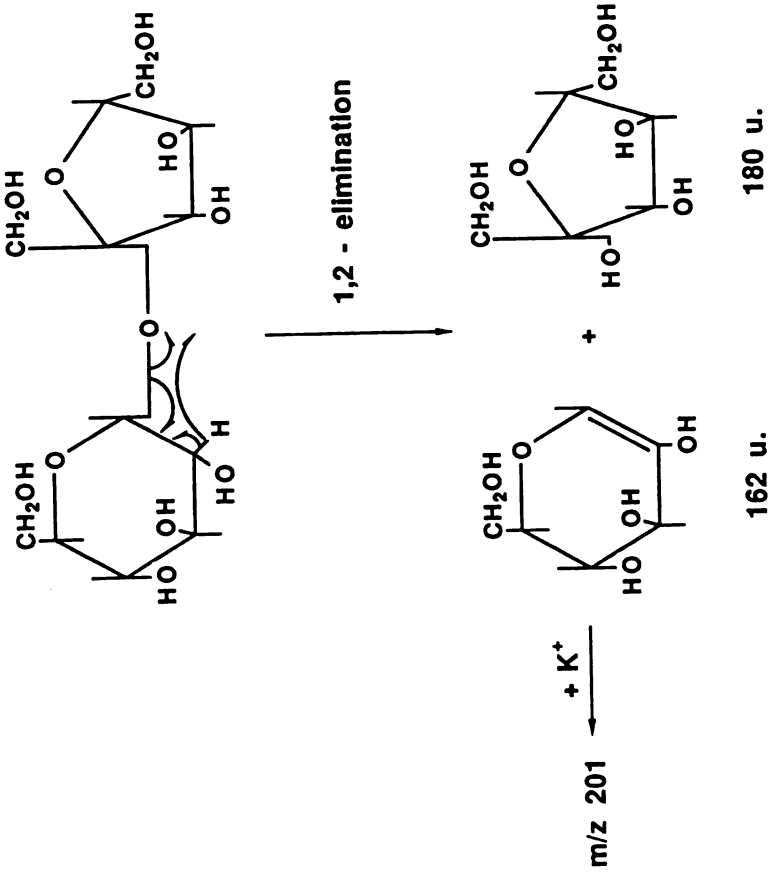

Figure 2.1 Example of the 1,2-elimination mechanism for the thermal degradation of sucrose.

bonds with little degradation of the analyte. Other researchers have utilized different materials for sample supports to achieve the same results of enhancing the sample volatility. Materials used as sample support surfaces primarily for DCI techniques include polyimide-coated wires,[35] various metals,[36] Vespel,[37] nitrocellulose,[38] and SE-30-coated glass (SE-30 is a dimethyl siloxane polymer).[39] This variable of sample support surface and its effect on the volatilization of thermally labile compounds has not been pursued to date with the K^+IDS technique. It is an area of future study that may prove necessary when trying to extend the mass range of this technique and to work with more thermally fragile compounds.

Beuhler and coworkers also suggest the use of "rapid heating" of a sample for volatility enhancement.[30] This is based on the kinetics of competitive desorption versus thermal degradation processes. They showed how the rate at which energy is deposited in a solid sample can enhance desorption of the intact molecule over thermal degradation of the sample on the surface. Arrhenius plots can be used to illustrate how kinetic considerations of vaporization versus degradation can be used to control the amount of decomposition that occurs upon rapid heating of thermally labile samples. The rate of vaporization of a neutral fragment is related to the activation energy for decomposition.[30] This activation energy is lower than the activation energy for evaporation of the intact parent molecule. The Arrhenius equation (Equation 2.4) provides a relationship between the rate of product formation, k, and the activation energy, E_a, and the inverse temperature, $1/T$.

$$k = A \exp\left(-\frac{E_a}{RT}\right) \qquad 2.4$$

$$\text{or} \quad \ln k = \ln A - \left(\frac{E_a}{RT}\right) \qquad 2.5$$

Therefore, Arrhenius plots of the relative ion abundances of the intact molecule and thermal degradation products (which are a function of ln k) versus 1/T must intersect at some crossover temperature (T_c) since the activation energies and, thus, slopes of the plots are different for these two processes of desorption of the intact molecule and thermal degradation. A

generic Arrhenius plot for desorption and degradation is given in Figure 2.2. At low temperatures ($1/T > 1/T_c$), the rate of degradation is greater than the rate of desorption and, therefore, mostly K^+ adducts of thermal degradation products would be observed in the K^+IDS experiment. At high temperatures ($1/T < 1/T_c$), the rate of desorption is greater than the rate of decomposition and K^+ adducts of the intact molecule also would be observed in the K^+IDS mass spectrum. Therefore, rapidly heating the sample allows for the crossover temperature to be exceeded while there is still enough sample to allow desorption of the thermally labile compound to dominate. The selection of the heating rate of the sample may be used to control the information obtained during the K^+IDS experiment. Molecular weight information is obtainable at high rates of heating. Structural information, from thermal degradation products, is available at lower rates of heating and lower final temperatures.

Monitoring the surface temperature from which sample desorption occurs also provides other interesting information. Williams and coworkers investigated the kinetics of the volatilization process for thermally labile compounds.[40] Both slow (1-5K/min) and rapid (1000 K/sec) heating techniques were utilized in these experiments. The N-acetyl(L-alanine)$_n$ methyl esters were studied with the slow heating rates while rapid heating chemical ionization was applied to polyalcohols and saccharides. The two techniques gave similar results regarding the temperature dependence of the rate of ion production of the molecular adduct ions. The activation energies for the volatility of the intact sample molecules were calculated from the slopes of the Arrhenius plots of the abundance of the molecular adduct ion versus the reciprocal of the surface temperature. The activation energies calculated increased with molecular weight within a class of compounds such as the methyl esters. These activation energies also quantitatively resembled the heats of vaporization obtained experimentally. Since intermolecular hydrogen bonding is a dominant interaction that is reflected in the heat of vaporization, the activation energies obtained for volatilization of the sample may be quantitatively related to the degree of hydrogen bonding. Ideally these temperature studies can be applied to the K^+IDS technique to allow for the determination of the relative activation energies for the volatilization of different compounds and of different fragmentations from a given compound.

The first indication that temperature could be used to alter the mass spectra obtained with the K^+IDS technique was from early studies

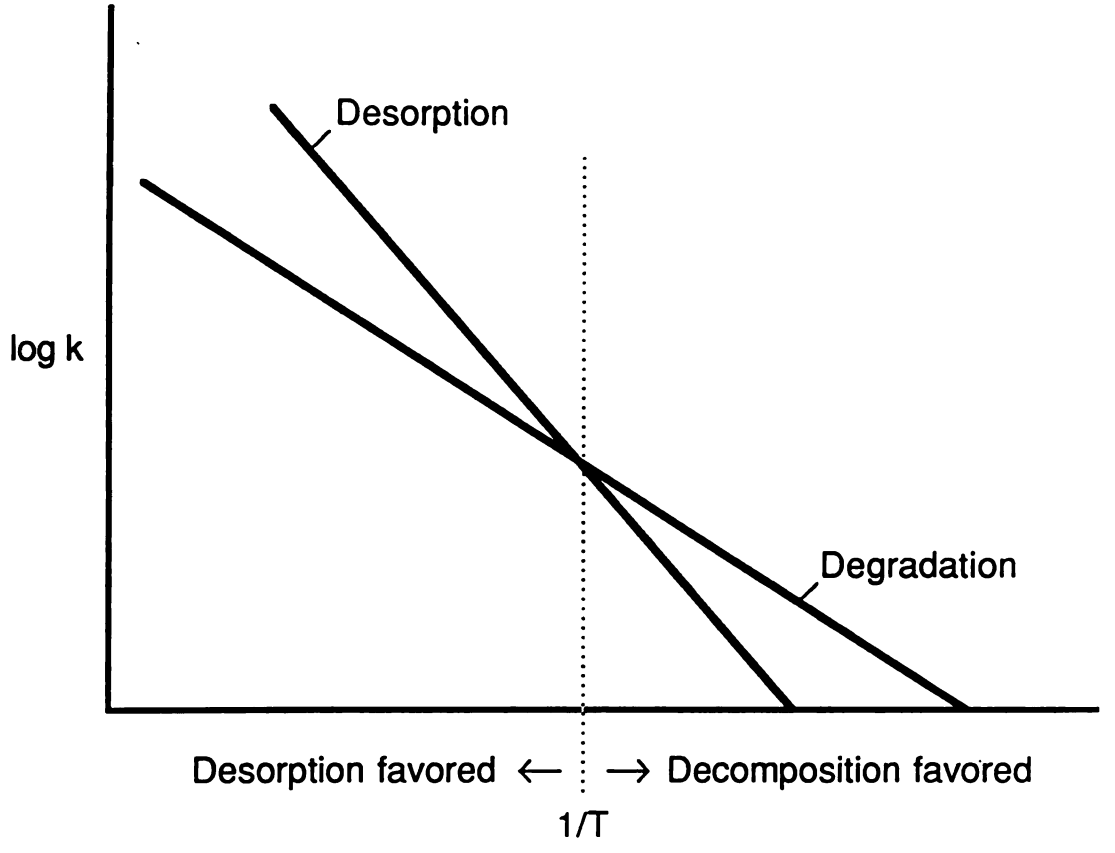

Figure 2.2. Arrhenius plot of the log k vs. 1/T for desorption and thermal degradation processes. The slope of the line is a function of the activation energy.

with tristearin. Tristearin is a fatty acid derivative of glycerol; the structure is shown in Figure 2.3. The arrows on the figure show the fragmentations that are observed during the K^+IDS analysis and the resulting m/z values of the K^+ adduct ions produced. Varying the current applied to the K^+ emitter for each analysis, produces different K^+IDS mass spectra. At higher currents and thus faster heating rates and higher final temperatures, only the K^+ adduct ions of the intact molecule are observed. At lower currents and thus lower heating rates, more thermal degradation products are observed as K^+ adduct ions. In addition, variations in the K^+IDS mass spectra can be observed at intermediate heating rates within one experiment, when there is sufficient sample present. This is illustrated in Figure 2.4 which is a plot of the relative abundance versus scan number (time) for a variety of K^+ adduct ions of thermal degradation products and of the intact molecule of tristearin. Early in the experiment, the thermal degradation products are abundant as the temperature is close to the crossover point and, thus, the rate of vaporization and degradation are competitive. Later in the experiment as the temperature increases, the rate of vaporization is greater than the rate of thermal degradation and thus the mass spectrum mainly contains the $[M]K^+$ ion at m/z 929. Figure 2.5 shows two K^+IDS mass spectra of tristearin obtained by averaging the spectra in these two different regions of the experiment. Mass spectrum A is from the early part of the experiment and mass spectrum B is from the latter part of the same experiment. These within-run variations prompted interest in pursuing this temperature variable as a means of controlling the information obtainable with the K^+IDS technique.

It is the goal of this part of the research to exploit these variations in the K^+IDS mass spectra and alter the K^+IDS mass spectra obtained with the use of the temperature/heating rate variable. The ideal mass spectrum of any compound contains both molecular weight and structural information. Alteration of this temperature variable may allow for the production of K^+IDS mass spectra that contain both molecular weight and structural information. The main difficulty with this endeavor is the dynamic nature of the K^+IDS experiment and the short-lived signals which typically last less than one minute. Modifications to the probe design and experimental conditions are made to allow for better control of this heating rate variable and to increase the lifetime of the adduct ion signal.

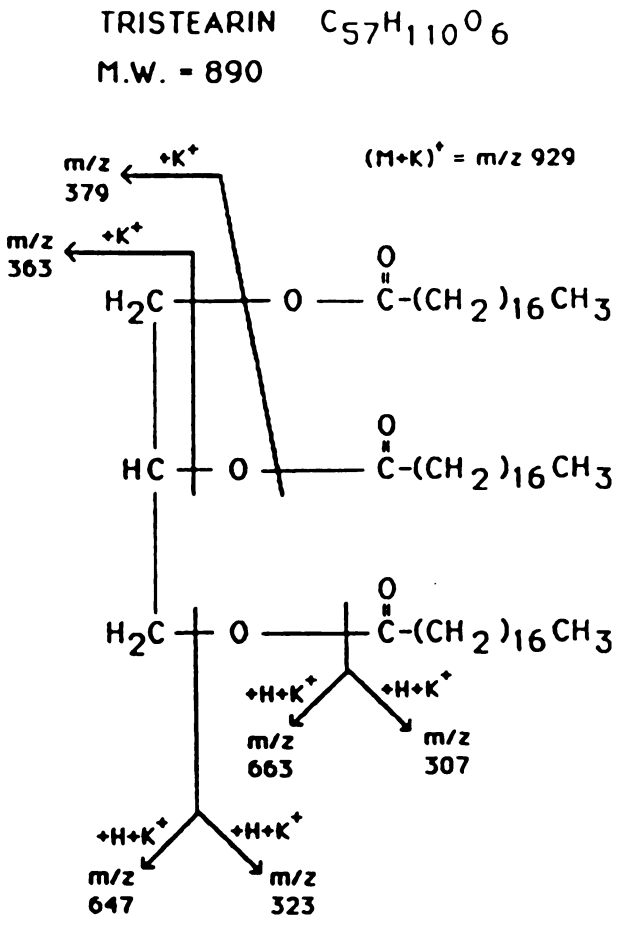

Figure 2.3 Structure of tristearin and the thermal degradations observed as K+ adduct ions in the K+IDS mass spectra.

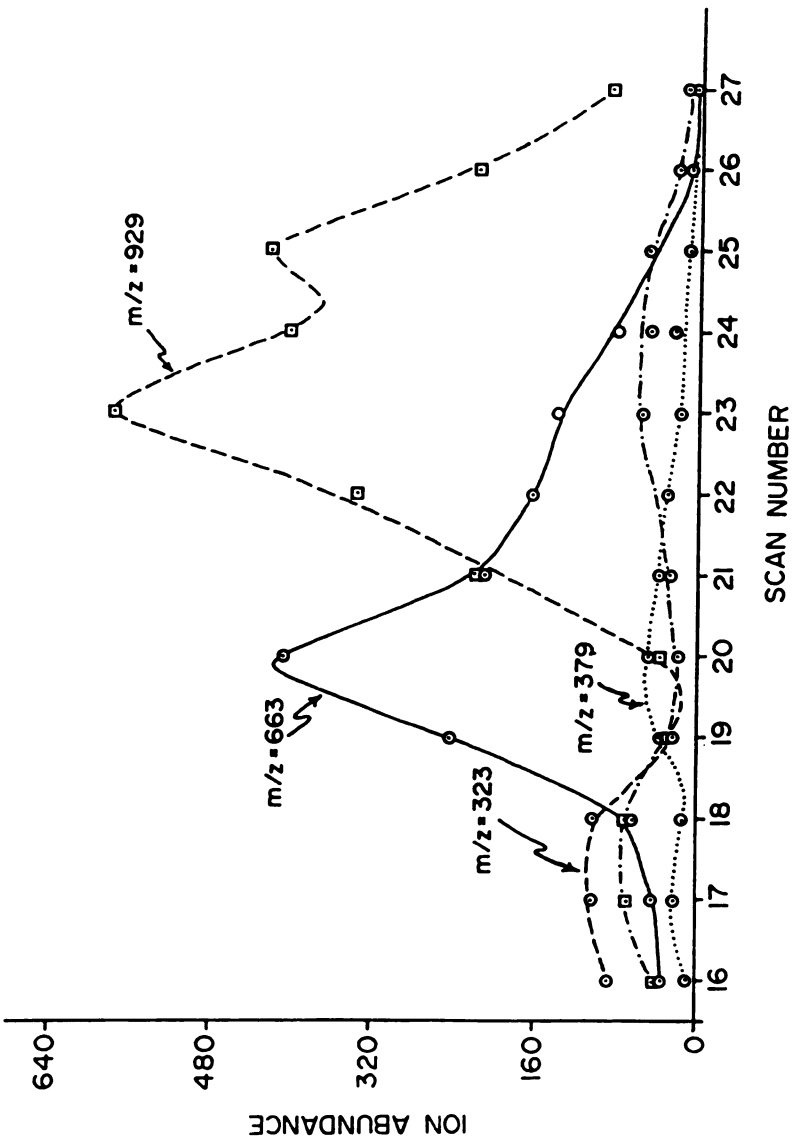

Figure 2.4 The abundances of the K^+ adduct ions of the intact molecule (m/z 929) and of the thermal degradation products of tristearin versus scan number.

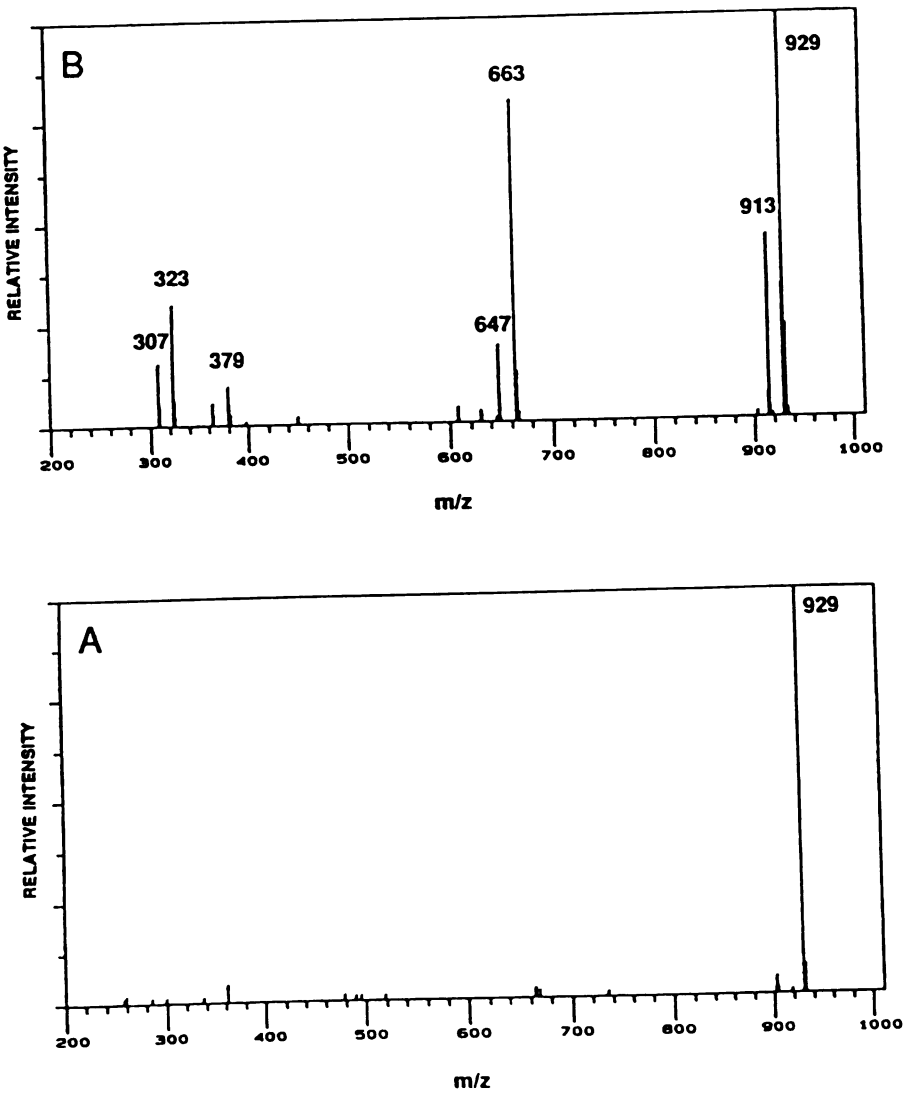

Figure 2.5 K^+IDS mass spectra of tristearin averaged over scans early (A) and late (B) in the same analysis.

2. CHARACTERIZATION AND MODIFICATION OF THE K+IDS PROBE

A. ORIGINAL SINGLE FILAMENT PROBE DESIGN

As mentioned in Chapter 1, the most important aspect of the K+IDS technique is the temporal and spatial overlap of the emission of K^+ ions in the gas phase and the desorption of neutral molecules and thermal degradation products of the sample. Characterization of the K+IDS probe was performed to determine the overlap of these two processes and to formulate ways of improving the sensitivity of the technique. Experiments were designed to monitor the two processes of K^+ emission and sample desorption individually and correlate the results to determine the temporal overlap. EI was used to monitor the desorption of the sample from the probe tip. The sample, suspended or dissolved in solvent, was applied in the normal manner for a traditional K+IDS experiment on the tip of the K^+ bead. After the solvent evaporated, the probe was inserted into the instrument with the probe tip positioned just at the edge of the ion source. This placement was chosen so that the K^+ bead did not interfere with the path of the electrons from the EI filament and to insure that desorption of the sample was from the current applied to the probe and not from electron bombardment of the surface. There were no ions detected from the sample with only the EI filament on. However, sample desorption was detected almost immediately (by EI) after the current was applied to the K^+ bead. The K^+ emission was monitored in a separate experiment with the normal K+IDS setup with the exceptions that the mass range was adjusted to detect m/z 39 (K^+) and the multiplier voltage was lowered so that the strong m/z 39 signal did not saturate the detector. In this case there was a lag time of approximately eight seconds before K^+ emission began. (This time lag for K^+ emission varies with the thickness of the K^+ glass covering the filament wire.) The TIC chromatograms of these two experiments are overlaid and shown in Part A of Figure 2.6. For both experiments, the current was applied to the K^+ bead at the same time (scan 7) and the scan rate of the quadrupole was 1 second/scan over the mass range of 20-420 daltons. From this overlap, it can be seen that most of the gas-phase sample molecules were gone by the time K^+ ions were produced in a large abundance. This poor

A. ORIGINAL PROBE TIP DESIGN

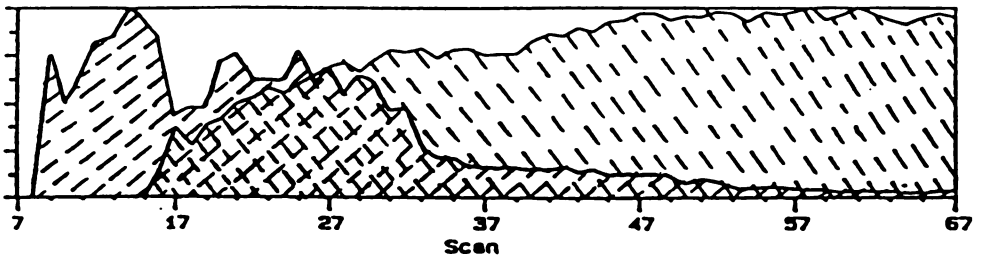

I applied to emitter

K^+ emission

sample desorption

B. TWO-FILAMENT PROBE TIP DESIGN

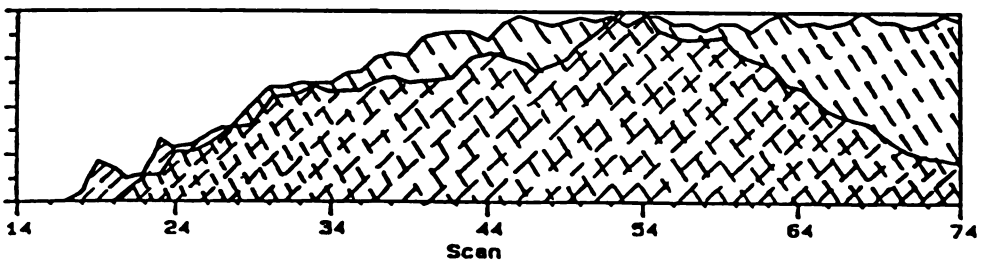

Figure 2.6 TIC chromatograms of the sample desorption of a fatty acid mix obtained by EI overlapped with the K^+ emission for the original probe tip design and the new two-filament probe tip design.

overlap resulted in poor sensitivity of the K^+IDS technique as most of the sample was desorbed too rapidly and, thus, was not detected.

B. DUAL FILAMENT PROBE DESIGN

To improve on the poor overlap of the two processes involved in the K^+IDS technique, new probe designs were proposed and tested for improvement in this overlap and for ease of construction. The goal was to substantially improve upon this overlap by either speeding up the onset of K^+ emission or by slowing down the onset of sample desorption. Many different ideas were addressed to solve this overlap problem including physically separating the two processes and providing two different power supplies for independent control of the K^+ bead and sample heating. Logistically, the independent temperature control of the two processes was not feasible. Only one probe inlet was available for a 1/4 inch outer diameter probe. This small diameter greatly limited the design possibilities. The final design for the new probe tip chosen after many tests with different wires, ribbons and other support materials is shown in Figure 2.7. This design resembles the two-filament "push-rod" probe tip design reported by Rollgen and co-workers for the production of alkali metal adduct ions of thermally labile compounds.[19] The probe tip shown in Figure 2.7 has a separate sample post very similar in design to the original K^+ bead filament. A 0.007" diameter wire (usually tungsten/rhenium instead of the pure rhenium used for K^+ bead filament for economical reasons) is threaded through a two-holed ceramic support post with a loop of wire left at the top. This sample wire is spot welded to two support posts that are cemented into a four-holed ceramic in the tip of the probe. This sample support is not directly heated, but is radiatively heated by the K^+ bead when in close proximity to the tip of the bead (the distance between the K^+ emitter and the sample wire is less than or equal to one millimeter).

The same overlap test of the K^+ emission and sample desorption was performed with this two-filament probe design. The sample is now placed only on the wire loop at the tip of the sample support post. (A twist in the wire loop just above the ceramic post helps prevent the sample from creeping down the wire and into the ceramic post). The desorption of the sample is observed by EI in the same manner as in the previous test. The results of this overlap test are

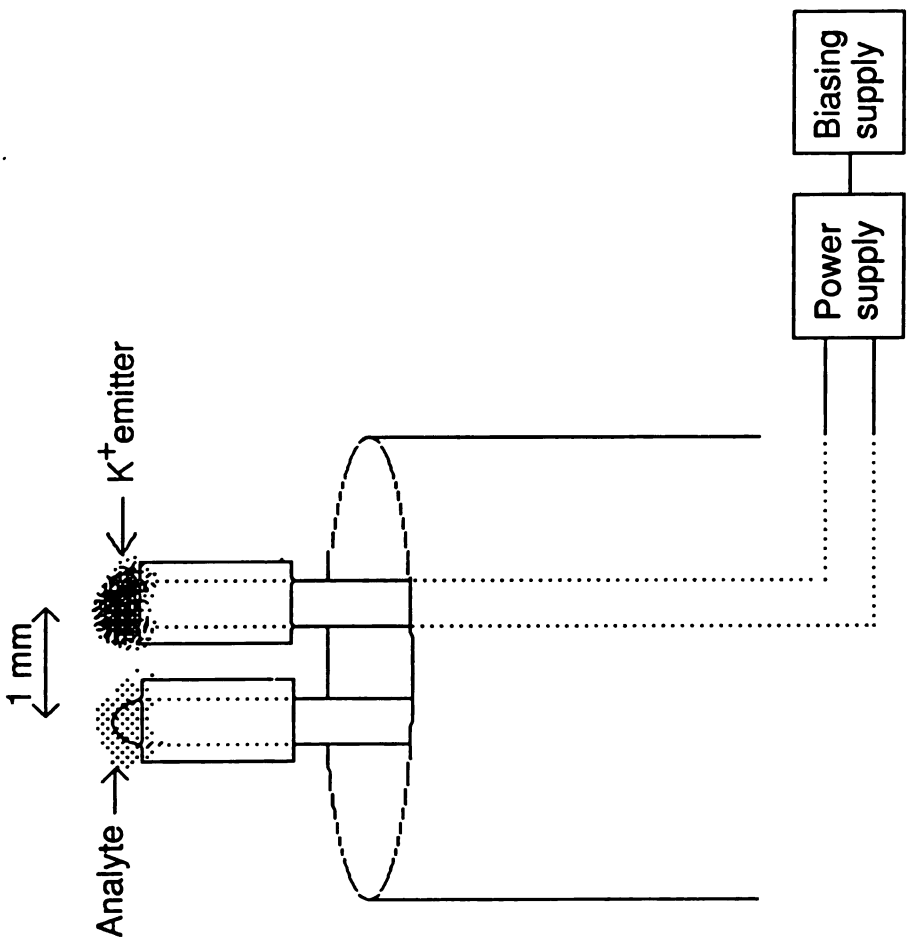

Figure 2.7 Two-filament K^+ IDS probe tip design.

shown in Figure 2.6 B. A much improved overlap of the two processes is now obtained. The K^+ emission began sooner due to the absence of sample covering the K^+ bead as in the previous design. But more importantly, the onset of sample desorption occurred later with respect to application of current to the emitter. Thus, the temporal overlap of K^+ emission and sample desorption is greatly improved. The sensitivity of the K^+IDS technique improved 30- to 40-fold with the development of this two-filament probe design. Kassel documented the increase in sensitivity of this two-filament probe design for the analysis of methyl stearate,[41] which is a compound typically used for determining relative sensitivities of ionization techniques such as EI and CI. Monitoring the $[M]K^+$ ion of methyl stearate with selected ion monitoring (SIM), the absolute peak height obtained with the original single filament probe design was 140 arbitrary units and the peak area was 2,300 arbitrary units squared. For the two-filament K^+IDS probe, the absolute peak height was 5,100 arbitrary units and the peak area was 26,000 arbitrary units squared for the $[M]K^+$ ion of methyl stearate of equal sample volume. These results show the large increase in sensitivity obtained with the two-filament probe design for the K^+IDS technique. This increased sensitivity is obtained for most other thermally labile compounds. Kassel determined the detection limit of the K^+IDS technique with the two-filament probe tip for the analysis of methyl stearate to be 3 ng in the SIM mode and 10 ng in the full scanning mode (50-450 daltons and 0.5 sec/scan) at a signal-to-noise ratio of five.[41] This two filament probe design is used to obtain the remainder of the K^+IDS mass spectral data presented, unless otherwise noted.

The success of this two-filament probe design introduces some uncertainty as to why the K^+IDS technique works well for the analysis of thermally labile compounds. The new design produces relatively the same K^+IDS mass spectra as were previously obtained with the original single filament probe design. However, the heating rates of the K^+ bead surface (where sample was originally placed) and the separate sample post are not the same. This prompted more detailed studies of the temperatures of these different surfaces and the actual heating rates needed to desorb the thermally labile compounds studied. The term "rapid heating" is generic in nature, as is the Arrhenius plot in Figure 2.2 which provides no idea of the actual temperature needed to reach the crossover point and promote vaporization of the intact thermally labile molecule. Beuhler reported that the volatilization

of sucrose reaches half of the maximum rate by 111°C and that rapid heating of the peptide TRH to 215°C produces twice as much protonated parent ion as fragment ion.[34] These temperatures are much lower than previously expected to promote vaporization of thermally labile compounds based on the understanding of the K^+IDS technique. In the original probe design, the sample was deposited directly onto the K^+ bead surface which reached very high temperatures (approximately 1000°C) at the onset of the K^+IDS experiment. Thus, it was assumed that these high temperatures were actually needed to desorb the thermally labile molecules intact. The success of the two filament probe design, however, questions this original assumption since the sample is no longer achieving the same high temperatures and yet the same K^+IDS mass spectra are obtained. Several experiments were designed to gain a better understanding of these heating rates and temperatures needed for the desorption of thermally labile compounds.

3. TEMPERATURE STUDIES OF THE K^+IDS TWO-FILAMENT PROBE DESIGN.

A. DETERMINING SURFACE TEMPERATURES IN A VACUUM CHAMBER

The first experiments to study the temperatures of the different surfaces of the K^+IDS probe were performed in a glass vacuum chamber separate from the mass spectrometer for easier access to the probe. The experimental design is shown in Figure 2.8. An evacuated three-neck round bottom flask was used to mimic the ion source of the mass spectrometer. An optical pyrometer was initially used to measure the temperature of the K^+ bead surface. It was determined that the emitter reached temperatures between 800 to 1250°C when K^+ emission was observed (heating currents > 2.0A). Heating the K^+ emitter inside the clear glass vacuum chamber allowed for visual inspection of the heating process and the differences of the two filaments. The K^+ bead tip glowed bright red at low currents (1.0 to 2.0A) and became bright white when the heating currents were greater than 2.0A. The ceramic post of the K^+ bead remained an orange-tinted glow throughout most of the experiments. In contrast, the sample filament did not show any physical signs of heating, which was the first evidence of the drastic temperature differences between the two surfaces. This visual observation prompted further studies of the temperatures of the two surfaces and of the heating

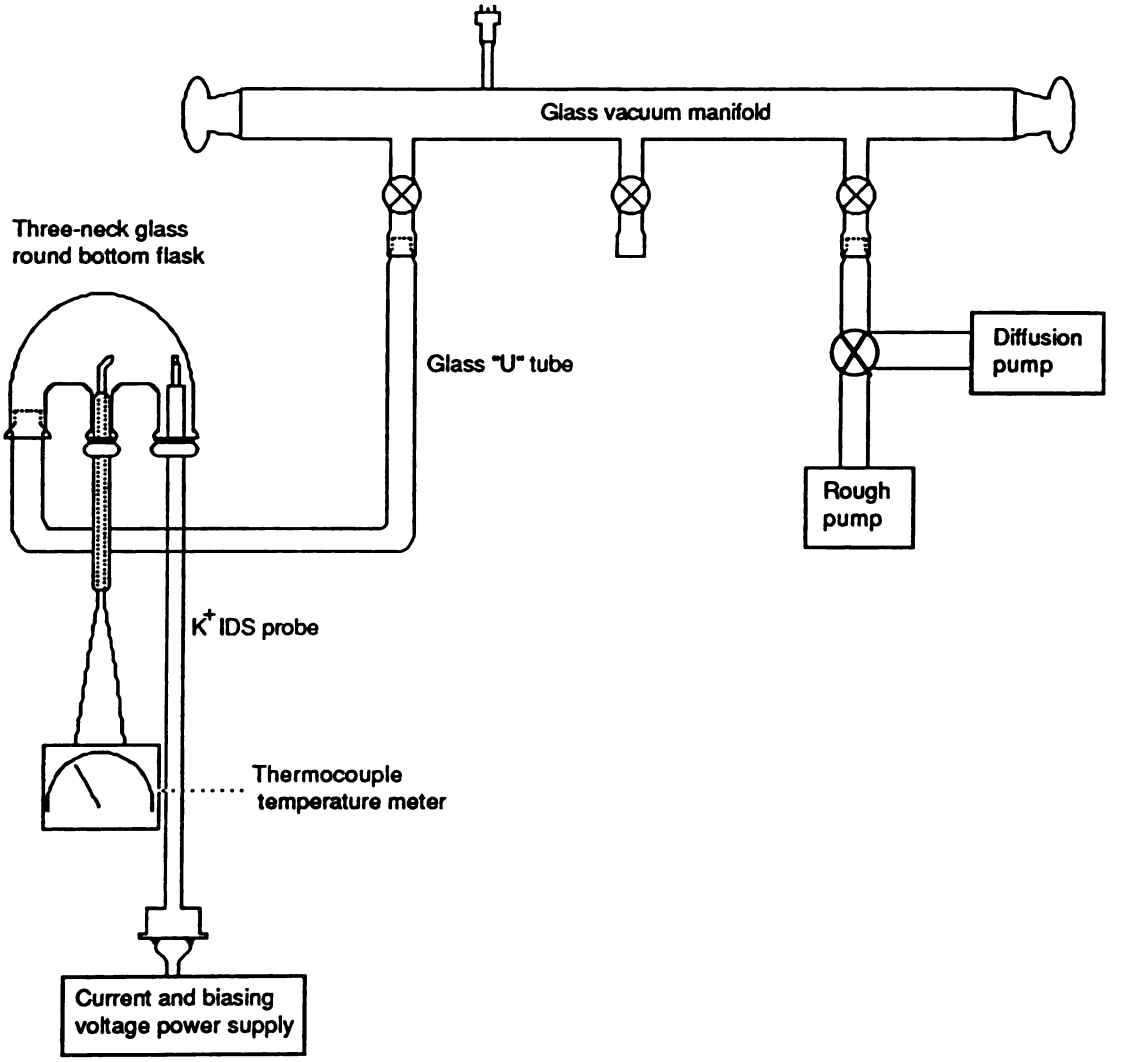

Figure 2.8 Experimental setup for the temperature measurements of the K^+ IDS probe performed inside a glass vacuum chamber.

rates of the surfaces when different currents are applied to the K^+ emitter filament.

1. EXPERIMENTAL DESIGN

To determine the heating rates, a thermocouple that had a fast response time and could respond to a wide temperature range (25-1400°C) was needed. Two different kinds of thermocouples were obtained from OMEGA Engineering, Inc. (Stamford, CT) as well as a monitoring device. Type K and Type C thin, bare wire thermocouples were obtained for their quick response to temperature changes. The Type K thermocouple is chromel/alumel with an upper temperature limit of 1250°C. The type C thermocouple is composed of two wires which are tungsten 5% rhenium/tungsten 26% rhenium and it has an upper temperature limit of 2320°C. Both of these thermocouples were converted into vacuum tight probes with glass tubing and epoxy. Small glass tubing was used to insulate the two thermocouple leads from one another. The wires and small tubing was threaded through a larger glass tube with an outer diameter of 0.25 inch and approximately six inches long. Five-minute epoxy was used to seal up both ends of the larger glass tube to make a vacuum tight probe. This probe and the K^+IDS probe were inserted into the round bottom flask, sealed with O-ring connectors and evacuated with the vacuum chamber. The tip of the thermocouple could be positioned on any surface of the K^+IDS probe, while under vacuum.

The Type K thermocouples obtained were 0.001 inch in diameter and, thus, could respond to temperature changes more quickly than the Type C thermocouples which were 0.003 inch in diameter. However, the Type K thermocouples were fine hair-like wires that broke easily and proved to be too difficult to work with. Thus, the Type C thermocouples were used for the initial heating rate studies. The Type C thermocouple leads were connected to an OMEGA DP-80 series thermocouple monitor that was equipped with an analog output option card so that a signal representing the thermocouple temperature could be sent to a chart recorder. The analog output was connected to a Houston Omnigraphic 2000 X-Y recorder and a temperature-versus-time plot was obtained. The X-axis was set at 25 sec/cm and the Y-axis was set at 1V/in. The OMEGA temperature monitor was programmed so the analog output of zero V corresponded to +25°C and 10V corresponded to +1525°C.

2. RESULTS

The heating rates were approximated from plots of temperature versus time at the different current values applied to the emitter. An example of the temperature vs. time plots for the two different probe tip surfaces (K^+ bead and sample wire support) is shown in Figure 2.9. The two measurements were made consecutively with the same thermocouple. The thermocouple was repositioned onto the different surface and the bead was cooled between experiments. For the data shown in Figure 2.9, 3.0A were applied to the K^+ emitter at the start of each experiment. As can be seen in these plots, not only is there a discrepancy in the final temperatures of these two surfaces, but also a difference in the heating rates of the two surfaces. This difference in heating rates is indicated by the slopes of the heating curves. This process was repeated for six different currents between 2.25A and 3.50A. Figure 2.10 shows a plot of the final temperatures of the K^+ emitter surface and the sample support surface as a function of current applied to the emitter measured with the Type C thermocouple probe. The heating rates of the two surfaces were approximated by dividing the temperature obtained at half the time it took to reach the maximum temperature by the half time, or $T_{1/2}/t_{1/2}$. The heating rate of the emitter surface is hard to determine with this method as the temperature is changing so rapidly that the monitoring device is not keeping up with the change. The heating rate ($T_{1/2}/t_{1/2}$) is approximately 200°C/sec during this initial heating period of the K^+ bead. The sample surface has a much lower heating rate and therefore changes in the heating rate as a function of the emitter current can be observed. Figure 2.11 shows a plot of the approximate heating rates ($T_{1/2}/t_{1/2}$) of the sample support surface as a function of current applied to the emitter. The data in Figures 2.10 and 2.11 demonstrate that the current applied to the emitter affects both the final temperatures of the surfaces of interest and the heating rates. As the current increases so does the final temperature and the heating rate (especially for the sample support surface). These figures also emphasize the major differences in the final temperatures and the heating rates of the two different surfaces.

This proof of the differences in heating rate and final temperature of the sample in the two different K^+IDS experimental designs prompts the need to explain why the K^+IDS mass spectra remain unchanged. One possible

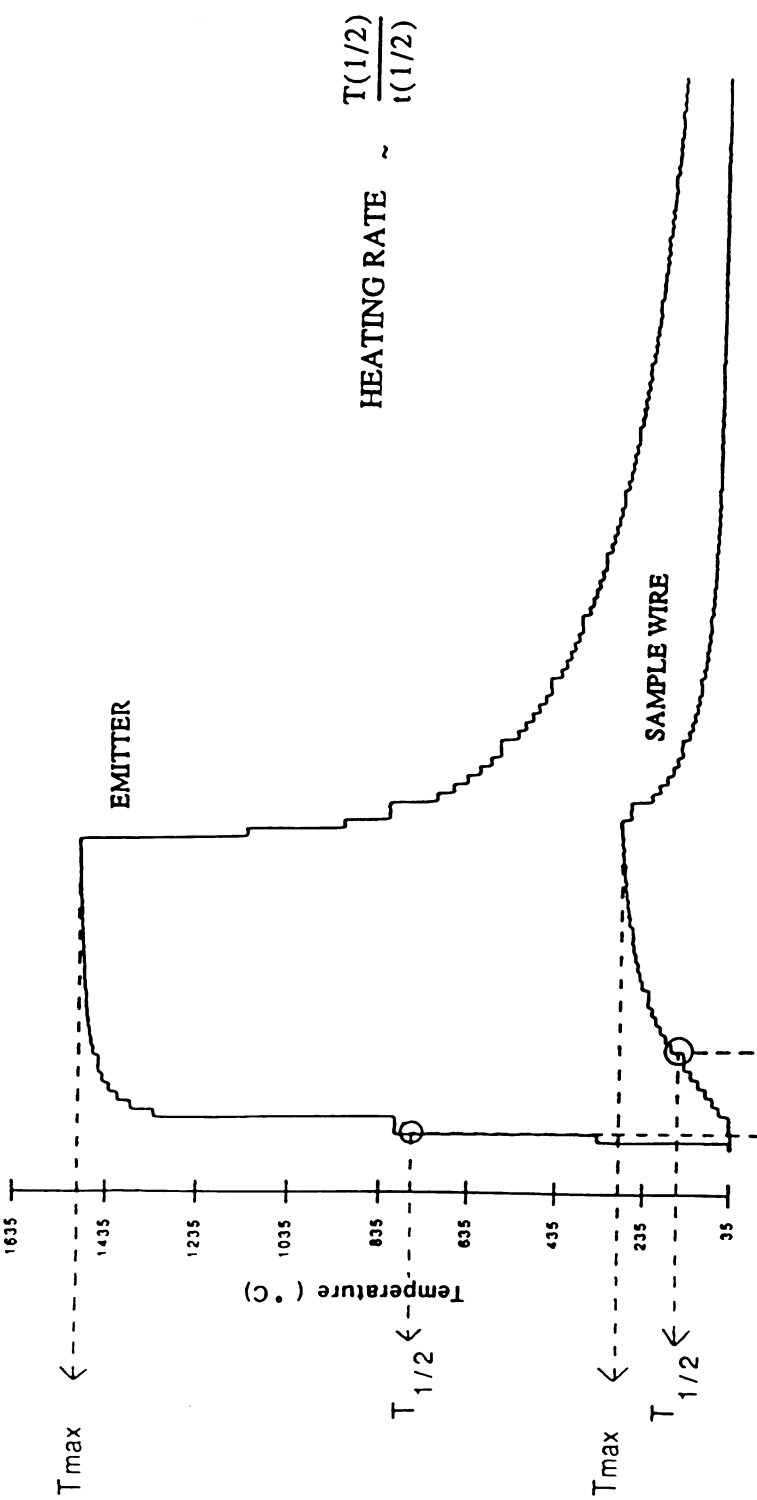

Figure 2.9 K^+ Emitter bead and sample filament wire temperature versus time when 3.0A is applied to the emitter.

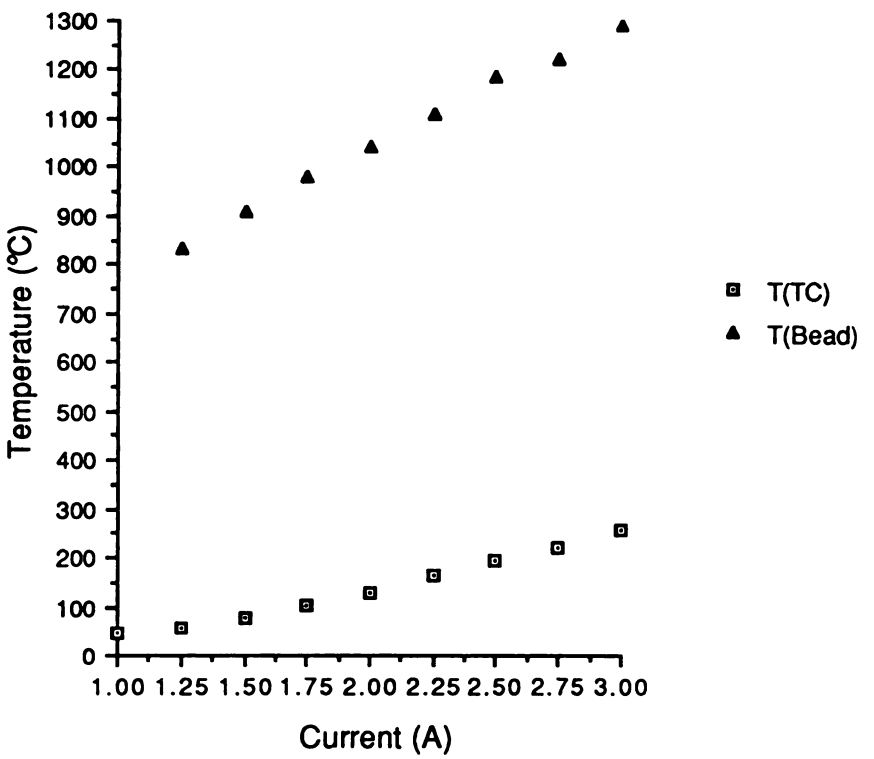

Figure 2.10 Temperature of the emitter surface and sample filament wire vs. current applied to the emitter.

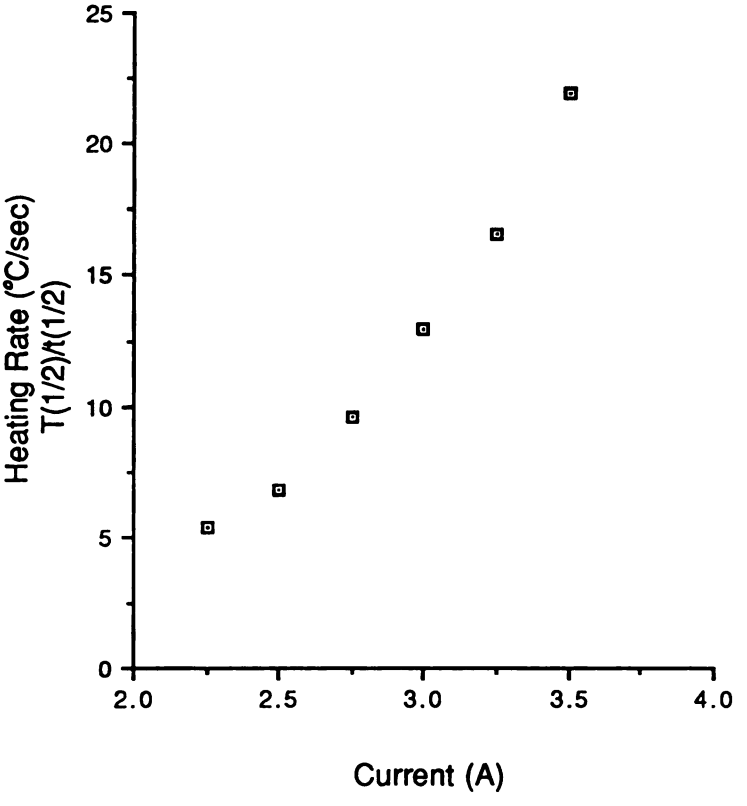

Figure 2.11 Heating rate of the sample filament wire vs. emitter current.

explanation for this may have to do with where the sample resides when applied to the K^+ bead versus the second filament support wire. It is possible, for instance, when applying sample that is suspended in a solvent such as methanol to the K^+ bead in the original probe design, that some of the sample may creep down the ceramic post of the emitter tip. The sample observed with K^+IDS utilizing the old probe design could be the result of desorbing sample from the ceramic and not from the tip of the K^+ bead which heats up so rapidly. The sample that resides directly on the tip of the K^+ bead may desorb too quickly, before the production of K^+ ions, and therefore not be detected. The temperature of the ceramic post of the K^+ bead was monitored in a manner previously described to test the heating rates. The thermocouple was consecutively positioned on the three different surfaces: the K^+ bead tip, the ceramic post of the K^+ bead, and the sample support wire. The temperature of each surface was monitored as a function of time with the same current applied to the K^+ bead for each experiment. These measurements were repeated for a range of currents between 2.25A and 3.00A applied to the K^+ bead. Just as before, the probe tip was allowed to cool down to approximately room temperature before each analysis. The results of this test are shown in Figure 2.12. The heating of the ceramic post closely resembles the heating of the sample support surface, which adds some experimental support to the above hypothesis. However, it is hard to prove this notion that the observed sample in the original design is desorbing from the ceramic below the bead as it is difficult to observe where the sample actually resides on the K^+ bead and post when applied to the tip. It is much easier to observe the deposition of the sample on the bare wire typically used for the second filament sample support.

The two-filament design fosters the notion that surface bombardment could play a role in the K^+IDS technique since the two filaments are in such close proximity. Another temperature-related experiment was designed to dispel this premise. If many K^+ ions were bombarding the sample surface, a temperature rise of the sample surface would be observed. Once the temperature of the sample surface equilibrated with a constant current being applied to the emitter, variations were made in the bias voltage applied to the tip of the K^+ emitter. Varying the bias voltage applied to the tip of the K^+ emitter from 0V to +150V at a constant heating current did not change the temperature of the sample surface significantly. This supports the notion that the sample support is being heated radiatively and not by bombardment. This

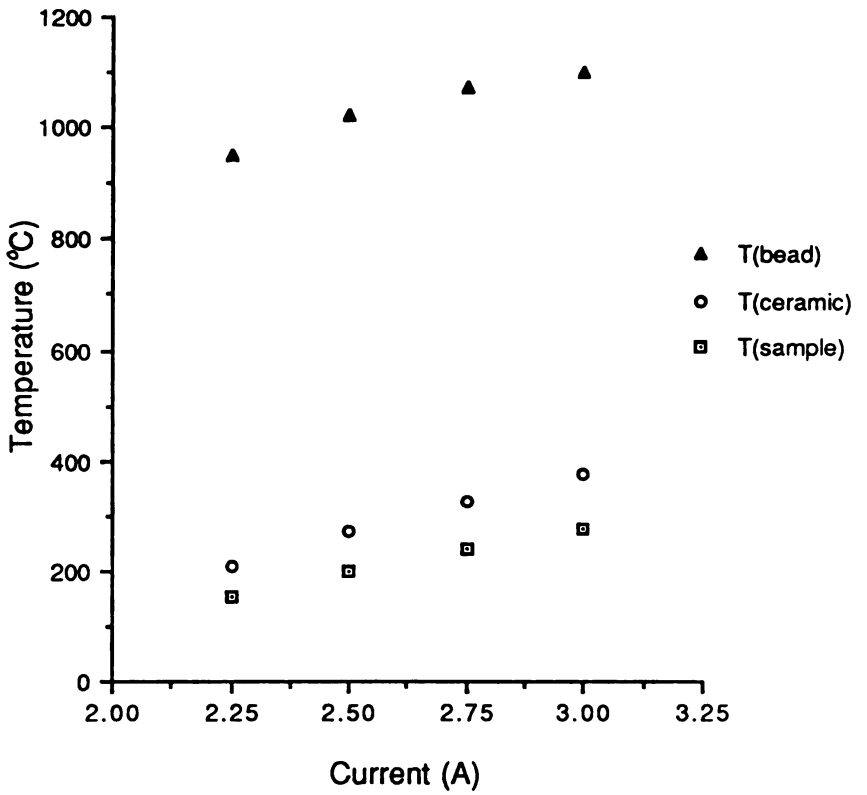

Figure 2.12 Temperature of the emitter surface, emitter ceramic post, and the sample filament wire vs. emitter current.

provides additional support to the mechanism of adduct formation that K^+ attachment is occurring in the gas phase and not on the surface.

Changes in heating rate, by changing the current applied to the emitter and the design of the probe tip, affect the K^+IDS mass spectra obtained. A series of K^+IDS experiments of tristearin with 2.0A, 2.5A, 3.0A, and 3.5A applied to the K^+ bead were performed with very interesting results. The onset of K^+ adduct ion formation varied with current and the relative appearance of the parent adduct ion of the intact molecule versus the K^+ adduct ions of thermal degradation products varied with current. The 3-D plots of these four experiments are shown in Figures 2.13 and 2.14. The current was first applied at scan number 10 for each analysis and the scan time was 0.5 sec/scan. From these plots it can be seen that increasing the current increases the heating rate of the surface and thus the K^+IDS mass spectra are observed earlier in the run. Also, there is some difference in the relative appearance time of the fragment ions versus the molecular adduct ion at m/z 929. For example, the experiment obtained at 2.5A shows that thermal degradation products are observed by scan 20 and the $[M]K^+$ ion is not observed until scan 27. This may be an example of a slower heating rate where the temperature is below the crossover point at the beginning of the experiment and thus thermal degradation products dominate. In agreement with the Arrhenius plot (Figure 2.2), the temperature has reached the crossover temperature at scan 27 and therefore vaporization of the intact molecule dominates. For the experiment at the higher current of 3.0A, the heating rate may be great enough that this crossover point is reached at the beginning of ion formation. It is also possible that in this case, the limiting factor in ion formation is the production of K^+ ions. Any thermal degradation occurring before scan 16 is not detected as K^+ emission has not begun. This is supported by the fact that the next experiment at 3.5A has the same lag time (16 scans, or 3 seconds after current is first applied) before any K^+ adduct ions are observed. The poor sensitivity of this last experiment of the series suggests that most of the sample has desorbed prior to the onset of K^+ emission. These changes in appearance times of different fragment ions and the intact molecule with changes in the surface temperature and heating rate support the idea that the thermal decomposition of the sample is occurring on the surface. The products are desorbed into the gas phase followed by K^+ attachment. K^+ attachment does not induce fragmentation, but merely samples the neutral gas-phase species.

Tristearin on sample wire I=2.0A

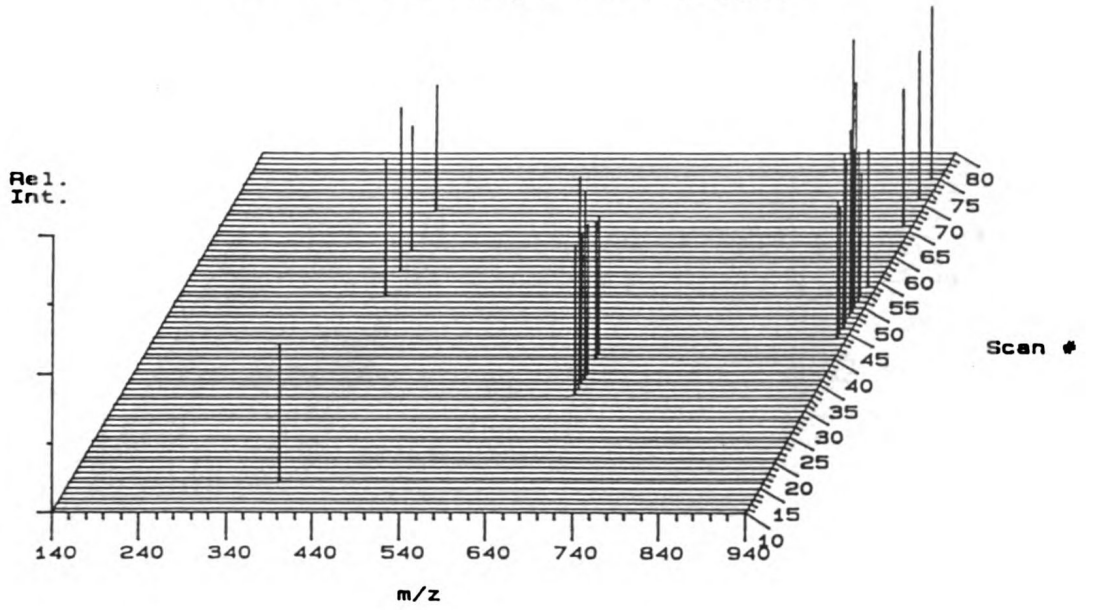

Tristearin on sample wire I=2.5A

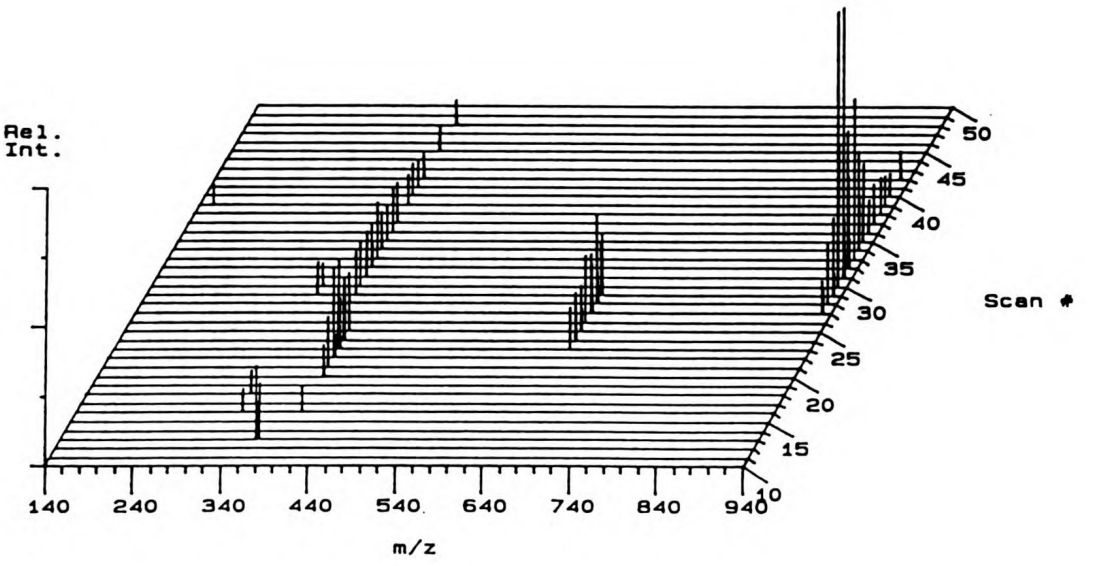

Figure 2.13 Plot of the K^+IDS mass spectra of tristearin when 2.0A and 2.5A are applied to the K^+ emitter and the sample is on the sample filament wire only.

Tristearin on sample wire I=3.0A

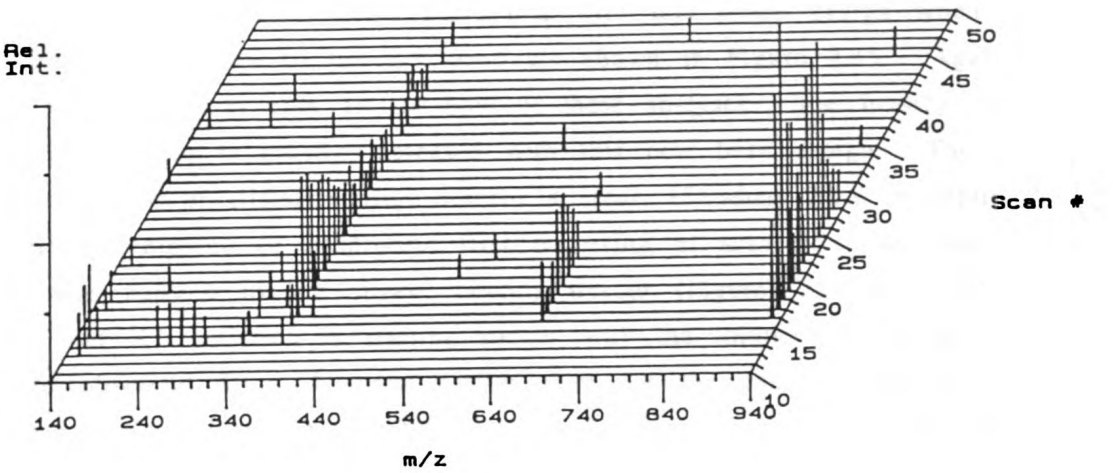

Tristearin on sample wire I=3.5A

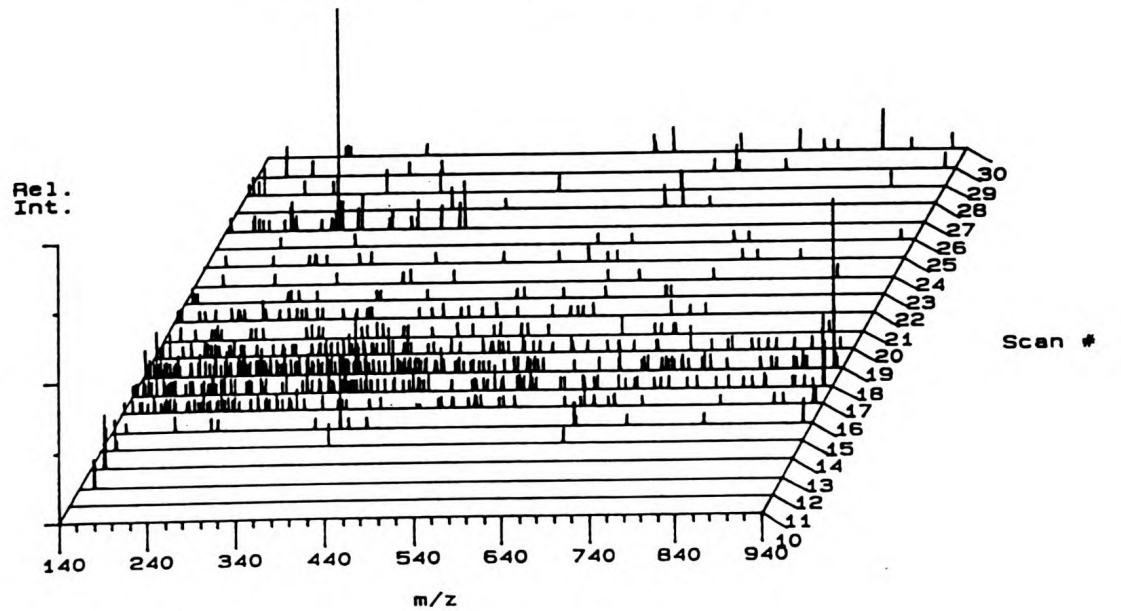

Figure 2.14 Plot of the K^+IDS mass spectra of tristearin when 3.0A and 3.5A are applied to the K^+ emitter and the sample is on the sample filament wire only.

This analysis was repeated with a different K^+ bead and sample support designed to decrease the heating rates of both surfaces. The thermal mass of the K^+ bead was reduced (thinner coating of aluminosilicate on the emitter wire) and the ceramic post on the sample support was reduced by half. The results of the K^+IDS experiments performed with this probe design when 2.0A and 3.0A were applied to the K^+ bead are shown in Figure 2.15. Again the current was applied at scan 10 for both of these analyses. The heating rate of the sample surface is greatly increased with this new bead design. The intact neutral molecule of tristearin first desorbs at scan 15 when 2.0A is applied to the emitter compared to desorption first occurring at scan 45 when the same current was applied to the slower heating design (Figure 2.13 A). Also, it appears that K^+ emission is starting sooner with the thinner emitter as adduct ions are observed 3 to 4 scans earlier than for the previous design. The thickness of the K^+ emitter and the amount of ceramic support post on the K^+ emitter and the sample filament affect the rate of heating of the sample and the onset of K^+ emission. These variables in the probe tip design may be adjusted to obtain the desired K^+IDS mass spectra, either promoting thermal degradation or desorption of the intact analyte molecule. For most thermally labile compounds studied to date with the two filament K^+IDS probe tip, the first design with more ceramic covering both the K^+ bead and the sample wires produces better results than the design with reduced thermal mass (less ceramic post).

B. CORRELATION OF K^+ IDS MASS SPECTRA WITH SAMPLE SURFACE TEMPERATURE

Preliminary K^+IDS studies, especially of mixtures, indicate that different compounds are observed at different times during a K^+IDS analysis and, therefore, require different surface temperatures to desorb and be observed. If these temperatures at which different compounds vaporize can be determined, then it is possible, based on the Arrhenius equation, that activation energies, or heats of vaporization, may be determined for desorption of these different compounds. K^+IDS provides a means of monitoring this sample desorption by the formation of $[M]K^+$ adduct ions for thermally labile compounds, M. It is assumed that the desorption of the analyte is the rate limiting step in the formation of the adduct ions, which is

Tristearin on sample wire with bare wire emitter I=2.0A

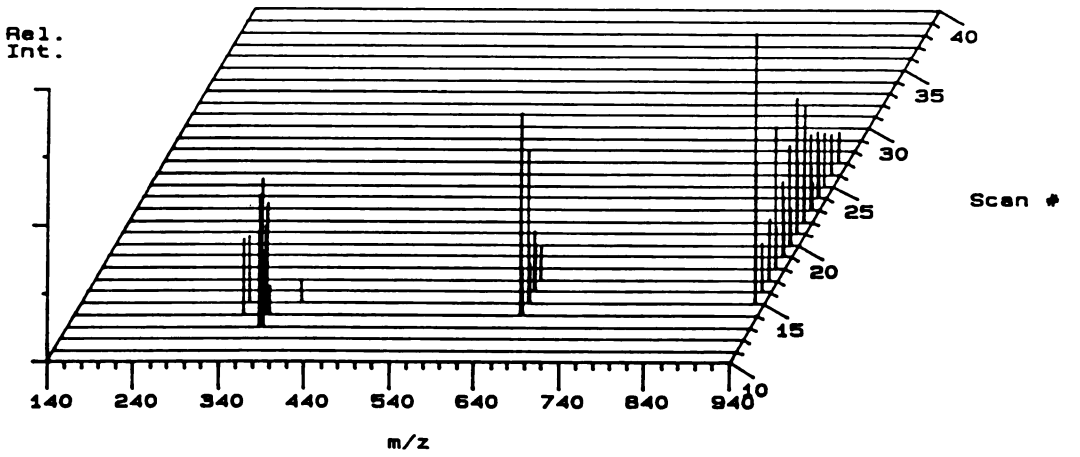

Tristearin on sample wire with bare wire emitter I=3.0A

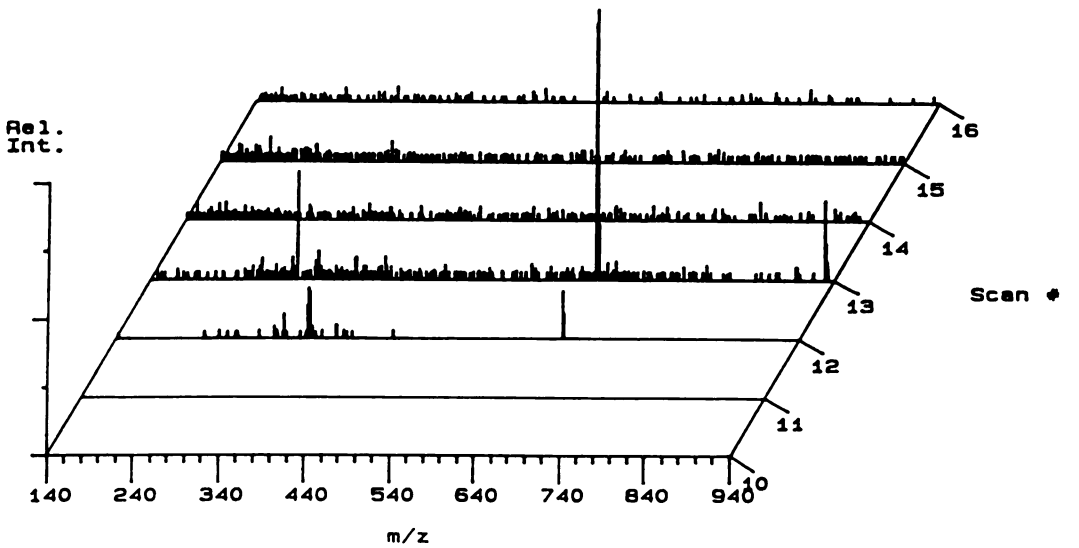

Figure 2.15 Plot of the K^+IDS mass spectra of tristearin when 2.0A and 3.0A are applied to the K^+ emitter. In this case, the thermal mass of the K^+ emitter was reduced by decreasing the length of the ceramic support rod.

explained in more detail later. Thus, by monitoring the surface temperature of the sample filament and the formation of $[M]K^+$ adduct ions, the temperature at which thermally labile compounds desorb can be determined. Beuhler et al. reported experimentally determined activation energies for the production of both parent and fragment ions of some small saccharides and erythritols.[39] These activation energies were calculated based on the Arrhenius plots of the rate of production of these sample ions as a function of the reciprocal of the absolute temperature of the sample support wire. The basic trend observed was an increase in activation energy with increasing molecular weight. The main discrepancy observed with the calculated activation energies was for the formation of the fragment ions of sucrose. Two of the fragment ions had very similar activation energies that were much lower than for the formation of the other fragment ion and the parent adduct ion. This suggests that there may be more than one mechanism involved and that there may be processes involving the monolayer molecules on the bare metal surface versus multilayer molecules on other molecules. Thus, the determination of activation energies for the formation of the different fragment ions and parent adduct ion observed may aid in the understanding of their origins.

The main goal of these K^+IDS temperature studies is to determine the temperatures required to desorb intact thermally labile compounds and produce thermal degradation products which are detected as K^+ adducts in a K^+IDS mass spectrum. Once this goal is achieved, the next step is to determine the activation energies of these desorption and degradation processes. The first experiments designed to correlate the temperature measurements of the sample support surface to the appearance of the K^+IDS mass spectra required two steps and two experimental designs. The temperature measurements of the sample support surface were performed in the vacuum chamber as previously described. Plots of temperature versus time for various currents applied to the K^+ emitter were obtained. Once the temperature measurements were completed, the same probe system was used to obtain K^+IDS mass spectra of compounds at the various currents used for the temperature measurements. Current was first applied to the K^+ bead at scan 10 and the scan rate was 0.5 sec/scan. From this information, the time of sample desorption could be calculated based on the formation of K^+ adduct ions. The previously acquired temperature versus time plot, obtained at the appropriate heating current, is

used to determine the temperature of the sample filament at the time of desorption.

The results of such experiments are shown for a variety of compounds. From the 3-D plot of the K^+IDS analysis of tristearin at 3.0A, Figure 2.14A, it was determined that desorption (observed as a peak at m/z 929 representative of the $[M]K^+$ ion) was first observed at scan 16. The temperature of the surface at scan 16 was extrapolated from the temperature vs. time plot of 3.0A to be 165°C. When only 2.5A was applied to the emitter (Figure 2.13B), the desorption of tristearin did not appear until scan number 27. In this case, the temperature was determined to be approximately 170°C at the onset of desorption. These two temperatures are within the experimental errors for the measurements. The lower heating current produces a slower heating rate for the sample wire and therefore it takes longer to reach the same temperature. The same types of 3-D plots are shown in Figures 2.16 and 2.17 for the K^+IDS analysis of sucrose and hexaglycine respectively. It was calculated from the temperature vs. time plots that sample desorption of the intact molecule for both of these compounds occurred when the sample wire temperature was 150°C. The structure of hexaglycine is shown in Figure 2.18. The thermal degradation of hexaglycine observed in the K^+IDS mass spectrum of this compound is labeled in Figure 2.18 along with the m/z values for the corresponding K^+ adduct ions.

This experimental design allows for the correlation of temperature measurements performed in the vacuum chamber to be made with the K^+IDS mass spectral data of several types of compounds to determine the temperatures of sample desorption. This experimental design, however, lends itself to much systematic error. One source of error is in the configuration of the K^+IDS probe itself. In order for these experiments to give accurate temperature measurements, the distance between the sample wire and the K^+ bead must remain constant while obtaining the temperature measurement and the K^+IDS mass spectrum. This distance greatly affects the heating rate of the sample wire. It is difficult to ensure that this distance remains constant during transportation between the two experimental setups for temperature measurement and K^+IDS mass spectral data collection. Another source of error in this design is with the mass spectrometer data system. It was discovered midway through these temperature studies that the data system does not always continuously collect data as previously assumed. When the data collection program is operated in the real time mode of monitoring the mass spectra, a

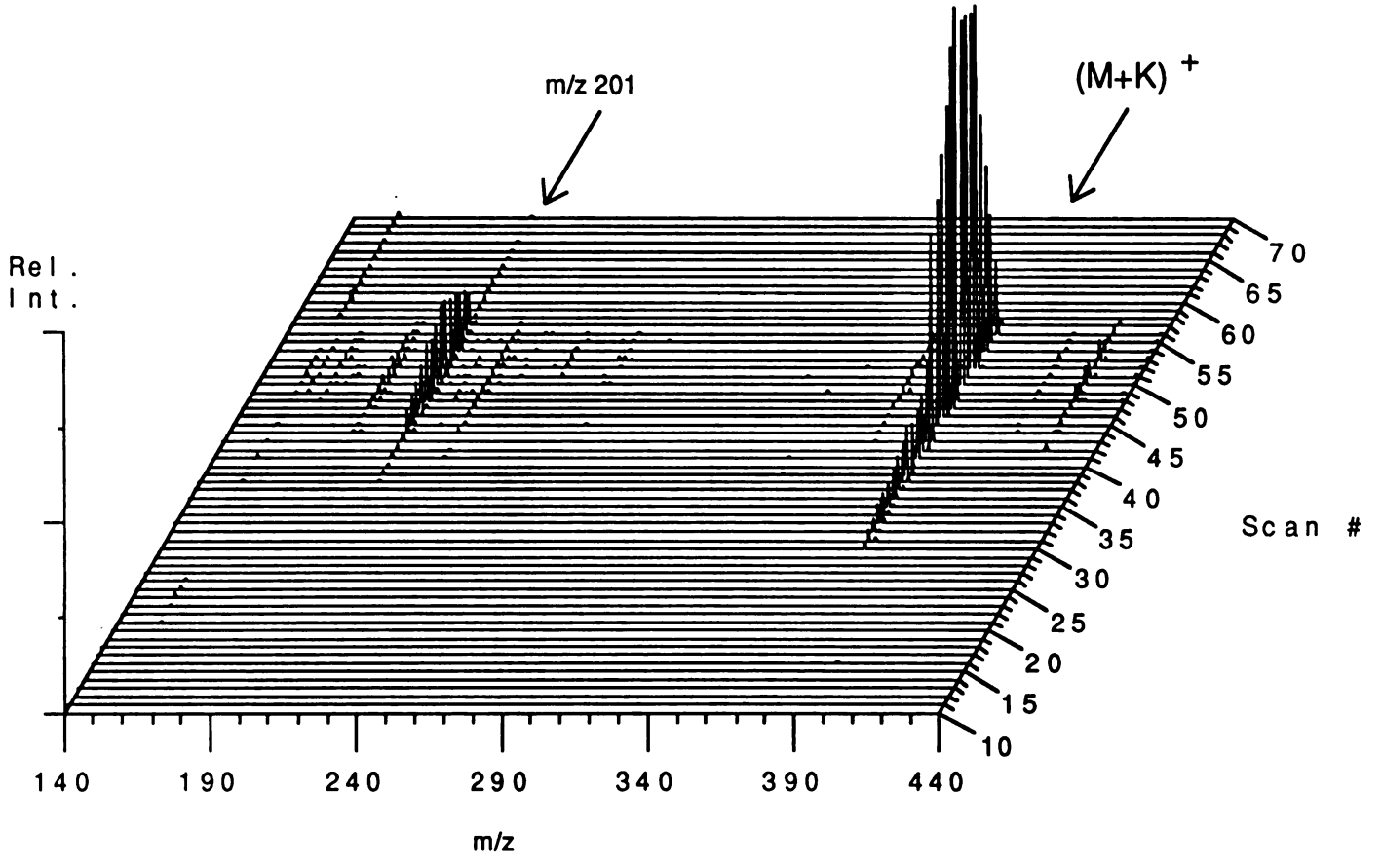

Figure 2.16. K^+ IDS mass spectrum of sucrose with sample on the support wire only. I = 2.5A
Sample desorption was first observed at scan 30. T(sample wire) = 150°C.

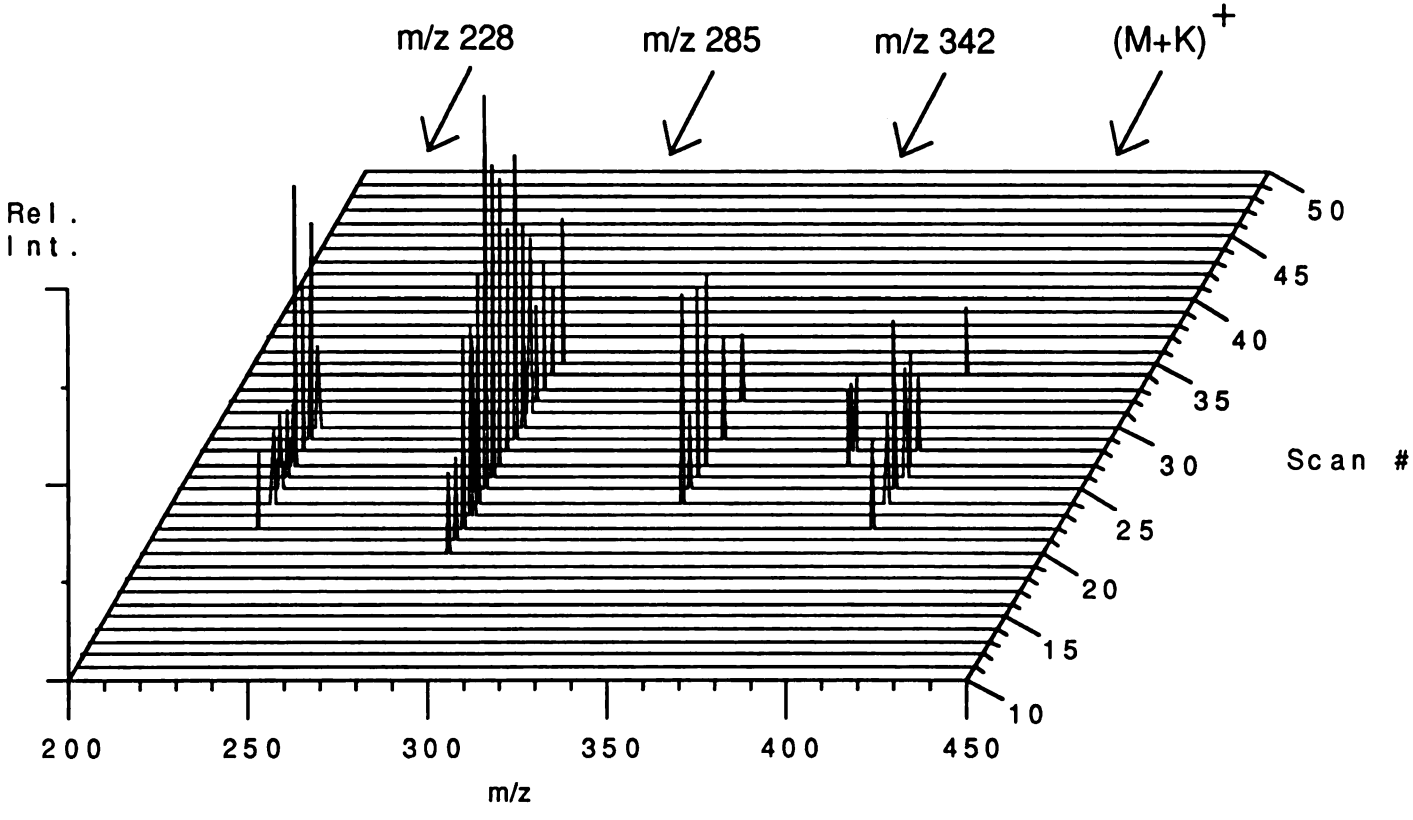

Figure 2.17. K^+ IDS mass spectrum of hexaglycine with the sample on the support wire only. I=3.0A
Sample desorption was first observed at scan 22. T(sample wire) = 150℃.

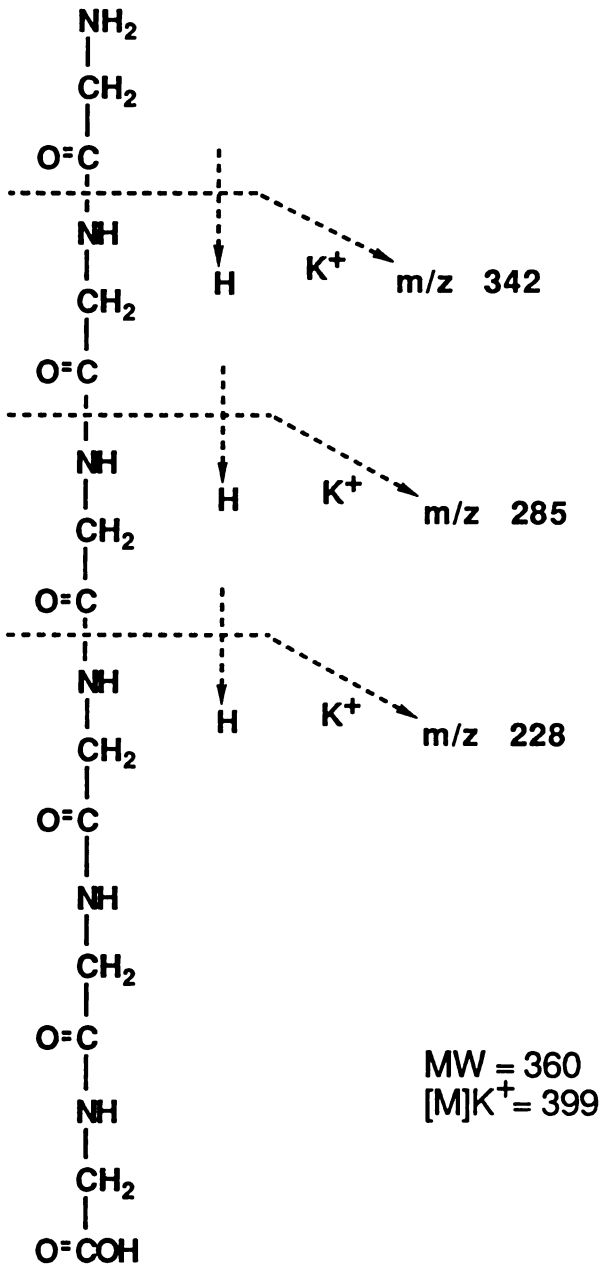

Figure 2.18 Structure of hexaglycine and the thermal degradations observed as K^+adduct ions.

delay time of four seconds occurs every time the computer redraws the mass axis at the bottom of the screen. During this four second delay, data are not being collected. This is a very serious problem for this project as the K^+IDS spectra are so short-lived and variable in nature that four seconds is a very large gap in data collection. Also, this lag time creates a problem when trying to calculate the time interval of sample desorption based on the scan number and, thus, time. This lag time was taken into consideration when calculating the temperatures of sample desorption discussed, but it still adds some uncertainty to the extrapolation.

C. REAL-TIME DETERMINATION OF SAMPLE DESORPTION TEMPERATURES.

1. EXPERIMENTAL DESIGN

The uncertainties in the temperature measurements described with the previous design led to the development of a simultaneous temperature and mass spectral data collection process. The ideal experiment would provide real time temperature measurement of the sample support surface while desorption via the K^+IDS technique is being monitored. In this case, collection of the K^+IDS mass spectrum is made simultaneously with collection of the temperature vs. time plots of the sample wire filament. The thermocouple is designed to be the sample support filament. Chromel and alumel wires 0.01 inch in diameter are threaded through the K^+IDS probe and spot-welded together at the tip to form the thermocouple junction for a Type K thermocouple. A small piece of two-holed ceramic is used at the tip to mimic the previous sample filament and provide the same heating characteristics. The thermocouple wires are obtained from OMEGA Engineering, Inc. with a teflon coating that provides electrical isolation of the wires through the length of the probe. The insulation has been removed at the tip where the wires are exposed so as not to interfere with the K^+IDS analysis. The sample is placed directly on the tip of the thermocouple and, therefore, the temperature of the surface can be measured directly as the sample desorbs from the surface. Apiezon Q sealing compound (Kurt J. Lesker, Inc., Clairton, PA) is used to create a temporary vacuum seal around the thermocouple leads at the back end of the probe. The thermocouple is connected to the same OMEGA DP-80 series monitor used in the previous studies. The output of the temperature

monitor is connected to a SOLTEC 1242 chart recorder to obtain a temperature versus time plot of the sample wire surface. There still exists some uncertainty with this design as the temperature is still extrapolated from the plot. However, the variable distance between the sample wire (thermocouple) and the K^+ bead is no longer a factor as the analyte surface temperature is monitored simultaneously with the collection of the K^+IDS mass spectra. Also, the mass spectral data are collected in the chromatographic display mode which is a constant data collection mode and do not suffer from the time lags previously mentioned for the real time spectral monitoring mode. Therefore, this experimental design should provide more accurate measurements of the surface temperature during sample desorption.

2. RESULTS

The goal of this experiment is to obtain a sample desorption profile in terms of the sample filament wire temperature in order to gain a better understanding of the temperatures needed to observe different thermal degradation products relative to the desorption of the intact molecule. K^+IDS provides a way of monitoring the production of these gas-phase degradation products and intact molecules by the production of K^+ adducts. The raw K^+IDS mass spectral data were correlated with the temperature measurements obtained from the chart recorder plots, in the same manner as the previous experimental design, to create adduct ion abundance versus temperature plots. The plot in Figure 2.19 shows the abundance of the molecular adduct ion (the $[M]K^+$ ion is represented by a peak at m/z 381) as a function of surface temperature for the K^+IDS analysis of sucrose. Each data point represents one mass spectral scan collected during the experiment. These data were obtained with a scan speed of 0.5 sec/scan over a mass range of 134-634 daltons. The erratic signal is characteristic of the results of these experiments. Some possible explanations for the origin of this adduct ion fluctuation are that the K^+ ion signal is fluctuating, the desorption of the neutral species is fluctuating, or there is some instrumental problem. A thorough cleaning of the entire instrument and repairs of weak electrical connections resulted in a decrease in these fluctuations, but not their complete elimination. The overall profile of Figure 2.19 resembles a Gaussian peak with observance of the $[M]K^+$ ion of sucrose being observed when the sample filament is between 225-365°C.

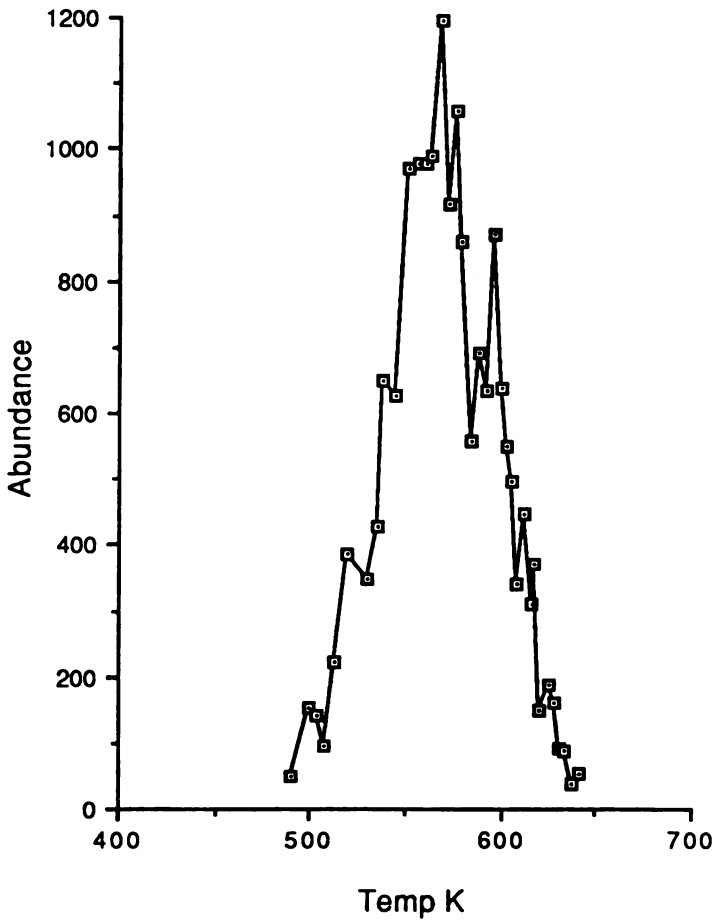

Figure 2.19 Abundance of the $[M]K^+$ ion of sucrose vs. Temperature (K) of the sample filament wire.

Another example of the abundance of the sample K^+ adduct ions versus temperature of the sample support wire is shown in Figure 2.20 for the K^+IDS analysis of melezitose. The relative abundance of the $[M]K^+$ ion (m/z 543) and the K^+ adduct ions of the most abundant thermal degradation products (m/z 363, m/z 201, and m/z 183) are plotted versus the temperature of the sample wire filament. The structure of melezitose and the origin of the fragment ions observed in the K^+IDS mass spectrum are shown in Figure 2.21. There is a slight variation in the temperatures at which the maximum abundance of these adduct ions are observed. A better comparison may be the differences in the overall adduct ion profiles as opposed to comparisons of the temperatures of maximum abundance. The adduct ion profile of the $[M]K^+$ ion of m/z 543 is slightly shifted to the right on the temperature axis with respect to the other K^+ adduct ion profiles of the degradation products. This shift is not substantial enough to suggest any major differences in the formation of these different K^+ adduct ions. Repetitive experiments with melezitose were performed and the plots of adduct ion abundance vs. sample filament temperature are provided in Appendix A. It has proven more difficult than expected to adjust the heating conditions to produce a K^+IDS experiment where the mass spectra are changing with time and analyte temperature. The main adjustments to the probe tip made in an attempt to change the heating rate of the analyte included changing the spacing between the two filaments and the amount of ceramic post present on both the emitter and sample filament. Reducing the amount of ceramic post on the sample wire filament seems to be a better way of increasing the heating rate than decreasing the amount of ceramic post on the K^+ emitter. Both of these changes would increase the heating rate of the sample, but the latter would result in bare wire on the K^+ emitter that typically results in mass spectra that contain more noise due to more chances of surface ionization and electron ionization.

Compounds with multiple functional groups are likely candidates for observing variations in the K^+IDS mass spectra within a single experiment as these compounds have many possible fragmentation sites. Methionine-enkephalin and leucine-enkephalin are pentapeptides that were studied with the hope of observing some variations in the K^+IDS mass spectra with time (sample wire temperature). Plots of the abundance versus temperature for the most abundant fragment ions, observed as K^+ adduct ions, of these peptides are provided in Appendix A. The desorption ion profiles of these fragment ions as

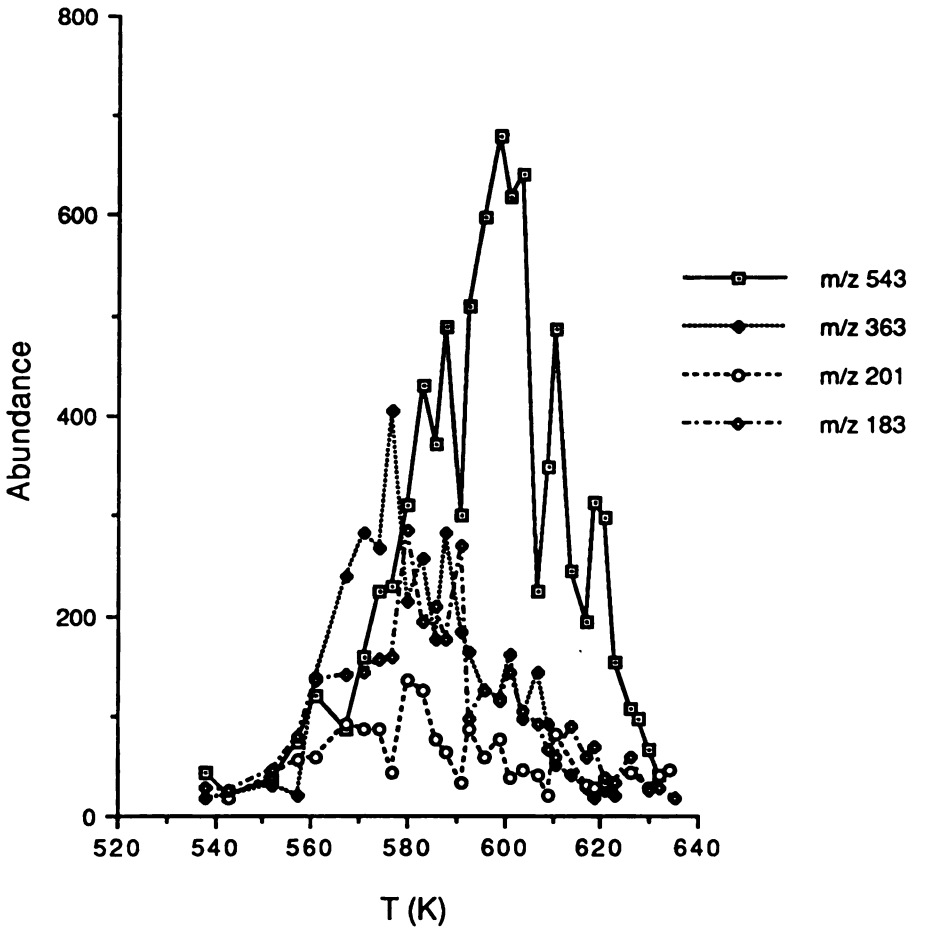

Figure 2.20 Abundance of the $[M]K^+$ ion and K^+ adduct ions of thermal degradation products of melezitose vs. temperature (K).

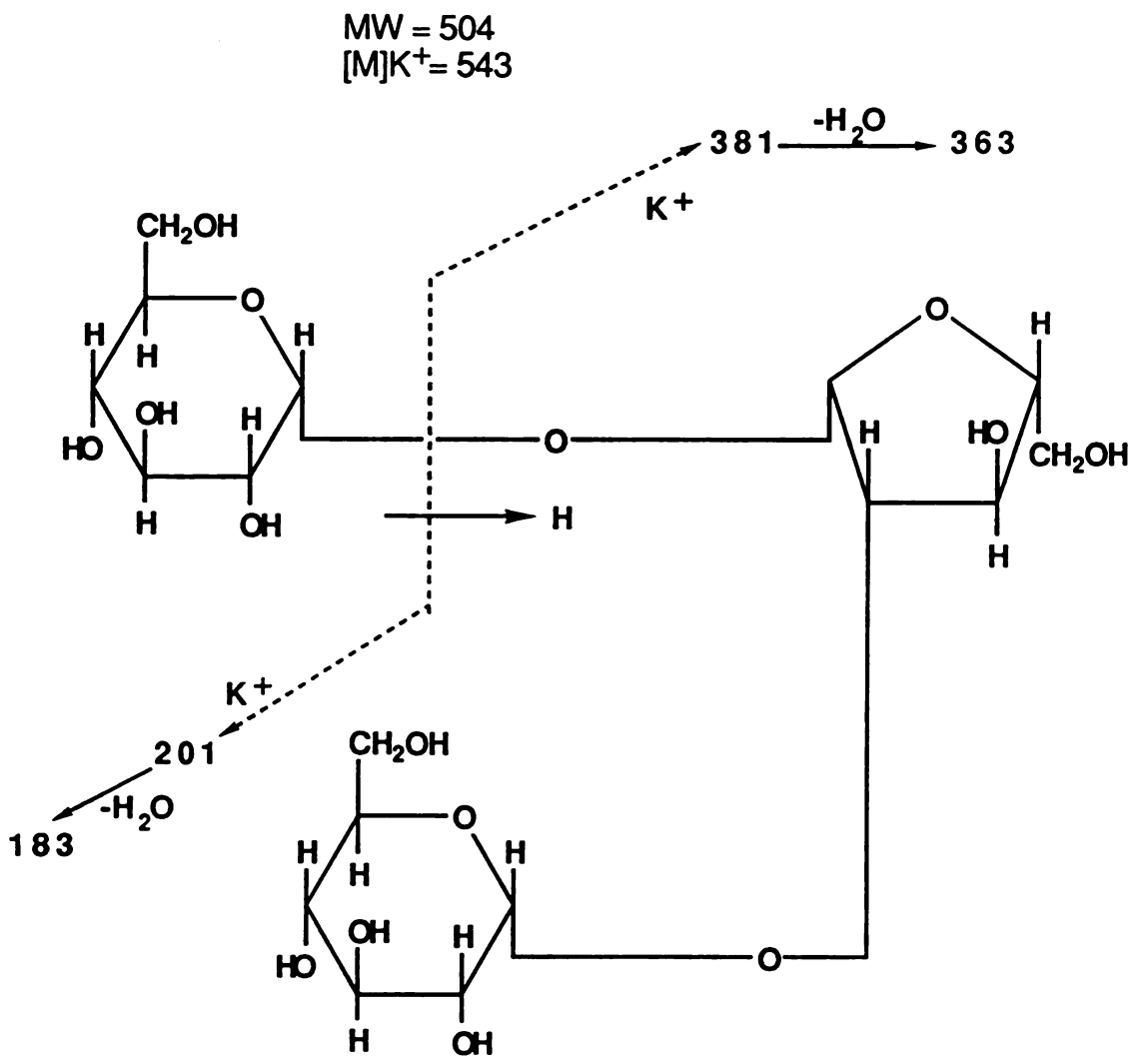

Figure 2.21 Structure of melezitose and the thermal degradation products that are observed as K^+ adducts.

a function of temperature overlapped substantially with no trend observed as to the order of desorption of the different thermal degradation product ions. The same is true for digoxin, which is a cardiac glycoside that is analyzed and discussed in detail later. There is little difference in the sample wire temperature when the fragment adduct ions of digoxin and the K^+ adduct ion of the intact molecule are observed. Shown in Figure 2.22 is the plot of the abundance of the K^+ adduct ions of the intact molecule (represented by a peak at m/z 819) and the thermal degradation products of digoxin (represented by peaks at m/z 169, m/z 299, m/z 429, m/z 559, and m/z 689) versus the temperature of the sample filament. The overlap of all these K^+ adduct ion profiles suggests that this experiment was performed near the crossover temperature where the rates of degradation are similar to the rate of desorption of the intact molecule.

Even though these within-run variations have proven difficult to reproduce, there does seem to be some temperature differences between the desorption of the intact molecule of different compounds. For example, Figure 2.23 contains the abundance of the molecular adduct ions, $[M]K^+$, versus surface temperature plots for sucrose (m/z 381) and melezitose (m/z 543) obtained when the analytes were codeposited onto the sample wire filament. As expected from the previous plots, observance of the K^+ adduct ions of intact sucrose molecules begins prior to observance of the K^+ adduct ions of intact melezitose molecules. The peak shapes of these K^+ adduct ion profiles of the intact analyte molecules resemble Gaussian shaped peaks that are shifted with analyte filament temperature. This shift can be used to indicate the relative thermal lability of the analytes. Instead of focusing on variations in the appearance of different K^+ adduct ions from one compound as a function of sample filament temperature, it may prove more beneficial to consider the appearance of $[M]K^+$ ions of different compounds as a function of temperature. A nonequimolar three-component mixture of palmitic acid, sucrose, and melezitose was analyzed by K^+IDS while monitoring the sample wire temperature. Three distinct $[M]K^+$ adduct ion profiles are obtained with this mixture for the three different components. The abundance vs. temperature plot for the $[M]K^+$ ion of each component is shown in Figure 2.24. The molecular adduct ion profiles shift to the right along the temperature axis with an increase in molecular weight of the analyte. This same trend was observed by Williams, et. al, when they calculated activation energies for the

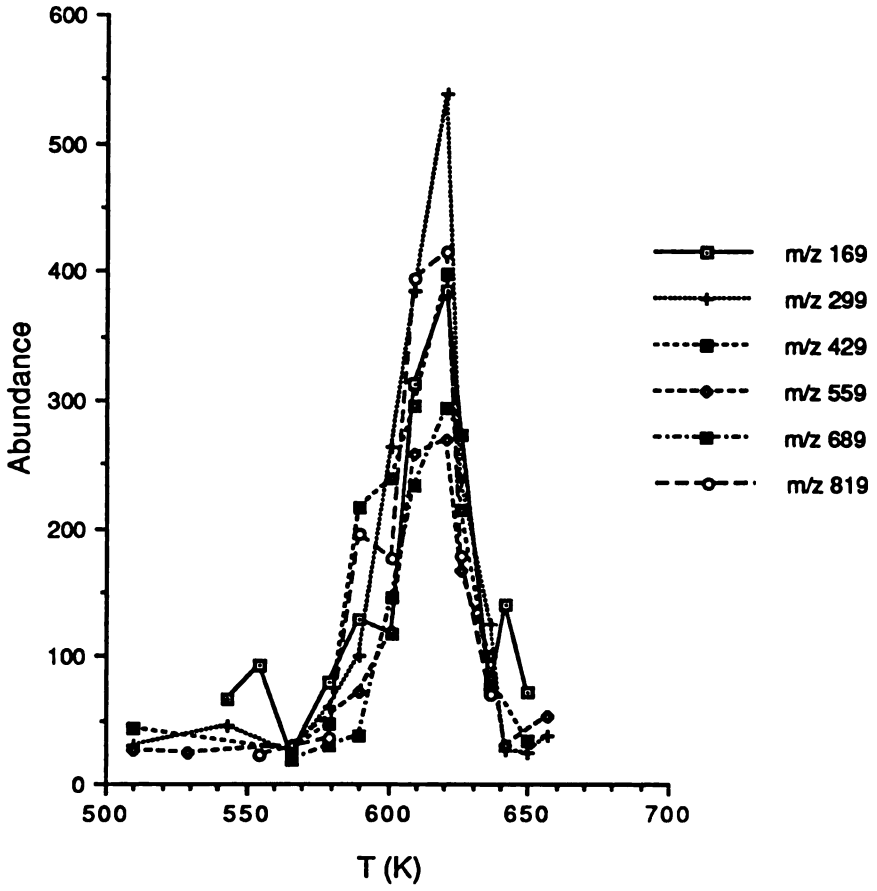

Figure 2.22 Abundance of the K^+ adduct ions of digoxin vs. sample filament wire temperature (K).

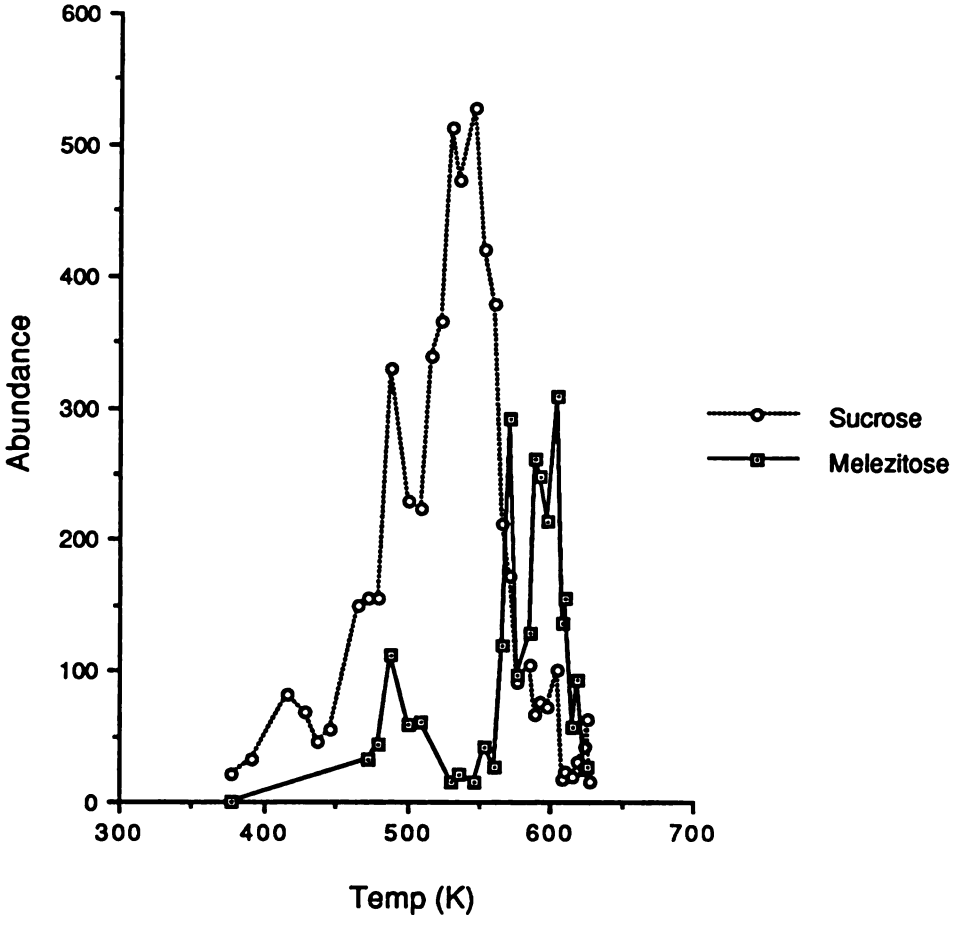

Figure 2.23 Abundance of the $[M]K^+$ ions of sucrose and melezitose vs. temperature (K) of the sample filament wire.

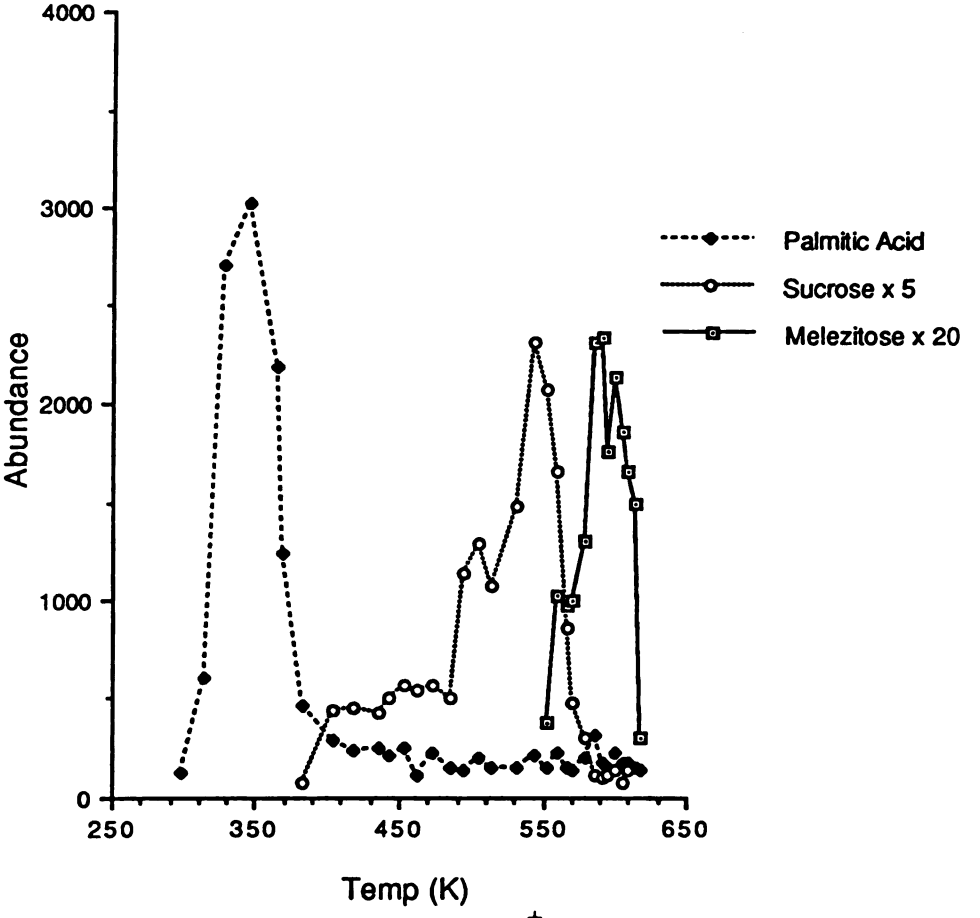

Figure 2.24 Abundance of the $[M]K^+$ ions of palmitic acid, sucrose, and melezitose vs. temperature (K) of the sample filament wire.

volatilization of a series of N-acetyl-L-alanyl methyl esters and noted a regular increase in activation energy with molecular weight.[40] The appearance of $[M]K^+$ ions as a function of temperature did follow this trend that an increase in molecular weight leads to higher temperatures required for desorption of the intact analyte. Additional plots of the abundance of the $[M]K^+$ and K^+ adduct ions of neutral thermal degradation products versus sample filament temperature for other compounds studied are provided in Appendix A for future reference.

D. ACTIVATION ENERGY DETERMINATIONS BASED ON K^+IDS ANALYSES

Activation energies for the processes leading to production of K^+ adduct ions of the intact molecule and neutral thermal degradation products can be determined from the log of the rate constant for producing these adduct ions as a function of the reciprocal of the absolute temperature of the sample filament. The rate of production of these K^+ adduct ions, or abundance, may be a good approximation for the rate constant of the volatilization of thermally labile compounds. Williams et al. determined activation energies for vaporization of thermally labile compounds by rapid heating and DCI using this approximation.[40] They assumed that the absolute abundance of the adduct ions was a function of the rate constant. Thus, by plotting abundance vs. 1/T, the activation energy was determined from the slope of the line of this Arrhenius plot. Activation energies, or heats of vaporization, for the desorption of the intact analyte molecule of palmitic acid and sucrose were determined by this method with the K^+IDS technique. Detection of the peaks representative of the $[M]K^+$ ions was used to monitor sample desorption. The plot of intensity of the peak representative of the $[M]K^+$ ion of sucrose versus 1/T is shown in Figure 2.25. It is assumed that at the maximum intensity, the sample is over half depleted. Therefore, the activation energy is calculated with the first half of the plot only, $1/T > 1.75 \times 10^{-3} K^{-1}$, when the amount of sample is not the limiting factor. From the slope of the best fit line, the activation energy, or heat of vaporization, of sucrose is calculated to be 13 kcal/mol. This is significantly lower than the activation energy for the formation of the $[M]NH_4^+$ ion of sucrose reported as 38.9 kcal/mol by Williams et al. obtained by rapid heating DCI.[40] This method of calculating the activation energy of vaporization does not take into account the competitive

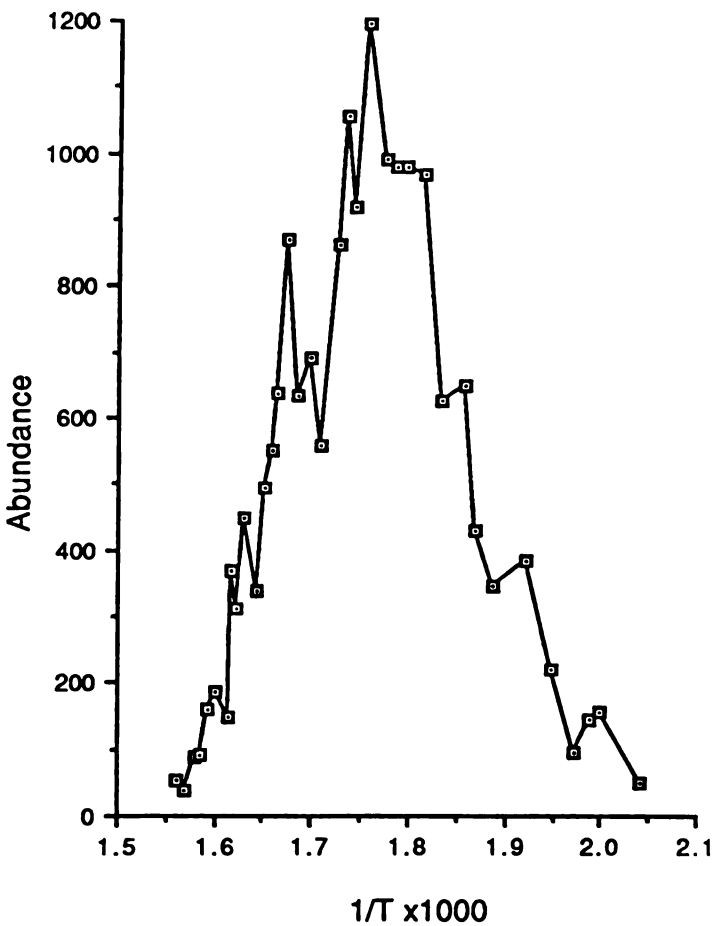

Figure 2.25 Abundance of the $[M]K^+$ ion of sucrose vs. 1/T (K). Ea calculated from the slope of the line of the first half of the experiment = 13 kcal/mol.

processes of thermal degradation of the sucrose molecule or the continual depletion of the sample with time. The more thermal degradation occurring, the less vaporization of the intact molecule can occur, both of which are also dependent on the amount of sample present on the sample wire. This could be the reason for the discrepancy in the heat of vaporization of sucrose calculated based on the K^+IDS technique compared to that calculated based on the DCI rapid heating experiment. The calculation of the activation energy for the desorption of palmitic acid, determined by the formation of $[M]K^+$ adduct ions, was performed with slightly better results. The plot of the intensity of the peak representing the $[M]K^+$ ion versus 1/T is shown in Figure 2.26. The slope of the first half of the experiment, when it is assumed that the sample supply is not the limiting factor, is used to calculate an activation energy of 23 kcal/mol. The literature value for the heat of vaporization of palmitic acid is 17.6 kcal/mol.[42] In this case, the compound does not undergo any thermal degradation and, therefore, essentially all of the sample can be desorbed intact and monitored by the production of $[M]K^+$ ions. No competing degradation reactions are present. This leads to a more accurate calculation of activation energy for the desorption process, based on the assumption that the formation of the $[M]K^+$ ion is a function of the rate of vaporization of palmitic acid. Other plots of abundance vs. 1/T, and the activation energy determinations for additional compounds are provided in Appendix A for future reference.

The formation of K^+ adduct ions depends on several factors that may not allow for this simplified analysis. The availability of K^+ ions, the amount of sample present, the competitive thermal degradation reactions, and the desorption processes all affect the production of K^+ adducts. A few of these possible reactions are shown below in equations 2.6-2.10 where M is the intact molecule in the solid phase (s) or the gas phase (g), and D is a neutral product of thermal degradation in the condensed phase (s) or the gas phase (g). Reaction 2.6 is the desorption of the intact analyte molecule into the gas phase. This reaction has a rate constant associated with it and the activation energy for this process is the heat of vaporization of the analyte, M. There is also a rate constant for the formation of the K^+ adduct ion of this gas-phase neutral through reaction 2.7. This reaction is assumed to be rapid once the analyte molecule is present in the gas phase and is not considered the rate-limiting step. The other option for the analyte species present on the surface is thermal degradation, represented by reaction 2.8. There is a rate constant

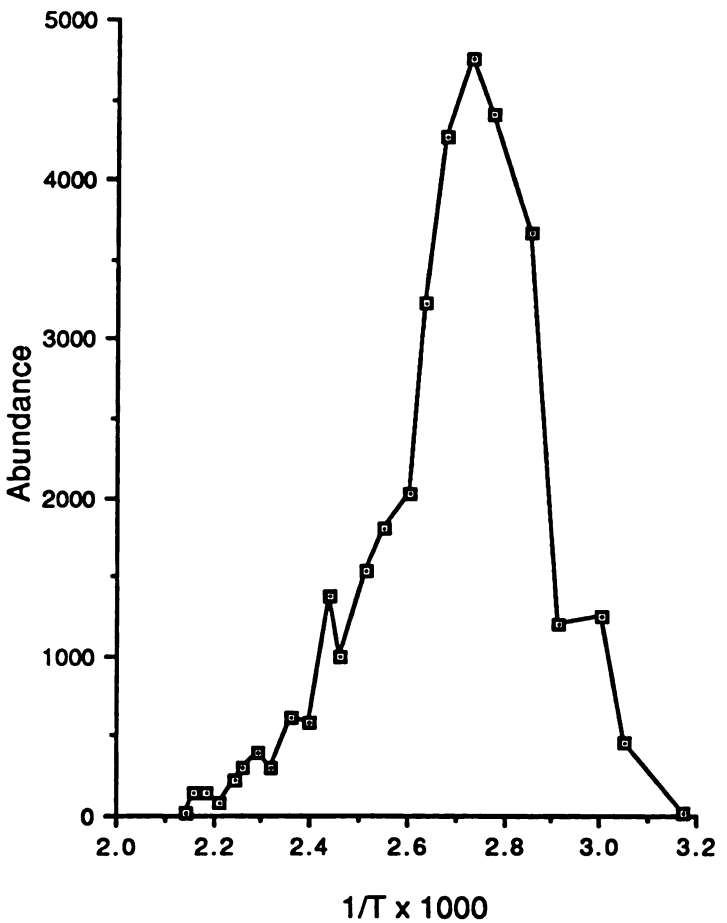

Figure 2.26 Abundance of the $[M]K^+$ ion of palmitic acid vs. 1/T (K). Ea calculated from the slope for 1/T > 2.7 = 23 kcal/mol.

$$M_s \rightarrow M_g \qquad 2.6$$

$$M_g + K^+ \rightarrow MK^+ \qquad 2.7$$

$$M_s \rightarrow D_s \qquad 2.8$$

$$D_s \rightarrow D_g \qquad 2.9$$

$$D_g + K^+ \rightarrow DK^+ \qquad 2.10$$

associated with each degradation process. The vaporization of these degradation products each have a corresponding rate constant. Again, it is assumed that the K^+ adduct formation of these gas phase species, reaction 2.10, is not the rate-limiting reaction in the formation of $[D]K^+$. It is unclear whether the degradation process or the vaporization of the degradation products is the rate limiting step in observing the K^+ adduct ions of these products. Therefore, the activation energies for the formation of the gas phase degradation products could be dependent on either the degradation process or the vaporization process.

The most important factor in the production of K^+ adduct ions of the intact analyte molecule and thermal degradation products may be the finite sample supply on the sample filament. If first order kinetics is assumed for the depletion of sample with time, the following derivation may apply. A_0 is the total amount of sample initially applied to the filament (t=0) and A_t is the remaining amount of sample at time t. This analysis is for neutral species and the processes involved in the thermally induced conversion from the condensed phase to the gas phase. K^+IDS is a very useful technique in these analyses as the abundance of K^+ adducts, $[M]K^+$ and $[D]K^+$, reflect the abundance of the species M and D in the gas phase and thus provides a means of monitoring the vaporization of the analyte. From this derivation, the activation energy can be calculated from the slope of the plot of $\ln(\ln(A_0/A_t)$ versus 1/T. This assumes that ln(t) is negligible as a variable due to the short reaction time of the K^+IDS experiment (less than one minute). The difficulty with this derivation is in determining the amount of sample remaining as the analysis proceeds. This is especially true when the sample undergoes much thermal degradation and, thus, many pathways of sample depletion are

$$\frac{A_t}{A_o} = \exp(-t\,k) \qquad 2.11$$

which is equivalent to:

$$k = \frac{1}{t}\ln\left(\frac{A_o}{A_t}\right) \qquad 2.12$$

$$k = A\exp\left(-\frac{E_a}{RT}\right) \quad \text{Arrhenius equation} \qquad 2.4$$

$$\frac{1}{t}\ln\left(\frac{A_o}{A_t}\right) = A\exp\left(-\frac{E_a}{RT}\right) \qquad 2.13$$

$$\ln\left(\frac{1}{t}\right) + \ln\left(\ln\left(\frac{A_o}{A_t}\right)\right) = \ln A - \left(\frac{E_a}{RT}\right) \qquad 2.14$$

$$\ln\left(\ln\left(\frac{A_o}{A_t}\right)\right) = -\left(\frac{E_a}{R}\right)\frac{1}{T} + (\ln A + \ln t) \qquad 2.15$$

present. A simple compound that does not decompose during the K^+IDS analysis is a good starting point for these activation energy determinations. One such compound is palmitic acid which has a K^+IDS mass spectrum with only one ion, the $[M]K^+$ ion at m/z 295, indicating that the sample does not decompose when rapidly heated. This simplifies the determination of the ratio of A_o/A_t. Assuming complete vaporization of the sample, A_o is calculated as the sum of the abundance of the $[M]K^+$ ion for the entire experiment. A_t, the amount of sample left at time t, is calculated by the total $[M]K^+$ ion observed during the experiment, A_o, minus the sum of the $[M]K^+$ ion observed until time t. The plot of $\ln(\ln(A_o/A_t))$ versus 1/T for palmitic acid is shown in Figure 2.27. This data are from the same experiment as was used for the plot in Figure 2.26. The slope of the plot from the best fit line of the entire data set in Figure 2.27 is used to calculate an activation energy of 15 kcal/mol. The plot seems to have two regions, or two slopes. If the activation energy is calculated based only on the first half of the experiment ($1/T > 0.0027$), it would have a value of 25 kcal/mol. The activation energy calculated from the second half of the experiment ($1/T < 0.0027$) is 5 kcal/mol. The overall activation energy calculated as 15 kcal/mol is closest to the literature value of 17.6 kcal/mol.[42] Since this method of calculation takes into account the depletion of the sample

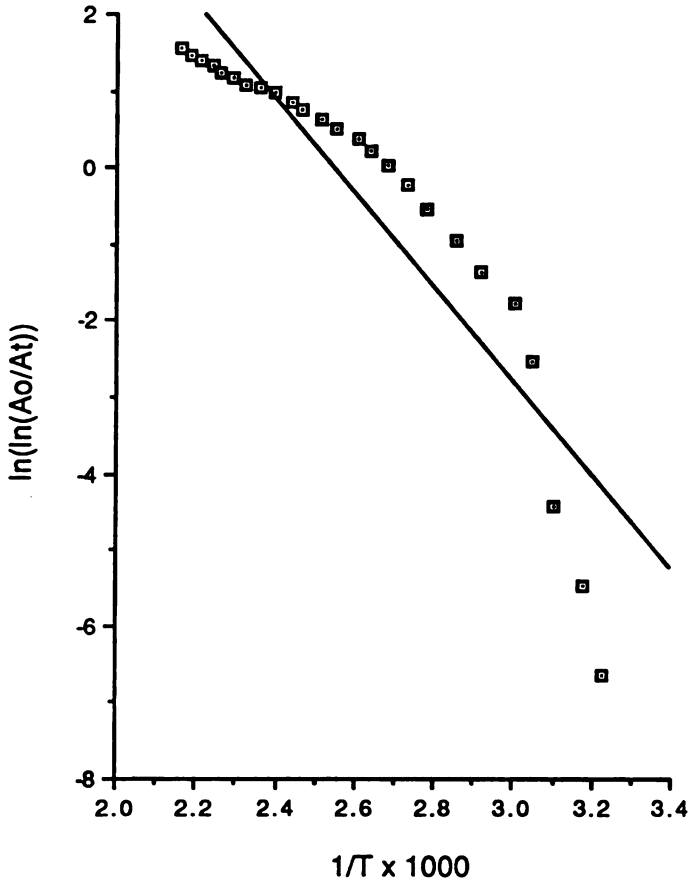

Figure 2.27 Arrhenius plot of ln(ln(Ao/At)) vs. 1/T for palmitic acid. Ea calculated from the slope = 12 kcal/mol.

with time, the entire plot should be representative of the activation energy and should be used in the calculation. Duplicate activation energy determinations for the vaporization of palmitic acid based on other K^+IDS experimental results are presented in Appendix A.

This method of activation energy determination may be applied to sucrose. In this case, the analyte does undergo thermal degradation which complicates the calculations. Initially, these thermal degradation products are ignored and A_o is calculated as the sum of the abundance of only the $[M]K^+$ ion of sucrose observed over the entire experiment. The A_t is calculated the same way as for palmitic acid, as if no analyte decomposition is occurring. The plot of $\ln(\ln(A_o/A_t))$ vs. $1/T$ for sucrose is shown in Figure 2.28. The data points are more linear than for the plots of the palmitic acid data. It appears that these assumptions for the calculation of A_o are valid based on the appearance of the plot. The activation energy is calculated as 28 kcal/mol which is close to the reported experimental activation energy of 38.9 kcal/mol for the vaporization of sucrose and formation of the NH_4^+ adduct ion.[40] These preliminary results of activation energy determinations lend some validity to the proposed method of analysis. The calculated activation energies are the same order of magnitude as reported values.[40,42] More replicate determinations of activation energies need to be performed in order to determine the reproducibility and validity of these results.

Methionine-enkephalin (met-enkephalin) is a pentapeptide that experiences much thermal degradation during a K^+IDS analysis. The structure of this peptide is shown in Figure 2.29. The fragmentation pathways that produce the most abundant thermal degradation products as observed by K^+ adduct formation are labeled in Figure 2.29. The $[M]K^+$ ion of this peptide is not observed as an abundant adduct ion in the K^+IDS mass spectrum. Therefore, only the activation energies for the production of the gas phase thermal degradation products that are observed as the most intense peaks representative of K^+ adduct ions can be calculated. Again, these activation energies could either be for the thermal degradation of the analyte or the vaporization of these thermal degradation products, whichever is the limiting step in being observed as K^+ adduct ions. The simplest approach would be to assume there is no interdependence of the thermal degradation processes and that each adduct ion can be considered independently. If this is pursued, then A_o and A_t can be determined for each adduct ion. The results of such

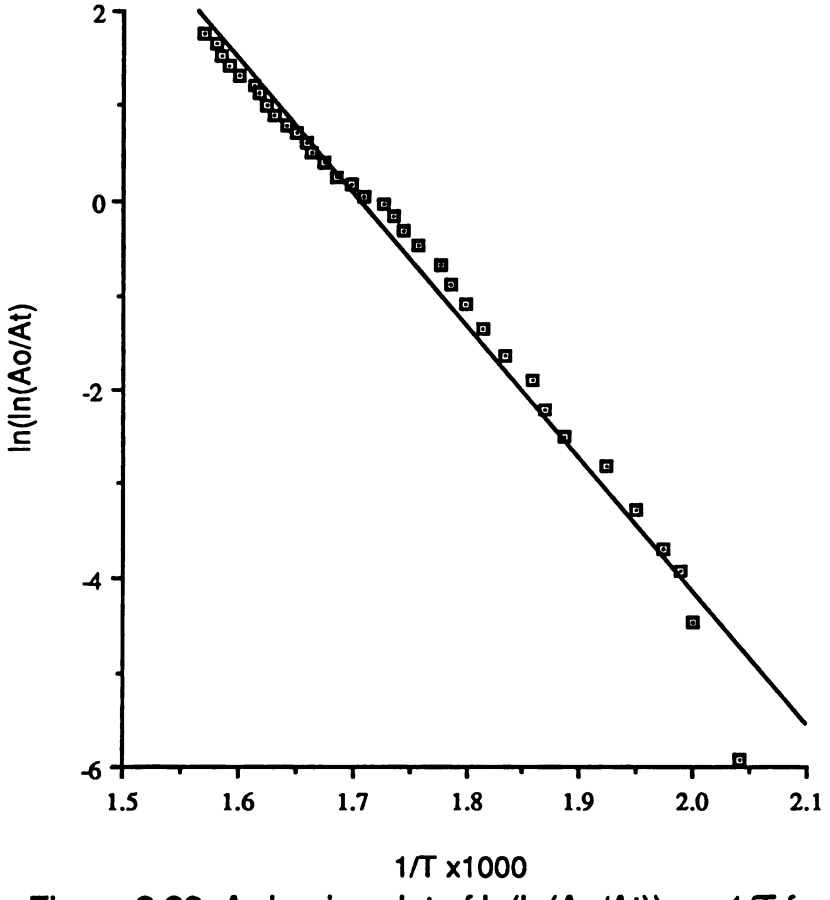

Figure 2.28 Arrhenius plot of ln(ln(Ao/At)) vs. 1/T for the $[M]K^+$ ion of sucrose. Ea calculated = 28 kcal/mol.

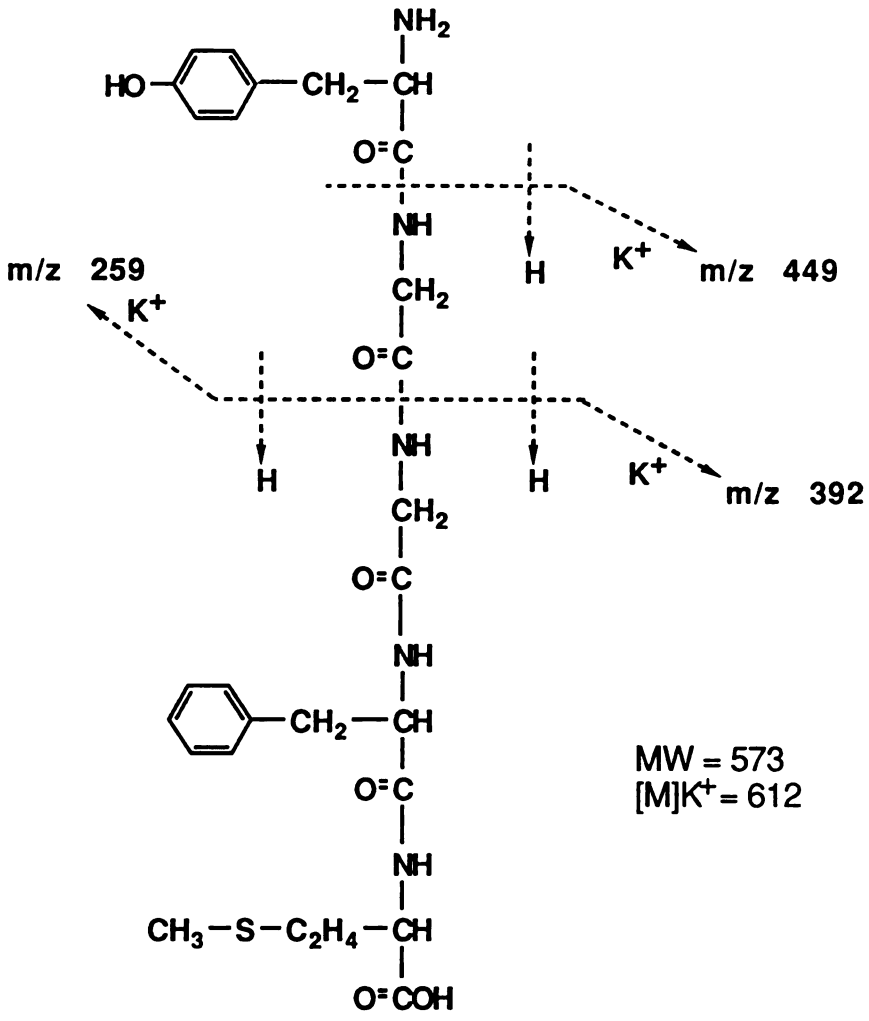

Figure 2.29 Structure of methionine-enkephalin and the thermal degradations observed as K^+ adduct ions.

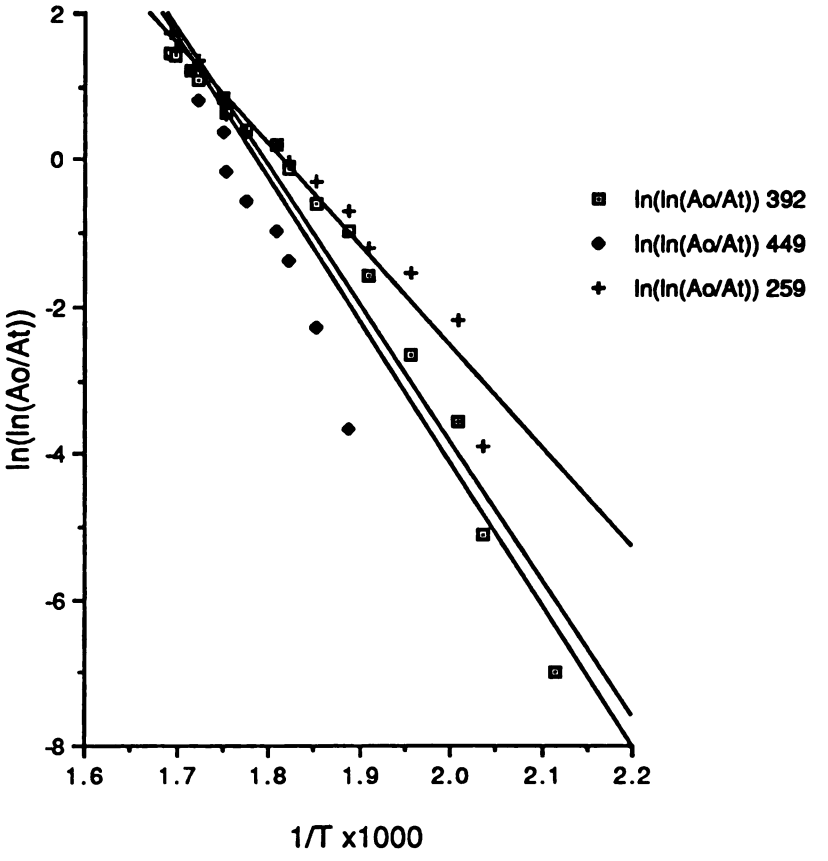

Figure 2.30 Arrhenius plot of ln(ln(Ao/At)) vs. 1/T for three fragment K^+ adduct ions of met-enkephalin.
Ea (259) = 27 kcal/mol, Ea (392) = 37 kcal/mol,
Ea (449) = 52 kcal/mol.

calculations are plotted in Figure 2.30 for K^+ adduct ions of three thermal degradation products. As expected, the activation energy for the production of gas phase thermal degradation products of met-enkephalin does increase with molecular weight of the decomposition product. The values of the activation energies calculated for these processes do seem to be reasonable based on the previous activation energy determinations for vaporization of thermally labile compounds. However, repetitive experiments of met-enkephalin indicate that these values are not reproducible within experimental errors. Additional Arrhenius plots of K^+IDS experiments are provided in Appendix A. The data from one experiment were used to calculate the activation energy for the formation of one of the fragment K^+ adduct ions (observed as a peak at m/z 259) as being 4 kcal/mol. This value is much below the experimentally acceptable deviation and points to a possible problem in the method of calculation. The assumptions used for these calculations, mainly that the thermal degradation processes are independent of each other, are probably over simplifications of the processes involved in the K^+IDS technique. This does, however, provide a starting point for the determination of activation energies based on K^+IDS experimental data. These preliminary results indicate that these determinations are possible with the K^+IDS technique, and that further studies and modifications are needed.

4. SUMMARY

Continuation of the temperature studies would benefit from further alterations in the experimental design. First of all, the computerization of the temperature measurement would be a significant improvement. The output of the OMEGA temperature monitor could either be connected to a separate computer or directly to the HP computer of the instrument for a digital readout of the temperature versus time. Ideally, the temperature measurement would be synchronized with the scanning of the mass spectrometer which would eliminate many of the sources of error currently present. This would allow for more accurate temperature determinations at specific times instead of the current manual measurement of the chart recorder temperature plots.

Another aspect of this study which needs further testing is the variable adduct ion signal that plagued many of the preliminary results obtained. A more detailed examination of this problem may lead to ways to reduce some of

this signal ion fluctuation. Possible sources of this varying signal are the K^+ emitter and the production of K^+ ions. In the past, this K^+ signal was relatively constant and very strong. However, when the sample adduct ion fluctuation was troublesome, the K^+ signal also appeared to fluctuate more than usual. If the source of K^+ ions fluctuated it would follow that the K^+ adduct ion production and signal would also fluctuate. Whether this K^+ variation was the result of the probe construction or the performance of the instrument is unclear.

One way to avoid this fluctuating signal may be to use selected ion monitoring (SIM) to monitor the production of just the $[M]K^+$ ion and one or two thermal degradation products. This data collection mode allows for more signal averaging and faster scanning capabilities than the full mass range scanning procedure typically used. However, one disadvantage to this mode, is the limited number of adduct ions that can be observed simultaneously. This would inhibit the ability to observe within run variations in the production of different adduct ions at different temperatures and times. The main advantage to using SIM is the increased data collection that could be obtained over the desorption profile of the sample. Since the K^+IDS experiment is typically very fast with analyte ion signals lasting less than one minute, this higher sampling rate could greatly improve the results of determining the temperatures at which desorption and thermal degradation processes of thermally labile compounds occur.

CHAPTER 3. APPLICATIONS OF THE K^+IDS TECHNIQUE

1. INTRODUCTION

Previous researchers have applied the K^+IDS technique to a wide variety of compounds. Bombick showed the utility of K^+IDS for the analysis of saccharides, peptides, steroids, antibiotics, and some salts. The K^+IDS technique also has proven to be very effective for the analysis of polymers in determining the average molecular weight, oligomer distribution, and impurities present.[43] Kassel extended the applicability of Na^+IDS to the determination of organic acids in complex mixtures and metabolic profiling.[44] (Na^+IDS is the same as K^+IDS except Na_2O is used in the aluminosilicate mixture instead of K_2O and, therefore, thermally produces Na^+ ions. Na^+IDS seems to be more sensitive for some compounds including the organic acids and induces more fragmentation than K^+ attachment does in other types of compounds). A procedure was developed based on the Na^+IDS technique for the rapid screening of urine samples for the detection of organic acidemias. These are physiological disease states caused by errors in certain metabolic pathways that can be characterized by elevated concentrations of one or more organic acids in the body's plasma or urine. Na^+IDS provided a simple, quick method for analyzing urine samples for these diseases.[44] Even in these early stages of development, the K^+IDS/Na^+IDS technique has proven to be a very useful DI technique for a wide variety of compounds.

2. K^+IDS MASS SPECTROMETRIC ANALYSIS OF CARDIAC GLYCOSIDES

DI techniques, in general, have been applied to a wide range of thermally labile compounds especially in the field of biochemistry where most compounds of interest contain a large number of functional groups and are considered thermally labile. One group of compounds that has received much attention in the DI field is the cardiac glycosides. These compounds contain a sugar portion and a steroid moiety. The cardiac glycosides are used as therapeutic agents for the treatment of congestive heart failure and certain heart arrythmias. These compounds have been studied by almost every mass spectrometric ionization technique.[45] FAB is the most widely used DI technique used to date for the analysis of thermally labile compounds.

Therefore, this technique will serve as a standard for comparison of the K^+IDS technique.

A reported FAB mass spectrum of digitonin is shown in Figure 3.1 and serves as a good example of the mass spectra obtained with FAB.[46] The structure of digitonin, which is a cardiac glycoside with a molecular weight of 1228 daltons, is shown in Figure 3.2 This mass spectrum is characteristic of the FAB technique with glycerol used as the matrix. In the molecular weight range, there are at least three peaks representative of the intact molecule; the $[M]H^+$ ion, the $[M]Na^+$ ion, and the $[M+glycerol]H^+$ ion. This multiple representation often complicates the molecular weight determination. Other protonated ions representative of the analyte from cleavages of the glycosidic bonds are observed in the middle mass range. The low-mass range is cluttered with many ions representative of the liquid matrix, glycerol. This makes it very difficult, if not impossible, to obtain information about the sample from this low-mass range of the mass spectrum. In summary, FAB mass spectra are often characterized by decreasing abundance of sample ions with increasing molecular weight (or m/z value), many fragment ions representative of the sample, protonated and glycerol adduct ions representative of the intact molecule, and a complicated low-mass region.

In contrast, the K^+IDS mass spectrum of digoxin is shown in Figure 3.3. Digoxin is a cardiac glycoside similar to digitonin with fewer sugar residues and, therefore, has a molecular weight (780 daltons) within the mass range of the quadrupole mass spectrometer used for K^+IDS. This mass spectrum is characteristic of K^+IDS mass spectra in that the peak representing the $[M]K^+$ ion is the most intense peak in the mass spectrum and the majority of the peaks observed represent the K^+ adduct ions of the intact molecule and neutral thermal degradation products of the analyte. The fragmentations are simple 1,2-eliminations about the glycosidic bonds. The mass spectrum is representative of the sample with no interference from addition of a solvent or liquid matrix. This comparison of FAB and K^+IDS for the analysis of cardiac glycosides shows the utility of the K^+IDS technique for the analysis of thermally labile compounds and some of its advantages over the FAB technique. This does not mean that it is expected for K^+IDS to replace FAB, but rather that the K^+IDS technique does have some advantages to offer for the analysis of thermally labile compounds. K^+IDS is a simple technique that produces relatively simple mass spectra that are representative of the sample.

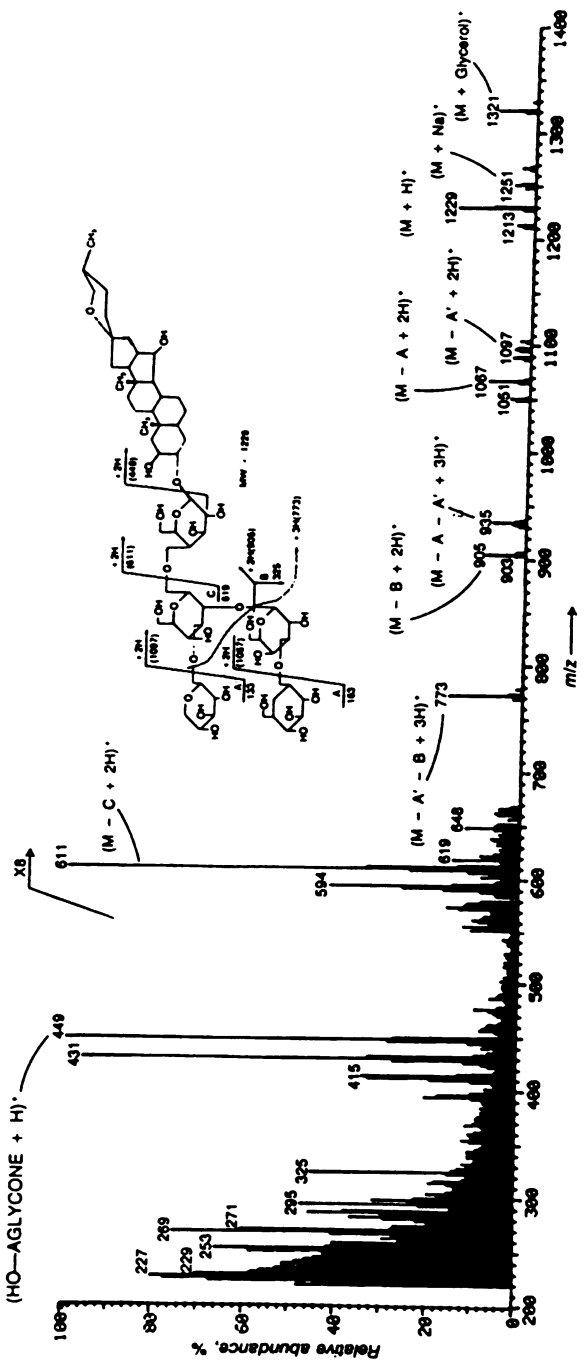

Figure 3.1 Published fast atom bombardment mass spectrum of digitonin.[45]

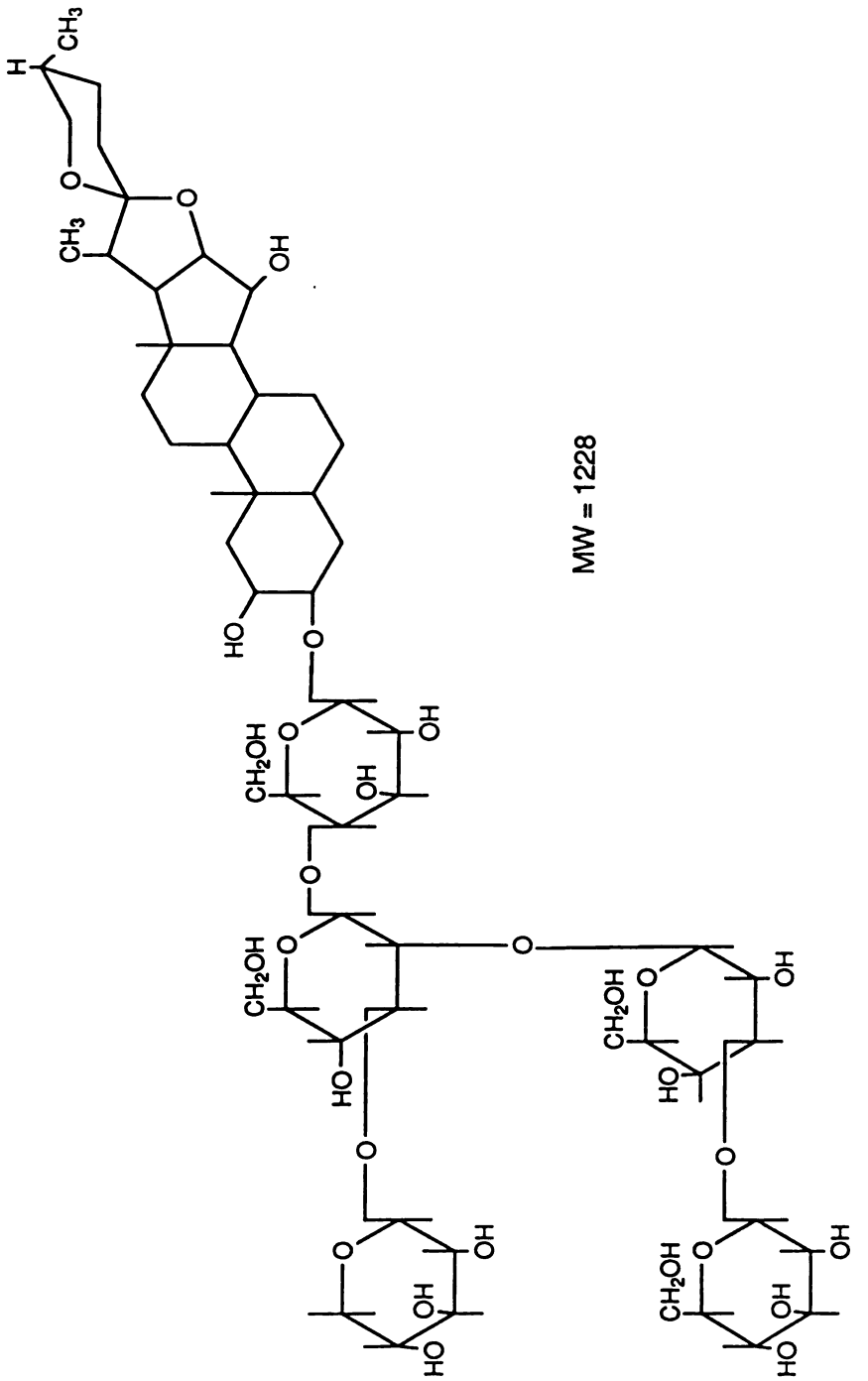

Figure 3.2 Structure of digitonin.

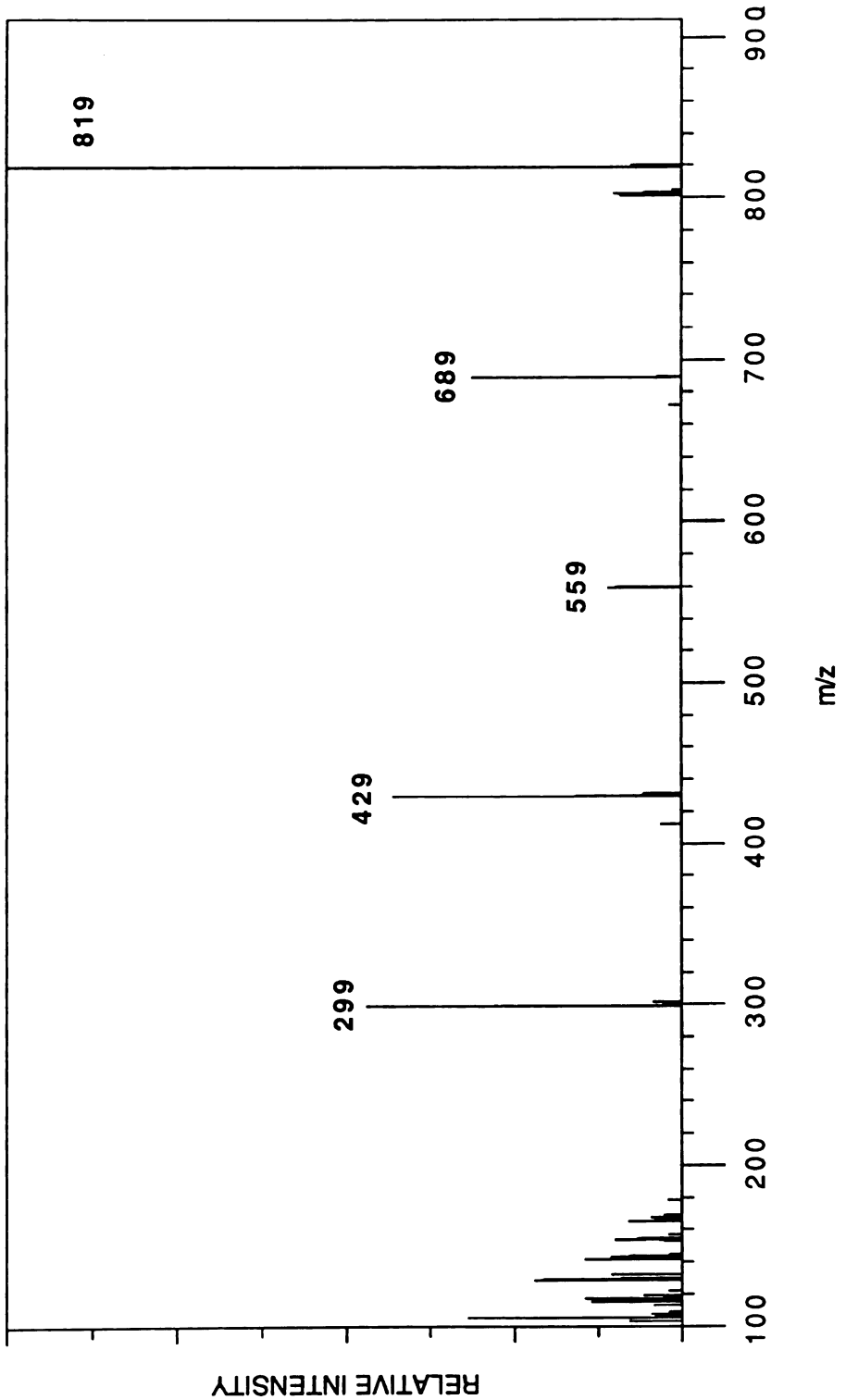

Figure 3.3 K^+IDS mass spectrum of digoxin.

The K^+IDS mass spectra are easy to interpret based on one mechanism of fragmentation, the 1,2-elimination mechanism.

Due to these encouraging preliminary results, K^+IDS was used to analyze several cardiac glycosides to allow for the evaluation of K^+IDS in the context of other DI techniques. The results of the K^+IDS mass spectrometric analysis of the cardiac glycosides have been published and this article is provided in Appendix B. The results of this study show the strengths of K^+IDS for the analysis of the cardiac glycosides and related compounds. The mass spectra are clean and only contain K^+ adduct ions representative of the sample. The base peak in the mass spectrum represents the $[M]K^+$ ion which provides molecular weight information. Also, thermal degradation products, primarily from fragmentation of the glycosidic bonds between the sugars, are observed as K^+ adduct ions. These ions provide structural information. All of the fragmentations observed can be explained by the 1,2-elimination mechanism (see Figure 2.2). Therefore, another useful application of the K^+IDS technique to these cardiac glycosides has been established.

3. UTILITY OF THE K^+IDS TECHNIQUE FOR MIXTURE ANALYSIS

One interesting aspect of the K^+IDS technique is the utility for mixture analysis. Bombick was able to accurately determine the average molecular weight of polymers that are composed of mixtures of oligomers.[43] Kassel successfully performed numerous studies utilizing Na^+IDS for analyzing the organic acids in urine samples with minimal sample preparation.[44] However, quantitative determinations of individual components within mixtures has proven difficult with the K^+IDS technique, as with other DI techniques. There seems to exist a mass dependence on the extent of desorption of free fatty acids. This is discussed in more detail elsewhere.[41] There are several characteristics of the K^+IDS technique that contribute to its applicability for mixture analysis. K^+ ions attach to neutral gas-phase species during the K^+IDS technique and do not induce any fragmentation. Therefore, K^+ adduct formation will not complicate the mass spectrum, but merely provide a good representation of the gas-phase neutral species representative of the sample. K^+IDS produces primarily $[M]K^+$ ions of most analyte species with some K^+ adduct ion formation of neutral thermal degradation products. Thus, the K^+IDS mass spectra of mixtures provide molecular weight information of the components.

Since the K^+IDS technique requires no matrix, the K^+IDS mass spectra of mixtures are less complex than the mass spectra obtained with other DI techniques, such as FAB, which do require liquid matrices. This simplifies the analysis of the K^+IDS mass spectra of mixtures.

The K^+IDS analysis of a mixture that contains different types of compounds also provides very encouraging results as to the utility of K^+IDS for mixture analysis. A mixture of fatty acids, low molecular weight organic acids, and steroids provides an interesting challenge. In order to analyze this mixture by more traditional EI or GC/MS analysis, several different sample preparation techniques and derivatizations would be necesary. An equimolar mixture of eight compounds representing these three groups was made and analyzed by Na^+IDS. This mixture contained three organic acids: salicylic acid (MW = 138), cinnamic acid (MW = 148) and mandelic acid (MW = 152); three saturated fatty acids: myristic acid (MW = 228), palmitic acid (MW = 256) and stearic acid (MW = 284); and two steroids: 5ß-pregnen-3ß-ol-20-one (MW = 316) and cholesterol (MW = 386). The Na^+IDS mass spectra of each of these eight compounds was obtained individually for identification of the components in the Na^+IDS mass spectrum of the mixture. All of the Na^+IDS mass spectra of the individual components, except for mandelic acid, represent only one abundant ion, the $[M]Na^+$ ion. The Na^+IDS mass spectrum of mandelic acid has a base peak (at m/z 157) corresponding to the $[M-H_2O]Na^+$ ion in addition to a strong peak at m/z 175 ($[M]Na^+$). One µliter of the equimolar mixture dissolved in methanol was applied to the sample support wire of the Na^+IDS probe and the solvent was evaporated. Approximately five µmoles of each component were present on the probe tip at the beginning of each analysis. The TIC mass chromatogram and the $[M]Na^+$ mass chromatograms of the eight components from the Na^+IDS mass spectrometric analysis of the mixture are shown in Figure 3.4. There is a considerable difference in the maximum abundance of each component as denoted on the chromatograms in Figure 3.4. For instance, the maximum abundance of the $[M]Na^+$ ion of myristic acid is labeled as 27,136, whereas the maximum abundance of the $[M]Na^+$ ion of cinnamic acid is 6,112. These differences could be the result of differences in the efficiency of desorption of the intact species and adduct ion formation. Another reason for these discrepancies in abundance is probably due to differences in the onset of desorption and the overlap of this process with the emission of Na^+ ions. This can be seen in the plot of the Na^+IDS mass spectra versus scan number of

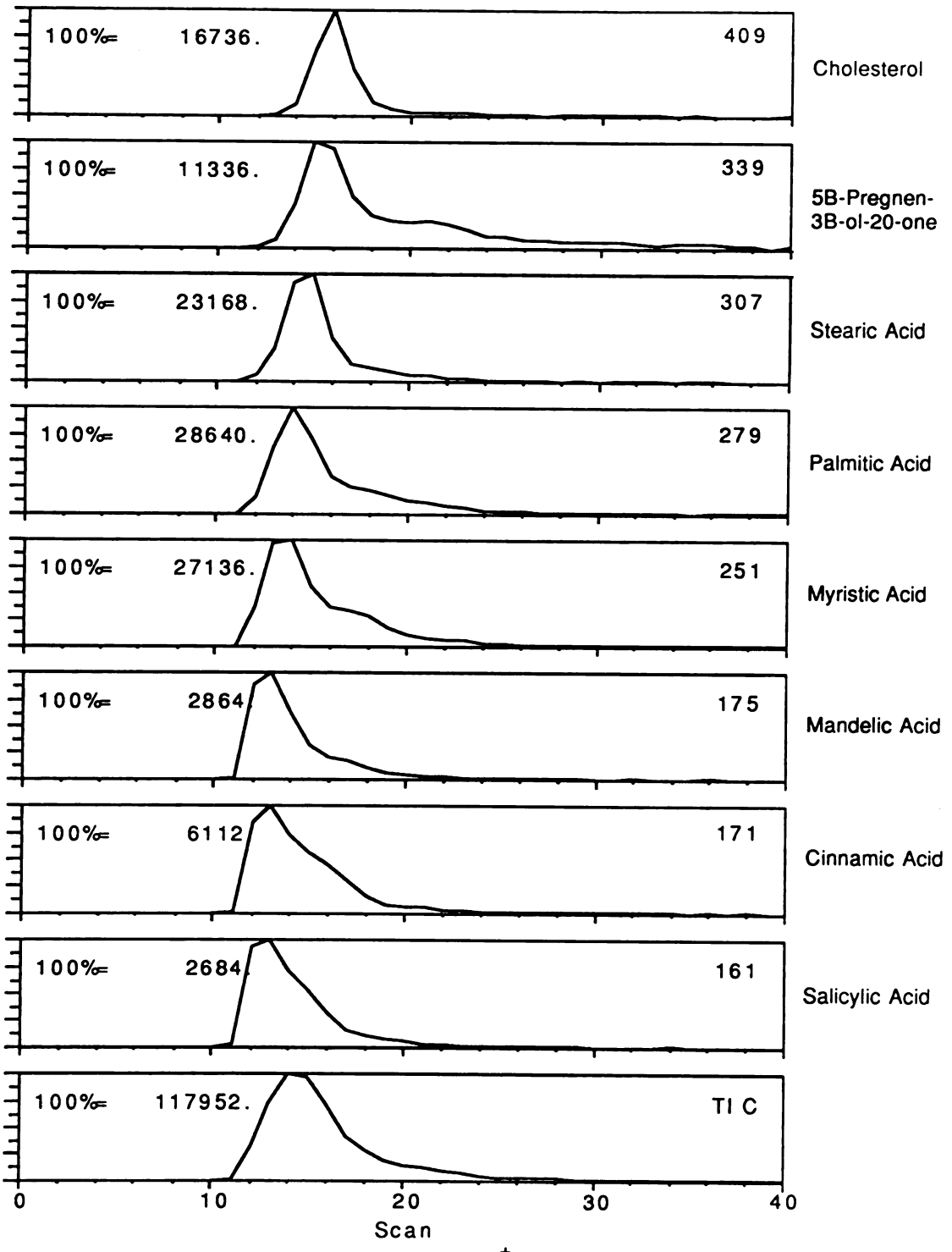

Figure 3.4 Mass chromatograms of the $[M]Na^+$ ions of the eight individual components present in the mixture.

this eight-component mixture shown in Figure 3.5. The x-axis is the m/z scale, the y-axis is scan number, and the z-axis is abundance. The low-mass ions are from the organic acids. Notice that these ions do not increase in abundance with scan number for the first few scans as is observed for all the other ions at higher m/z values. This suggests that the formation of these ions is limited by the production of Na^+ ions. The neutral molecules of these organic acids (salicylic, cinnamic, and mandelic acids) are probably desorbing before Na^+ ions are being produced from the Na^+ emitter. Therefore, when they are first observed, they are already at, or beyond, their maximum desorption. There is a slight delay in the observance of the $[M]Na^+$ adduct ions of the steroids of m/z 339 and 409 with respect to the observance of the fatty acids of lower m/z values. This is in agreement with the discussions presented in Chapter 2 that there is an increase in heat of vaporization with increasing molecular weight. Therefore, the lower molecular weight fatty acids desorb prior to the higher molecular weight steroids and are observed by their corresponding Na^+ adducts in the Na^+IDS mass spectrum before the $[M]Na^+$ adducts of the steroids. The Na^+IDS mass spectrum obtained from averaging scans 12-18 of this analysis of the mixture is shown in Figure 3.6. The $[M]Na^+$ adduct ions of the eight components are all observed. The m/z values of these $[M]Na^+$ ions are provided with their corresponding analyte names in Figure 3.6. The least abundant molecular adduct ions in this mass spectrum are from the three lower molecular weight organic acids. These components may be desorbing before the onset of K^+ emission and, thus, part of the sample is undetected. It is very interesting to note that all of the compounds, though differing in structure, are desorbed intact with the Na^+IDS technique and detected. Little thermal degradation is observed for any of these analytes, except mandelic acid which does exhibit dehydration. No evidence exists for any reaction between these eight components in the mixture, either on the surface or in the gas phase. As previously mentioned, K^+ and Na^+ ions primarily add to the neutral molecule without inducing any fragmentation. These results further support the utility of the Na^+IDS/K^+IDS technique for mixture analysis. Any reaction products observed in mixtures would probably be the result of interactions in the sample prior to analysis and are not the result of rapid heating.

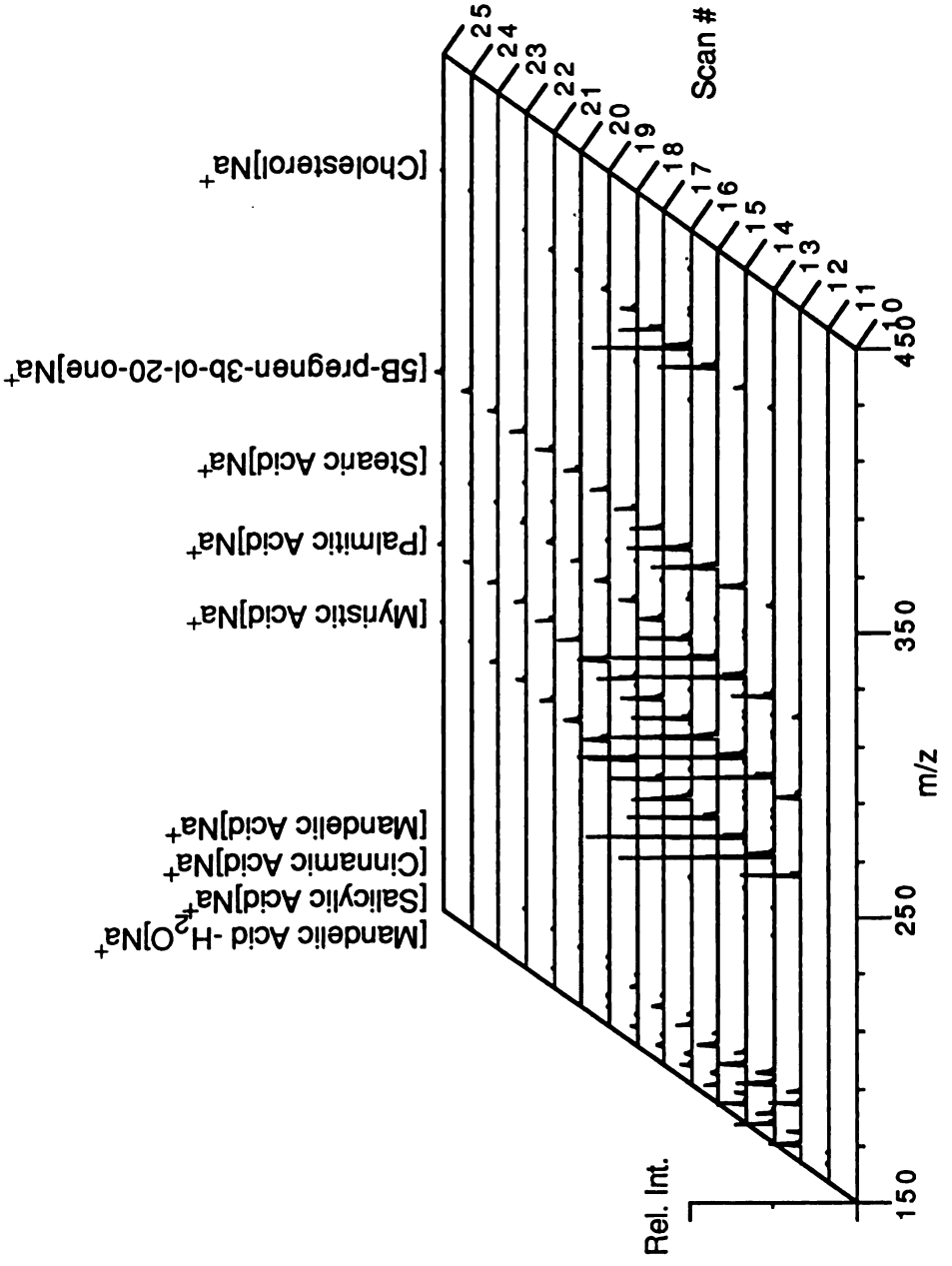

Figure 3.5 Plot of the Na^+ IDS mass spectra vs. scan number for the analysis of the eight component mixture.

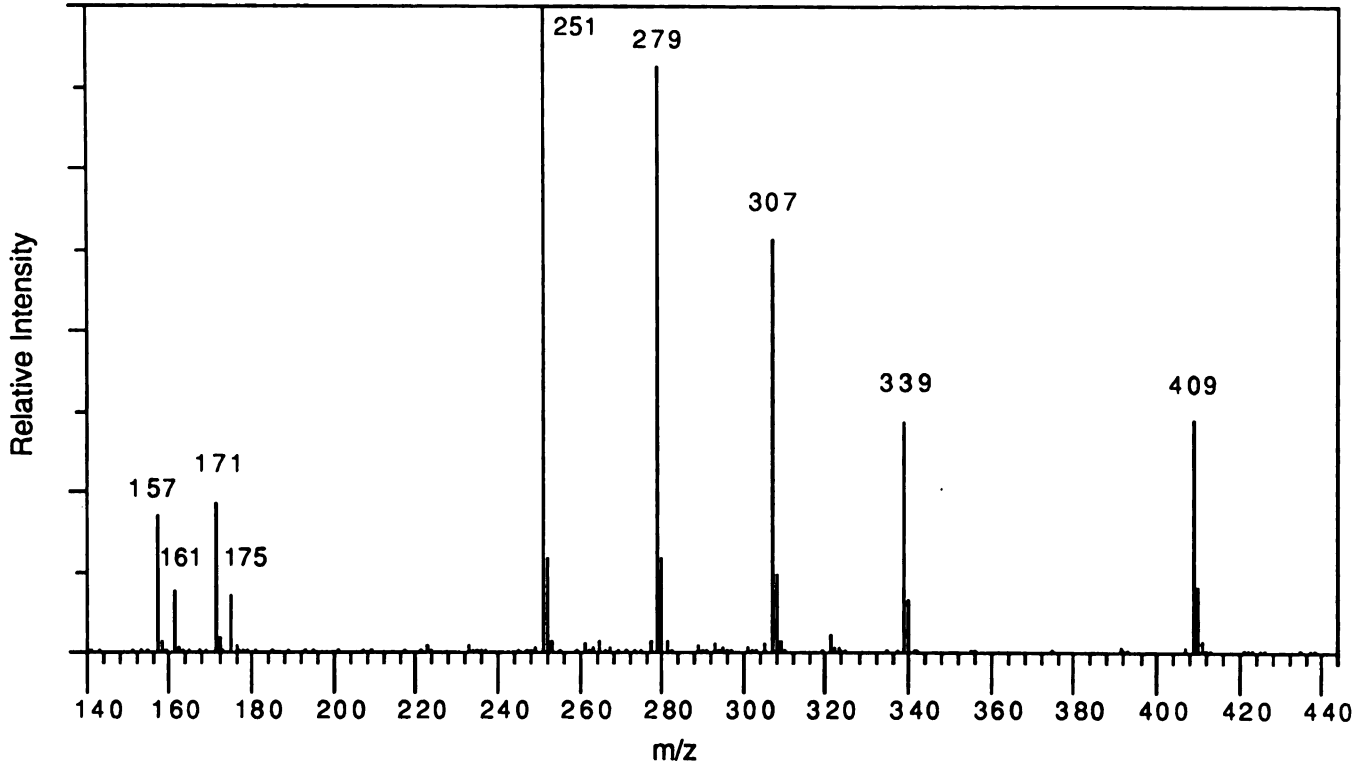

Compound, [M]	$[M]Na^+$	Compound, [M]	$[M]Na^+$
Salicylic Acid	161	Palmitic Acid	279
Cinnamic Acid	171	Stearic Acid	307
Mandelic Acid	175	5B -pregnen-3B -ol-20-one	339
Myristic Acid	251	Cholesterol	409

Figure 3.6 The averaged Na^+ IDS mass spectrum of the eight component mixture containing organic acids, fatty acids, and steroids.

4. FINAL COMMENTS

K^+IDS and Na^+IDS have been shown to be useful DI techniques for the analysis of a wide range of compounds including the cardiac glycosides. All of the ions observed in the K^+IDS mass spectra are K^+ adduct ions of the intact molecule or neutral thermal degradation products representative of the analyte, produced by the 1,2-elimination mechanism. Since K^+IDS requires no matrix, all of the ions observed are representative of the sample. Thus, K^+IDS mass spectra are typically cleaner with less chemical noise than the mass spectra produced by the more traditional DI techniques such as FAB.

In addition, K^+IDS provides an easy way to analyze mixtures as there is no matrix interference to complicate the already complex mass spectrum from the sample. Also, the mass spectrum is representative of the mixture with no mixing or interactions occurring as a result of the ionization process. Molecular weight information of the components in the mixture is usually obtained due to the intense peaks representing the $[M]K^+$ ions that are characteristic of the K^+IDS technique.

CHAPTER 4. Li^+IDS

1. INTRODUCTION

Often the K^+IDS analysis of thermally labile compounds produces only $[M]K^+$ ions and, thus, only molecular weight information is obtained. Ideally, mass spectrometric analyses provide both molecular weight and structural information concerning the analyte of interest. One way of adjusting the K^+IDS technique to obtain structural information is by altering the temperature and heating rate variables to change the rate of desorption versus the rate of thermal degradation. This was discussed in detail in chapter 2. Another variable that may be used to increase fragmentation of some compounds is the choice of the metal ion used with this DI technique. K^+ merely attaches to neutrals in the gas phase with all observed fragmentation occurring prior to K^+ attachment.

There are many possible metal ions that can be used for the cationization of thermally labile compounds that may induce fragmentation and thus provide more structural information. Blewett and Jones reported thermionic emitters that could produce Mg^+, Ca^+, Ga^+, In^+, Rb^+, and Al^+ in addition to the alkali ion emitters.[28] More recently, sources of ions such as Cu^+ and Ag^+ have been reported.[47] Extensive research has been performed on the gas-phase reactivity of transition metal ions such as Fe^+, Co^+, and Ni^+ with molecules containing functional groups and for alkanes.[48] Many of these metal ion reactions are specific enough to be useful for structural determination. Transition metal ions have been reportedly used for chemical ionization analyses.[49] The main difficulty with transition metal ions is that they have the higher ionization energies than alkali metals and, therefore, the transition metal ions are more difficult to ionize thermally. It may be difficult to create an emitter that produces a high enough flux of gas-phase transition metal ions for the "M^+IDS" technique. Some encouragement, however, has come with the report of thermally generated Cr^+ ions.[50] Volkening and Heumann used borosilicate matrices containing the transition metals as a source of the transition metal ions.[50] If this technique could be used to produce transition metal ions such as Co^+ or Fe^+, it would greatly expand the realm of the K^+IDS approach. Normal K^+IDS could be used to determine molecular weight information and Co^+IDS could be used to obtain

information concerning the structure of the analyte and functional groups present.

Li^+ has been shown to be a reactive ion and induce fragmentation in some organic molecules.[51] Allison and Ridge suggested a mechanism by which alkali ions may react with organic molecules such as alkyl halides and alcohols.[52] For example, Li^+ reacts with small alcohols such as t-butanol to form $Li(C_4H_8)^+$ and $Li(H_2O)^+$. The Li^+ ion induces fragmentation of this alcohol to produce the corresponding olefin and H_2O. Na^+ and K^+ only form adduct ions with t-butanol with no fragmentation observed. Li^+IDS may provide a way of obtaining structural information by inducing fragmentation of compounds that only desorb intact and, therefore, are only observed as $[M]K^+$ ions in the traditional K^+IDS technique.

2. EXPERIMENTAL CONSIDERATIONS FOR PRODUCING A Li^+ THERMIONIC EMITTER

The construction of a Li^+ thermionic emitter follows the design of the K^+IDS emitter. The aluminosilicate mixture is composed of $Li_2O:Al_2O_3:2SiO_2$. This mixture is more difficult to formulate into a bead than is the K^+ mixture. Two methods of making a K^+ bead on a rhenium wire loop were discussed in Chapter 2. One method is to use an oxygen/acetylene torch to melt the alkali aluminosilicate on a platinum crucible. The rhenium wire loop is then dipped into the molten mixture to make a bead. The melting temperature of the Li^+ aluminosilicate is higher than the K^+ aluminosilicate mixture. Therefore, the lithium mixture is harder to melt with the oxygen/acetylene torch without also melting the platinum crucible used as the support. This proves to be a very tedious way of forming a Li^+ emitter. The other procedure for making an emitter bead is with an acetone slurry of the aluminosilicate mixture. Some of the slurry is deposited onto the rhenium wire loop and the solvent is allowed to evaporate. Then the mixture is hardened in the flame of a bunsen burner. This slurry method of bead making is also more difficult with the Li^+ mixture. When the dry powder is inserted into the bunsen burner flame, much popping occurs probably due to the formation of NO_2 gas (from $LiNO_3$). This popping causes most of the aluminosilicate to fall off the wire. The best way to deal with this problem is to carefully melt the aluminosilicate mixture several times with the oxygen/acetylene torch, re-grinding between each melt. This

procedure will reduce most, if not all, of the $LiNO_3$ to Li_2O. For this procedure, the aluminosilicate does not have to be molten enough to submerge the wire in, but just melted enough for $LiNO_3$ to decompose. Therefore, it is easy to accomplish without melting the platinum. This acetone slurry method with premelted aluminosilicate powder proved to be the easiest way to make Li^+ beads.

Once the Li^+ emitter is made, the conditioning process is performed inside the ion source of the mass spectrometer as usual. It takes much longer to condition the Li^+ bead to achieve a strong Li^+ signal than it does for the K^+ bead to achieve a K^+ signal. This is primarily due to impurities of the other alkali metals present in the $LiNO_3$ and their relative ionization energies. The ionization energies for the alkali metals are as follows: Li is 5.392 eV, Na is 5.139 eV, K is 4.341 eV, Rb is 4.4177 eV, and Cs is 3.894 eV.[53] Therefore, any alkali metal impurities with lower ionization energies in the Li glass will be preferentially ionized, before Li.

The first Li^+ bead was conditioned for a long period of time in order to reduce the signals from other alkali ions present as impurities in the Li^+ bead. This extensive conditioning to produce a Li^+ emitter is similar to the process reported gy Weber and Cordes for the conditioning of a Na source to eliminate K^+ impurities by heating the source at 1000°C for over six hours.[54] After five hours of conditioning, the Li^+ emitter still produced 100 times more Na^+ ions than Li^+ ions. Varying the bias voltage applied to the tip of the bead did affect the ratio of the alkali ions observed. When the bias voltage was less than 1.0V, more Li^+ ions were observed than Na^+ ions. The bias voltage also affected the Li^+/K^+ ratio in a similar manner. However, the absolute abundance of these impurity alkali ions was still greater than desired. Another disturbing observation was the strong appearance of Na^+ and K^+ ions when current was first applied to a cold Li^+ bead. Only after heating for approximately 30-60 seconds did the Li^+ signal become the dominant metal ion observed. A second Li^+ bead was initially conditioned at a low-current (<2.0A) for approximately three hours with the goal of preferentially ionizing Na and K, which have lower ionization energies than Li. After this period of low current conditioning, the current and bias voltage were adjusted to obtain an optimum Li^+ signal. In this case, the Li^+ signal was much larger than the impurity K^+ and Na^+ signals. This low-current conditioning appears to be a good way of conditioning the Li^+ bead to decrease the presence of the impurities.

3. Li^+IDS MASS SPECTRA

This offshoot of the K^+IDS project was performed during the early stages of the development of the two-filament probe tip prior to the temperature studies and characterization of the probe tip design. Therefore, the data presented here should only be considered as preliminary results to show that Li^+ attachment to intact thermally labile molecules does occur and to suggest that this Li^+ attachment may lead to increased fragmentation. These results cannot be considered conclusive of the reactive nature of Li^+ ions (or nonreactive) upon attachment. In Chapter 2, evidence was presented that variations in the probe tip configuration and design can result in differences in the mass spectra obtained. During these Li^+IDS studies, little attention was given to these design details. Therefore, some of the differences in the Li^+IDS mass spectra compared to the Na^+IDS and K^+IDS mass spectra could be the result of the probe tip design instead of the reactive nature of Li^+ compared to Na^+ and K^+, however, the latter may still be a factor.

The polymer propylene glycol 725 (PPG 725) is one compound that does show some differences in the Li^+IDS mass spectra compared to the Na^+IDS mass spectra. The Na^+IDS mass spectrum of PPG 725 is shown in Figure 4.1 and the Li^+IDS mass spectrum of PPG 725 is shown in Figure 4.2. Both of these mass spectra are obtained by averaging over the entire experiment. The two mass spectra are very similar in the high-mass range where the ions are the corresponding Na^+ and Li^+ adduct ions, respectively, of the oligomers represented by $H[CH_2CH_2CH_2O]_nOH$ where n=8 to 16. The m/z values of the oligomer Na^+ and Li^+ adduct ions as a function of n are given in Table 4.1. The low-mass range of the two mass spectra in Figure 4.1 and Figure 4.2 show considerable differences in the abundance of dehydration products observed. The metal adduct ions of the low molecular weight oligomers (n=1 to 7) are of very low abundance in the Na^+IDS mass spectrum in Figure 4.1 compared to the Li^+IDS mass spectrum in Figure 4.2. Also, dehydration products of the low molecular weight oligomers are observed as Li^+ adduct ions with a large relative abundance. It is possible that the Li^+ attachment is inducing some of this observed dehydration. Figure 4.3 shows a plot of the Li^+ mass spectra of PPG 725 as a function of scan number. This is a good example of the changes in the Li^+IDS mass spectra with time during a single analysis. As the

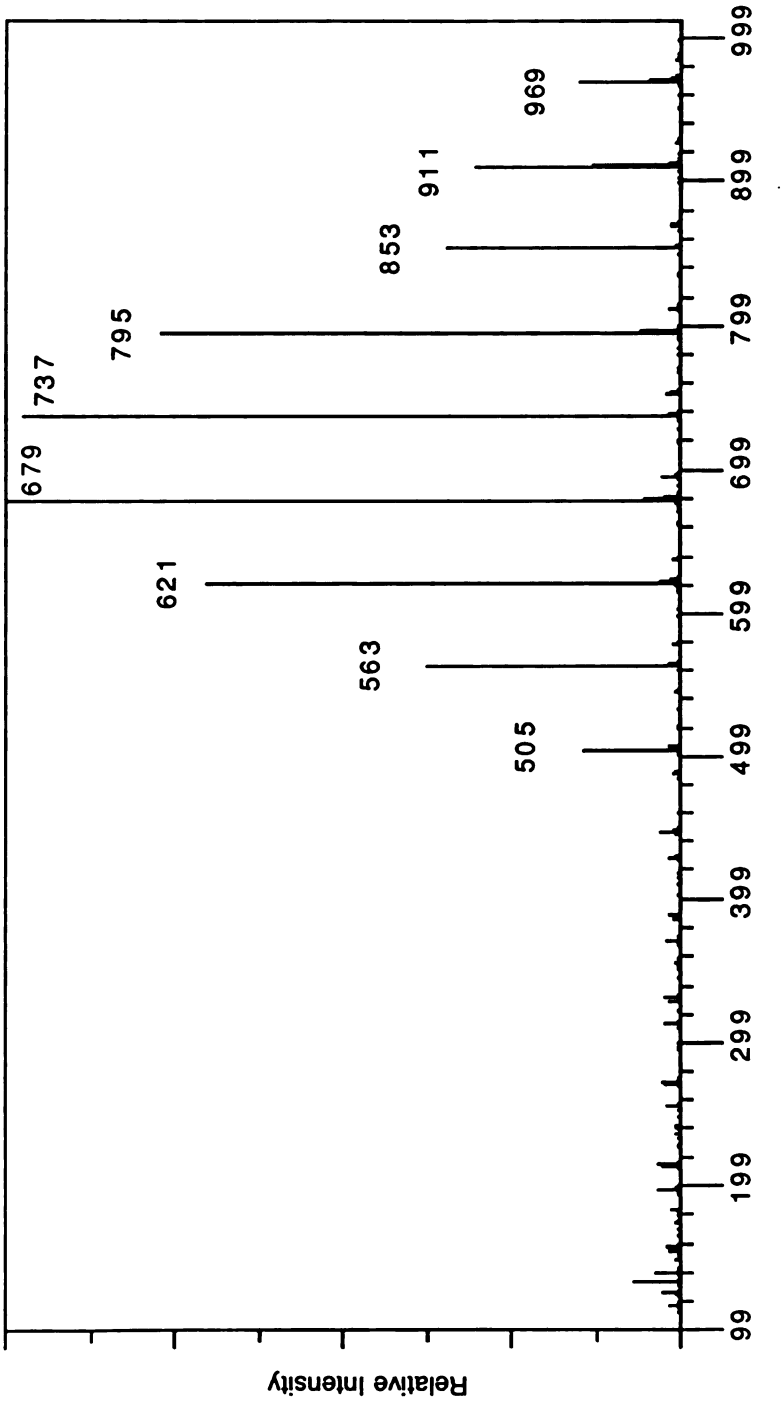

Figure 4.1 Na^+ IDS mass spectrum of PPG 725 averaged over the entire experiment.

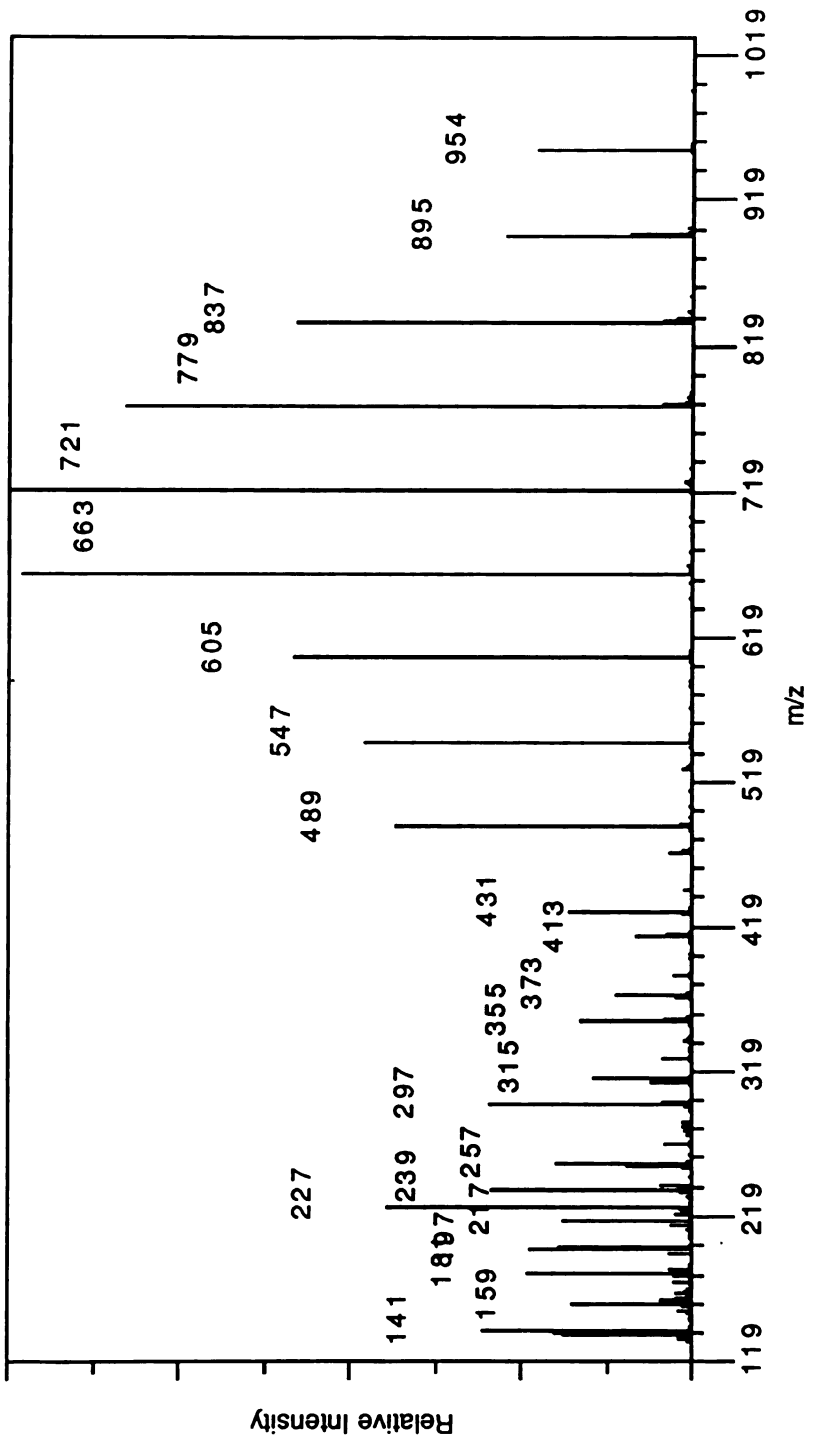

Figure 4.2 Li^+ IDS mass spectrum of PPG 725 averaged over the entire experiment.

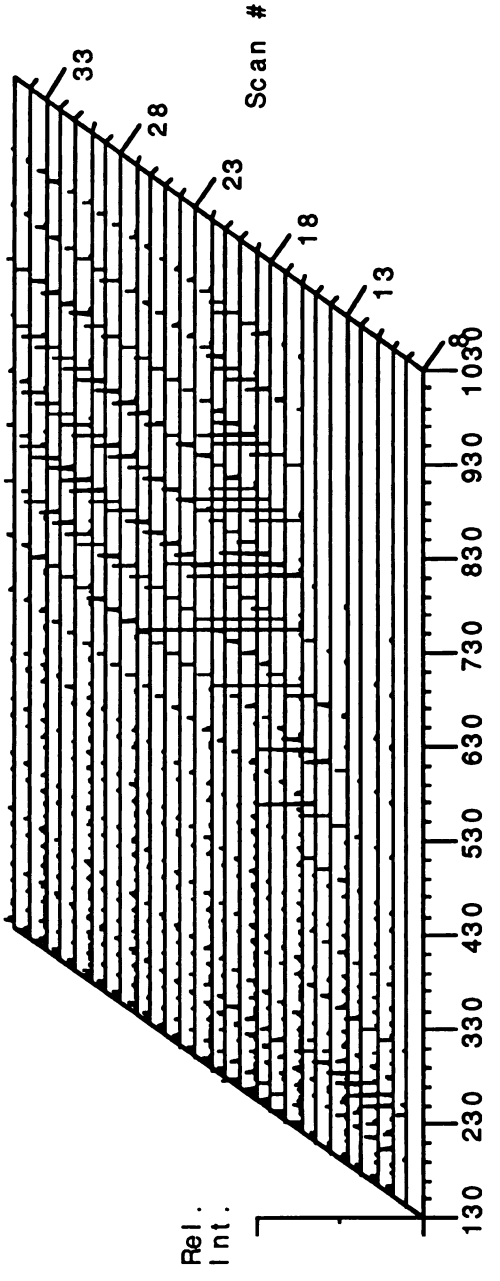

Figure 4.3 Li^+IDS mass spectra of PPG 725 versus scan number for a single experiment.

experiment progresses, the temperature of the sample wire filament increases, and the molecular weight of the observed oligomer adduct ion increases. This is consistent with the findings of the temperature studies in Chapter 2.

Table 4.1 The m/z values of the Na^+ and Li^+ adduct ions of the oligomers of PPG 725, $H[CH_2CH_2CH_2O]_nOH$.

n	m/z value of $[H[CH_2CH_2CH_2O]_nOH]Na^+$	m/z value of $[H[CH_2CH_2CH_2O]_nOH]Li^+$
1	138	122
2	197	181
3	255	239
4	313	297
5	331	315
6	389	373
7	447	431
8	505	489
9	563	547
10	621	605
11	679	663
12	737	721
13	795	779
14	853	837
15	911	895
16	969	953
17	1027	1011

Several other compounds were analyzed by the Li^+ emitter. The Li^+IDS mass spectrum of palmitic acid is shown in Figure 4.4. The base peak is the $[M]Li^+$ ion of m/z 263. If the lower-mass region is magnified, there are some other ions at very low abundance that may be the result of the fragmentation of palmitic acid. There is a significant peak at m/z 245 corresponding to the $[M-H_2O]Li^+$ ion. This dehydration is uncommon for the K^+IDS analysis of

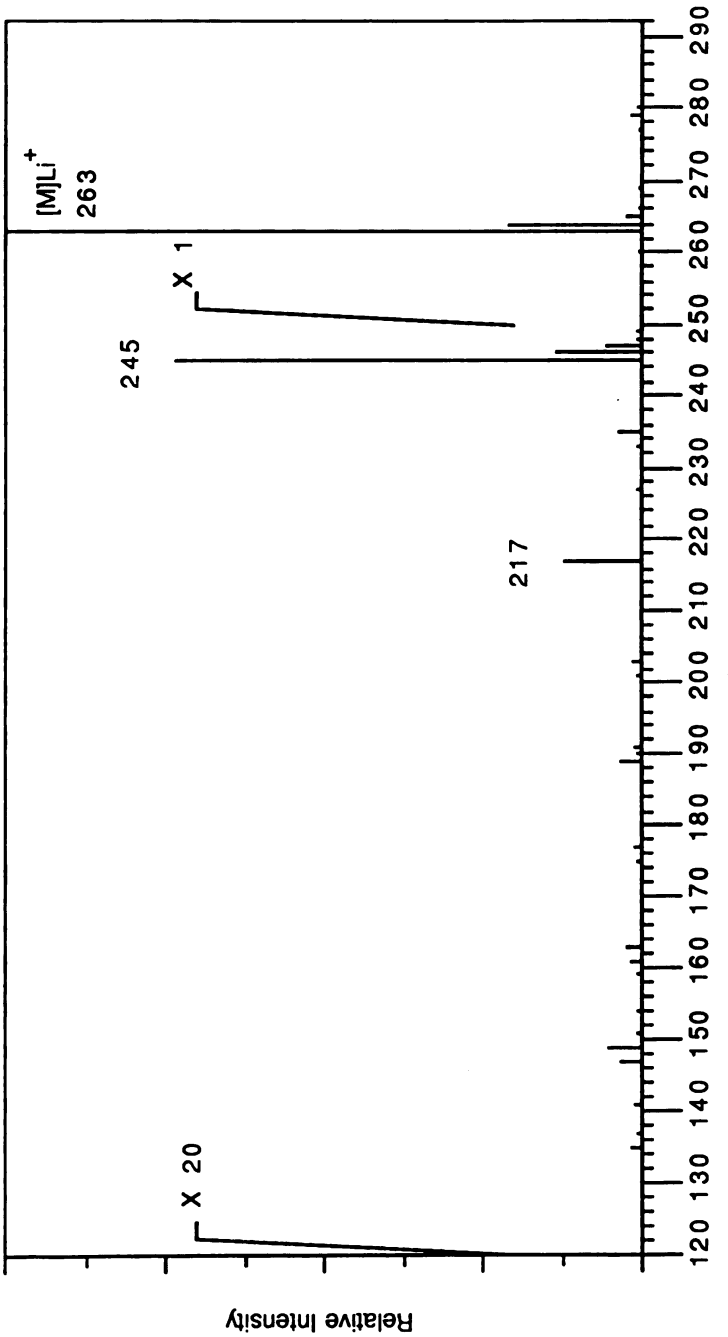

Figure 4.4 Li^+IDS mass spectrum of palmitic acid.

palmitic acid and, therefore, may be the result of Li^+ attachment. The ion of mass 217 is at a relatively low abundance, but could be explained as resulting form the loss of formic acid (HCOOH) from the $[M]Li^+$ ion of palmitic acid. Co^+, another reactive metal ion, has been shown to eliminate CH_2O_2 and H_2O in addition to other products from organic acids.[49b] This provides support for the possibility of Li^+ reacting with fatty acids to eliminate similar products.

Li^+IDS was used to analyze two steroid molecules to see if any induced fragmentation resulted from the ionization process. The Li^+IDS mass spectrum of cholesterol is shown in Figure 4.5. The base peak represents the $[M]Li^+$ ion of m/z 393. The Na^+ and K^+ molecular adduct ions are also observed with m/z 409 and m/z 425, respectively, as these metal ions are present as impurities in the Li^+ emitter. It was hoped that this steroid, which contains several functional groups, would exhibit more fragmentation due to the reactive Li^+ ion attachment. The low-mass ions in the m/z range 135-175 do not resemble typical adduct ions as they appear at odd and even m/z values unlike K^+ or Li^+ adduct ions that should only appear at odd m/z values for cholesterol. Compounds that contain only carbon, hydrogen and oxygen, as does cholesterol, should be represented by even-mass neutrals from both the intact molecule and from products of 1,2-elimination. Therefore all adduct ions formed by the attachment of Li^+ (m/z 7) or K^+ (m/z 39) to these even-mass neutrals should have odd m/z values. This discrepancy suggests that the low-mass ions observed in Figure 4.5 are surface ionization products. Figure 4.6 contains the Li^+IDS mass spectrum of digitoxigenin which is the steroid portion of digitoxin (a member of the cardiac glycoside family). The $[M]Li^+$ ion is observed as the base peak at m/z 381. Again, some molecular adduct ions of digitoxigenin from the alkali metal impurities are present to a small extent at m/z 397 ($[M]Na^+$) and m/z 413 ($[M]K^+$). No major fragmentation is observed in the Li^+IDS mass spectrum of digitoxigenin. There are some low-mass ions present in this mass spectrum that are from residual PPG 725 present either on the probe tip or in the source. This polymer was analyzed just prior to the analysis of digitoxigenin. It is not uncommon for residual polymer to be present for the next few experiments. Other Li^+IDS mass spectra of thermally labile compounds are provided in Appendix A.

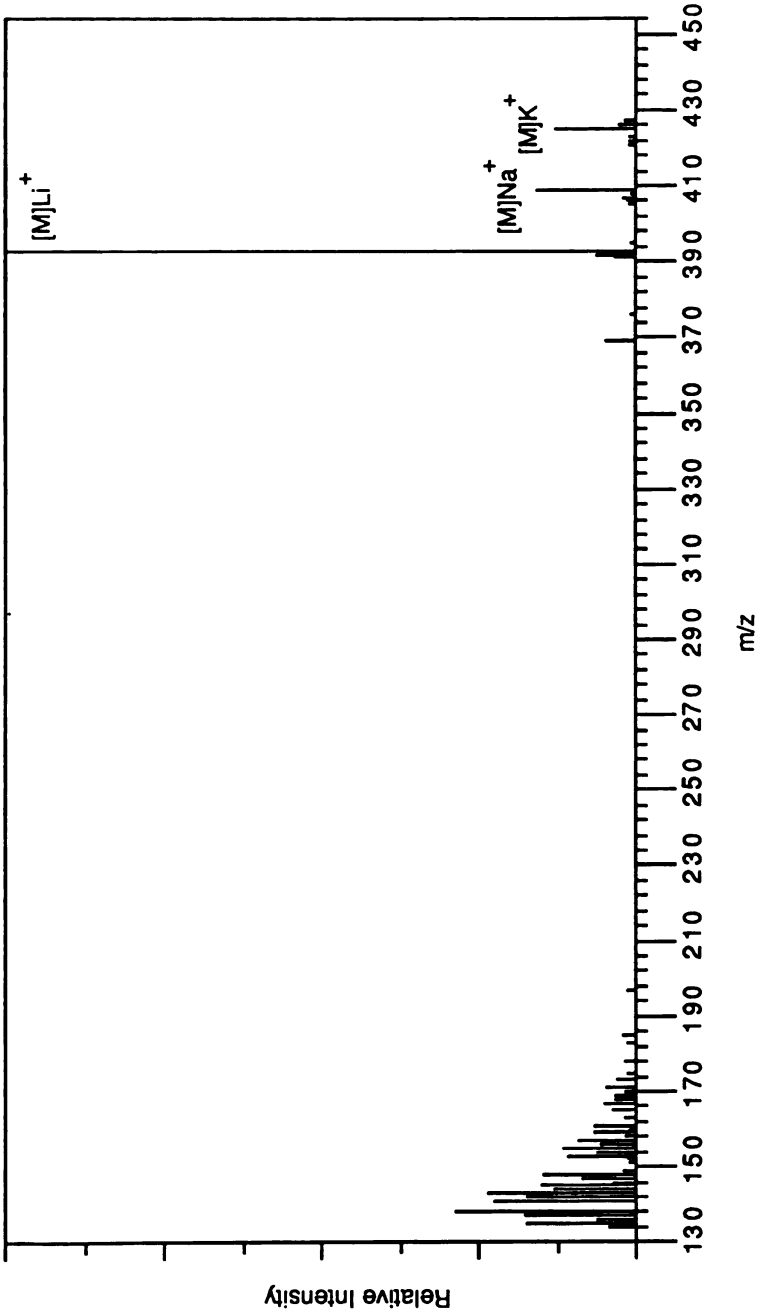

Figure 4.5 Li^+ IDS mass spectrum of cholesterol.

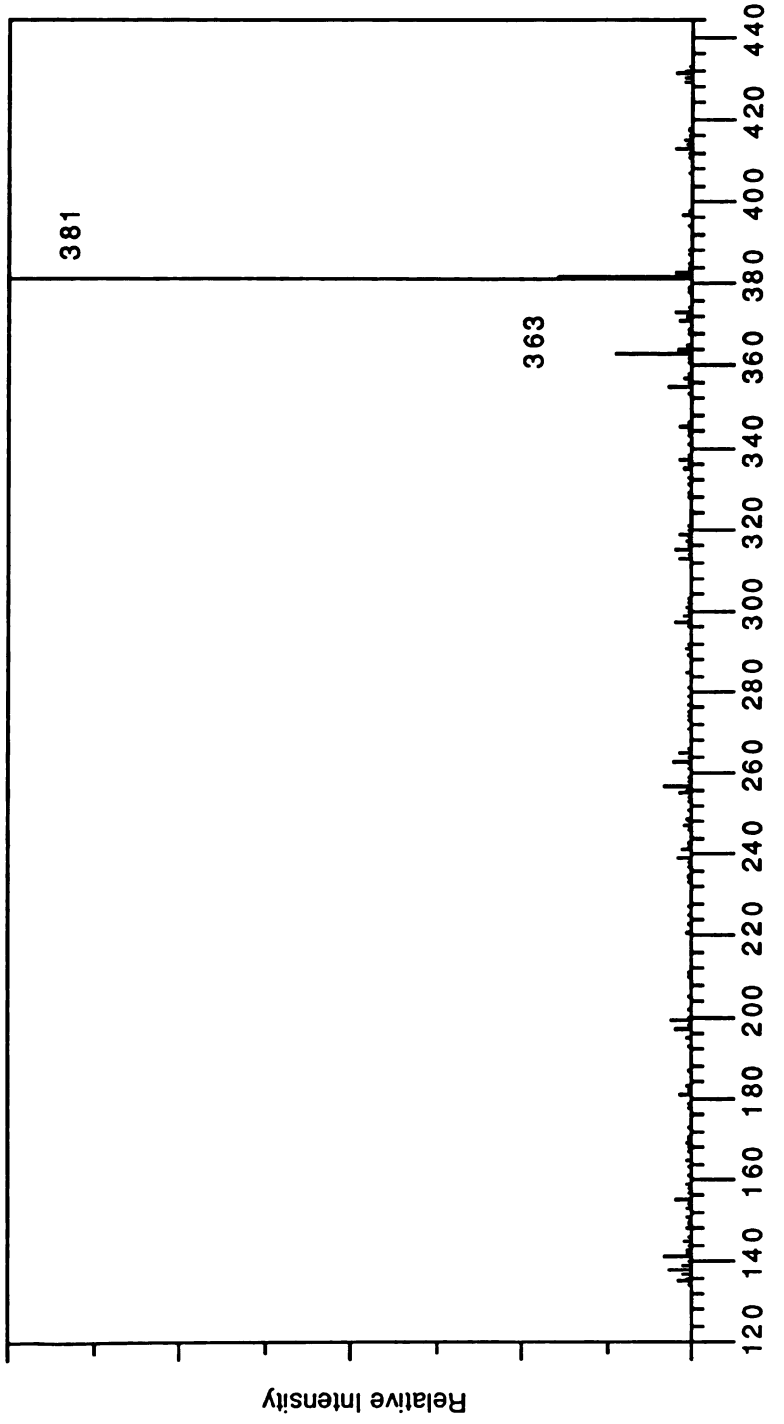

Figure 4.6 Li^+ IDS mass spectrum of digitoxigenin.

4. FINAL COMMENTS

These preliminary results show that it is possible to obtain Li^+ attachment to the intact molecule of several thermally labile compounds including cholesterol, digitoxigenin and palmitic acid, and to the oligomers of the polymer PPG 725. The Li^+IDS mass spectra obtained did show some possibility of induced fragmentation of the analyte from Li^+ attachment. This is primarily in the form of dehydration of the intact analyte molecule. More carefully controlled studies need to be performed to accurately compare the results of Li^+IDS with K^+IDS and/or Na^+IDS and ascertain whether the Li^+IDS technique will provide a means of obtaining more structural information from the different thermally labile compounds. None of the emitters used for this preliminary study were used for more than one day as the direct insertion probe was converted back to K^+IDS for use with other on-going research projects. This makes it very difficult to control all of the variables that affect the mass spectra with this technique, including the size of the emitter bead, the amount of ceramic support post present, and the distance between the sample wire surface and the emitter. Recently, more modified direct insertion probes have been constructed for the K^+IDS project and, thus, it would be feasible to dedicate one probe to the Li^+IDS technique for an extended period of time. This would allow for more extensive studies with Li^+IDS to determine whether more structural information is obtainable than with the traditional K^+IDS. Also, consecutive Li^+IDS and K^+IDS analyses of the same samples could be made with all instrumental parameters constant. This would provide ideal conditions for comparing the results obtained with Li^+IDS and K^+IDS to determine if Li^+ attachment does induce any fragmentation for the thermally labile compounds studied. The preliminary results are encouraging, but more experimentation is necessary to determine the utility of using a Li^+ ion emitter for the "K^+IDS" technique.

CHAPTER 5. IMPLEMENTATION OF THE K^+IDS TECHNIQUE ON A DOUBLE-FOCUSING MASS SPECTROMETER.

1. INTRODUCTION

Another offshoot of the original research project was to determine the mass limit of the K^+IDS technique. The current trend in the development of DI techniques is towards extending the mass range of these mass spectrometric methods. All previous work with K^+IDS was performed on a quadrupole mass spectrometer with a mass limit of 1,000 daltons. Therefore, to determine the mass limit of this technique, it was apparent that another mass spectrometer was needed. The instrument readily available for such an endeavor was the JEOL HX-110 double-focusing mass spectrometer which has a mass limit of 14,000 daltons. Modifications were made to adapt the K^+IDS technique for use on this magnetic sector instrument. The JEOL HX-110 mass spectrometer is more automated than the HP 5985 quadrupole mass spectrometer previously used in terms of the direct inlet probe and electronic controls, and is not designed for easy modification. Also, the inherent differences between magnetic sector and quadrupole mass spectrometers, such as the ion source voltage, add to the complexity of the modifications needed.

Initial efforts to implement the K^+IDS technique on the double-focusing mass spectrometer dealt with modifying the existing direct chemical ionization (DCI) probe and DCI electronics of the JEOL HX-110 mass spectrometer, since the DCI filament closely resembles that used for the K^+IDS technique. DCI involves placing a nonvolatile sample directly on the surface of an extended probe and inserting the probe tip into the ion source.[55] Often the tip of the probe is heated with a programmable current control as is provided on the JEOL instrument. This heating promotes desorption of thermally labile compounds into the gas phase, followed by traditional CI or EI (DEI). The main differences between this technique and K^+IDS are the rate of heating of the sample (slow ramping for DCI and rapid heating for K^+IDS) and the CI reagent ions (typically ions of ammonia or methane for DCI versus K^+ ions for K^+IDS). The JEOL HX-110 DCI probe consists of a platinum wire filament loop connected to the probe tip through which a heating current is applied. A second method for implementing K^+IDS on the JEOL HX-110 mass spectrometer dealt with using the modified DCI probe of the mass spectrometer combined with the

original K^+IDS power supply. These two experimental designs are explained in detail and the results obtained with each setup are presented and evaluated.

2. EXPERIMENTAL DESIGN

The automated nature of the JEOL HX-110 vacuum system makes it difficult to construct a direct insertion probe suitable for the K^+IDS technique. The JEOL DCI probe, however, can be modified to make a K^+IDS probe very similar in appearance to the original probe design used with the quadrupole instrument. The normal DCI filament is converted to a K^+ emitter by threading the filament wire (0.007" Re) through a two-holed ceramic support post (identical to that used with the standard K^+IDS probe) and then making the K^+ glass bead on the wire loop protruding from the ceramic. This is shown in Figure 5.1. A sample support loop also can be spot-welded to the outer cone of the DCI probe. The instrument controls (parameter files and control panel) must be set in the DCI mode, as the DEI mode was never completed in the software package of the instrument. The source may still remain in the EI mode, however. A sample parameter file used to perform the K^+IDS experiment on the JEOL HX-110 mass spectrometer with the modified DCI probe is shown in Figure 5.2. Calibration of the mass axis was performed by positive

CTRL Type: SCAN Group: 1 of 1 MS Unit: 0 File: HSPAR.PAR Date: 22-NOV-88

DA5000 Acquisition Parameters

A1: DY HSCSKPOS 2: ST HSSTATIC
B1: Acell.V.: 6.0kV/DAC 2: Ion Mode: DCI 3: Polarity: POS. 4: Temp.
C1: Resolution: 1000 2: Filter: AUTO 3: Inlet: DIR 4: Store: ALL
< Value Manual >
D1: Scan Slope: 1.0 2: Cycle Time: 1.0[0.7 + 0.3] 3: M. Field:HS
E1: Max Run Time 2: Scan Type: MF, LI, UP, DA 3: DataType: MZ, HE
F1: Thres.: 500-500 2: Valley: 50% 3: Accum.: Range 4: Amp.Sw: 2/60%/100

	<E/D	Range AMP
G1:	2:	100.000-1500.000

Q1: Note: K^+IDS with modified DCI probe and K^+IDS power supply.

Figure 5.2. Parameter file for data collection on the JEOL HX-110 with the modified DCI/K^+IDS probe and K^+IDS power supply.

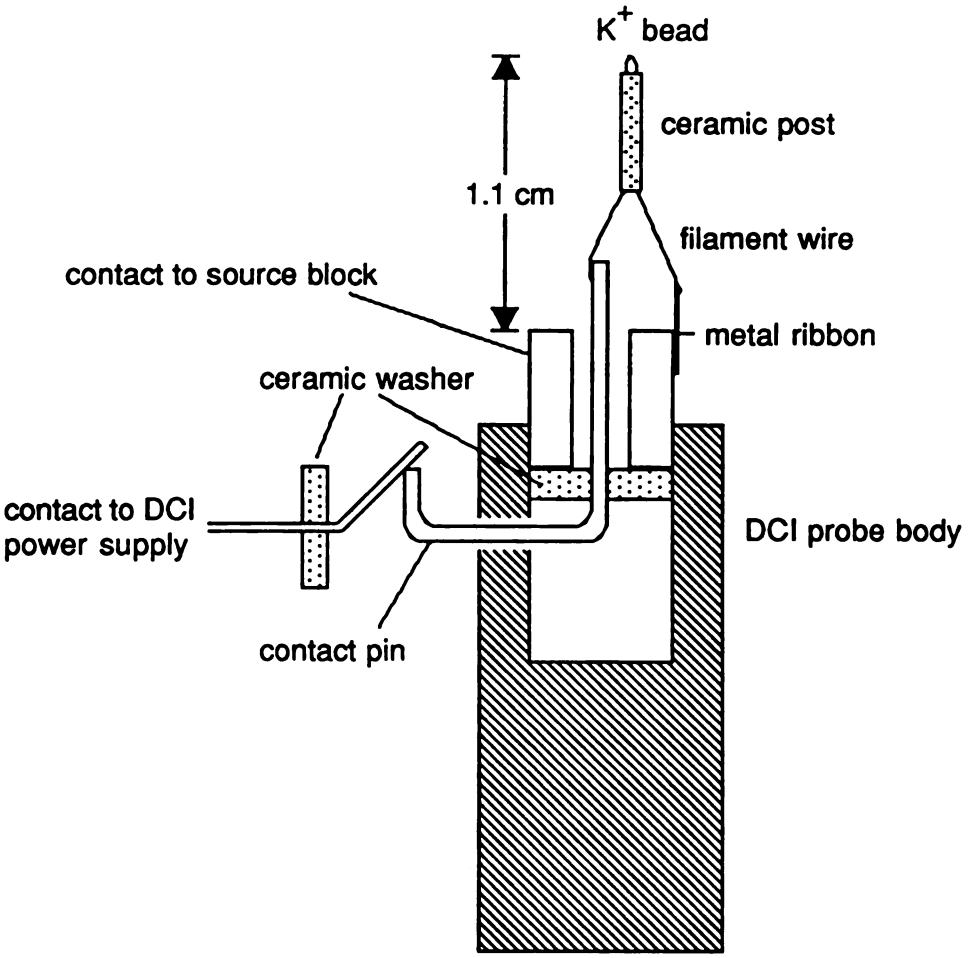

Figure 5.1. Schematic of the modified JEOL HX-110 DCI probe tip for use with the K^+ IDS experiment.

FAB with CsI/KI with the same scan slope as used for the K^+IDS/DCI experiments. The variables that need further study are the scan slope and cycle time. The K^+IDS experiment is very fast and most of the sample is depleted within 1 minute. Therefore, fast scan rates are necessary to obtain all the information possible from this DI technique. Typical scan rates used for FAB are 1 scan/minute, or slower. Fast scanning results in poor ion statistics and possible problems with the mass axis calibration. A detailed analysis of the limitations of the JEOL HX-110 instrument regarding fast scanning needs to be performed to determine the optimum scan slope and cycle time for the K^+IDS technique at the desired mass ranges (e.g., 100-1000 daltons and 100-1500 daltons). Preliminary studies show that a one-second scan slope is often too great, depending on the mass range, and often leads to erroneous results as the magnet and data system can not keep up with the fast scanning. The result is the appearance of peaks at erroneous values and a distorted or poorly calibrated mass axis.

A. MODIFICATION OF THE DCI POWER SUPPLY.

The existing DCI power supply of the JEOL HX-110 mass spectrometer was modified so that it could be used as the power supply for the K^+IDS technique. The DCI power supply was originally designed to apply current through a filament similar to that used for the K^+IDS emitter. However, instead of a sudden input of a constant preset current, as is used for K^+IDS, the JEOL DCI power supply was designed to produce a current ramp that varied from 1/32 to 4A per minute with continuous repetition of this current cycle. There was no way to hold the current at the maximum value and no way to control the maximum current obtainable. Also the ramping rates were all too low to heat up the K^+ emitter as rapidly as needed for optimum results with the K^+IDS technique. The maximum current obtainable with the original electronic design and with a K^+ bead on the filament was approximately 1A. This is below the optimum current for a traditional K^+IDS probe which usually requires 2-3A for the best results.

The first modification to the DCI controls was the addition of two "TEST" buttons placed on the front panel of the DCI power supply that allowed for by-passing the current ramping controls. In the test mode, the current can

immediately be placed at the maximum value and be held at that current until the "MIN" switch is activated. With this addition, the current supplied to the DCI/K^+IDS filament can be immediately set at the maximum current with the "MAX" button and remain constant. These "TEST" buttons are used to provide the maximum rate of heating, but do nothing to increase the maximum current available. Originally there were two 4Ω resistors (R20 and R21 on the schematic diagram) in the current system that were replaced by two 1Ω resistors. Thus, the overall resistance was changed from 2Ω to 0.5Ω. With this modification the maximum current obtainable is approximately 2A with the K^+ bead connected (3A with no load). The DCI current meter on the main instrument panel no longer reads the correct current that is passing through the DCI filament due to the modifications with the resistors. The meter value times four gives the approximate current flow. Therefore, the maximum current of 2A is read as 0.5A on the meter. This was still not enough current to perform the K^+IDS experiment optimally. Also, the inability to control the value of the constant current applied to the K^+ bead was another major drawback of this experimental design.

B. CONVERSION OF THE K^+IDS POWER SUPPLY TO CONTROL THE DCI/K^+IDS PROBE.

The second attempt at applying the K^+IDS technique to the JEOL HX-110 instrument centered around floating the K^+IDS power supply so that it could be connected to the DCI probe and used as the controllable current source for the DCI/K^+IDS probe. An isolation transformer was purchased from Heyboyer Transformer, Grand Haven, MI to float the K^+IDS power supply at the high voltage of the source in the magnetic sector instrument. The transformer and K^+IDS power supply were placed inside a wooden crate to protect the user from the power supply which is floating at the acceleration voltage (typically 6-10 kV). Plexiglass was placed on the front of the crate to allow for monitoring and controlling the current supplied to the bead. The REF IN for the bias voltage was left unconnected. At this point, no bias voltage has been applied to the K^+ bead as it is difficult to find a true reference voltage that would not interfere with the current loop. Therefore, the bias voltage is set to zero. The two current connections are made with pins inside the surge filter located behind the panel under the vacuum control diagram. One lead is connected to pin #6 which is the contact to the source block and the other lead is connected

to the top lead (from the source) that was connected to pin #10 (from the DCI control box). The DCI control box is now disconnected from the system and the K^+IDS power supply is connected to the DCI probe contacts through the surge filter. Many precautions need to be taken when using this system. All the connections should be clear and not be touching anything. The panel safety rollers must be taped in to override the safety switch and allow for the acceleration voltage to be turned on. The maximum accelerating voltage used with this setup should be 6 kV. Accelerating voltages higher than this result in overloading and destroying the K^+IDS power supply bias voltage meter (and possibly other components). There are holes in the Plexiglass cover of the crate to change the current and turn the power supply off and on with a rubber hose or wooden dowel.

3. RESULTS

The first modifications to the DCI control unit, the addition of the test switches and the replacement of the resistors, did allow for K^+IDS experiments to be performed on the JEOL HX-110 mass spectrometer, but with only marginal results. The only compounds for which acceptable K^+IDS mass spectra were obtained with this system was the polyethylene glycols (PEG). The K^+IDS mass spectra of PEG 1000 obtained with these modified DCI controls on the JEOL HX-110 are shown in Figure 5.3. The m/z values for the K^+ adduct ions of the oligomer series ions are given in Table 5.1. These spectra closely resemble those obtained on the HP 5985 for similar compounds of lower mass (that are within the mass limit of the HP quadrupole instrument). There is a time dependence for these mass spectra where the lower-mass fragments are observed as K^+ adduct ions earlier during the run and higher-mass adduct ions are observed later during the run. This can be seen in Figure 5.4 in the mass chromatogram of several K^+ adduct ions of different oligomers. The averaged mass spectrum over this entire desorption profile from scan 15 through 50 is shown in Figure 5.5. This shows a very interesting distribution of adduct ions throughout the mass range. These are the same results as are obtained with the K^+IDS performed on the quadrupole instrument. A detailed analysis of polymers by K^+IDS has been made elsewhere.[43] The main problem with this design for K^+IDS is the limited current that can be applied and the lack of

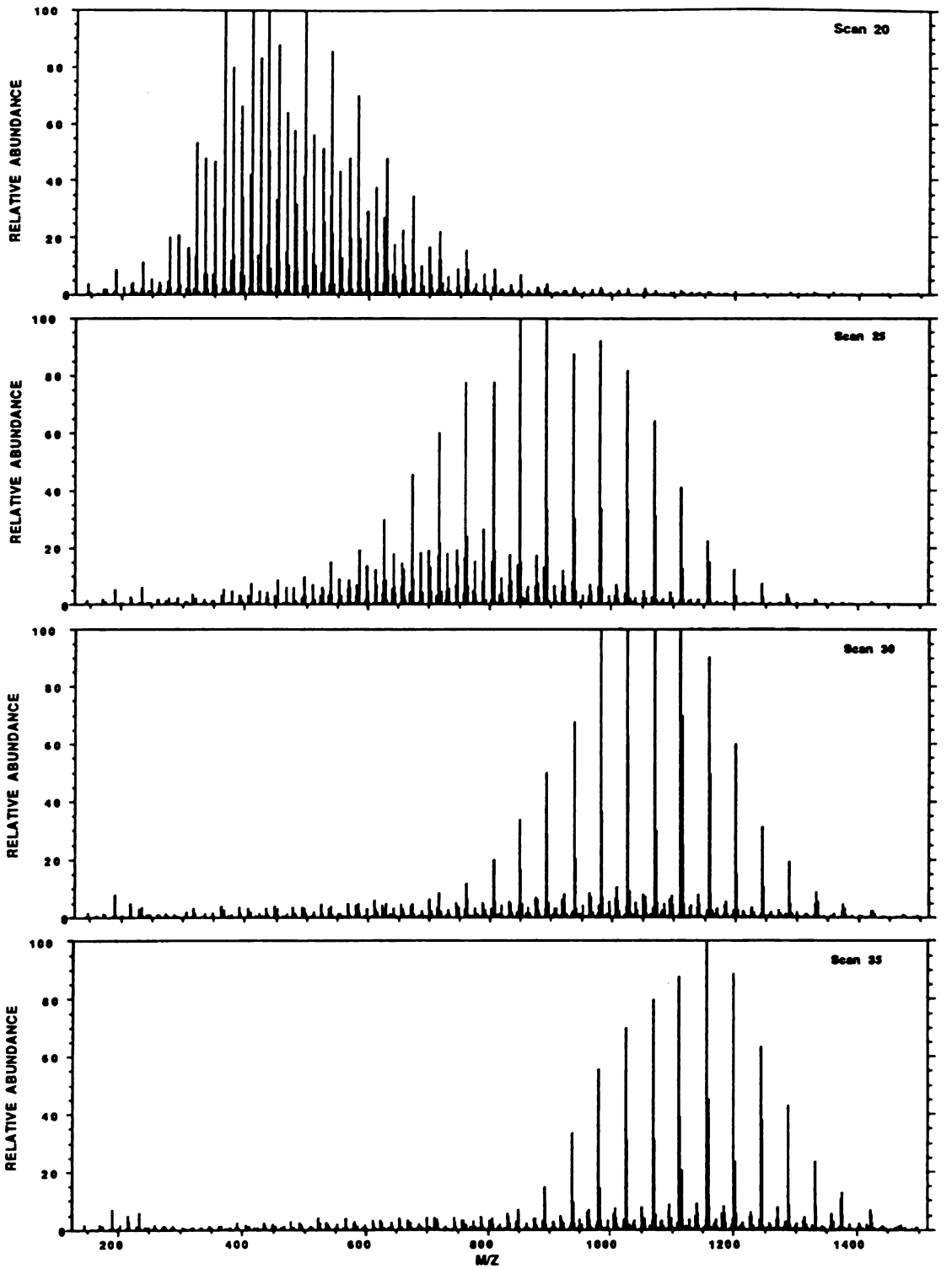

Figure 5.3. Temporal dependence of the K^+IDS mass spectra of PEG 1000 obtained with the JEOL HX-110 double-focusing mass spectrometer.

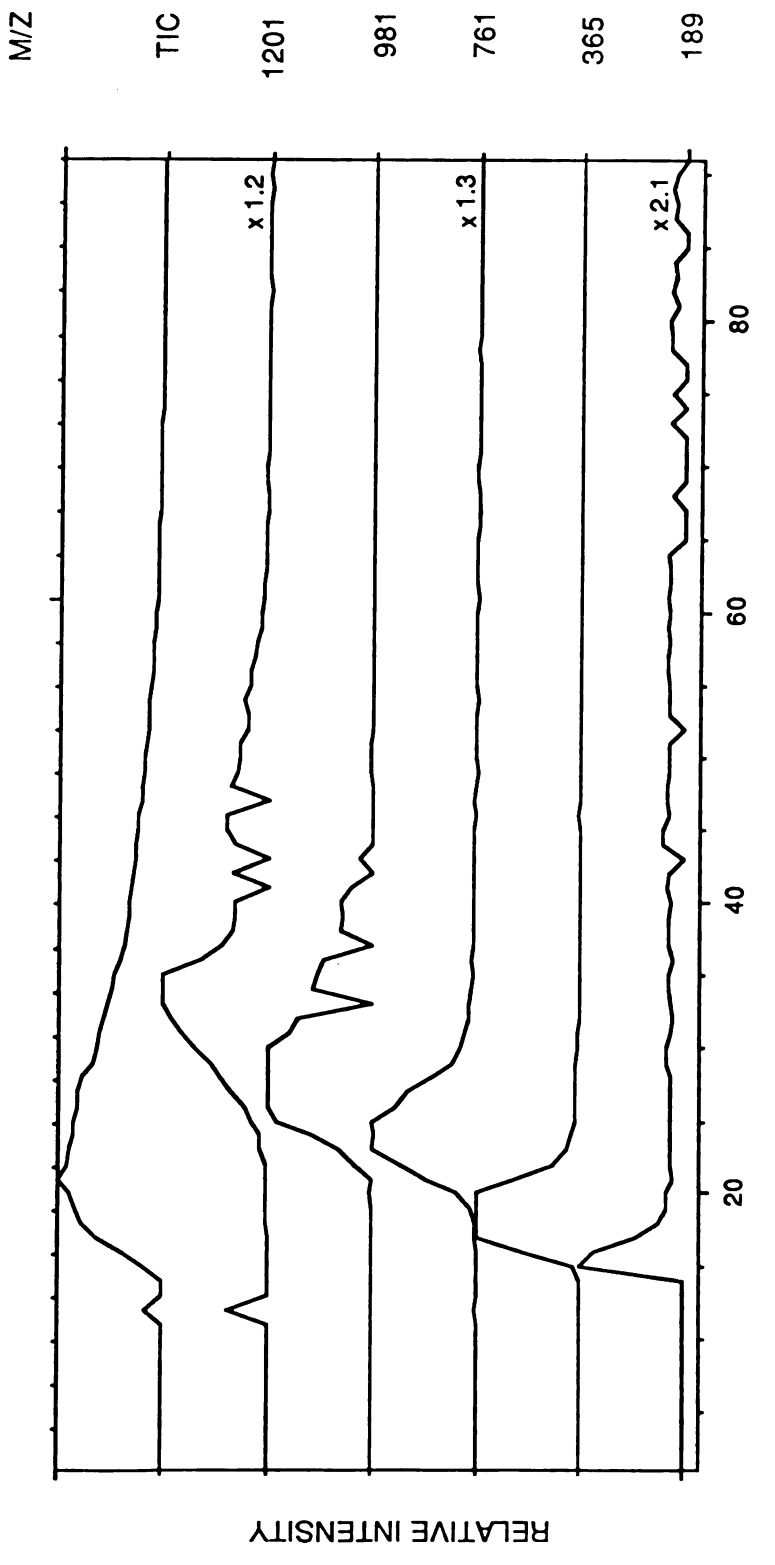

Figure 5.4. Mass chromatograms of the TIC and selected K^+ adduct ions produced by the K^+IDS analysis of PEG 1000.

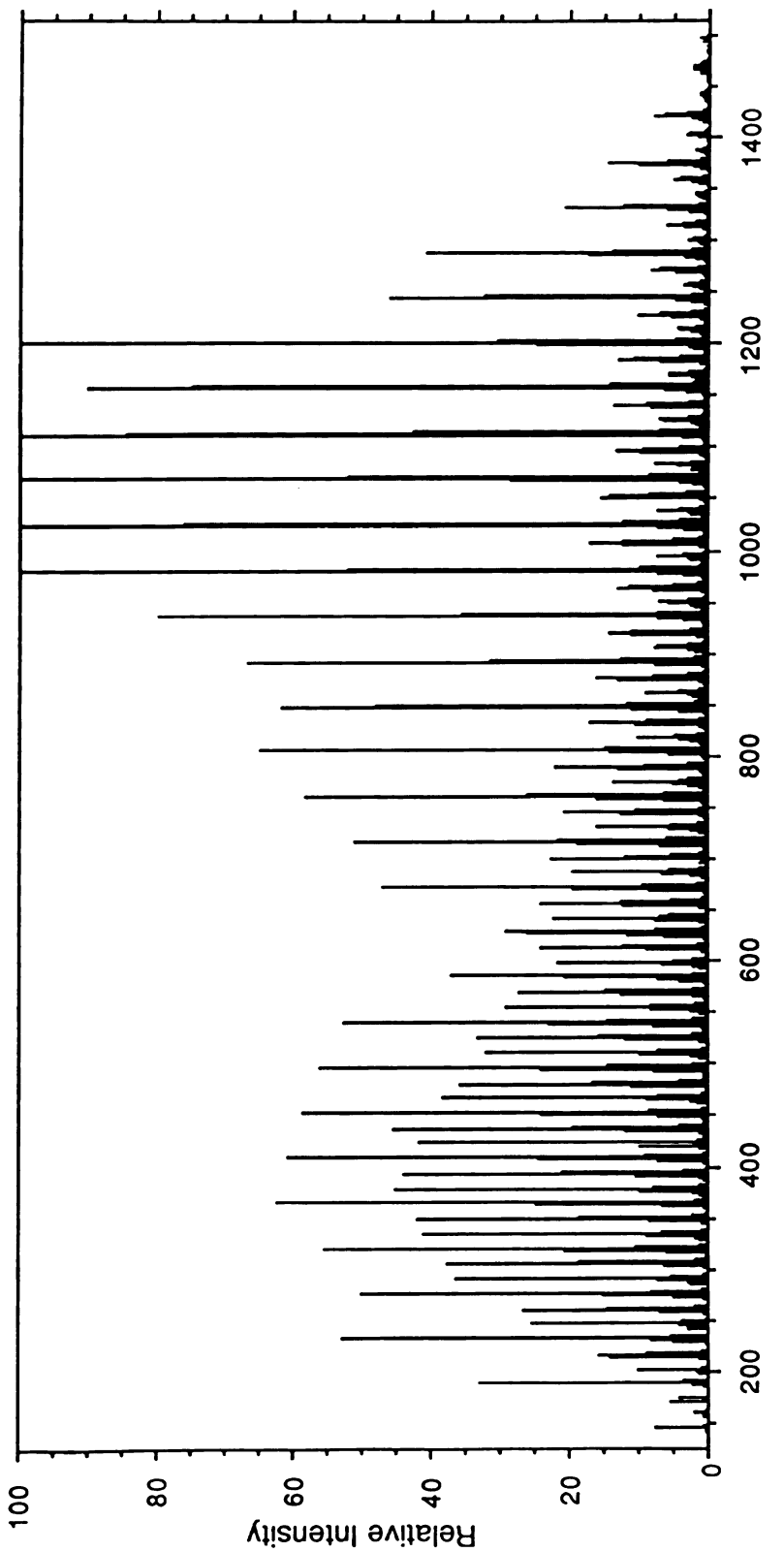

Figure 5.5. The averaged K^+ IDS mass spectrum of PEG 1000 from scans 15-40 obtained on the JEOL HX-110 double-focusing mass spectrometer.

Table 5.1 Values of m/z for the K^+ adduct ions of the oligomers of polyethylene glycol 1000.

n	$H[OCH_2CH_2]_nOH]K^+$	n	$H[OCH_2CH_2]_nOH]K^+$
1	101	18	849
2	145	19	893
3	189	20	937
4	233	21	981
5	277	22	1025
6	321	23	1069
7	365	24	1113
8	409	25	1157
9	453	26	1201
10	497	27	1245
11	541	28	1289
12	585	29	1333
13	629	30	1377
14	673	31	1421
15	717	32	1465
16	761	33	1509
17	805	34	1553

control over this current. Different types of compounds require different heating currents and energy to desorb with little or no fragmentation and be detected as K^+ adduct ions. As the search for the upper mass limit of K^+IDS continues, higher final currents and heating rates will probably be needed to desorb larger molecules intact. Therefore, this initial design proved incapable of replicating the K^+IDS technique satisfactorily and providing control over the current.

The second design, which utilizes the K^+IDS power supply to apply current to the DCI/K^+IDS probe, does allow for the maximum current to be controlled and optimized for different types of compounds. The K^+IDS mass spectrum of digoxin obtained with the K^+IDS power supply providing current to the DCI probe is shown in Figure 5.6. As can be seen, this mass spectrum closely resembles the K^+IDS mass spectrum of digoxin obtained on the quadrupole mass spectrometer (see Appendix B). Not all of the fragment

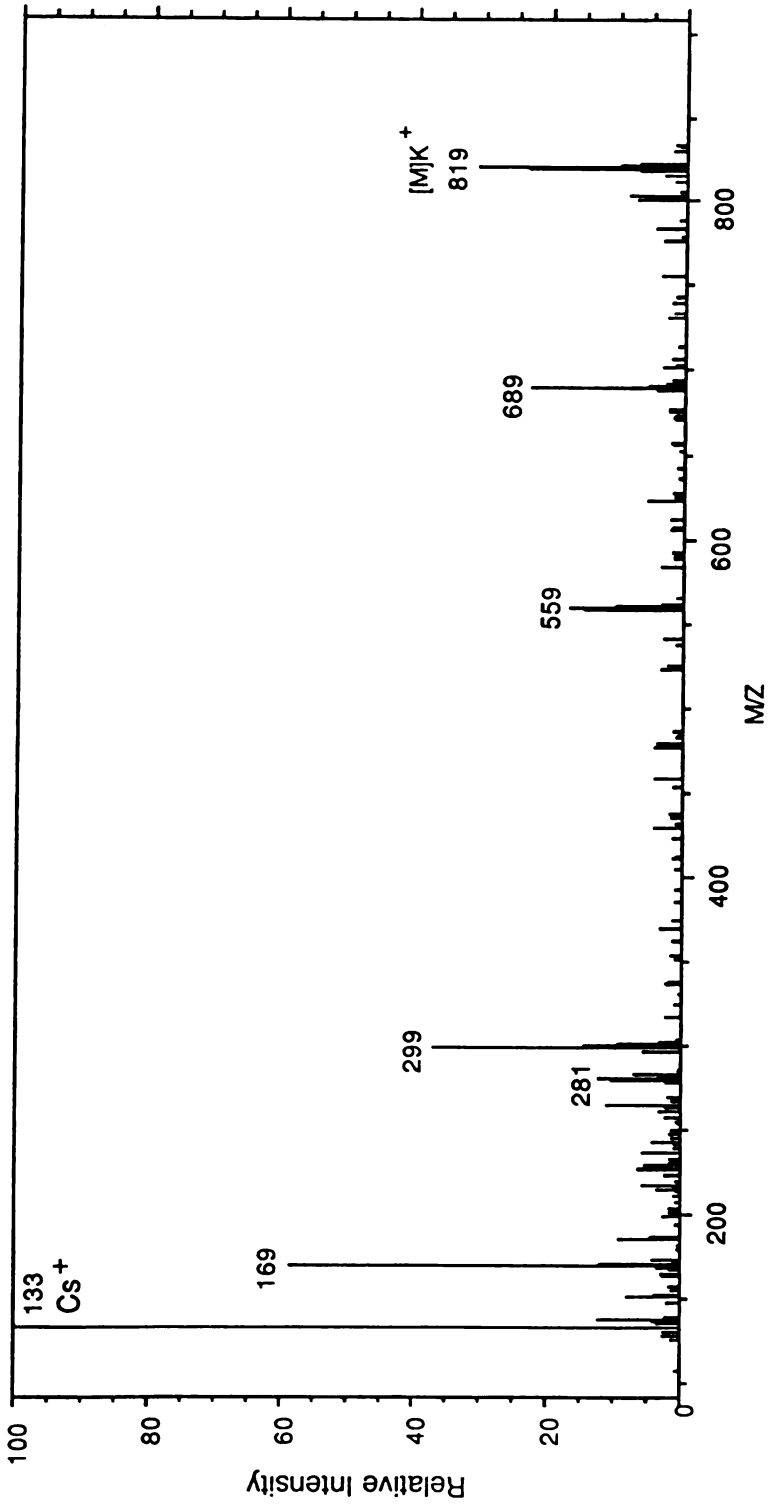

Figure 5.6. K^+ IDS mass spectrum of digoxin obtained on the JEOL HX-110 double-focusing mass spectrometer.

adduct ions and $[M]K^+$ ion are detected at the correct masses. This is most likely due to the fast scanning rate, pushing the limits of the magnet and the data system, and affecting the mass axis calibration. The major problem with the application of the K^+IDS technique to the JEOL HX-110 magnetic sector mass spectrometer is the scan rate limitation.

4. FINAL COMMENTS

The dynamic nature of the K^+IDS technique and the short-lived signals (less than one minute) makes it highly unlikely that implementation of this technique to the JEOL HX-110 double-focusing mass spectrometer will be a successful endeavor. The scan rates needed to observe the desorption of the analyte and the changes in the K^+IDS mass spectra with time are too great for the magnetic sector instrument to handle them with good results. The K^+IDS technique is more suited to quadrupole mass spectrometers or time-of-flight instruments that can handle scan rates of 1 scan/second or greater.

This application of K^+IDS to the HX-110 mass spectrometer may be useful in the study of mechanisms of ion formation and fragmentation of the FAB technique. Since K^+ ions only attach to neutral species and do not induce fragmentation, the formation of K^+ adduct ions provide information about the origin of fragmentation. Any thermal degradation products that are formed on the surface and desorb into the gas phase as neutrals should be observed as K^+ adduct ions. Whereas, any fragmentations induced by the initial protonation of the molecule will not be observed as K^+ adduct ions. This combination of K^+IDS with FAB may provide a way of determining whether fragmentations are occurring in the gas phase following protonation or prior to ionization during the desorption process. The K^+ emitter provides a good means of injecting a large flux of K^+ ions into the gas phase, a process which is required for the formation of K^+ adduct ions. Therefore, it may be beneficial to combine these two techniques to gain a better understanding of the mechanisms of fragmentation and ionization of FAB. The combination of the traditional FAB technique for desorption and K^+ adduct formation in the gas phase for ionization (K^+ chemical ionization) is currently being pursued in our lab.[5,6]

CHAPTER 6. FAB MASS SPECTROMETRIC ANALYSIS OF CARDIAC GLYCOSIDES.

1. INTRODUCTION

Interest in desorption ionization (DI) techniques and the understanding of the mechanisms of ionization and fragmentation led to a side project that utilizes FAB. One goal of this study was to gain a better understanding of a more traditional DI technique, FAB, compared to K^+IDS in terms of sample preparation, experimental procedures required, and the mass spectra obtained. Ultimately, a direct comparison of these two DI techniques in terms of mechanisms of ion formation and fragmentation would be ideal, but is beyond the scope of this minor research project. Since much work was done with cardiac glycosides utilizing the K^+IDS technique, these compounds were chosen for this comparative FAB study. The previous K^+IDS study of these biomolecules showed very interesting results as molecular weight and sequence information was easily obtainable from the K^+IDS mass spectra (Appendix B). However, K^+IDS is a technique that does not induce fragmentation upon ionization. All fragmentation occurs prior to ionization in the condensed phase and K^+ ions merely attach to the neutral species present in the gas phase. FAB, on the other hand, is a DI technique where ionization (protonation) often induces fragmentation which may lead to further structural information. Therefore, it was of interest to study the FAB mass spectra of the cardiac glycosides to investigate the types of fragmentation of these multifunctional compounds that occur with this DI technique and whether the mechanisms of fragmentation can be determined.

2. EXPERIMENTAL SECTION

The cardiac glycosides were obtained from Sigma Chemical Co., St. Louis, Mo. and were used without further purification. Acetyldigitoxin was purchased from ICN K&K Laboratories, Cleveland, OH. The samples were dissolved in methanol to concentrations of approximately 1μg/μl. One to two-μl aliquots were transferred to the FAB probe sample target and mixed with the glycerol matrix. The FAB analyses were performed on a JEOL HX-110 double-

focusing mass spectrometer of forward geometry with an accelerating voltage of 10kV and a FAB gun voltage of 6kV with Xe as the FAB gas.

3. RESULTS

A. POSITIVE FAB MASS SPECTRA OF SOME CARDIAC GLYCOSIDES

The structures of four of the cardiac glycosides studied are shown in Figure 6.1. Digoxin was chosen for a detailed mechanistic study due to its relative ease of ionization by FAB and the abundance of fragment ions observed with FAB. The goal was to determine if the information obtainable from a double-focusing mass spectrometer (i.e., peak matching, B/E linked scanning, and FAB) was sufficient for use in deducing the structural formulas of the ions and the fragmentation pathways. The results of this study are published and this article is presented in Appendix C. Many fragment ions are observed in the FAB mass spectrum of digoxin as seen in Figure 6.1. There are fragment ions representative of both ends of the molecule. However, the majority of the types of fragment ions of digoxin contain the aglycone portion of the molecule which suggests that this steroid structure may be directly involved in the ionization of this molecule and carries the charge in the fragment ions. Based on the results obtained from the linked scanning and peak matching experiments, it is determined that the majority of the fragment ions observed can be formed by remote site fragmentation of the protonated molecule with the charge localized on the aglycone portion of the molecule. Even though this seems to be the dominant mechanism of fragment ion formation, it is possible that some of the fragment ions which do not contain the aglycone could be the result of charge-initiated fragmentation from protonation of one of the glycosidic bonds. These mechanisms are explained in more detail in the article in Appendix C.

During the preliminary FAB study, FAB mass spectra of all the cardiac glycosides shown in Figure 6.1 were obtained. An analysis of these mass spectra, with comparison to the FAB mass spectrum of digoxin provide some interesting differences due to only minor differences in the structures of these compounds. Figure 6.2 contains the published FAB mass spectrum of digoxin to provide a basis for these comparisons. The proposed fragment ion assignments for digoxin, gitoxin, digitoxin, and acetyldigitoxin are given in

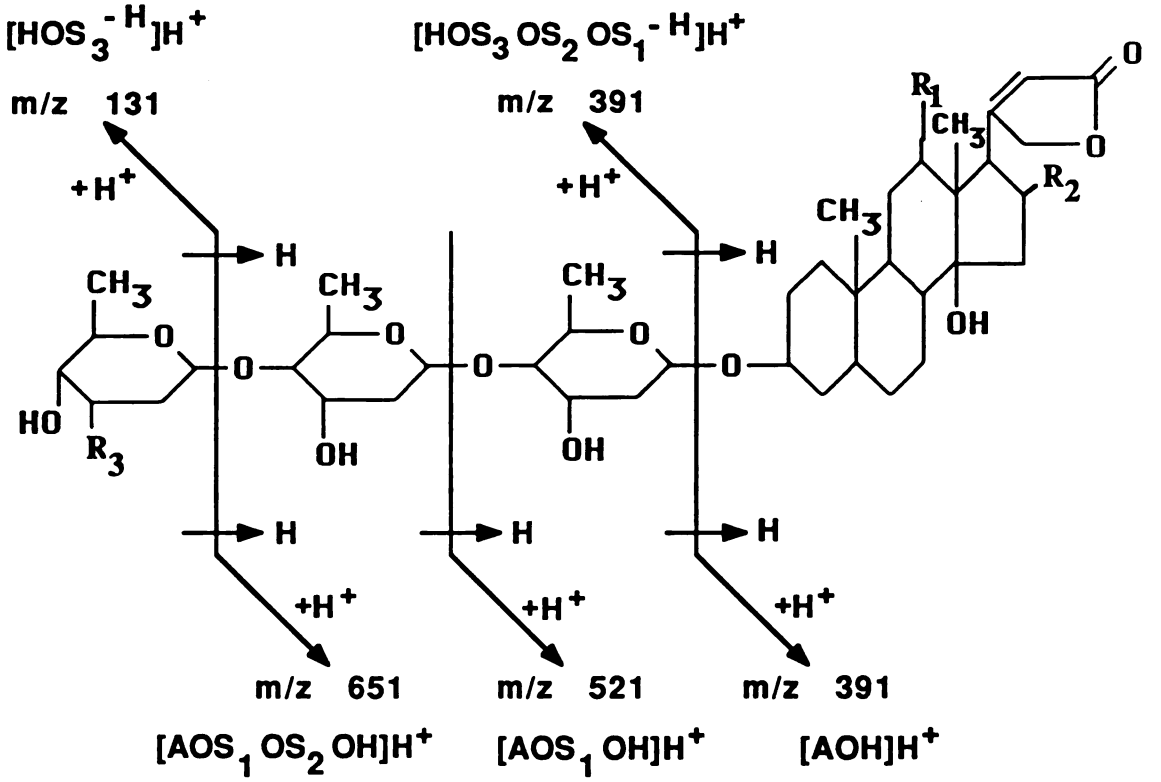

D=Digoxin
R_1= OH
R_2= H
R_3= OH

F=Acetyldigitoxin
R_1 = H
R_2= H
R_3= OAc

E=Digitoxin
R_1 = H
R_2= H
R_3= OH

G=Gitoxin
R_1 = H
R_2= OH
R_3= OH

Figure 6.1 Structure of digoxin and other similar cardiac glycosides studied. The fragmentations observed in the FAB mass spectrum of digoxin are labeled.

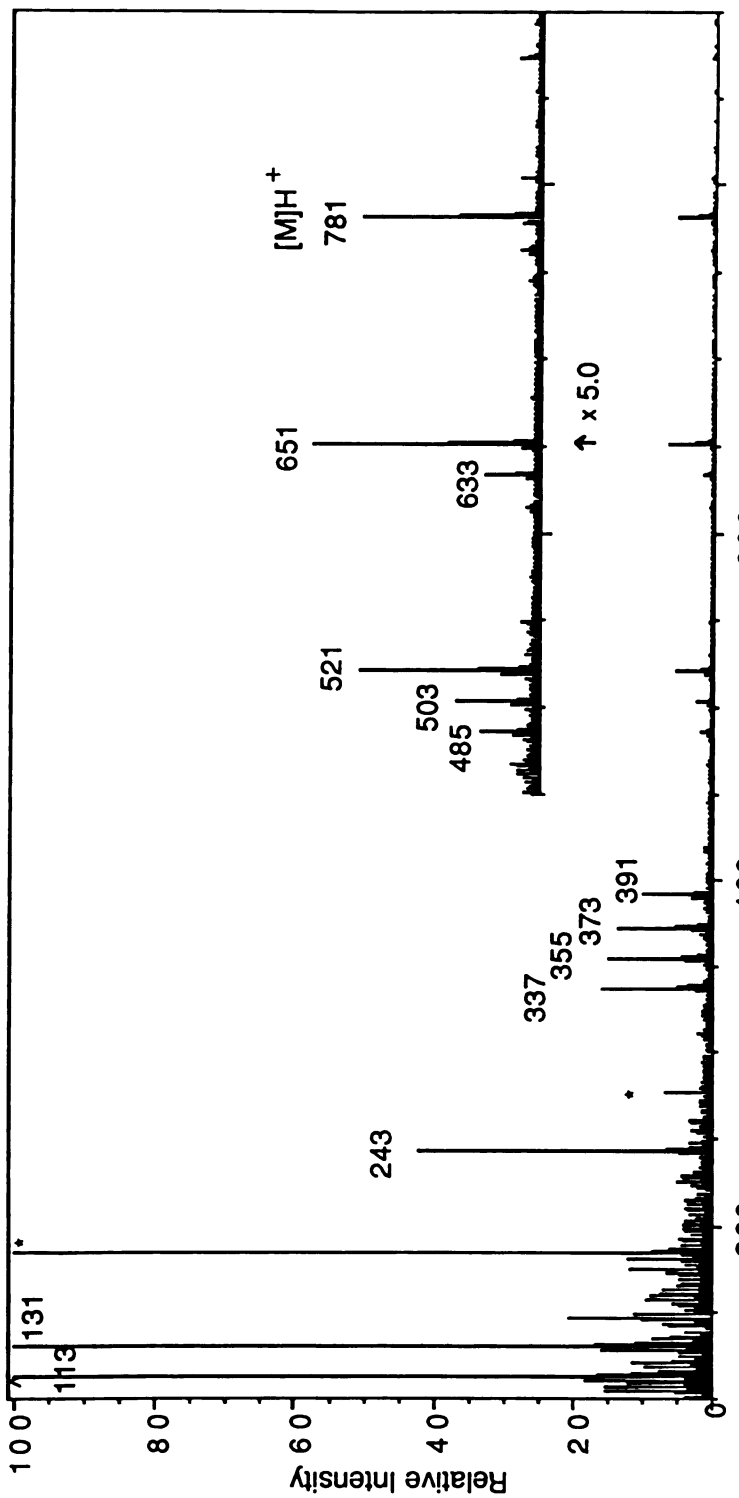

Figure 6.2 Positive FAB mass spectrum of digoxin. The glycerol cluster ions are denoted by *.

Table 6.1. The assignments are designated by the LKA nomenclature scheme, which is explained in detail in Appendix B.

TABLE 6.1 Fragment ion assignments for digoxin, digitoxin, gitoxin, and acetyldigitoxin.

Assignment[a]	m/z Value		
	digoxin and gitoxin	digitoxin	acetyldigitoxin
$[M]H^+$	781	765	807
$[AOS_1OS_2OH]H^+$	651	635	635
$[AOS_1OS_2OH\text{-}H_2O]H^+$	633	617	617
$[AOS_1OH]H^+$	531	505	505
$[AOS_1OH\text{-}H_2O]H^+$	513	487	487
$[AOH]H^+$	391	375	375
$[HOS_3OS_2OS_1\text{-}^{H}]H^+$	391	391	433
$[AOH\text{-}H_2O]H^+$	373	357	357
$[HOS_3OS_2OS_1\text{-}^{H}\text{-}H_2O]H^+$	373	373	415
$[AOH\text{-}2H_2O]H^+$	355	339	339
$[HOS_3OS_2OS_1\text{-}^{H}\text{-}2H_2O]H^+$	355	355	397/355[b]
$[AOH\text{-}3H_2O]H^+$	337	NA[c]	NA[c]
$[HOS_3OS_2OS_1\text{-}^{H}\text{-}3H_2O]H^+$	337	337	379/337
$[HOS_3OS_2\text{-}^{H}\text{-}H_2O]H^+$	243	243	285/243
$[HOS_3\text{-}^{H}]H^+$	131	131	173/131
$[HOS_3\text{-}^{H}\text{-}H_2O]H^+$	113	113	155/113

a. These assignments are based on the Light, Kassel, Allison (LKA) nomenclature scheme. For an explanation, see Appendix B.

b. There are two possible m/z values for this fragment ion with and without the acetyl group on the terminal sugar.

c. This fragment is not applicable to the compound. Digitoxin can not lose $3H_2O$ from its aglycone since there are only 2OH groups present.

The FAB mass spectrum of gitoxin is shown in Figure 6.3. This compound has the same molecular weight as digoxin, but varies in the position of one -OH group on the aglycone, as shown in Figure 6.1. The $[M]H^+$ ion of gitoxin is present in the FAB mass spectrum at m/z 781. There is less fragmentation (lower abundance of fragment ions) of gitoxin, where the retention of the charge is on the aglycone, than was observed in Figure 6.2 for

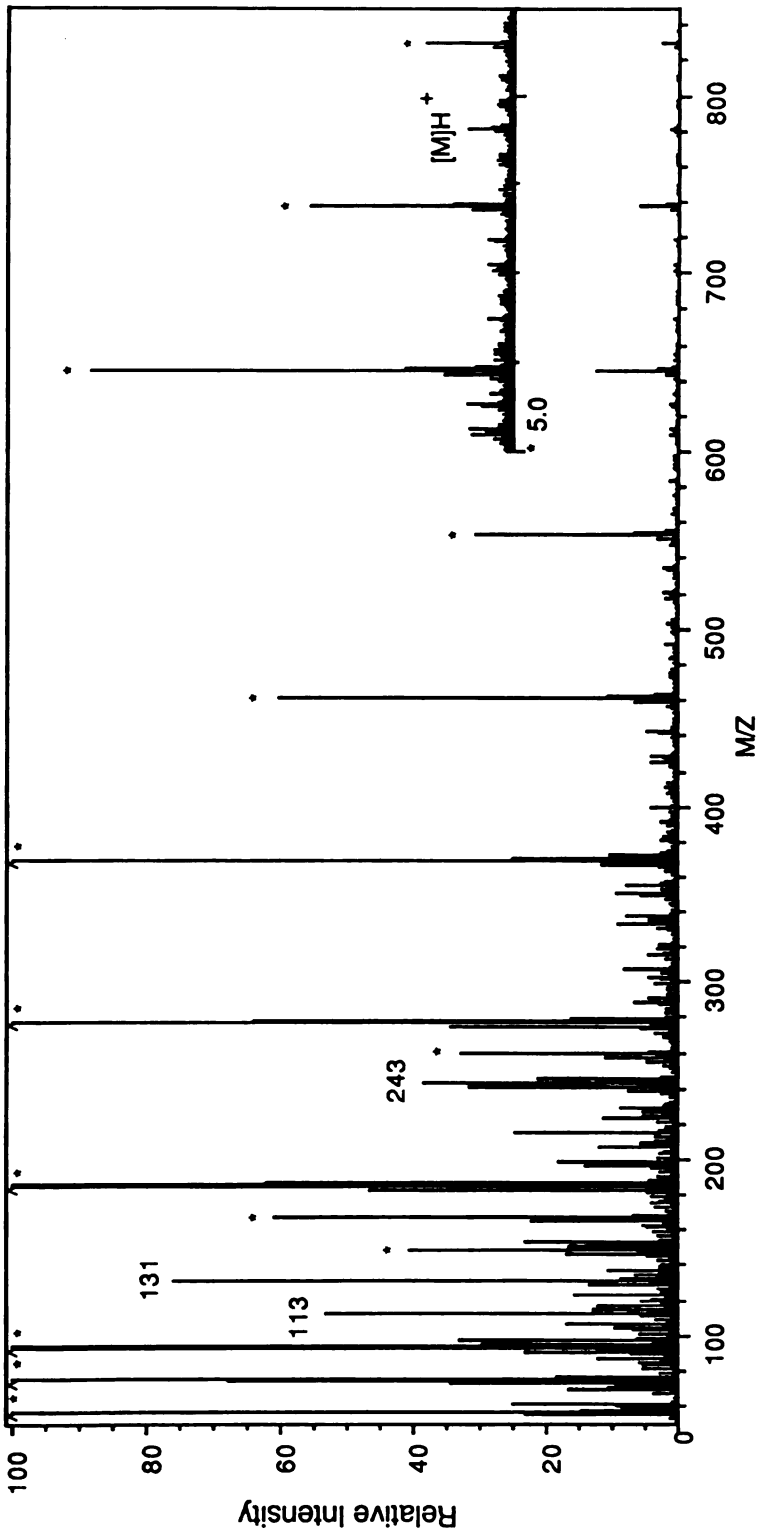

Figure 6.3 Positive FAB mass spectrum of gitoxin. The glycerol cluster ions are denoted by *.

digoxin. The low-mass fragment ions, with charge retention on the sugar portion of the molecule, are observed in the gitoxin spectrum. It should be noted that while concentrations of the cardiac glycosides in solution that are used in this preliminary study are approximately equal, the ratio of sample solution to glycerol matrix is not accurately controlled. Therefore, among these cardiac glycoside FAB mass spectra, the ratio of peaks representing matrix ions to sample ions (both molecular and fragment) may vary between different spectra. The fragment ion abundance vs. molecular ion abundance of one mass spectrum can be compared to the same abundance ratio for another compound.

The FAB mass spectrum of another similar cardiac glycoside, digitoxin, is shown in Figure 6.4. This compound differs from digoxin in that it has one less -OH group on the aglycone and, hence, the molecular weight is 16 daltons lower. The mass spectrum of digitoxin does contain a peak at m/z 765 representing the $[M]H^+$ ion. The "mass symmetry" that is present in the digoxin molecule between the aglycone and the sugars does not exist for digitoxin. Therefore, the series of fragment ions in the 300-400 dalton mass range, that each had two structural assignments for digoxin, are now split by 16 daltons due to the difference in the aglycone. Each fragment ion in the 300-400 dalton mass range in the digitoxin mass spectrum has one structural assignment and is less abundant than the corresponding doublet fragment ion in the mass spectrum of digoxin which has two structural assignments. For example, the peak at m/z 373 in the FAB mass spectrum of digoxin has two structural assignments. In the digitoxin FAB mass spectrum, one of these stuctures is respresented by a peak at m/z 373, while the other is represented by a peak 16 daltons lower at m/z 357. The low-mass sugar ions of m/z 113, m/z 131, and m/z 243 are present in the mass spectrum of digitoxin as they are for digoxin.

Acetyldigitoxin is another cardiac glycoside that is similar to digitoxin except for the presence of an acetyl group on the terminal sugar (digitoxose). The structure is shown in Figure 6.1 and the FAB mass spectrum of acetyldigitoxin is given in Figure 6.5. The peak at m/z 807 represents the $[M]H^+$ ion and the peaks at m/z 635 and m/z 505 are representative of the loss of one and two sugars from the compound, with charge retention on the aglycone. The ion of m/z 415 represents the structure $[HOS_3OS_2OS_1{}^{-H}\text{-}H_2O]H^+$ where S_3 contains the acetyl group. There are no peaks observed in the mass

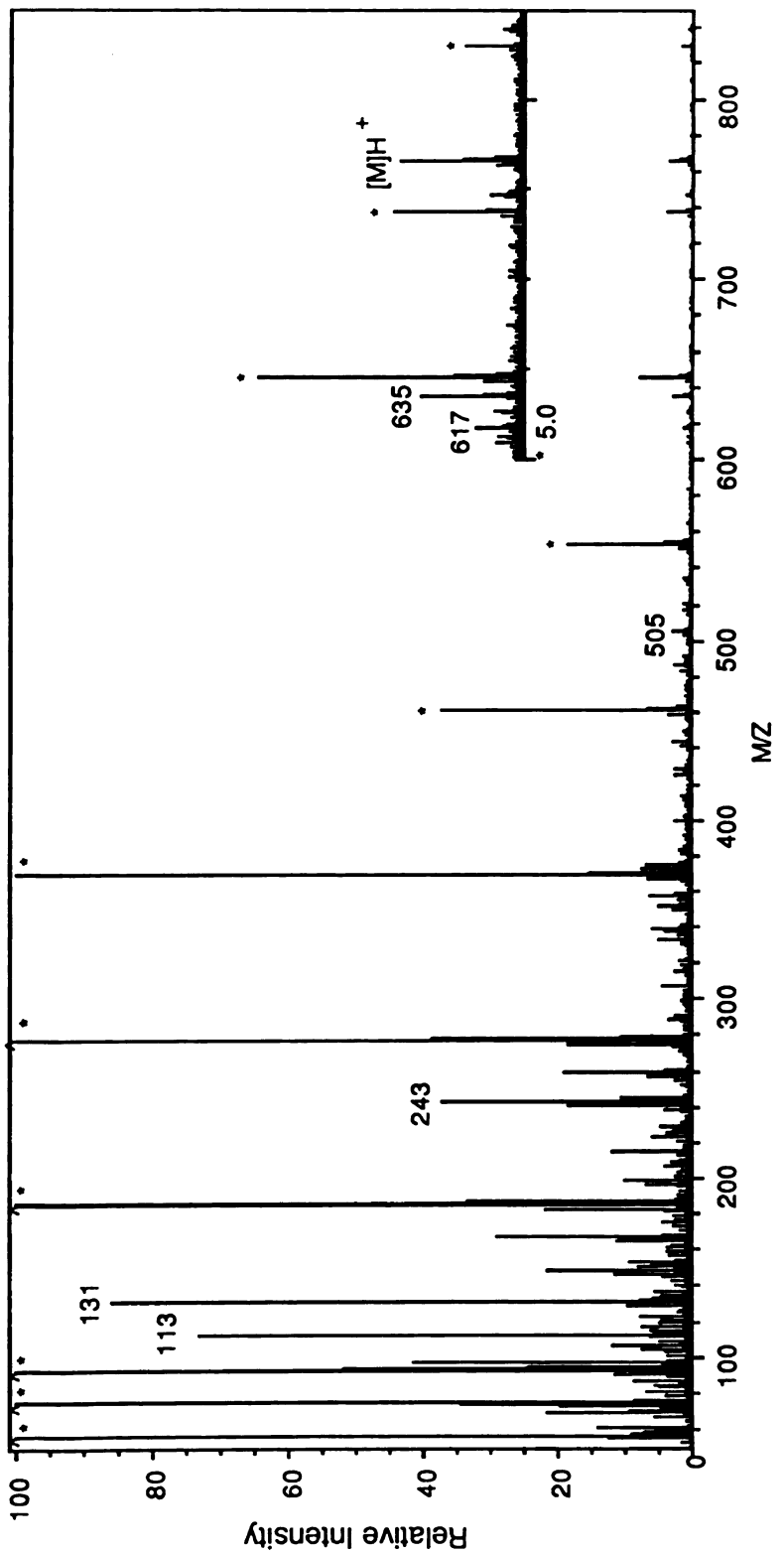

Figure 6.4 Positive FAB mass spectrum of digitoxin. The glycerol cluster ions are denoted by *.

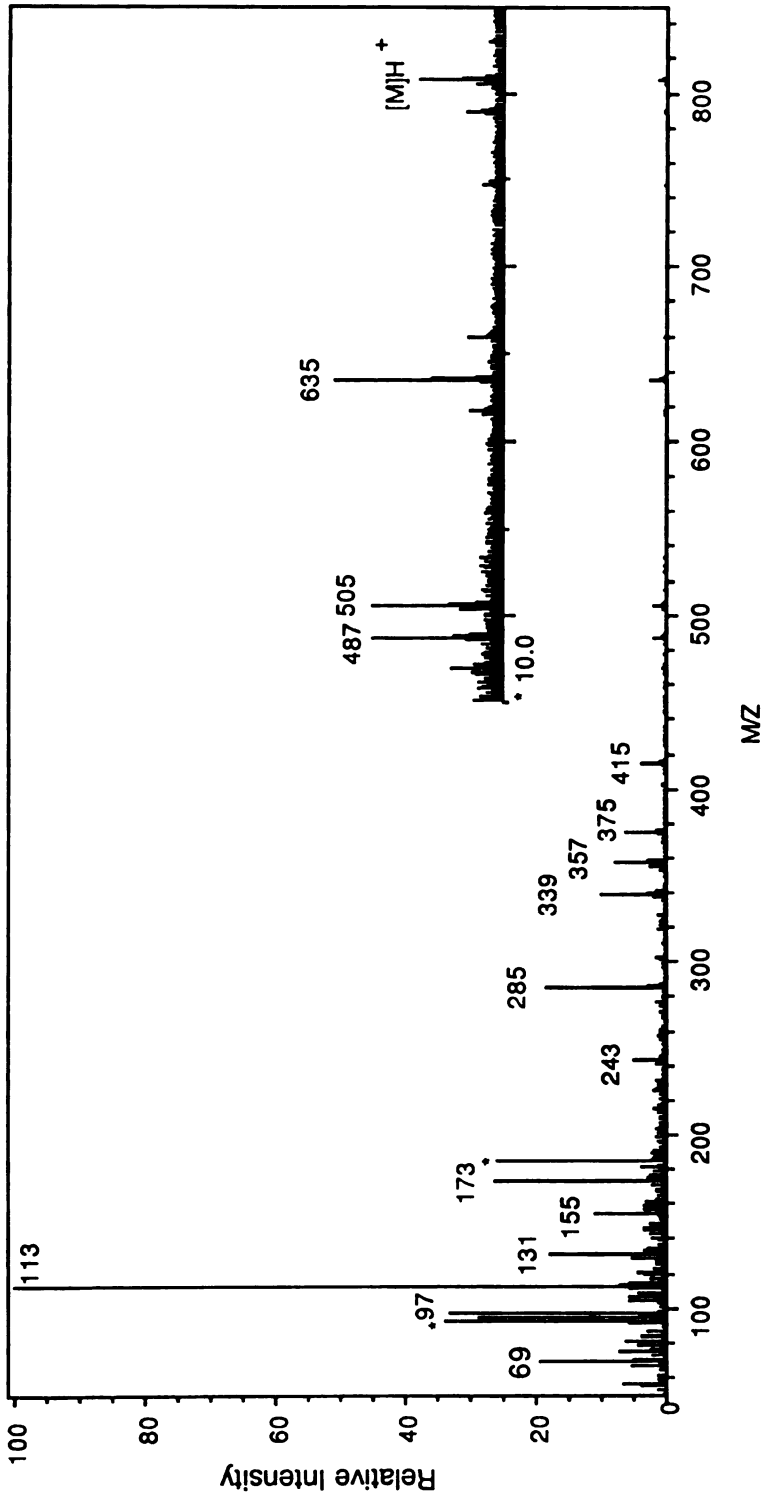

Figure 6.5 Positive FAB mass spectrum of acetyldigitoxin. The glycerol cluster ions are denoted by *.

spectrum that represent H_2O losses from this peak at m/z 415. The aglycone fragment $[AOH]H^+$ is observed as a peak at m/z 375 and does exhibit water loss that is represented by peaks at m/z 357 and m/z 339. The peak at m/z 285 represents a sugar ion that contains the acetyl group on the terminal sugar, with a structure $[HOS_3OS_2{}^{-H}\text{-}H_2O]H^+$. This fragment is also represented by the peak at m/z 243 without the acetyl group in which case the "H_2O" loss is the acetylated hydroxy group on the terminal sugar. The peaks representative of a single sugar are observed at m/z 113 and 131 when no acetyl group is present and at m/z 155 and 173 when the acetyl group is present on the sugar moiety.

The minor differences in the structures of these cardiac glycosides created observable differences in the FAB mass spectra in comparison to digoxin. For all of these compounds, peaks representing an $[M]H^+$ ion and basically the same fragment ions were observed in the FAB mass spectra. However, the structural differences did seem to affect the overall desorption ionization efficiency of the sample, as the relative intensities of the peaks representing the $[M]H^+$ ions differed. Many of the differences observed were due to mass shifts caused by the structural changes. Other noticeable differences were in the relative intensities of peaks representing the fragment ions from dehydration products. More detailed mechanistic studies of these other cardiac glycosides need to be performed before many conclusions can be drawn based on these preliminary observations.

B. NEGATIVE FAB MASS SPECTRA

The negative FAB mass spectra of digoxin and ouabain were obtained for preliminary comparison of the behavior of cardiac glycoside compounds under conditions of negative vs. positive ion formation. Similar studies of both positive and negative FAB mass spectra of cardiac glycosides utilizing different FAB matrices have been performed by Pare et al.[57] Figure 6.6 shows the negative FAB mass spectrum of digoxin. The peak at m/z 779 corresponds to the $[M\text{-}H]^-$ ion, which is more intense in this mass spectrum than the corresponding peak at m/z 781 representing the $[M]H^+$ ion in the positive FAB mass spectrum (Figure 6.2). This suggests that ionization occurs more readily in the negative ion mode and/or subsequent fragmentation is less prevalent. The fragmentations at the glycosidic bonds, with charge retention on the aglycone-containing portion, are observed at m/z 649 and m/z 519 in the

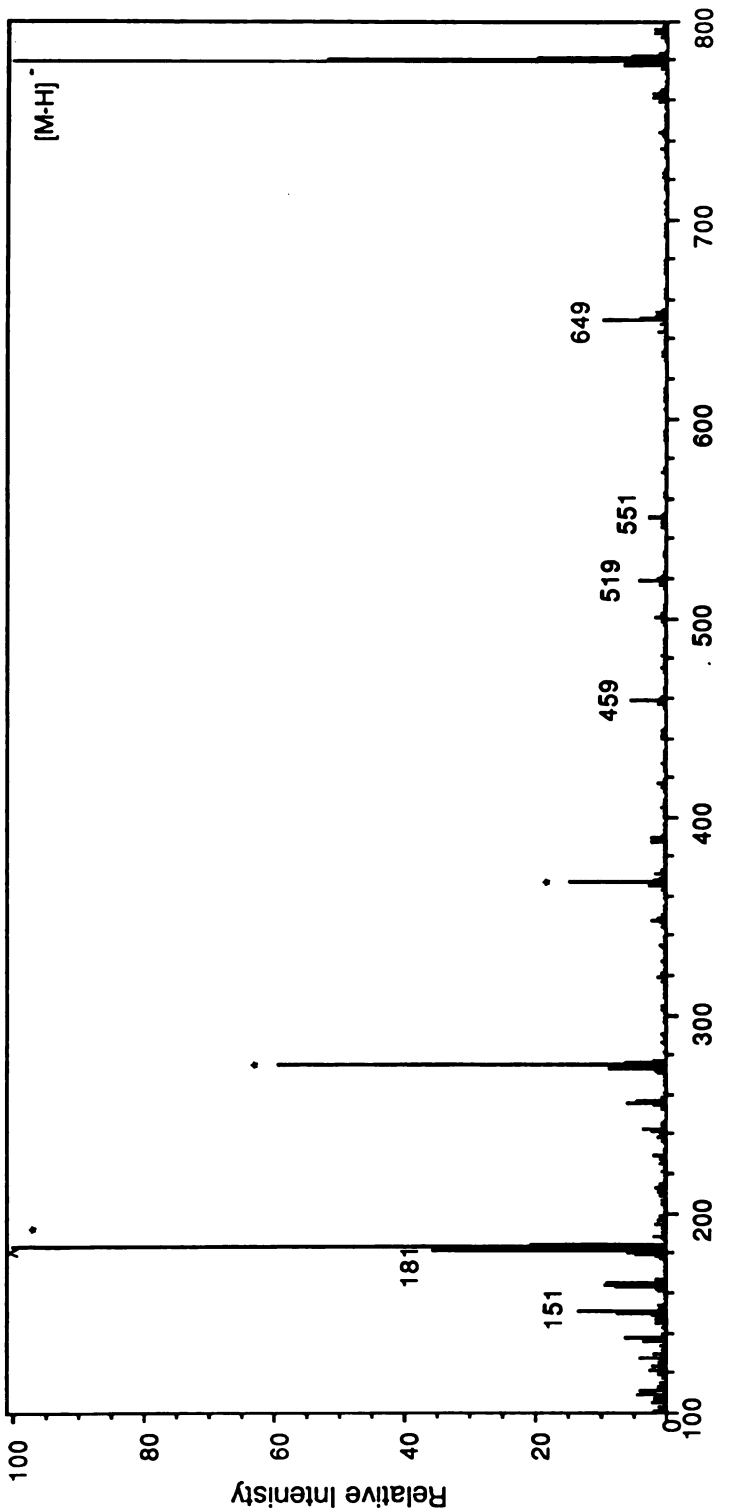

Figure 6.6 Negative FAB mass spectrum of digoxin. The glycerol cluster ions are denoted by *.

negative FAB mass spectrum. The low-mass sugar ions, which are very abundant in the positive mode, are practically non-existent in the negative mode. This suggests there may be interesting differences in ion formation and fragmentation between the negative FAB and positive FAB mass spectrometric analysis of digoxin, and suggests the need for a similar mechanistic study of digoxin to be carried out in the negative mode as was presented in Appendix C for digoxin in the positive mode.

Another cardiac glycoside for which both positive and negative FAB mass spectra were obtained is ouabain. The structure of this compound is shown in Figure 6.7. This cardiac glycoside contains only one sugar and the aglycone contains many more functional groups than the aglycone of digoxin. The positive ion mass spectrum of ouabain is shown in Figure 6.8 and the negative ion mass spectrum is shown in Figure 6.9. The m/z values and possible assignments of the analyte ions observed in both the positive and negative FAB mass spectra of ouabain are given in Table 6.2.

Table 6.2. Fragment ions observed in the positive and negative FAB mass spectra of ouabain and possible assignments based on the LKA nomenclature (see Appendix B).

Positive Ion FAB Mass Spectrum		Negative Ion FAB Mass Spectrum	
Assignment	m/z	m/z	Assignment
$[M]H^+$ or $[AOS_1OH]H^+$	585	583	$[M-H]^-$ or $[AOS_1O]^-$
$[AOH]H^+$	439	437	$[AO]^-$
$[A^{-H}]H^+$	421	419	$[A^{-2H}]^-$
$[A^{-H}-H_2O]H^+$	403	401	$[A^{-2H}-H_2O]^-$
$[A^{-H}-2H_2O]H^+$	385	383	$[A^{-2H}-2H_2O]^-$
$[A^{-H}-H_2O-OCH_2]H^+$	373	371	$[A^{-2H}-H_2O-OCH_2]^-$
$[A^{-H}-3H_2O]H^+$	367	369*	$[A^{-2H}-H_2O-CH_3OH]^-$
$[A^{-H}-2H_2O-OCH_2]H^+$	355	353	$[A^{-2H}-2H_2O-OCH_2]^-$
$[A^{-H}-4H_2O]H^+$	349	347	$[A^{-2H}-4H_2O]^-$
$[A^{-H}-3H_2O-OCH_2]H^+$	337	331	$[A^{-2H}-3H_2O-OCH_2]^-$
$[A^{-H}-4H_2O-OCH_2]H^+$	319	319	$[A^{-2H}-4H_2O-OCH_2]^-$
		163	$[HOSO]^-$

* There are several ions near this m/z value in the negative FAB spectrum shown in Figure 6.9 that may provide structural information. The assignment provided for the ion of m/z 369 is only proposed as one possible assignment.

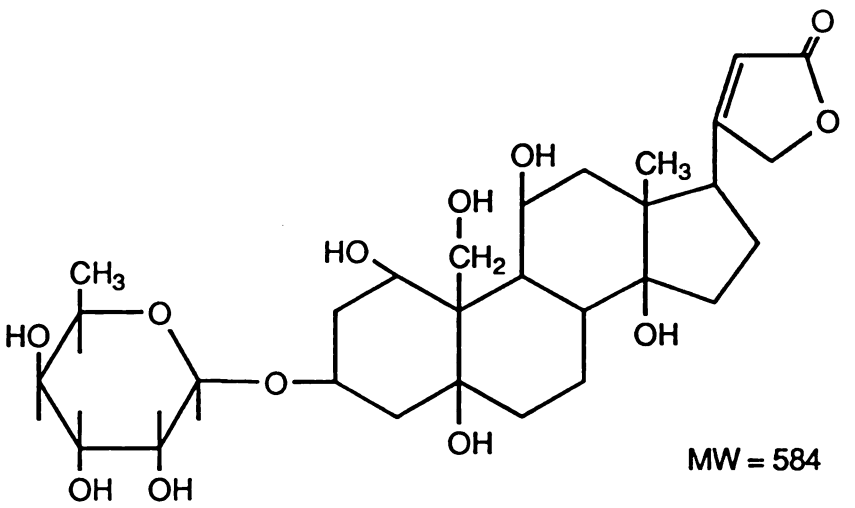

Figure 6.7 Structure of ouabain.

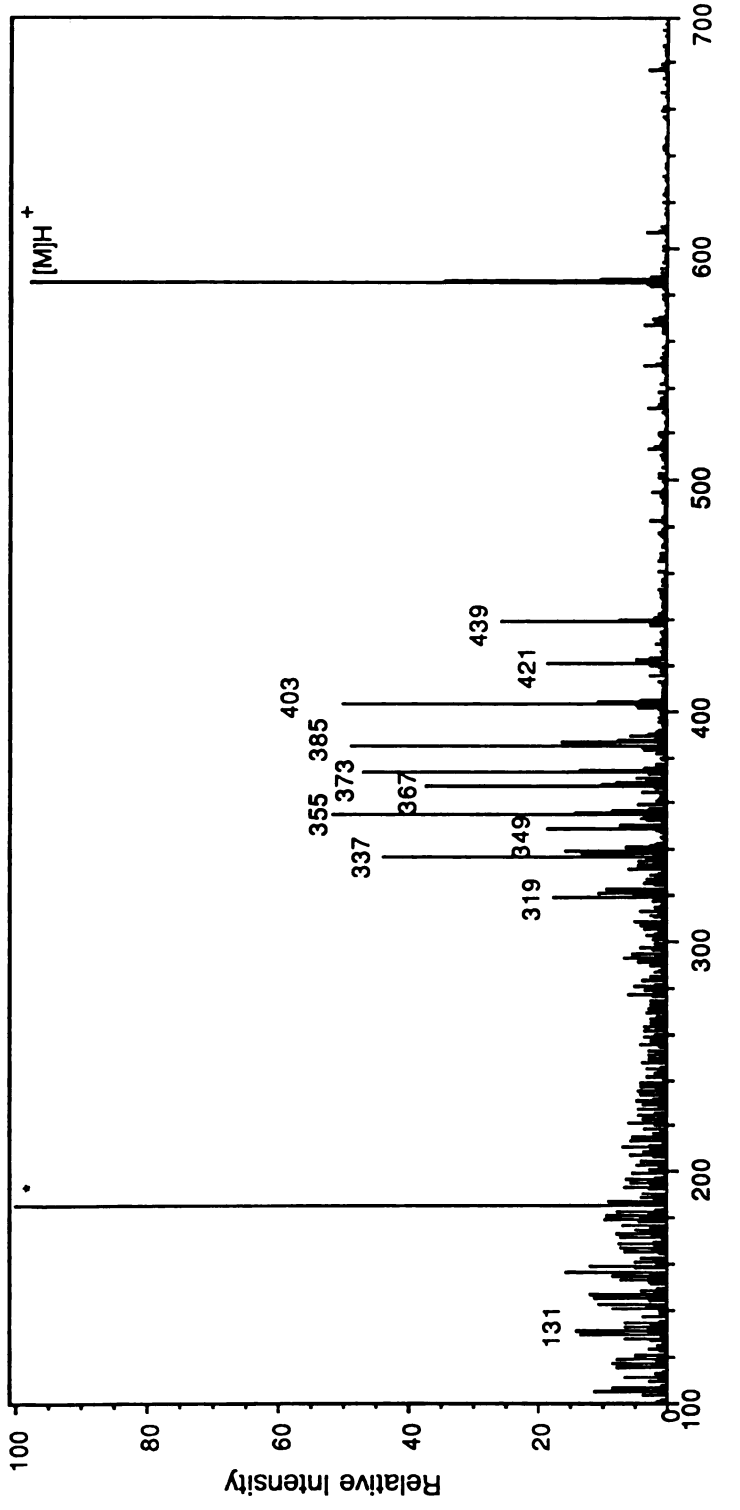

Figure 6.8 Positive FAB mass spectrum of ouabain. The glycerol cluster ions are denoted by *.

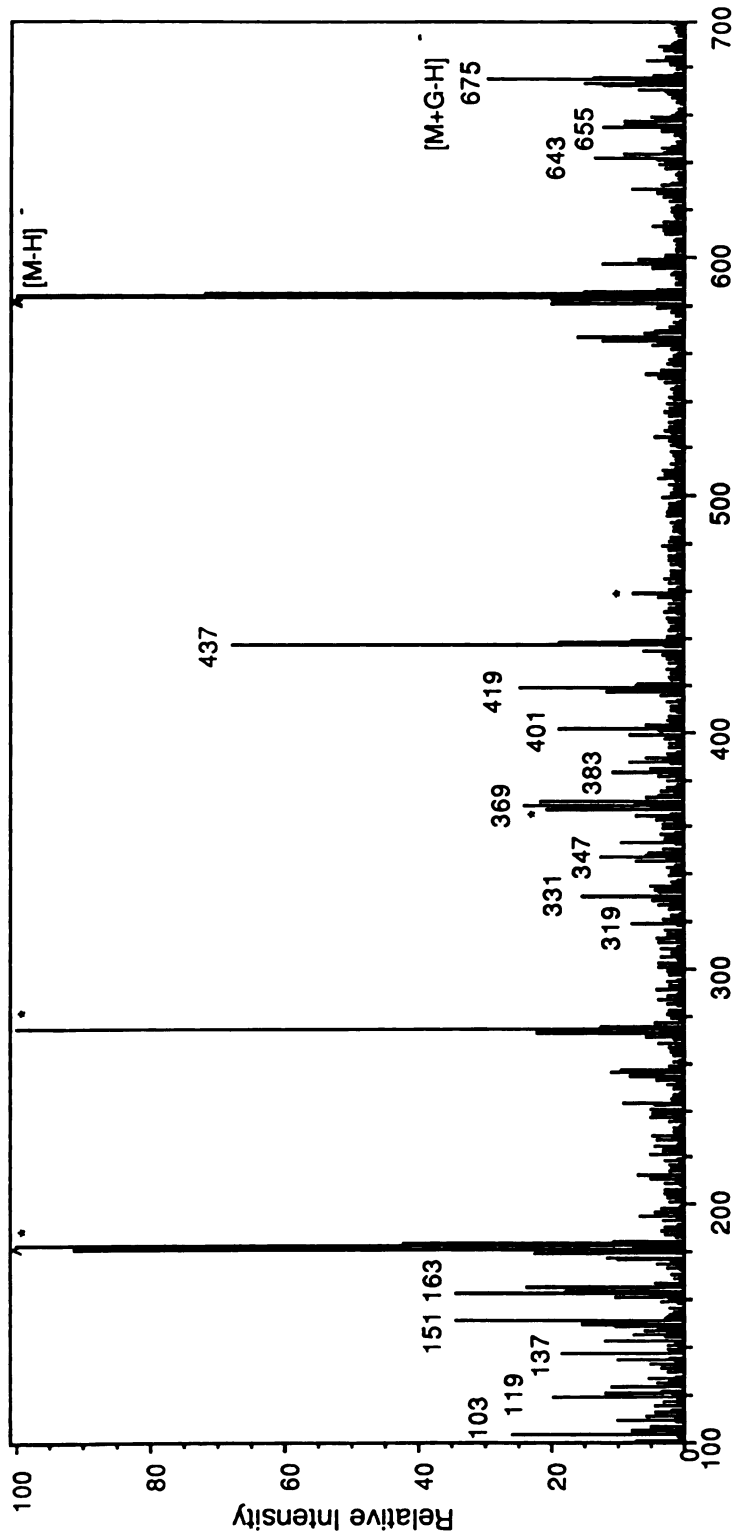

Figure 6.9 Negative FAB mass spectrum of ouabain. The glycerol cluster ions are denoted by *.

In the positive ion mass spectrum, there is a peak representing the $[M]H^+$ ion, and much fragmentation of the aglycone is observed in the m/z 300-400 dalton mass range. These fragment ions are probably from multiple dehydrations and loss of the functional groups of the aglycone. Very few low-mass sugar ions are observable to a significant extent. In the negative FAB mass spectrum, there is an intense peak at m/z 581 representing the $[M-H]^-$ ion. The same fragment ions from dehydration of the aglycone are present, but they have a lower relative abundance than those in the positive ion mode. The negative mass spectrum does, however, contain low-mass fragment ions from the sugar portion of the compound. The peak at m/z 369 in the negative FAB mass spectrum does not fit the pattern with the rest of the fragment peaks that are 2 daltons lower than corresponding positive ion fragments. It appears that there is some different mechanism in operation for the formation of this fragment ion. There are several peaks in this mass range of 365-371 daltons that may provide structural information. However, before "over-analysis" of these results is attempted these experiments should be repeated for verification.

IV. SUMMARY

The positive FAB mass spectra of the cardiac glycosides contained some very interesting differences due to slight structural variances. Understanding how these structural differences are responsible for the changes in the FAB mass spectra requires more detailed studies similar to the one completed with digoxin, which is presented in Appendix C. One interesting observation made from these FAB experiments is the static nature of the FAB mass spectra over the long-lived signals (> 15 minutes). This is in contrast to the K^+IDS mass spectra where the spectra often change with time and the signals are very short-lived (< one minute). There appear to be more variables to control in the K^+IDS technique, such as current and bias voltage applied to the emitter and the distance of the sample from the emitter, that may affect the mass spectra obtained and possibly increase the information obtainable. For instance, as described in Chapter 2, the order in which fragmentations and desorption of the intact molecule occur may provide some insight into the nature of those fragmentations or the corresponding products formed. FAB has few variables that can be changed to alter the mass spectra

obtained. The main variable is the matrix used which primarily affects the ionization efficiency and the longevity of the signal. Changing the matrix used for FAB does not change the fragment ions observed or the overall appearance of the FAB mass spectrum. Therefore, K^+IDS may have an advantage over the FAB technique in that several variables can be used to modify the mass spectra obtained for the desired results. This is contigent, however, on the ability to control all of these variables of the K^+IDS technique.

From these preliminary negative FAB mass spectra of digoxin and ouabain, it appears that there may be some interesting differences between positive and negative ion formation of the cardiac glycosides by FAB ionization. It may prove interesting to try some other matrices, that may be more amenable to formation of the $[M-H]^-$ ions of these molecules, such as triethanolamine (TEA) which is often used as a matrix for negative FAB. Also, the ratios of sample to matrix can be adjusted to obtain the optimum sample ion formation and fragmentation.

APPENDIX A

Plots of K^+ adduct ion abundance vs. sample filament wire temperature (K).

Figure A1. Abundance of fragment adduct ions of met-enkephalin vs. sample filament wire temperature (K).

Figure A2. Abundance of fragment adduct ions of met-enkephalin vs. sample filament wire temperature (K).

Figure A3. Abundance of fragment adduct ions of met-enkephalin vs. sample filament wire temperature (K).

Figure A4. Abundance of fragment adduct ions of leu-enkephalin vs. sample filament wire temperature (K).

Figure A5. Abundance of fragment adduct ions of leu-enkephalin vs. sample filament wire temperature (K).

Figure A6. Abundance of the $[M]K^+$ ion of sucrose vs. sample filament wire temperature (K).

Figure A7. Abundance of the $[M]K^+$ ion of sucrose vs. sample filament wire temperature (K).

Figure A8. Abundance of the K^+ adduct ions of melezitose vs. sample filament wire temperature (K).

Figure A9. Abundance of the K^+ adduct ions of melezitose vs. sample filament wire temperature (K).

Figure A10. Abundance of the K^+ adduct ions of melezitose vs. sample filament wire temperature (K).

Figure A11. Abundance of the K^+ adduct ions of melezitose vs. sample filament wire temperature (K).

Figure A12. Abundance of the K^+ adduct ions of melezitose vs. sample filament wire temperature (K).

Figure A13. Abundance of the K^+ adduct ions of melezitose vs. sample filament wire temperature (K).

Figure A14. Abundance of the K^+ adduct ions of melezitose vs. sample filament wire temperature (K).

Figure A15. Abundance of the K^+ adduct ions of melezitose vs. sample filament wire temperature (K).

Figure A16. Abundance of the $[M]K^+$ ions of sucrose and melezitose vs. sample filament wire temperature (K).

Figure A17. Abundance of the $[M]K^+$ ions of sucrose and melezitose vs. sample filament wire temperature (K).

Figure A18. Abundance of the $[M]K^+$ ion of palmitic acid vs. sample filament wire temperature (K).

Figure A19. Abundance of the $[M]K^+$ ion of palmitic acid vs. sample filament wire temperature (K).

Figure A20. Abundance of the $[M]K^+$ ions of palmitic acid, sucrose, and melezitose vs. sample filament wire temperature (K).

Figure A21. Abundance of the $[M]K^+$ ions of palmitic acid, sucrose, and melezitose vs. sample filament wire temperature (K).

Figure A22. Abundance of the $[M]K^+$ ion of glycerol vs. sample filament wire temperature (K).

Figure A23. Abundance of the $[M]K^+$ ion of glycerol vs. sample filament wire temperature (K).

Figure A24. Abundance of the $[M]K^+$ ion of triethylene glycol vs. sample filament wire temperature (K).

Figure A25. Abundance of the $[M]K^+$ ion of triethylene glycol vs. sample filament wire temperature (K).

Activation energy determinations based on plots of K^+ adduct ion abundance vs. 1/T

Figure A26. Ea determinations from the Arrhenius plot of the abundance of m/z 392 of met-enkephalin vs. 1/T.

Figure A27. Abundance of the $[M]K^+$ ion of palmitic acid vs. 1/T. Ea calculatedd from the slope = 23 kcal/mol.

Figure A28. Abundance of the $[M]K^+$ ion of palmitic acid vs. 1/T. Ea calculated = 4 kcal/mol.

Figure A29. Abundance of the $[M]K^+$ ion of glycerol vs. 1/T (K).

Figure A30. Abundance of the $[M]K^+$ ion of glycerol vs. 1/T (K).

Figure A31. Abundance of the $[M]K^+$ ion of glycerol vs. 1/T (K).

Activation energy determinations based on plots of ln(ln(Ao/At)) vs. 1/T.

Figure A32. Arrhenius plot of ln(ln(Ao/At)) vs. 1/T for the $[M]K^+$ ion of palmitic acid. Ea calculated = 14 kcal/mol.

Figure A33. Arrhenius plot of ln(ln(Ao/At)) vs. 1/T for the $[M]K^+$ ion and a K^+ adduct ion of a fragment of melezitose. Ea(543) = 22 kcal/mol and Ea(363) = 47 kcal/mol.

Figure A34. Arrhenius plot of ln(ln(Ao/At)) vs. 1/T for the $[M]K^+$ ion and a K^+ adduct ion of a fragment of melezitose. Ea(543) = 35 kcal/mol and Ea(363) = 40 kcal/mol.

Figure A35. Arrhenius plot of ln(ln(Ao/At)) vs. 1/T for the $[M]K^+$ ion and a K^+ adduct ion of a fragment of melezitose. Ea(543) = 41 kcal/mol and Ea(363) = 47 kcal/mol.

Figure A36. Arrhenius plot of ln(ln(Ao/At)) vs. 1/T for the $[M]K^+$ ions of melezitose (m/z 543) and sucrose (m/z 381). Ea(543) = 20 kcal/mol and Ea(381) = 15 kcal/mol.

Figure A37. Arrhenius plot of ln(ln(Ao/At)) vs. 1/T for the m/z 392 fragment adduct ion of met-enkephalin. Ea calculated = 37kcal/mol.

Sample Li^+IDS mass spectra.

Figure A38. Li^+IDS mass spectrum of polyethylene glycol 600 averaged over scans 30-55.

Figure A39. Plot of the Li^+IDS mass spectra of polyethylene glycol 600 vs. scan number.

Figure A40. Li^+IDS mass spectrum of methionine-enkephalin.

Figure A41. Li^+IDS mass spectrum of triphenylamine.

Figure A42. Li^+IDS mass spectrum of violuric acid.

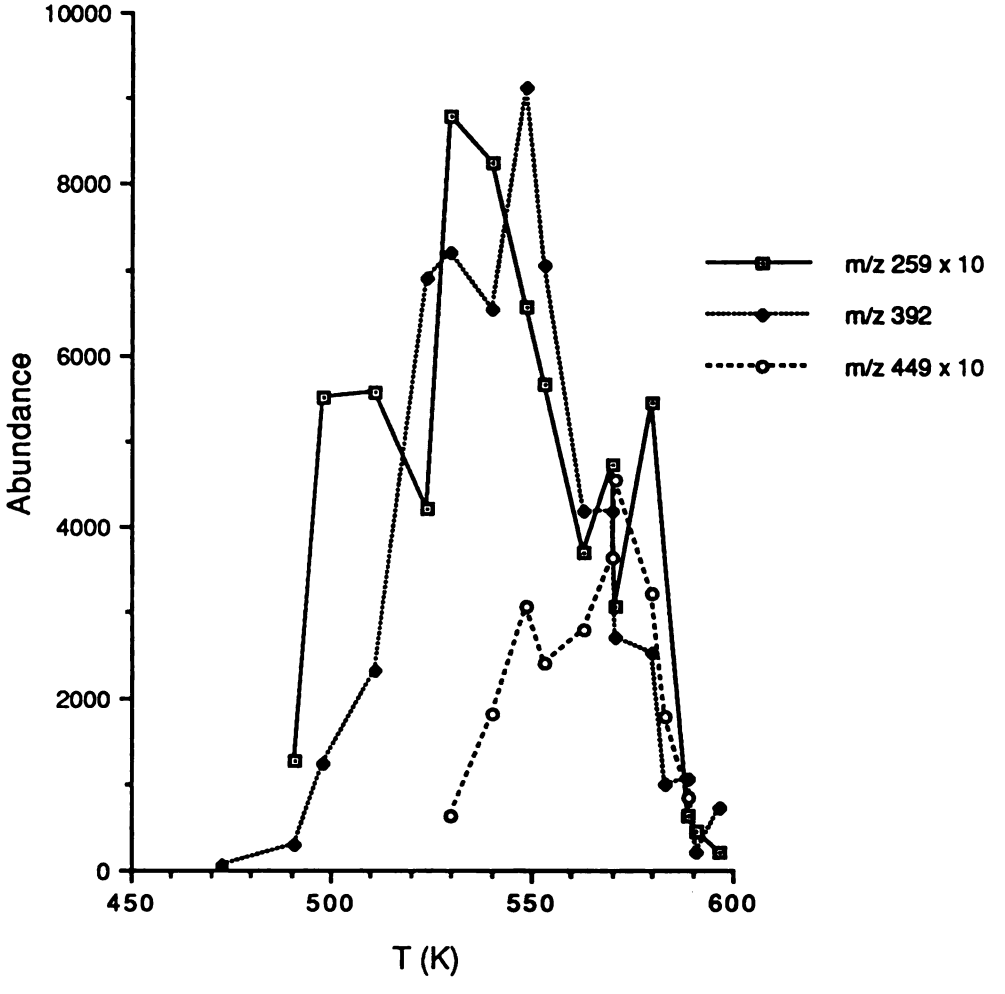

Figure A1. Abundance of fragment adduct ions of met-enkephalin vs. sample filament wire temperature (K).

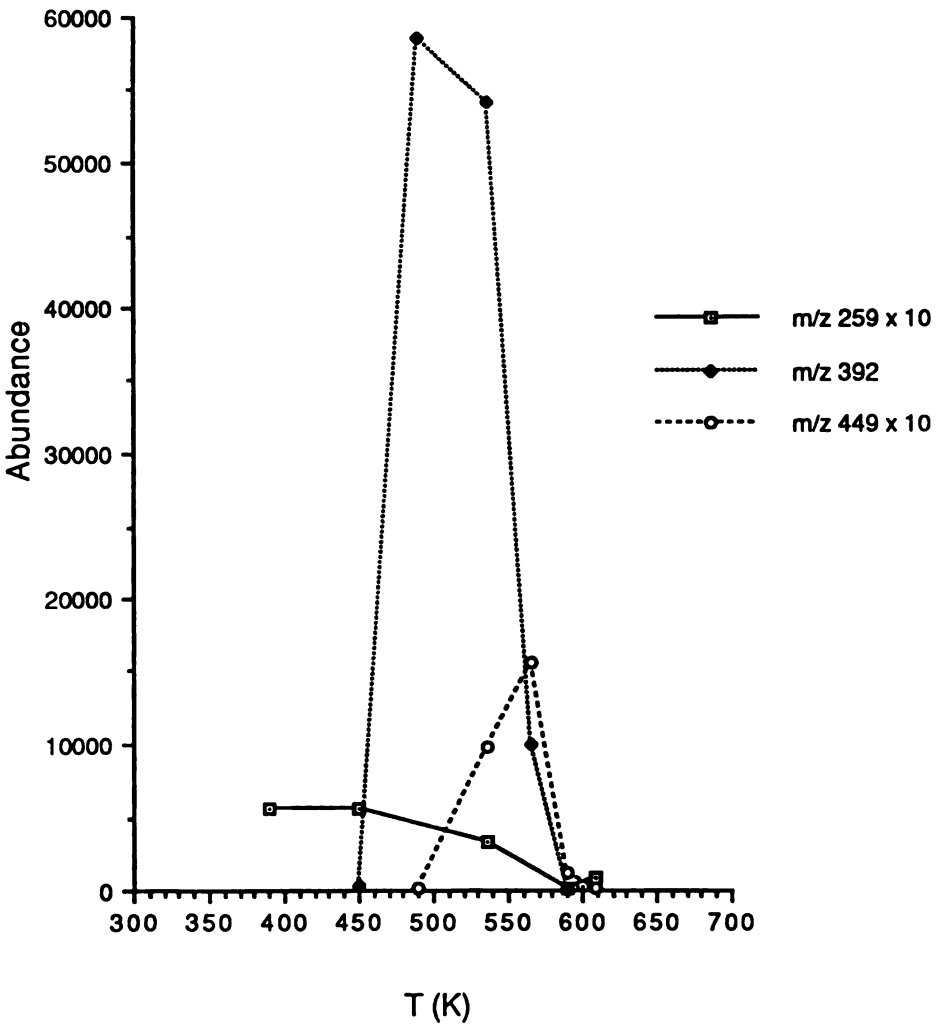

Figure A2. Abundance of fragment adduct ions of met-enkephalin vs. sample filament wire temperature (K).

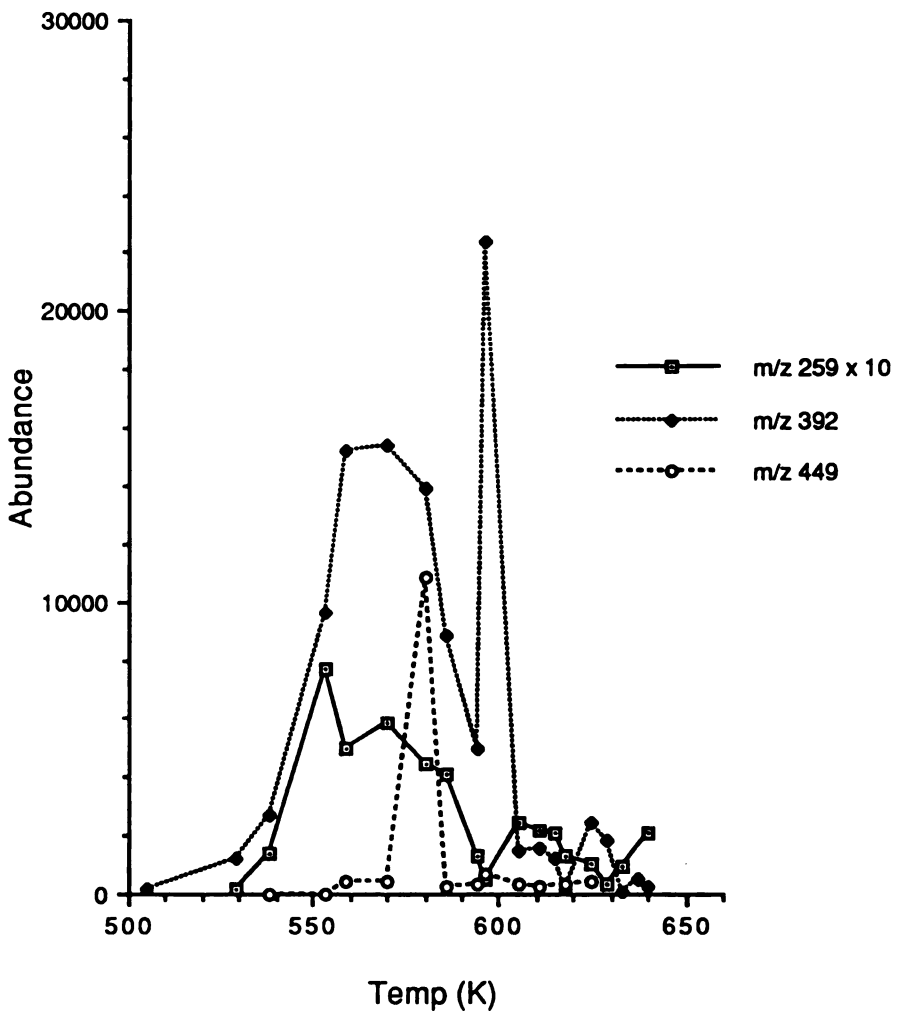

Figure A3. Abundance of fragment adduct ions of met-enkephalin vs. sample filament wire temperature (K).

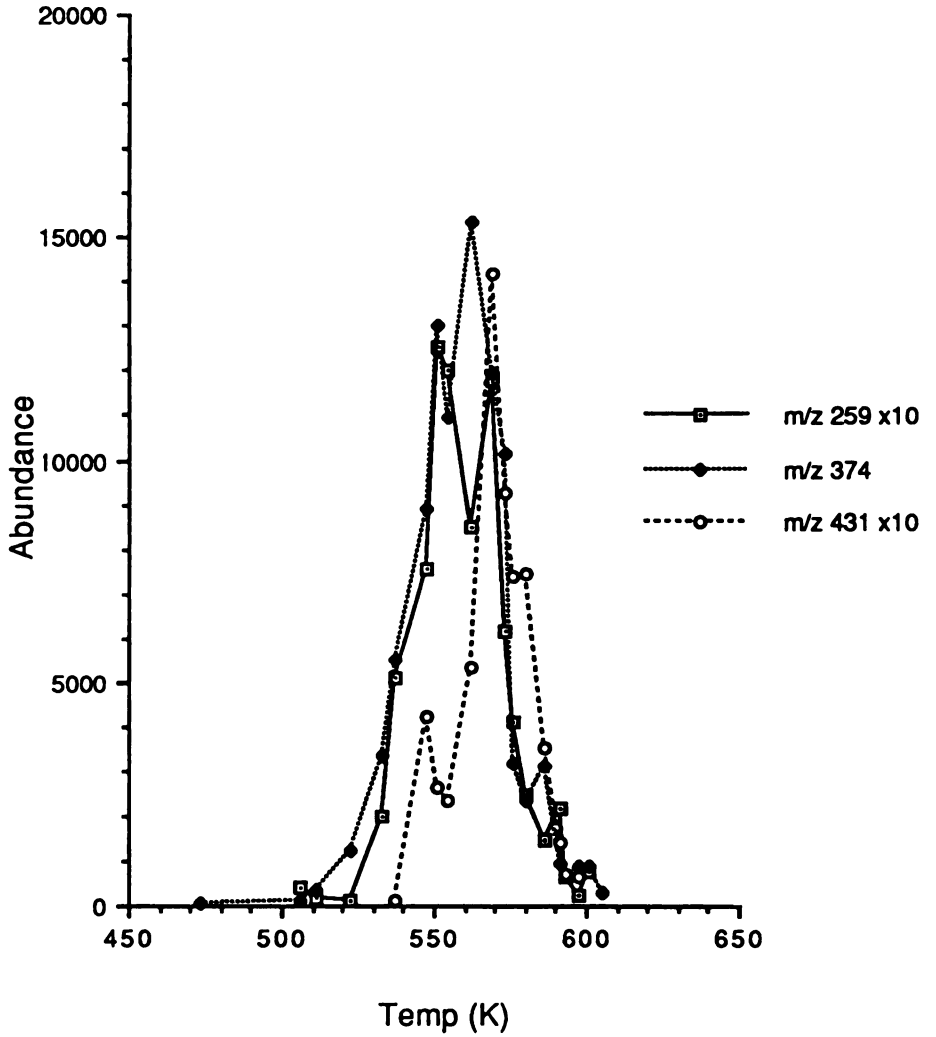

Figure A4. Abundance of fragment adduct ions of leu-enkephalin vs. sample filament wire temperature (K).

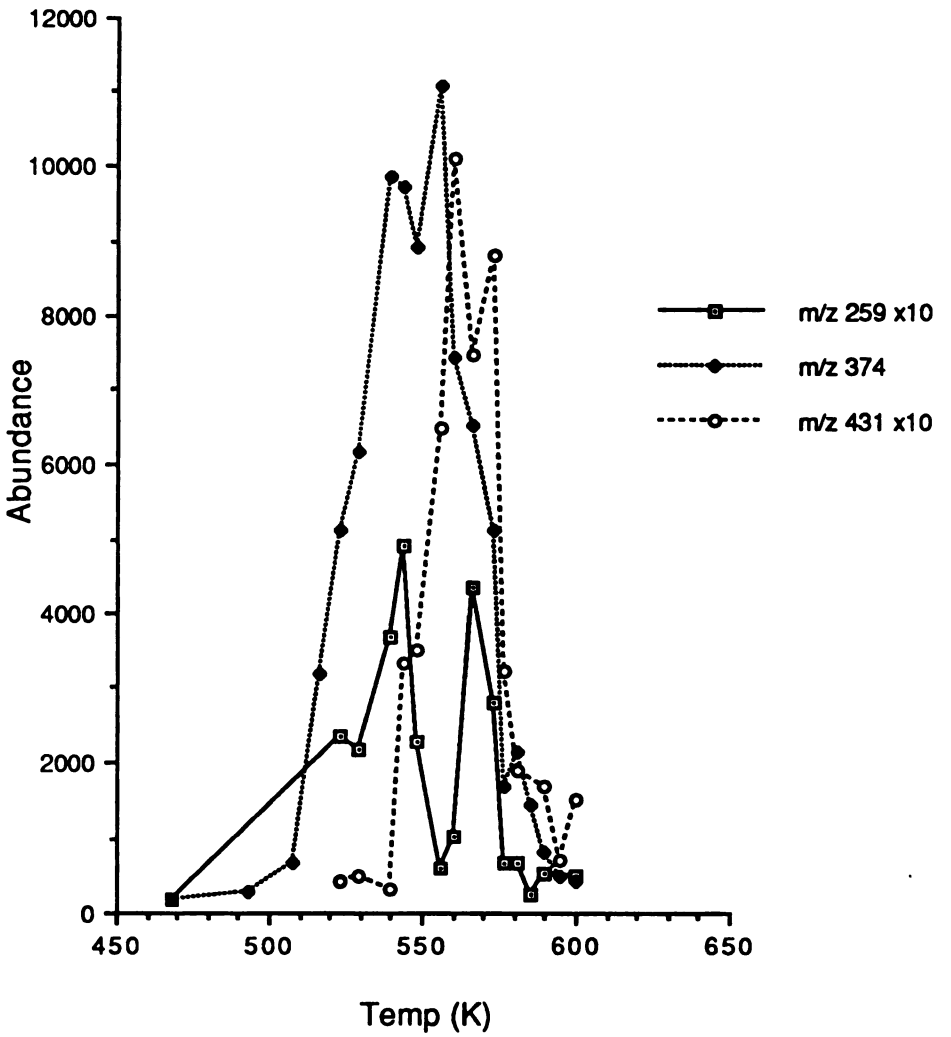

Figure A5. Abundance of fragment adduct ions of leu-enkephalin vs. sample filament wire temperature (K).

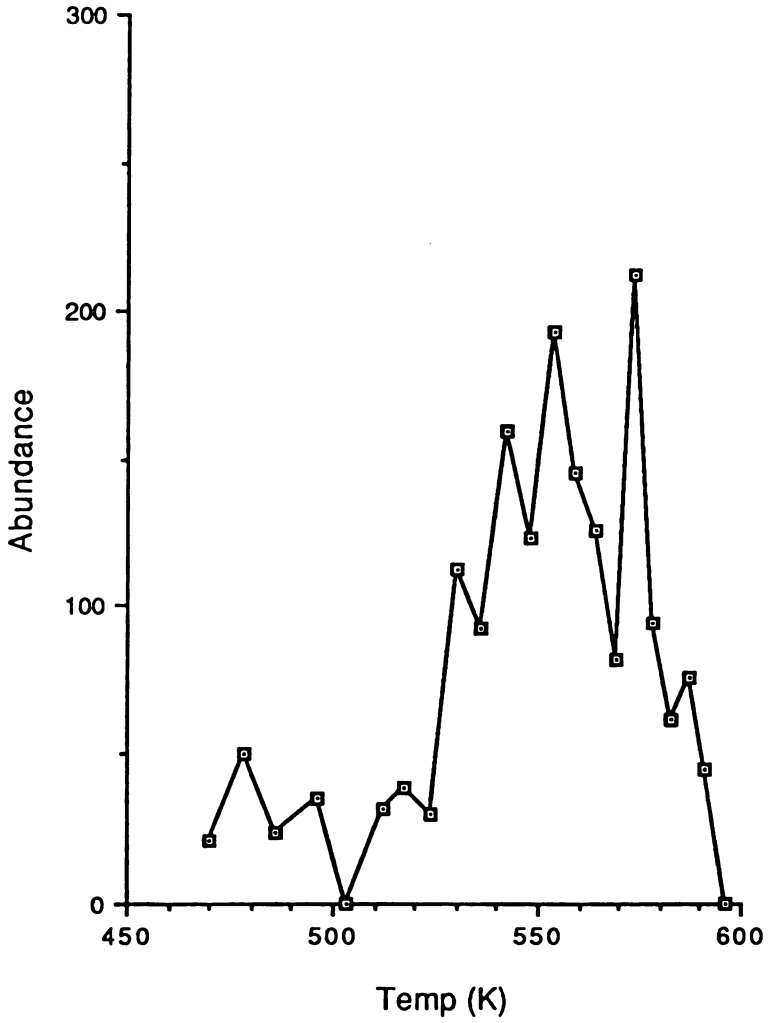

Figure A6. Abundance of the $[M]K^+$ ion of sucrose vs. sample filament wire temperature (K).

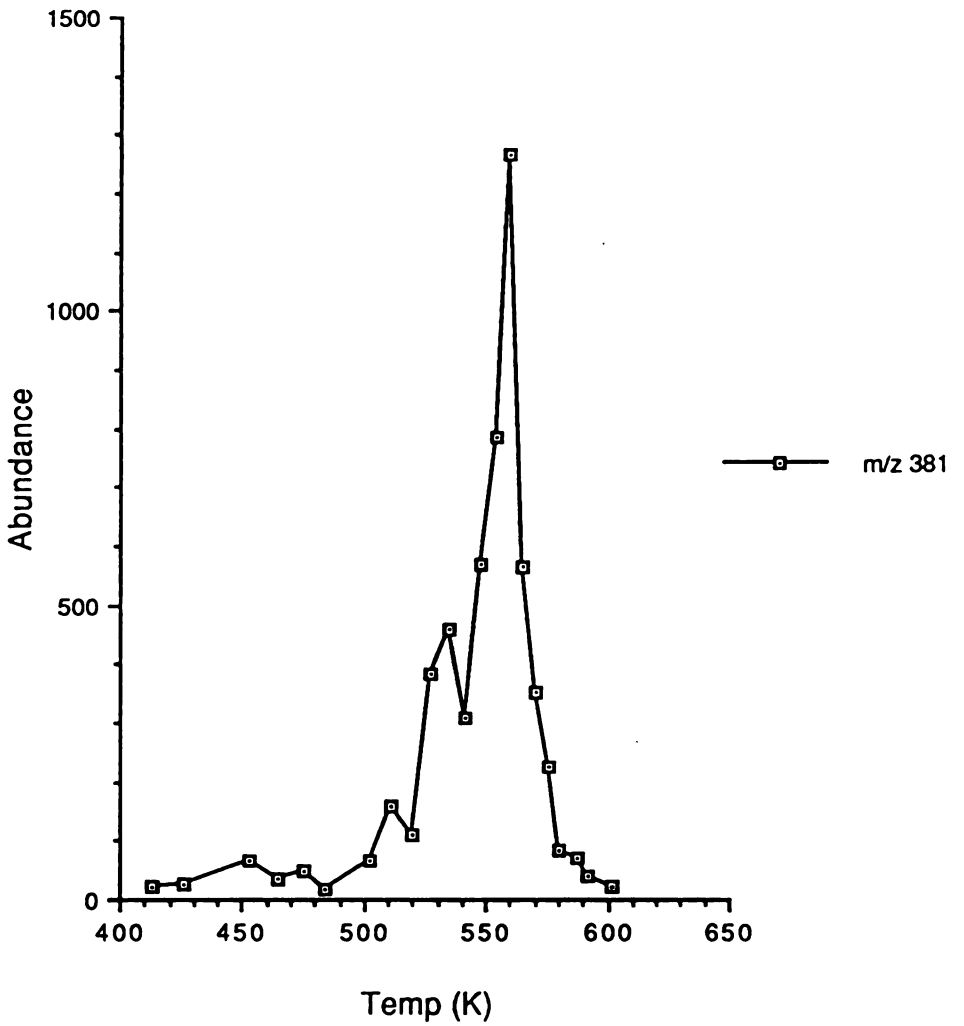

Figure A7. Abundance of the $[M]K^+$ ion of sucrose vs. sample filament wire temperature (K).

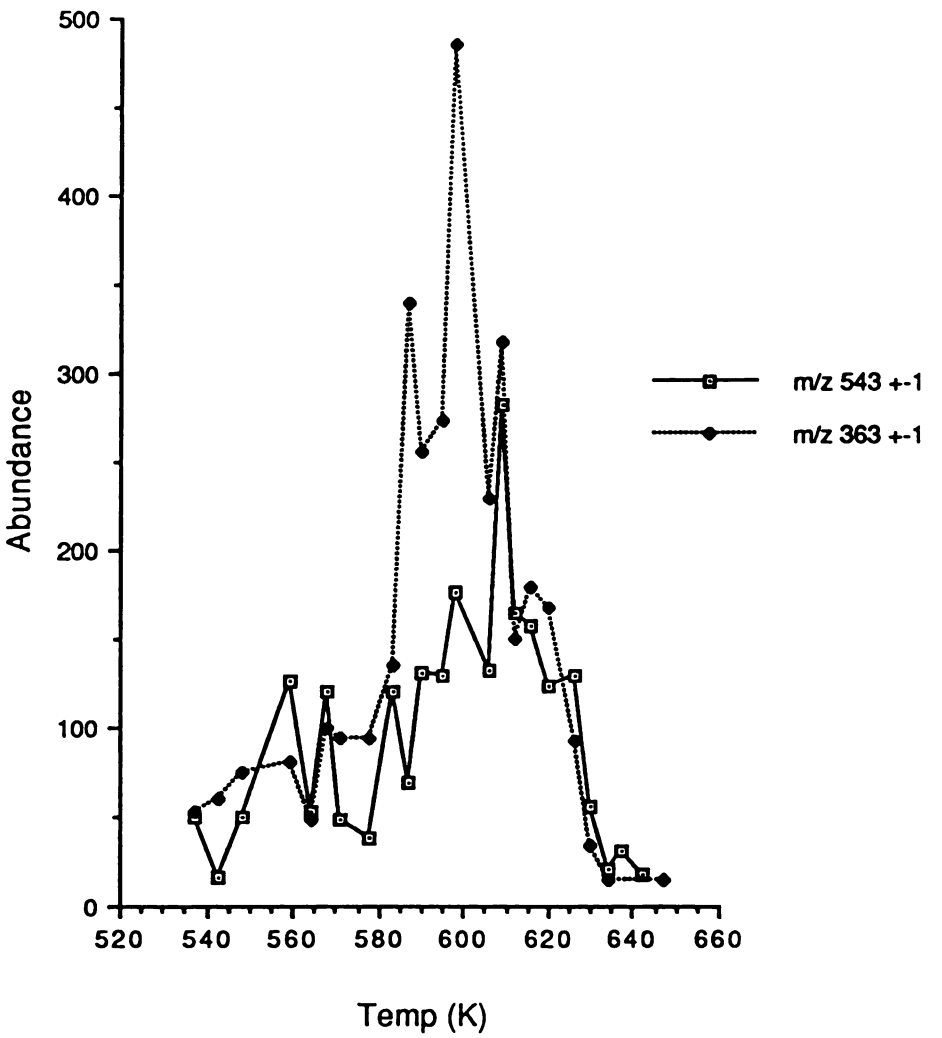

Figure A8. Abundance of the K^+ adduct ions of melezitose vs. sample filament wire temperature (K).

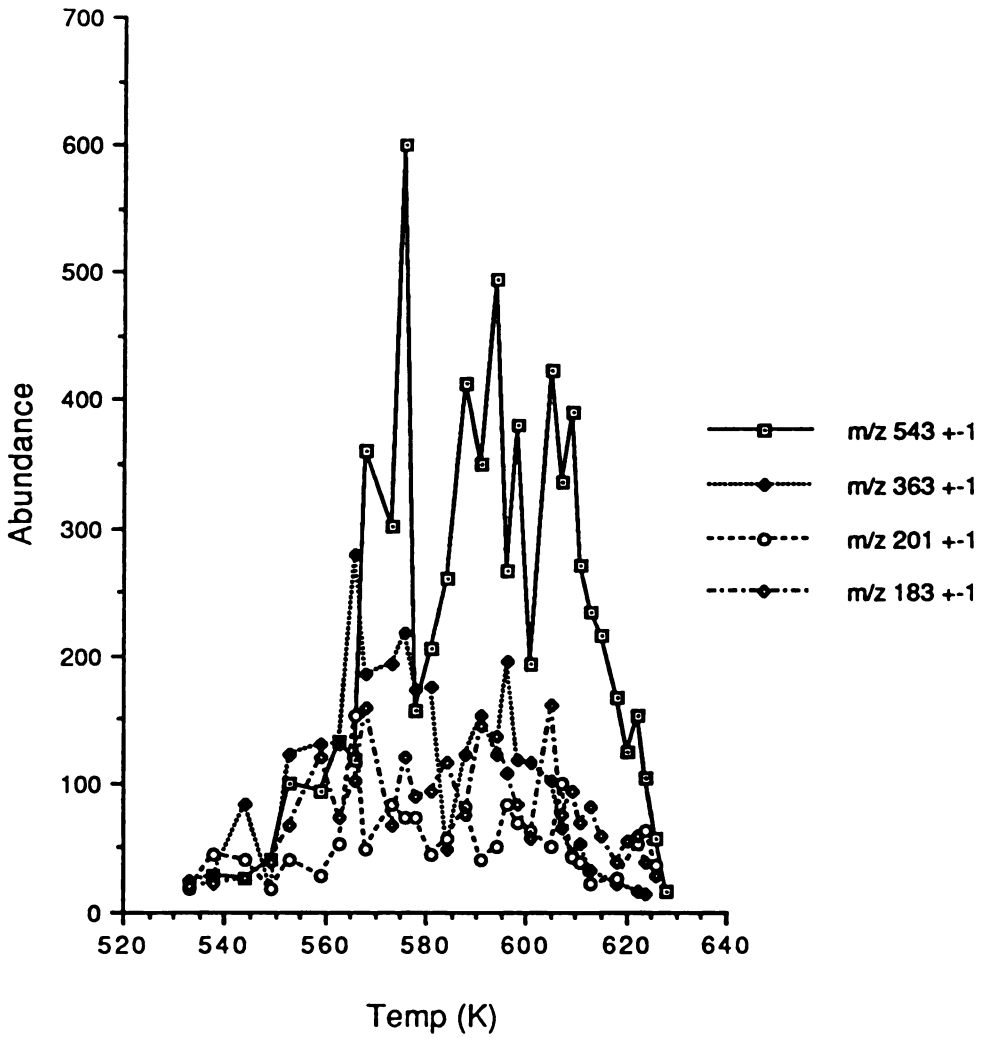

Figure A9. Abundance of K^+ adduct ions of melezitose vs. sample filament wire temperature (K).

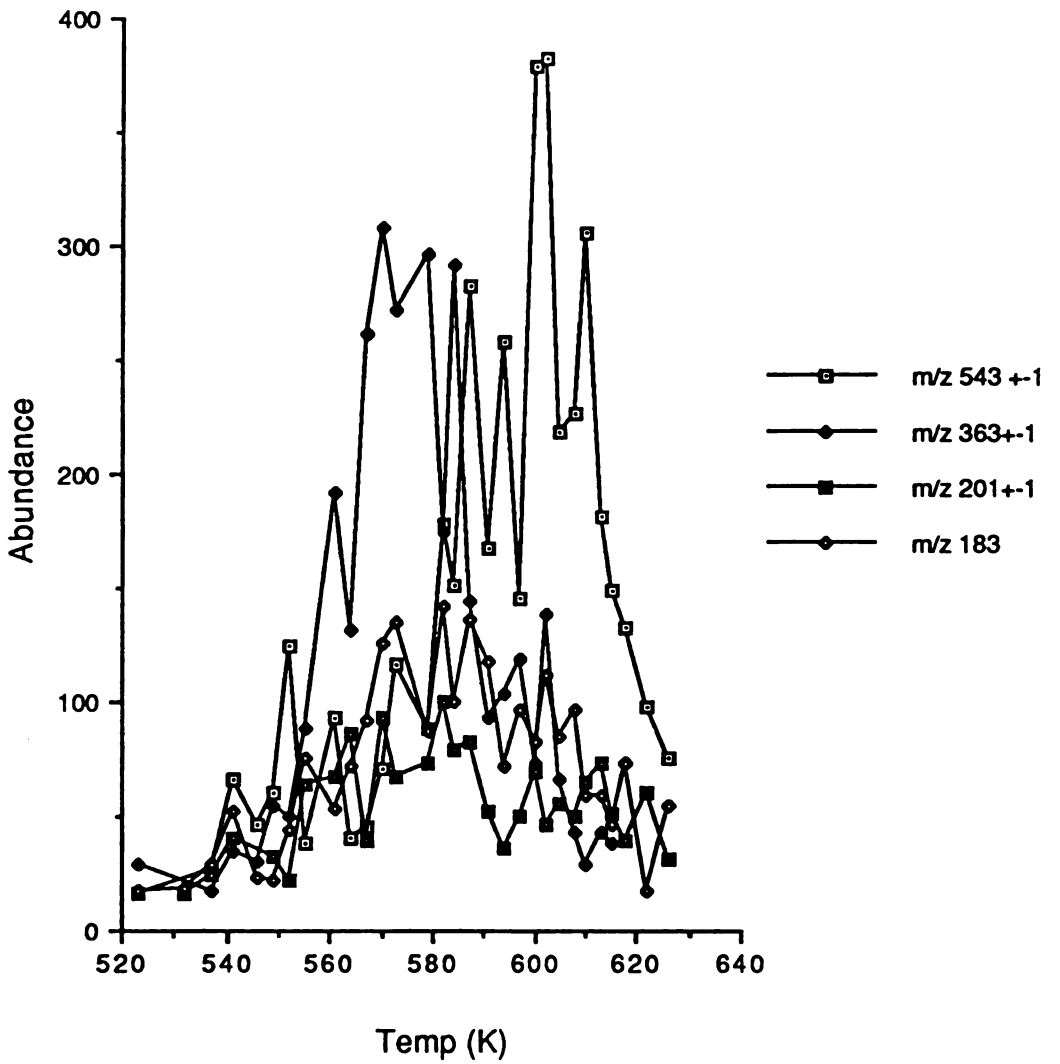

Figure A10. Abundance of the K^+ adduct ions of melezitose vs. sample filament wire temperature (K).

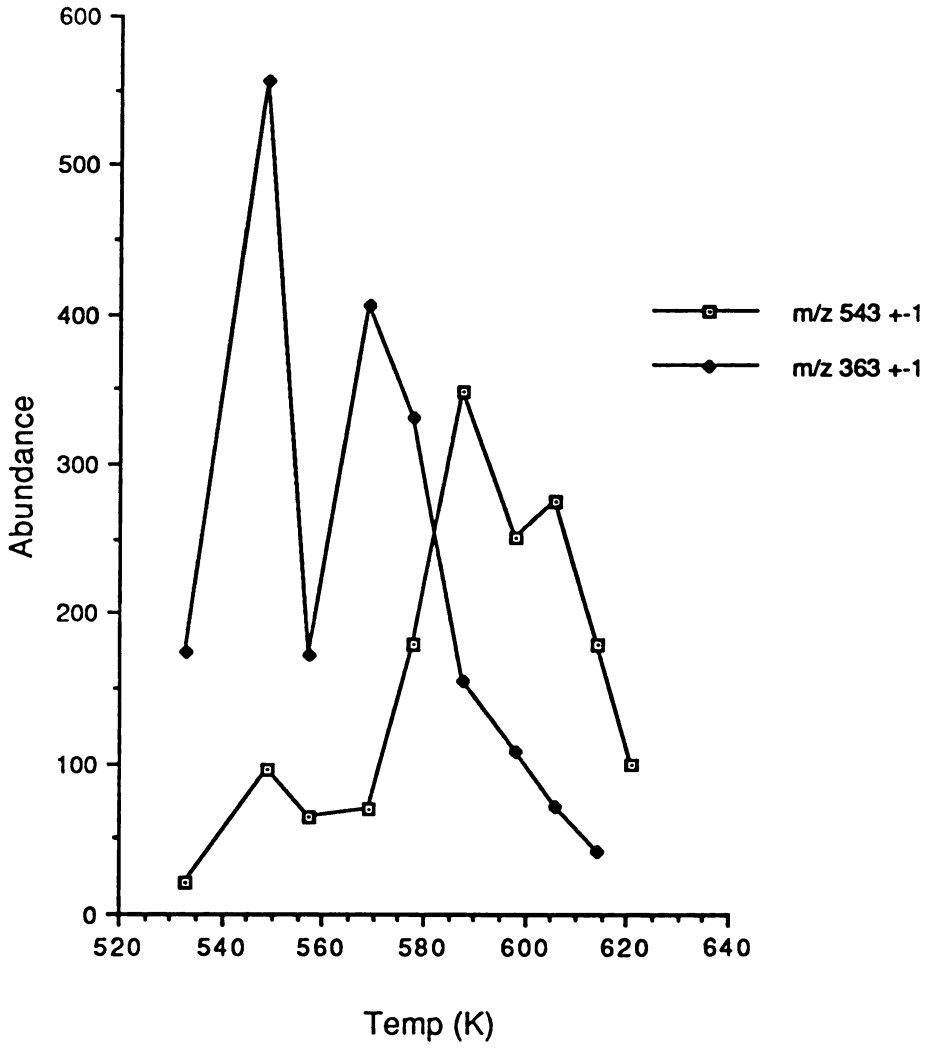

Figure A11. Abundance of the K^+ adduct ions of melezitose vs. sample filament wire temperature (K).

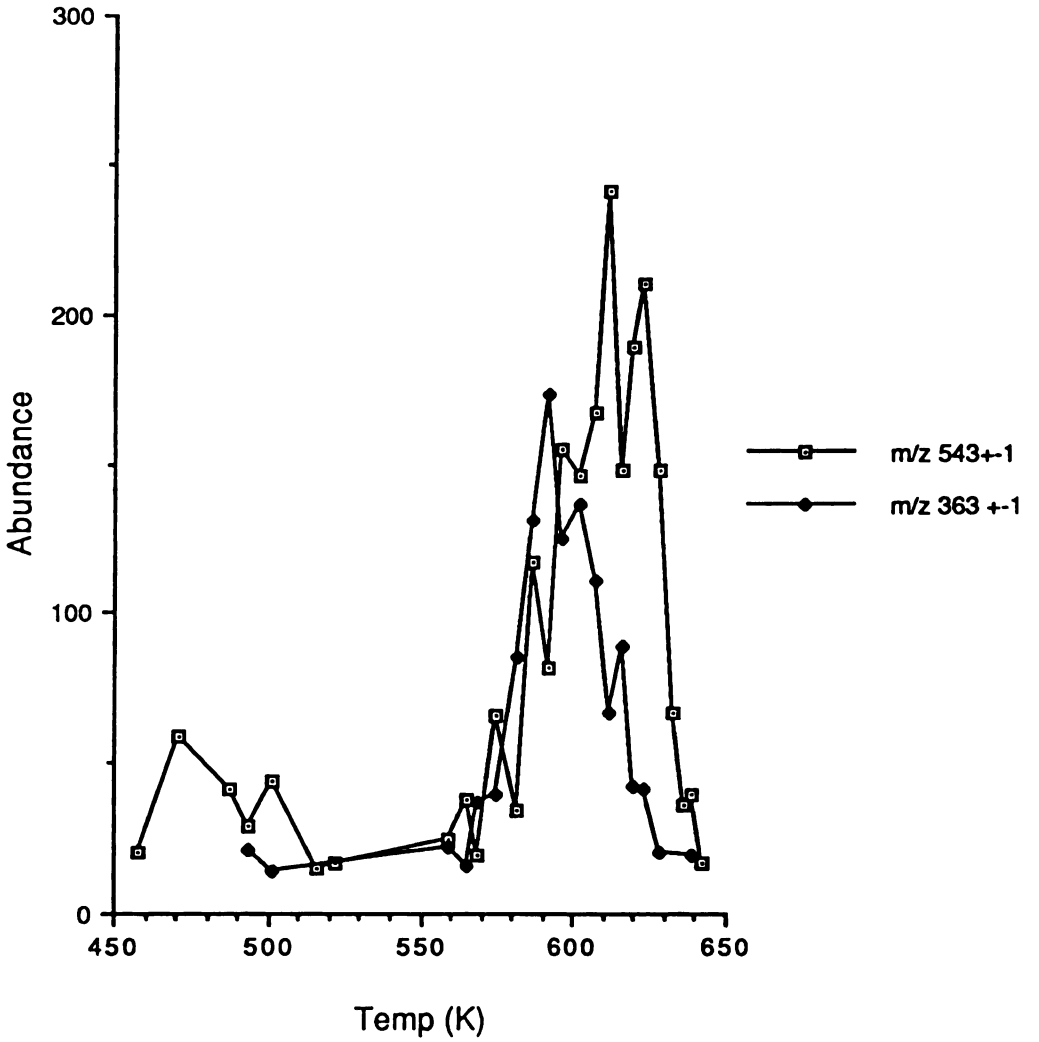

Figure A12. Abundance of the K^+ adduct ions of melezitose vs. sample filament wire temperature (K).

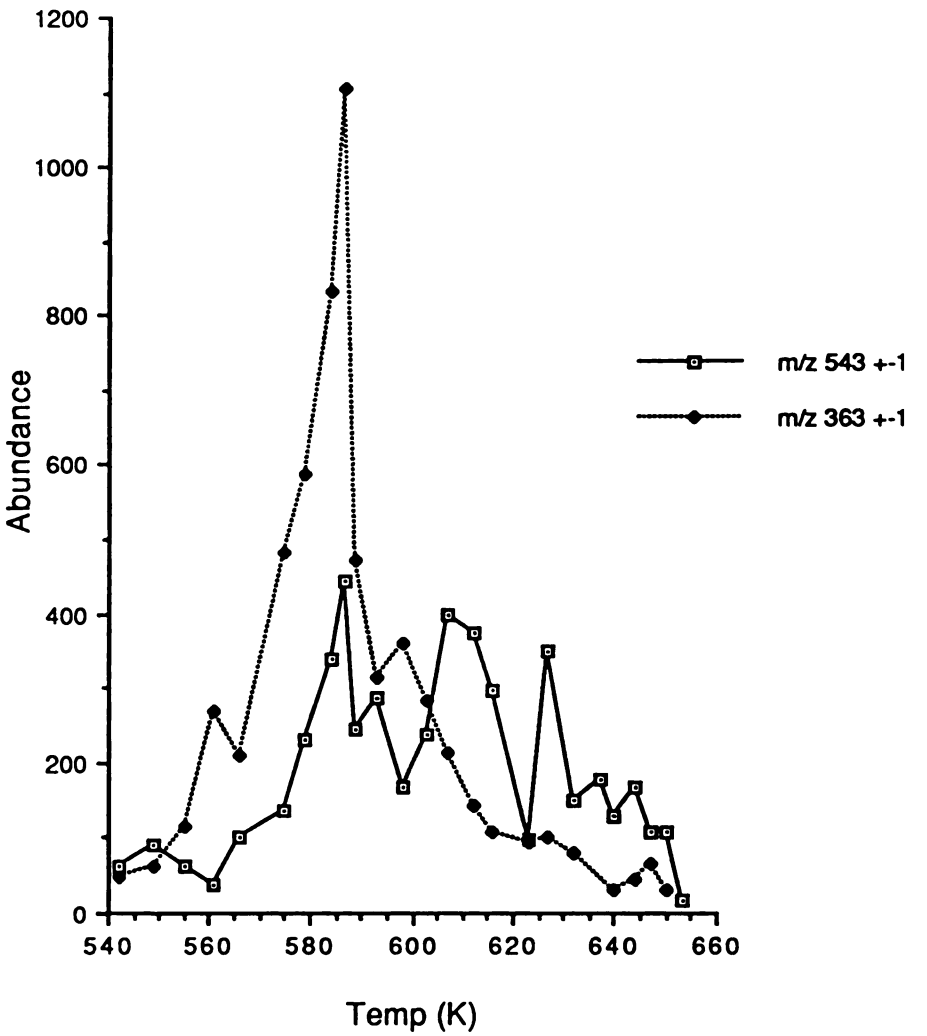

Figure A13. Abundance of K^+ adduct ions of melezitose vs. sample filament wire temperature (K).

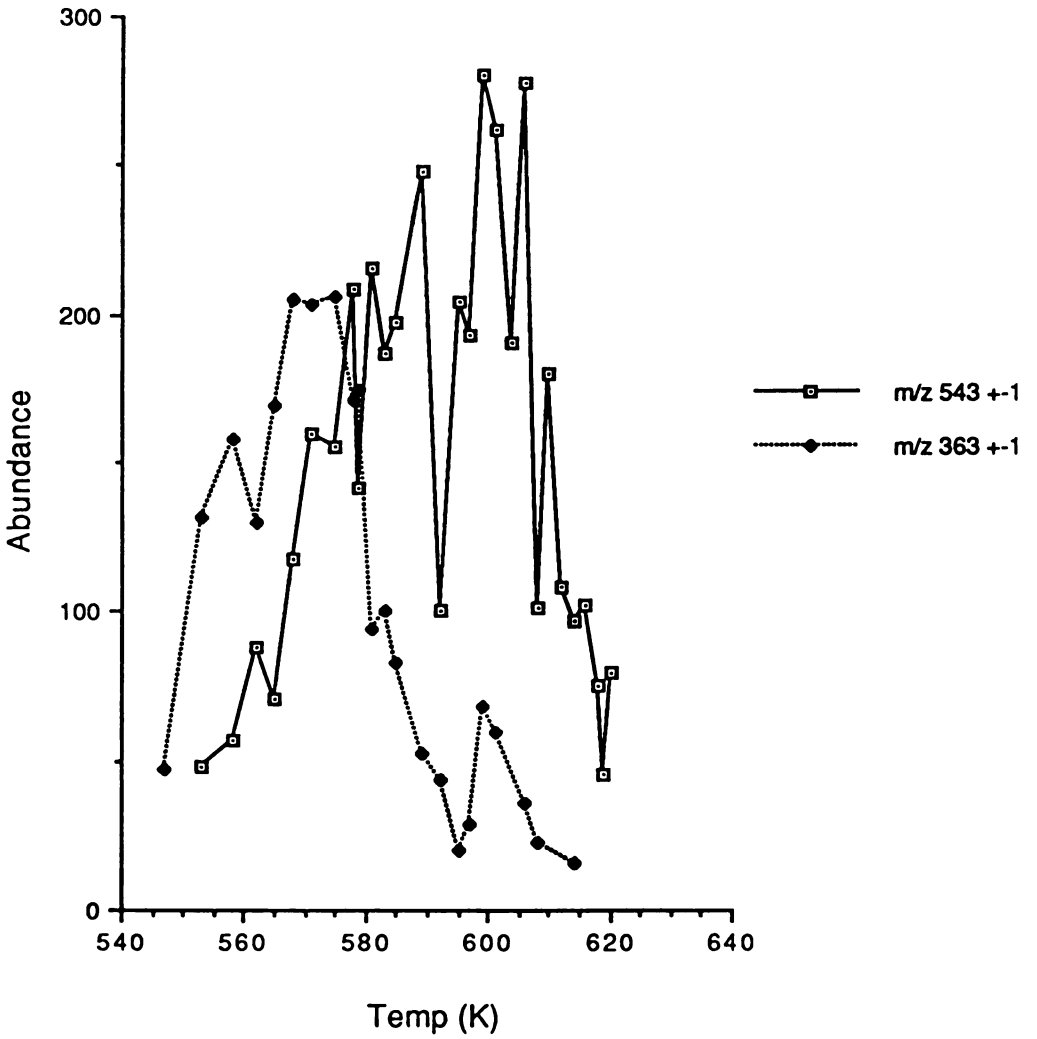

Figure A14. Abundance of the K^+ adduct ions of melezitose vs. sample filament wire temperature (K).

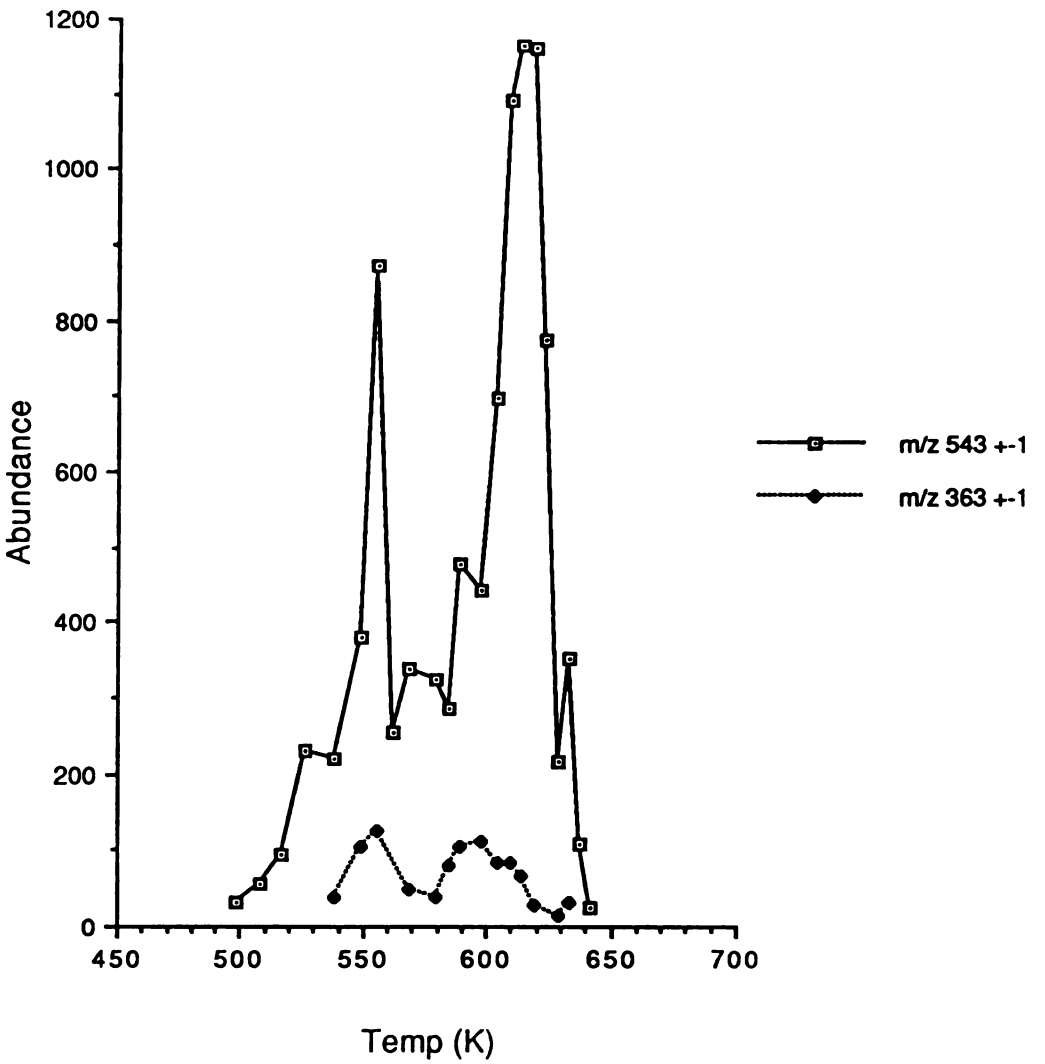

Figure A15. Abundance of the K^+ adduct ions of melezitose vs. sample filament wire temperature (K).

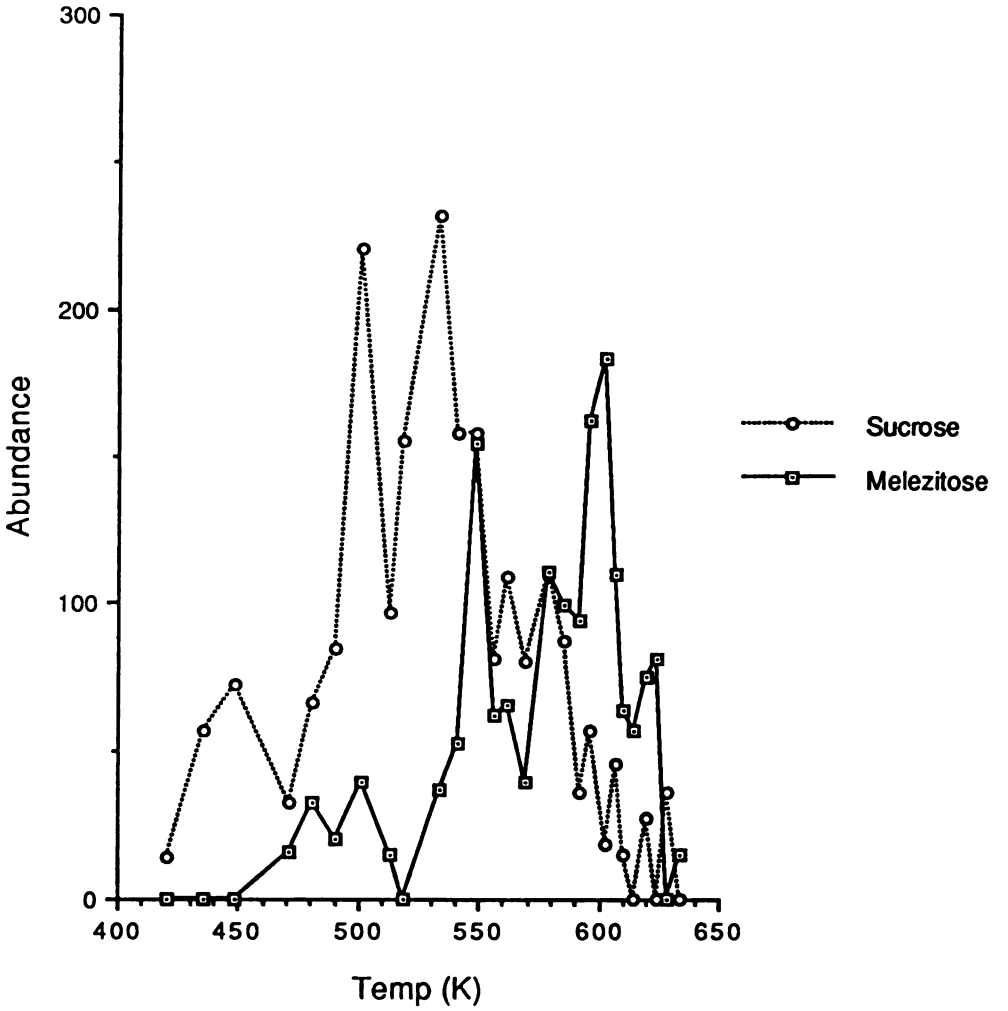

Figure A16. Abundance of the $[M]K^+$ ions of sucrose and melezitose vs. sample filament wire temperature (K).

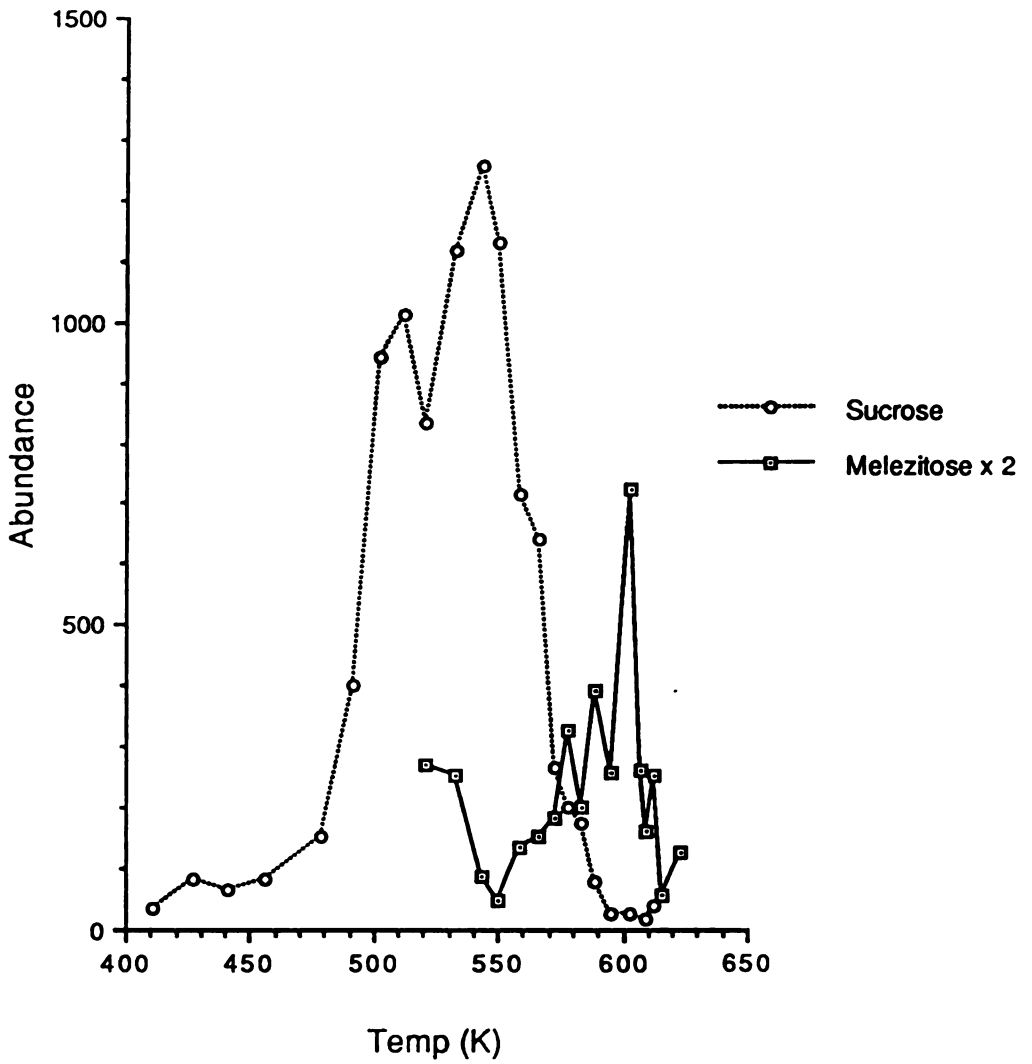

Figure A17. Abundance of the $[M]K^+$ ions of sucrose and melezitose vs. sample filament wire temperature (K).

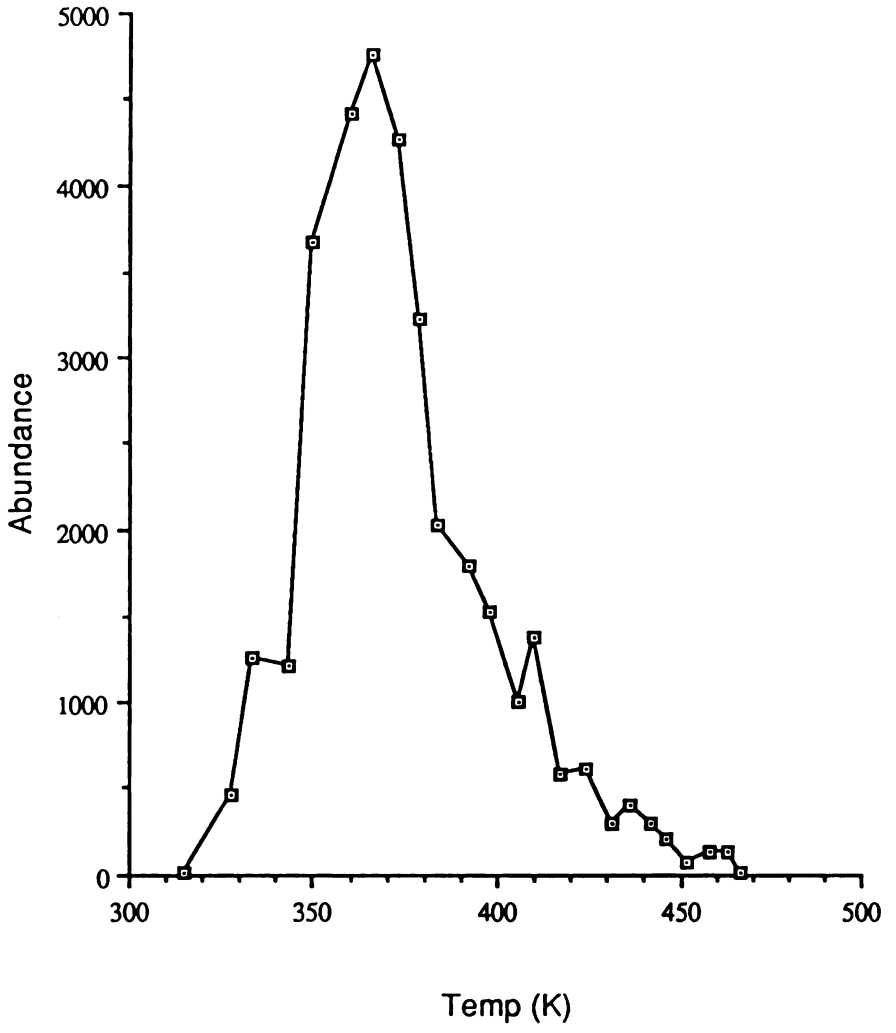

Figure A18. Abundance of the $[M]K^+$ ion of palmitic acid vs. sample filament wire temperature (K).

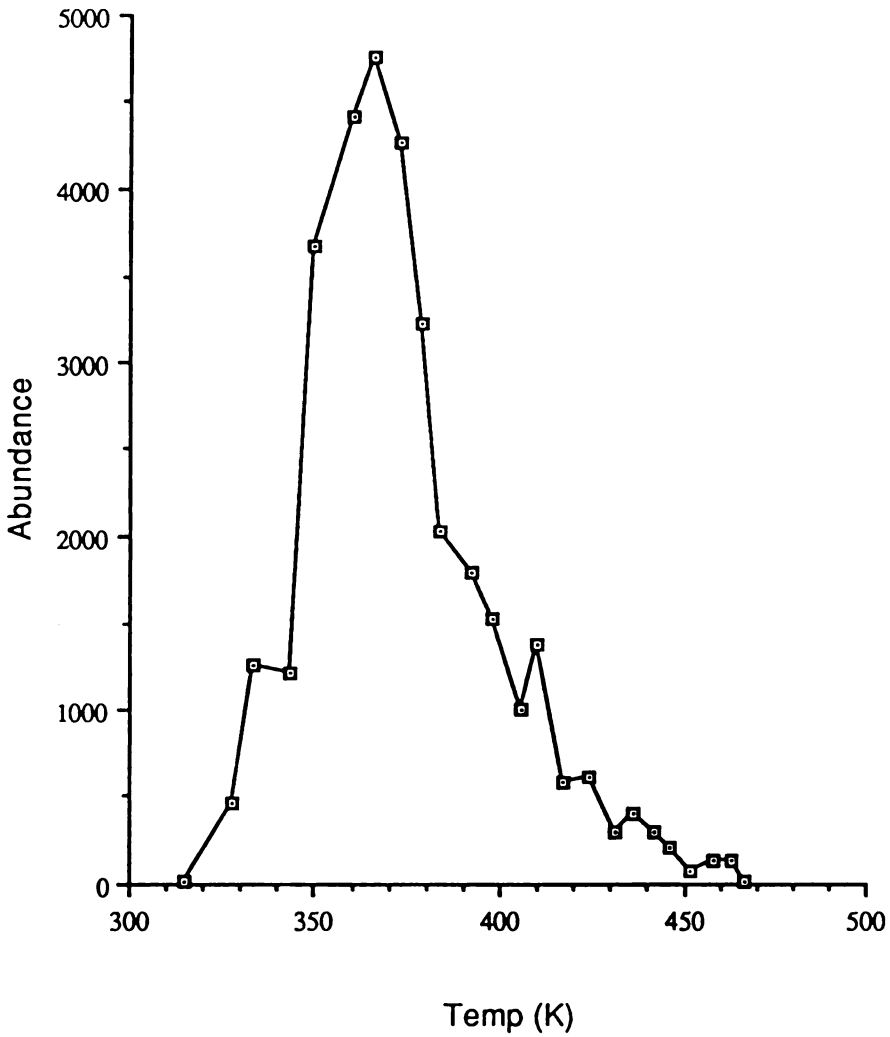

Figure A18. Abundance of the $[M]K^+$ ion of palmitic acid vs. sample filament wire temperature (K).

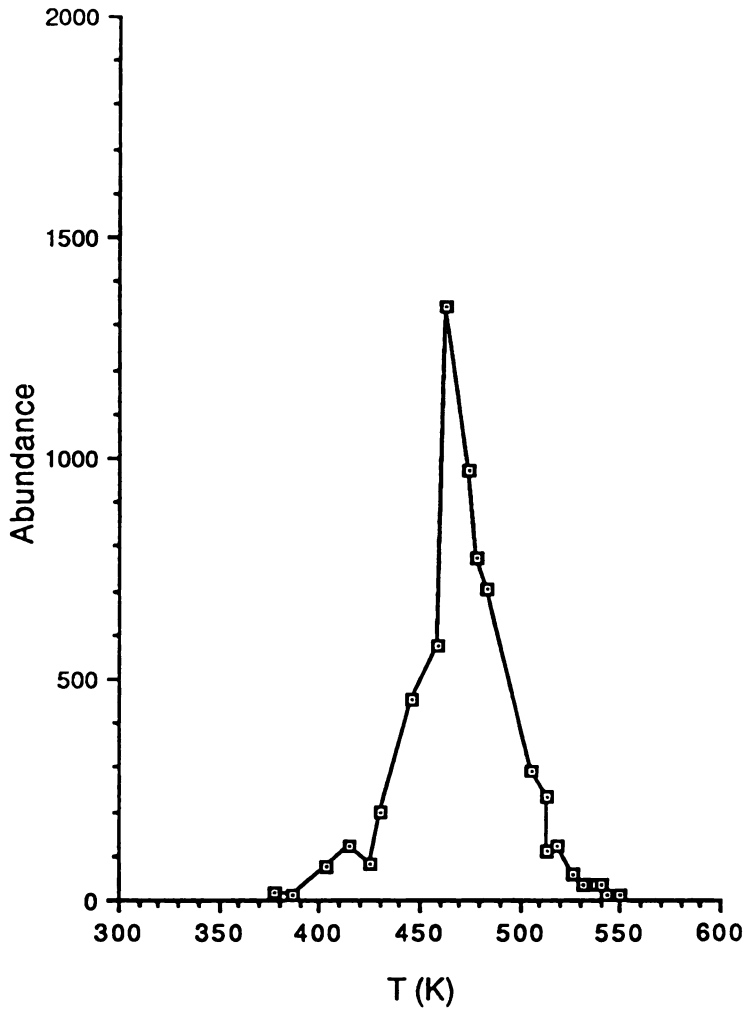

Figure A19. Abundance of $[M]K^+$ ion of palmitic acid vs. sample filament wire temperature (K).

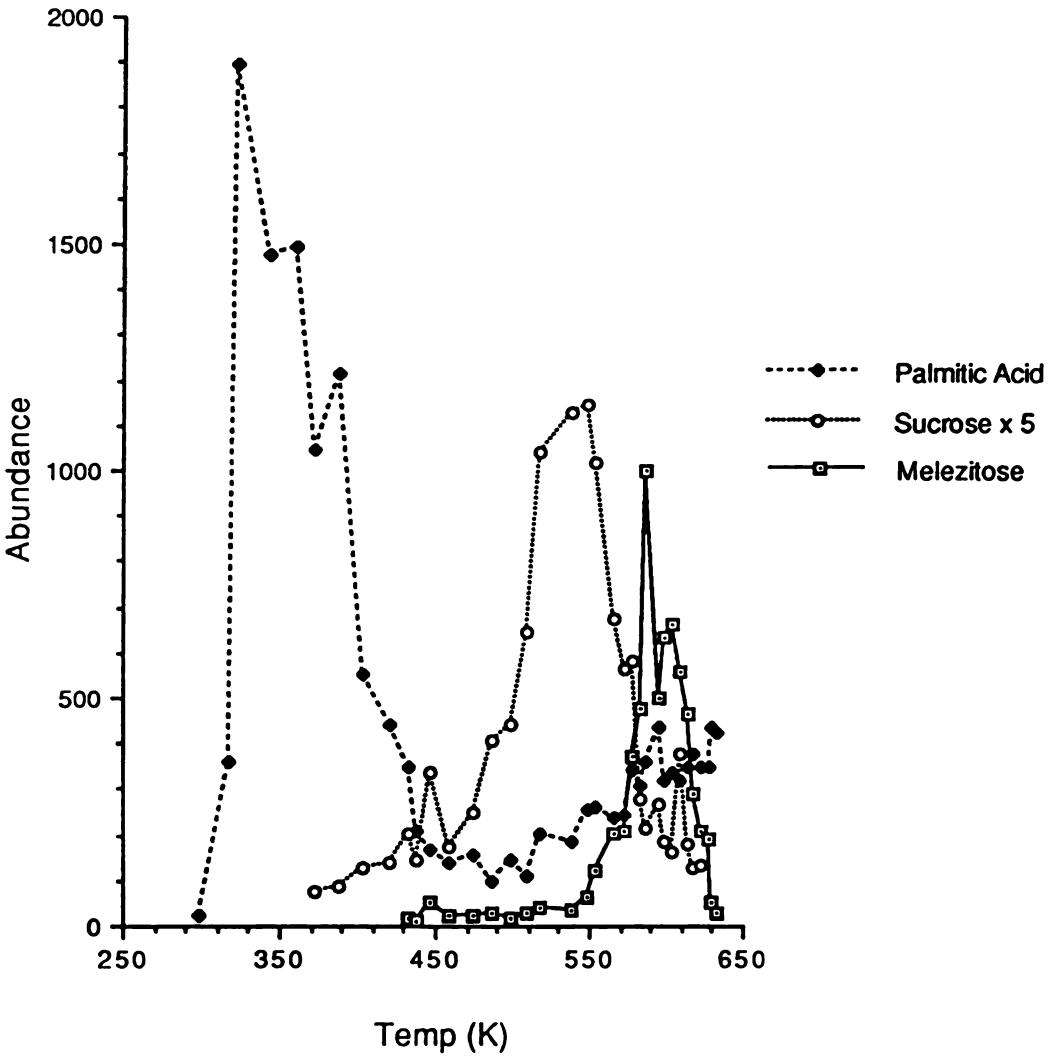

Figure A20. Abundance of the $[M]K^+$ ions of palmitic acid, sucrose, and melezitose vs. temperature (K).

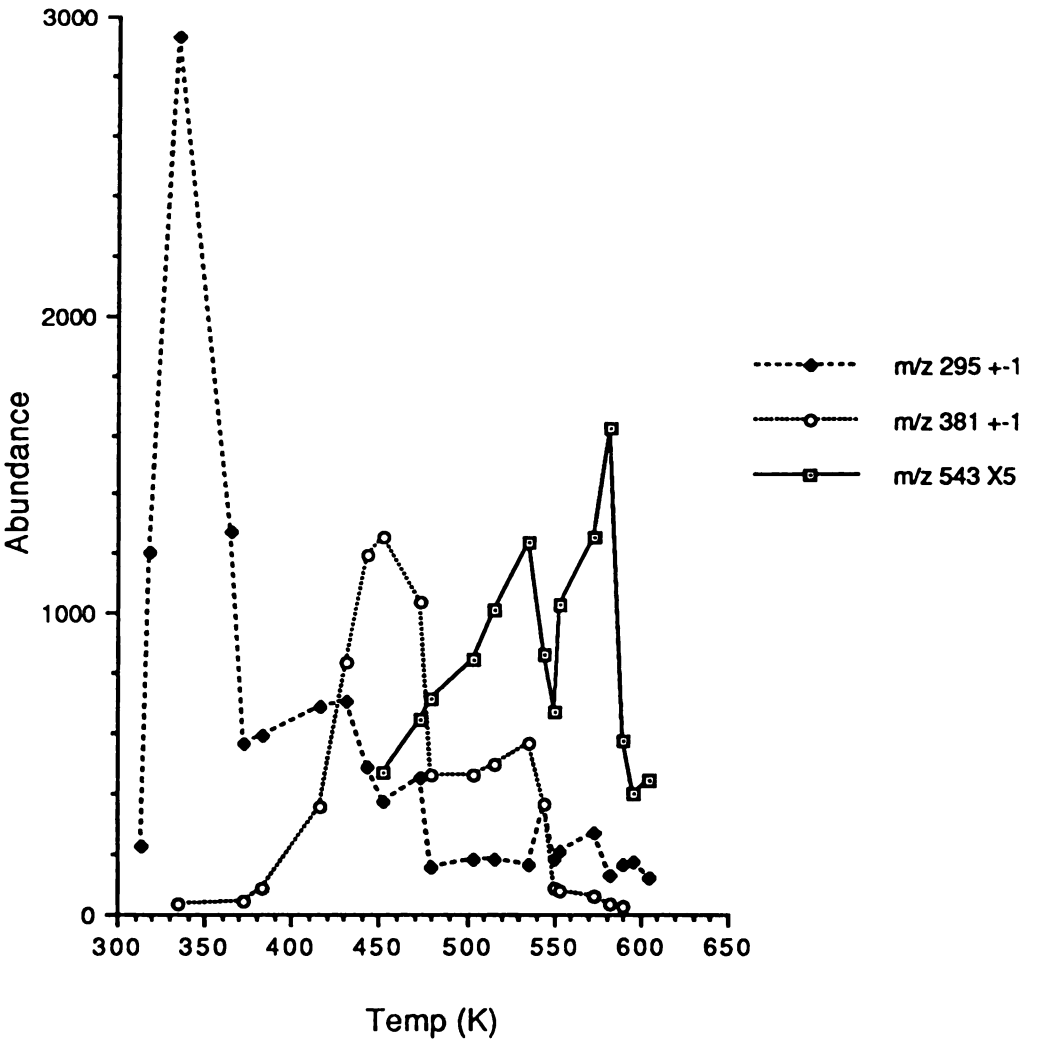

Figure A21. Abundance of the $[M]K^+$ ions of palmitic acid, sucrose, and melezitose vs. temperature (K).

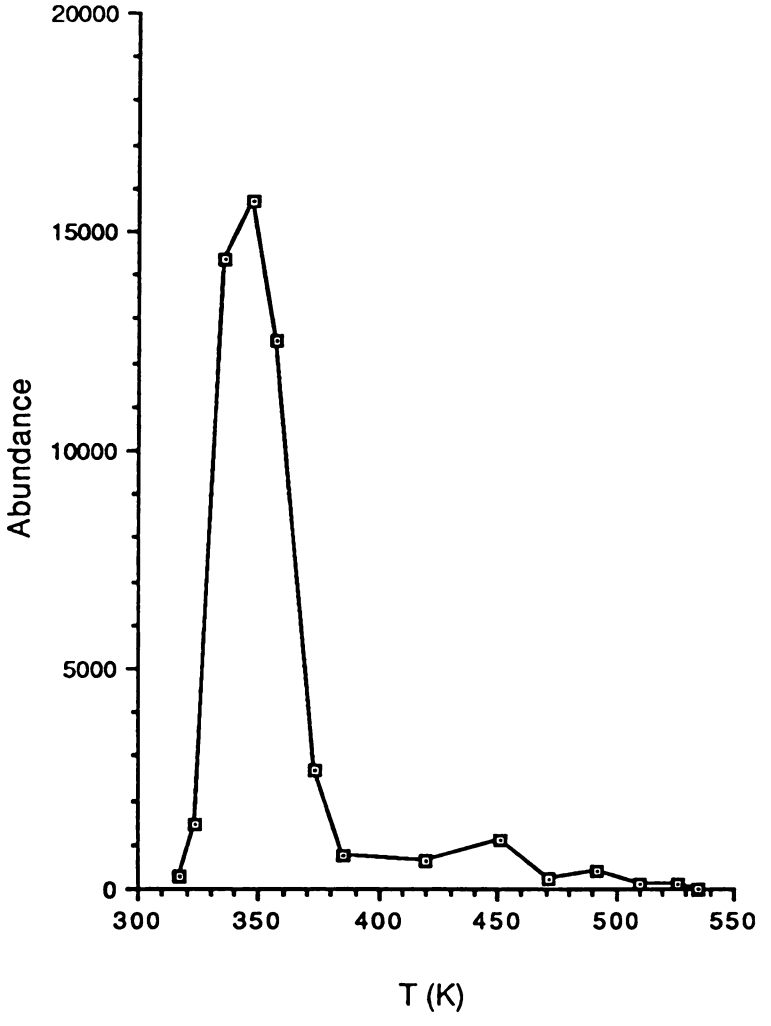

Figure A22. Abundance of the $[M]K^+$ ion of glycerol vs. the sample filament wire temperature (K).

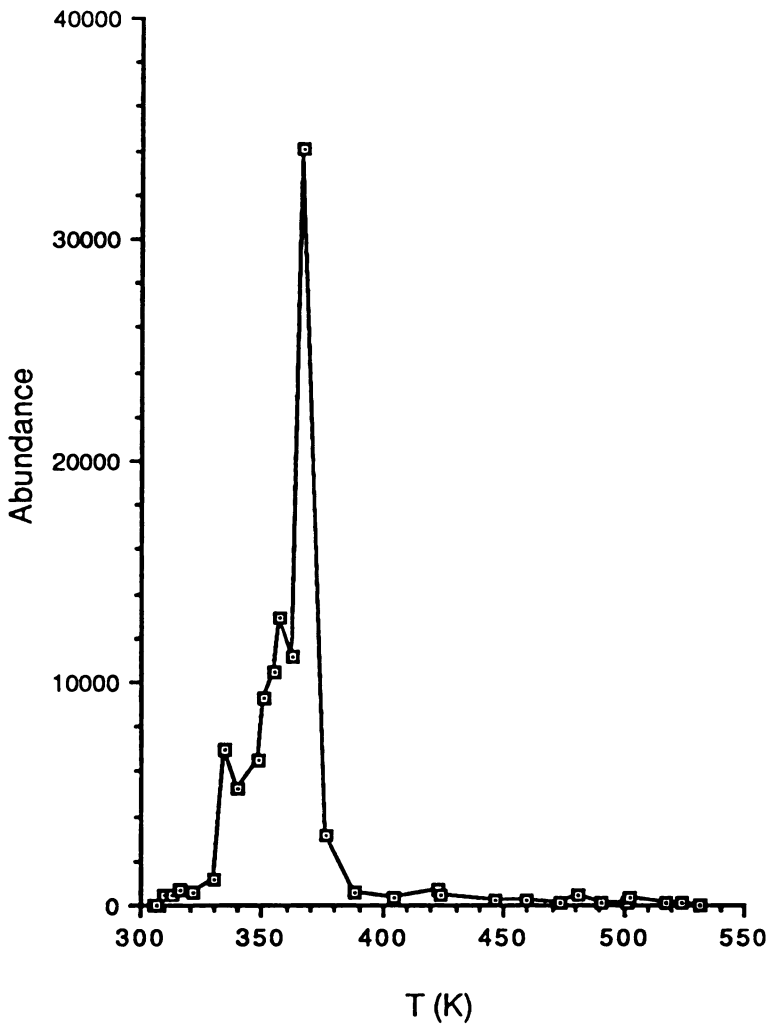

Figure A23. Abundance of the $[M]K^+$ ion of glycerol vs. the sample support surface temperature (K).

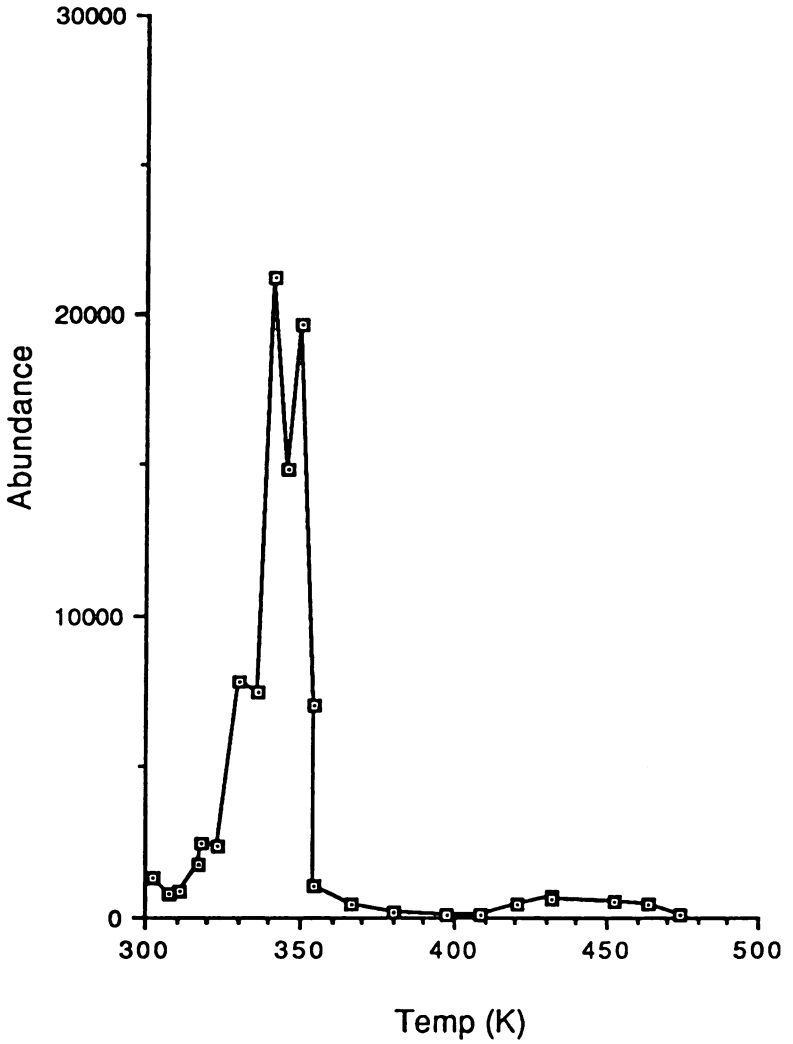

Figure A24. Abundance of the $[M]K^+$ ion of triethylene glycol vs. sample filament wire temperature (K).

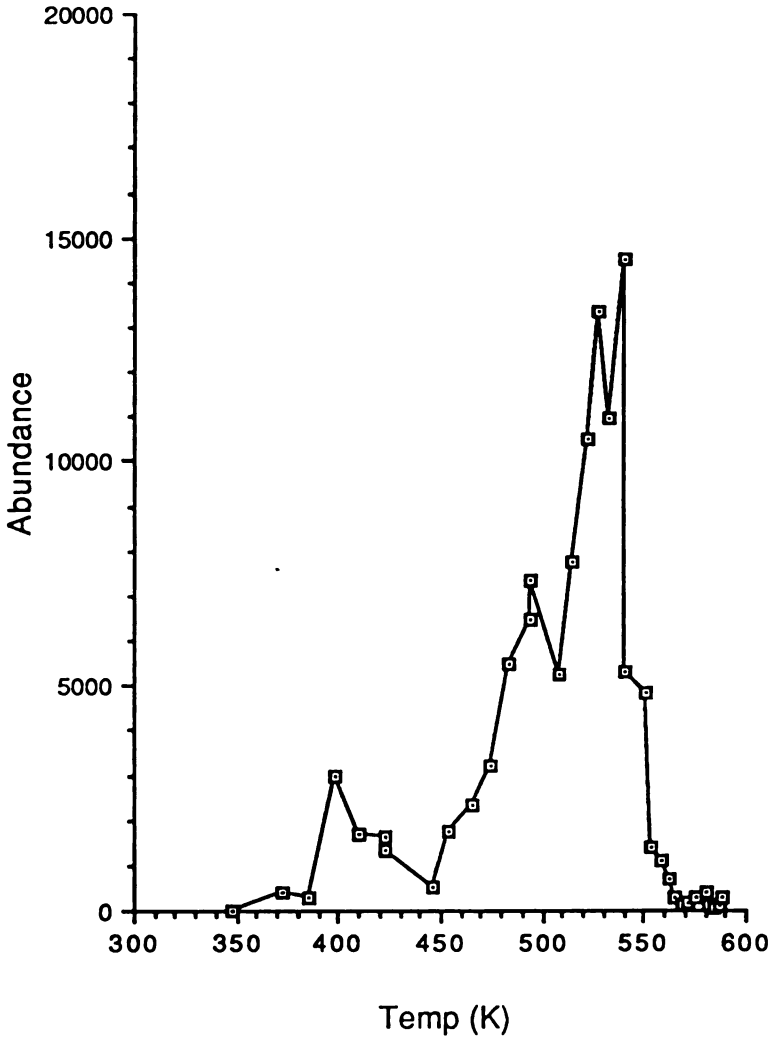

Figure A25. Abundance of the $[M]K^+$ ion of triethylene glycol vs. sample filament wire temperature (K).

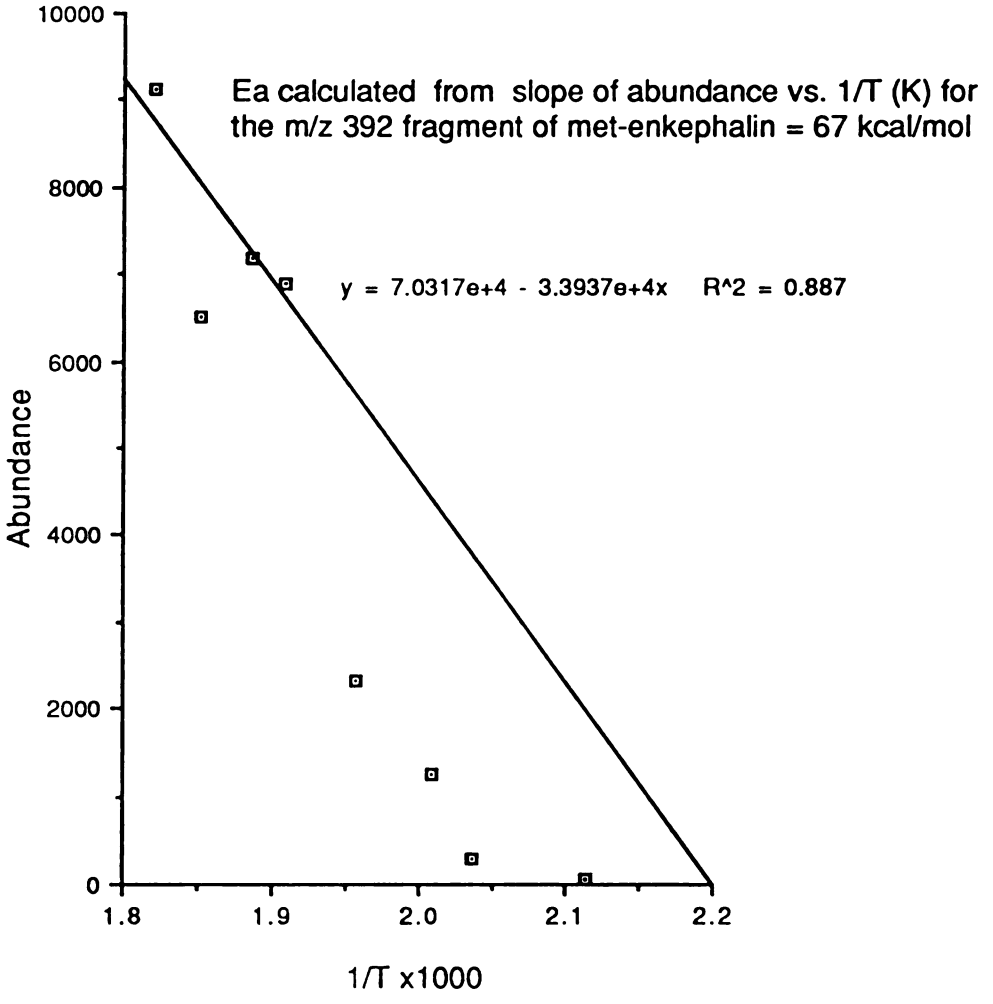

Figure A26. Ea determination from the Arrhenius plot of the abundance of m/z 392 of met-enkephalin vs. 1/T

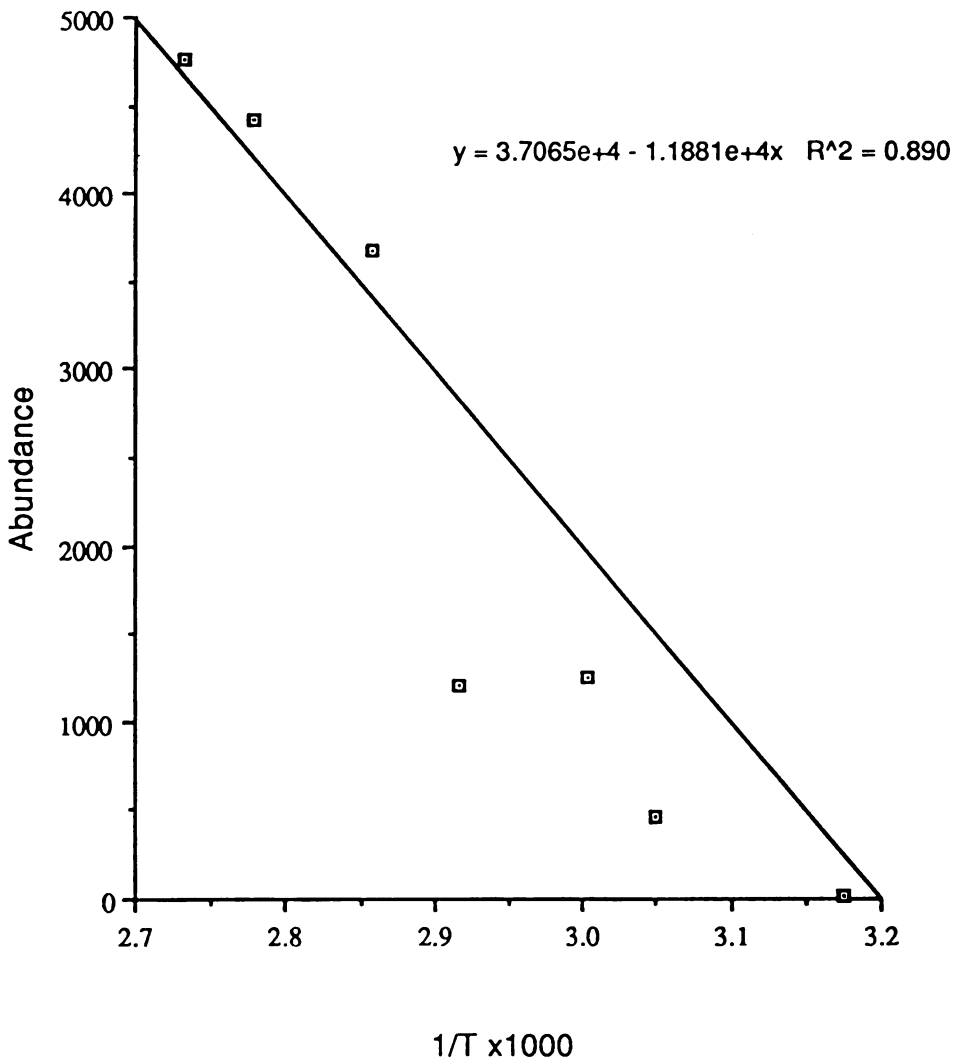

Figure A27. Abundance of the $[M]K^+$ ion of palmitic acid vs. 1/T Ea calculated from slope = 23 kcal/mol.

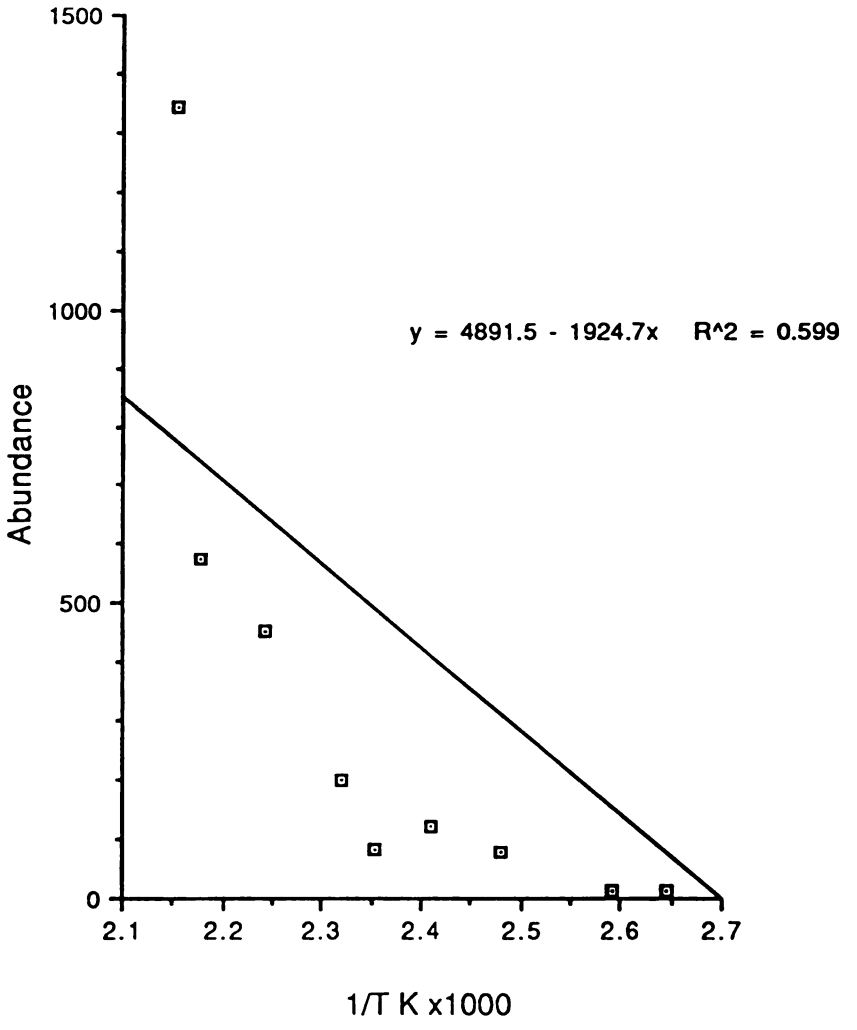

Figure A28. Abundance fo the $[M]K^+$ ion of palmitic acid vs. 1/T. Ea calculated = 4 kcal/mol.

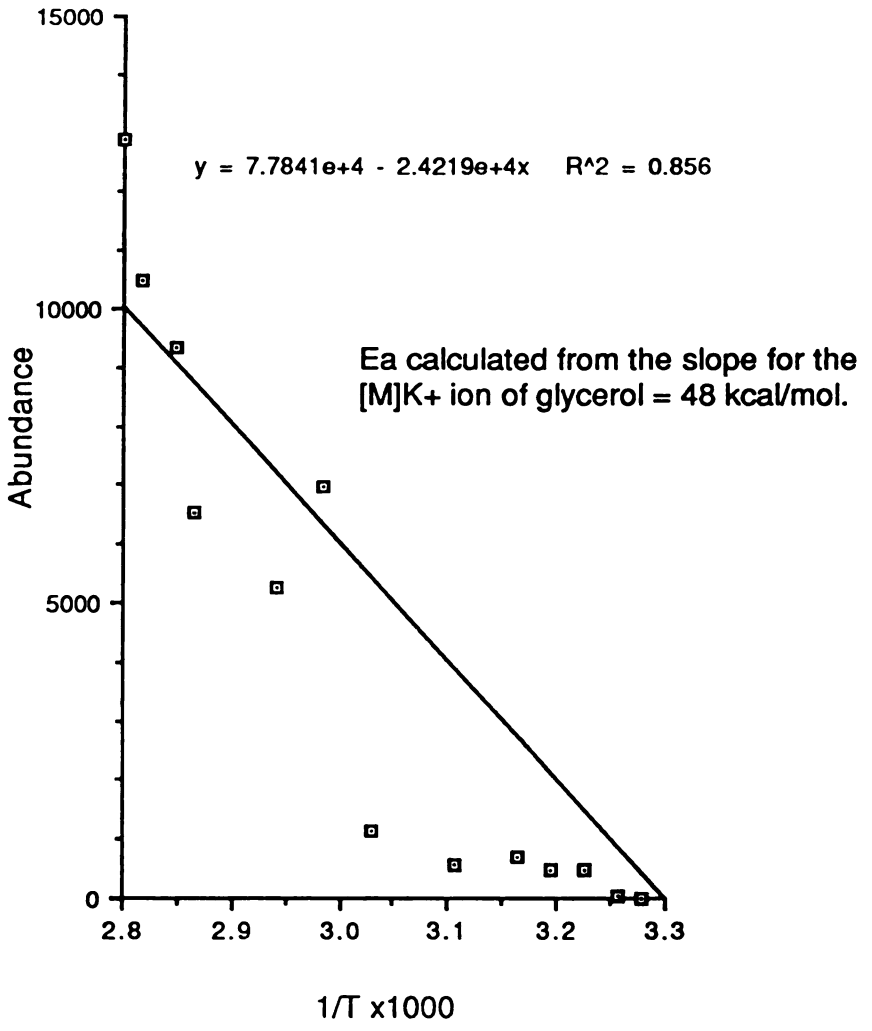

Figure A29. Abundance of the $[M]K^+$ ion of glycerol vs. 1/T (K).

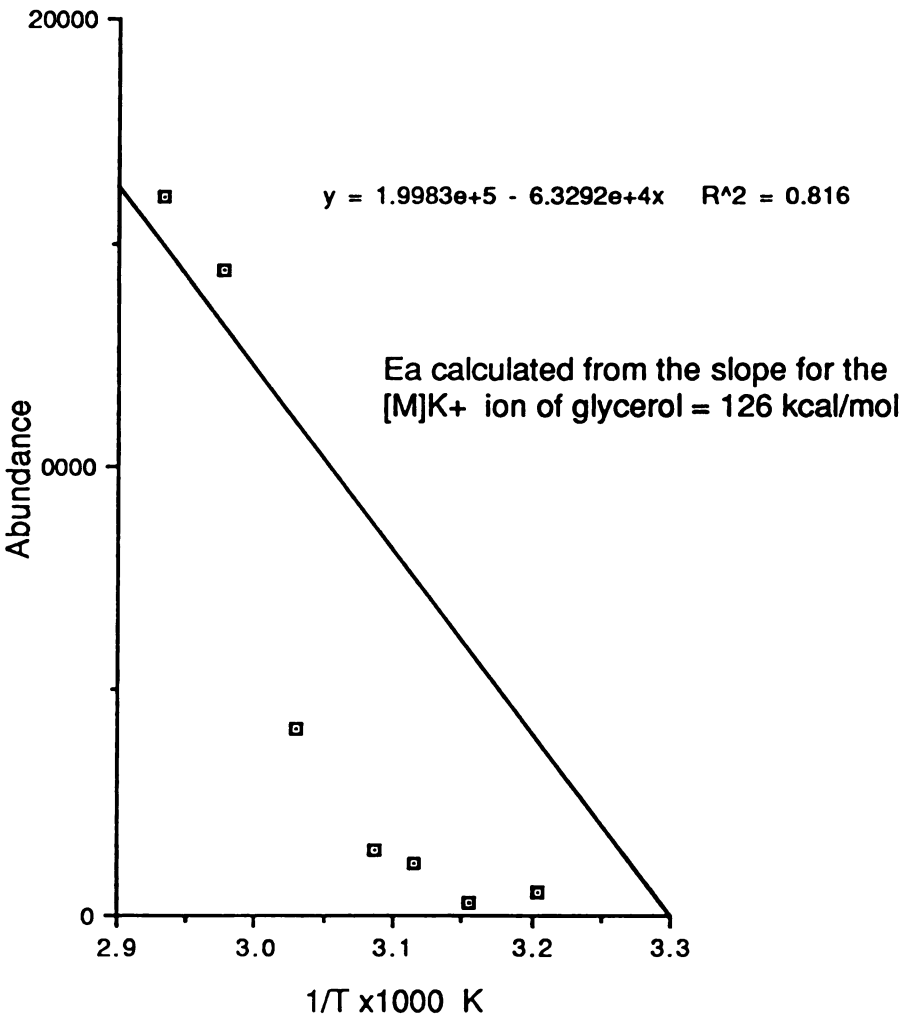

Figure A30. Abundance of the $[M]K^+$ ion of glycerol vs. 1/T K.

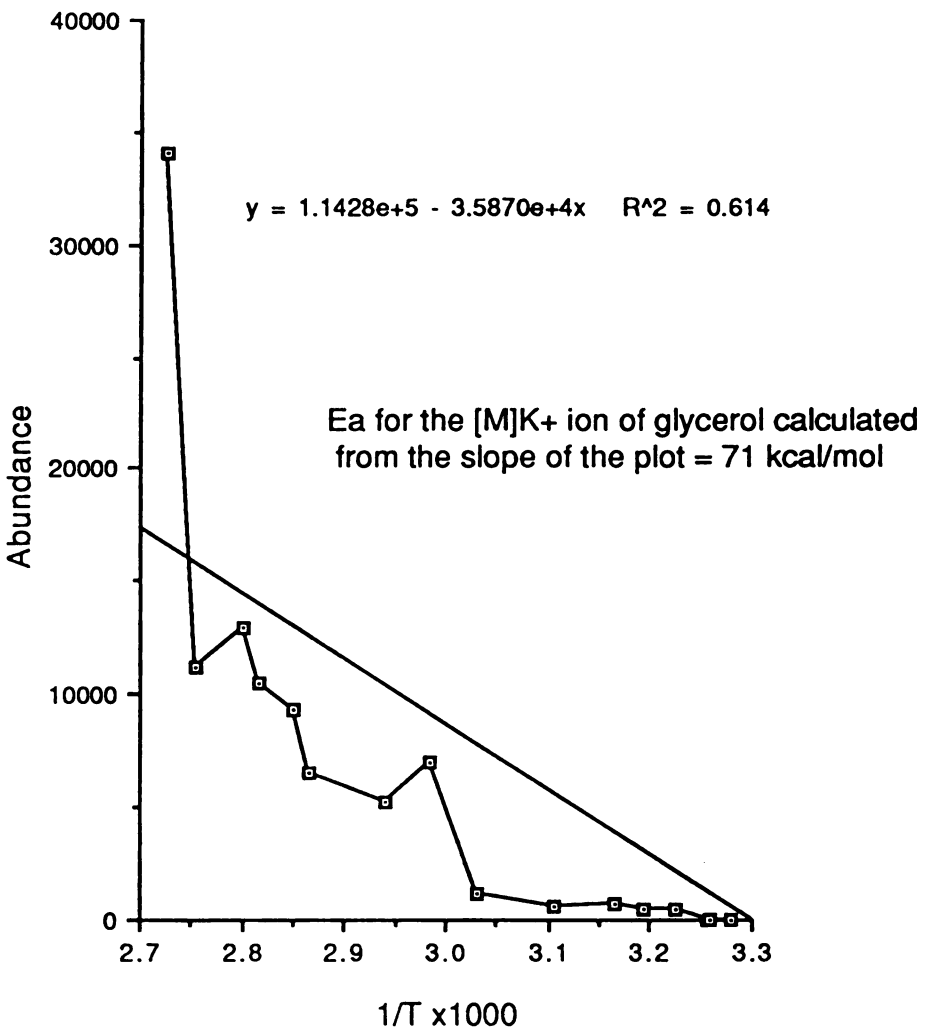

Figure A31. Abundance of the $[M]K^+$ ion of glycerol vs. 1/T (K).

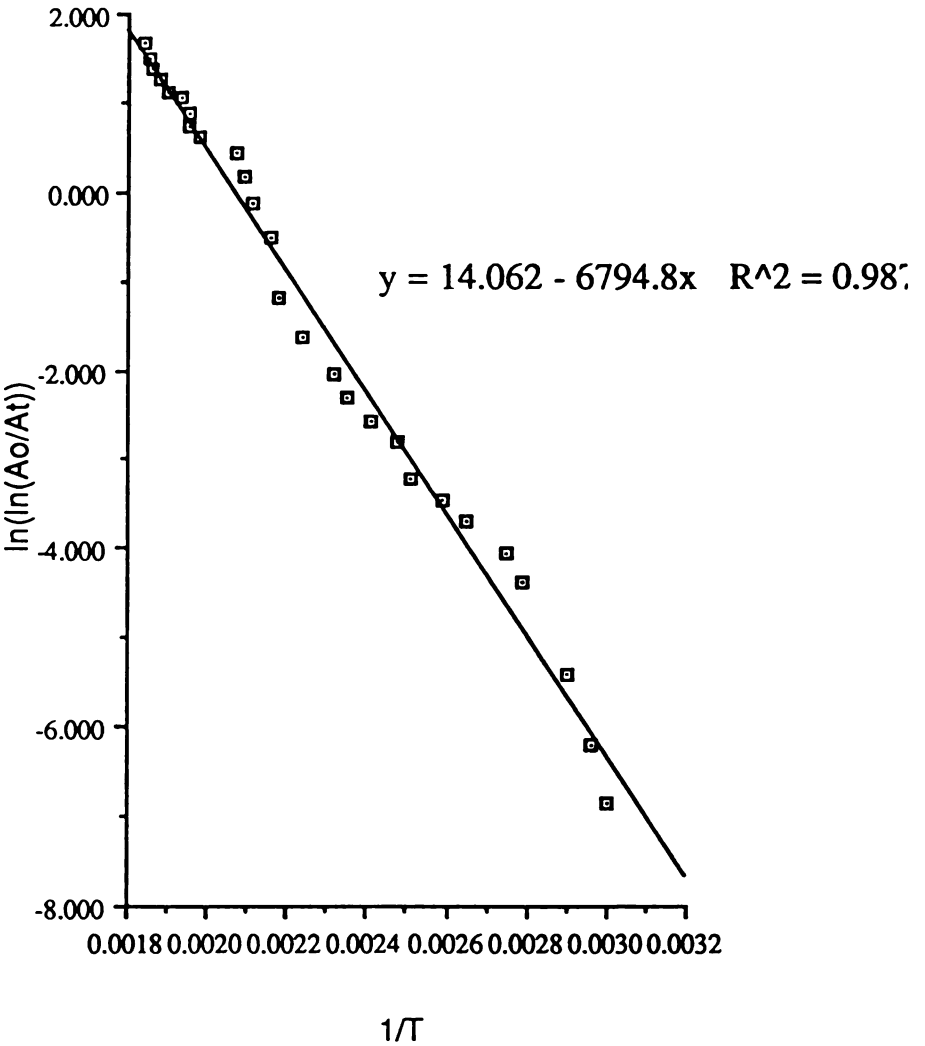

Figure A32. Arrhenius plot of ln(ln(Ao/At)) vs. 1/T for the $[M]K^+$ ion of palmitic acid. Ea calculated = 14 kcal/mol.

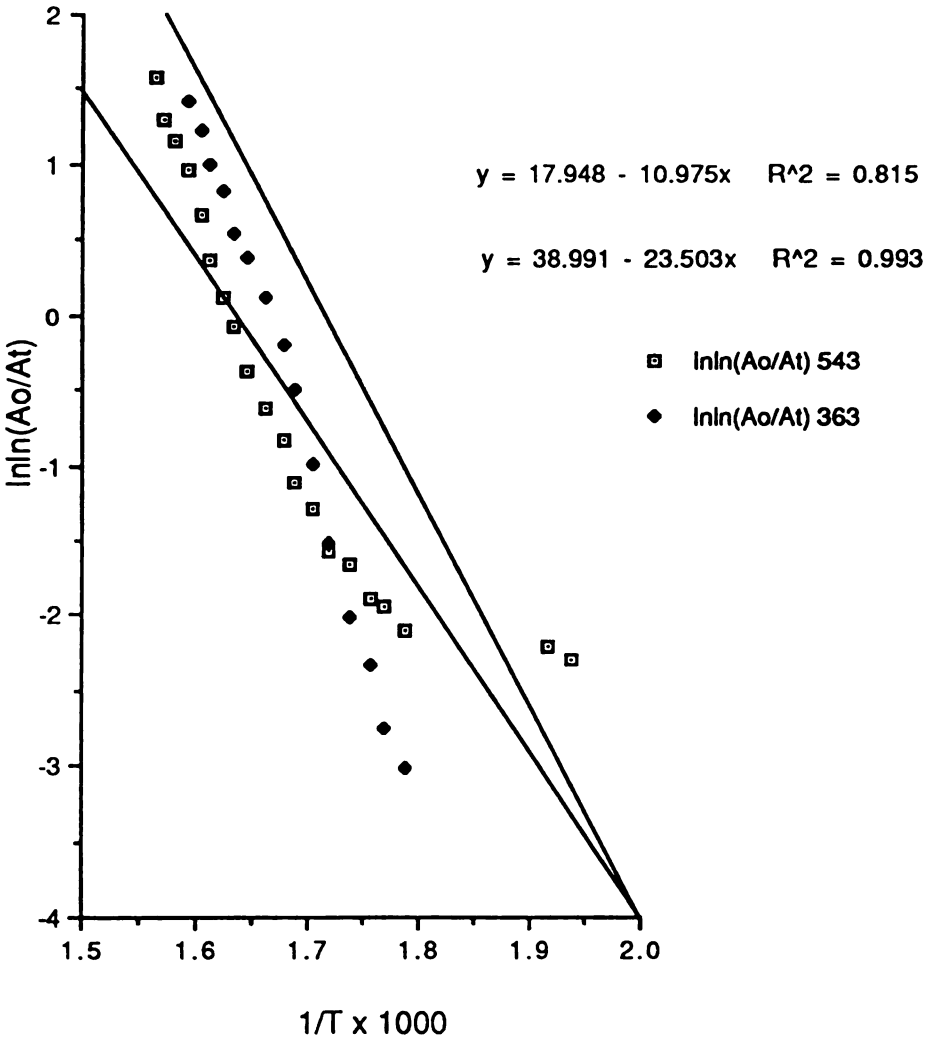

Figure A33. Arrhenius plot of ln(ln(Ao/At)) vs. 1/T for the $[M]K^+$ ion and a K^+ adduct ion of a fragment of melezitose. Ea(543) = 22 kcal/mol and Ea(363) = 47 kcal/mol.

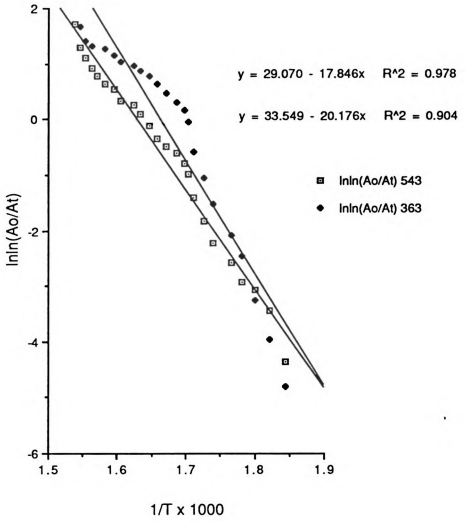

Figure A34. Arrhenius plot of ln(ln(Ao/At)) vs. 1/T of the $[M]K^+$ ion and a K^+ adduct ion of a fragment of melezitose. Ea(543) = 35 kcal/mol and Ea(363) = 40 kcal/mol.

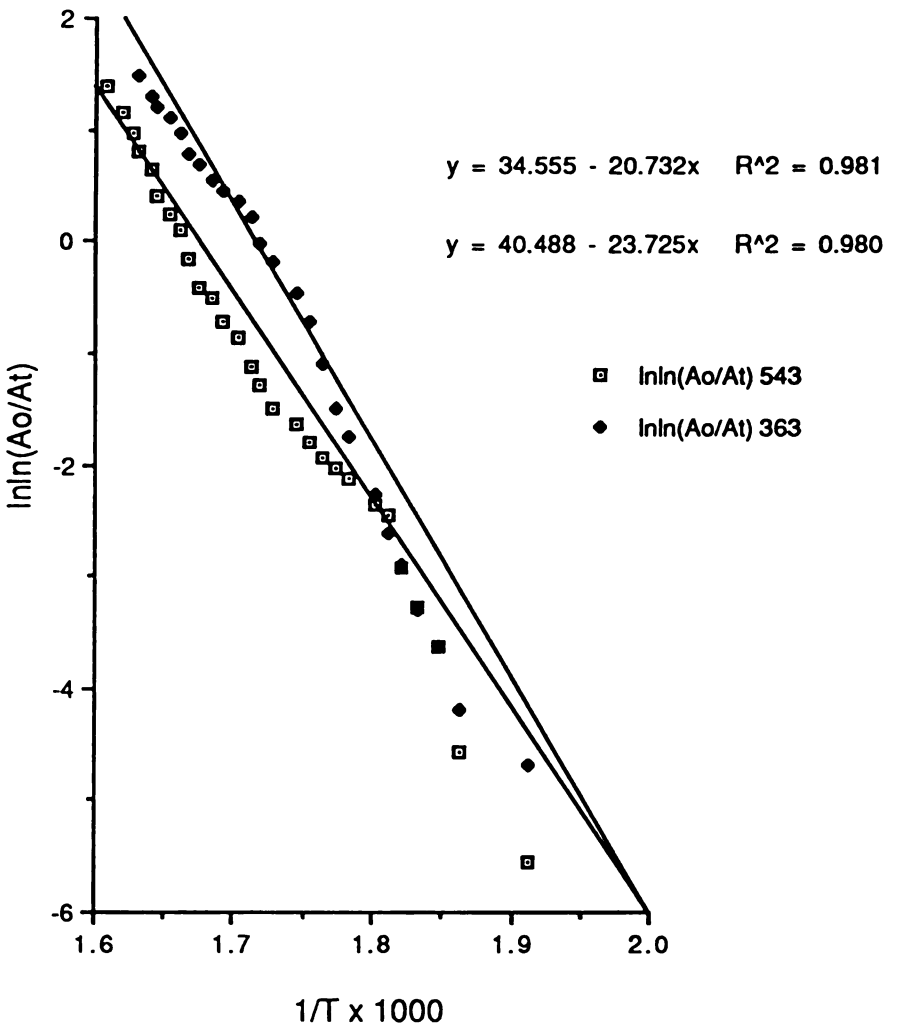

Figure A35. Arrhenius plot of ln(ln(Ao/At)) vs. 1/T for the $[M]K^+$ ion and K^+ adduct ion of a fragment of melezitose. Ea(543) = 41 kcal/mol and Ea(363) = 47 kcal/mol.

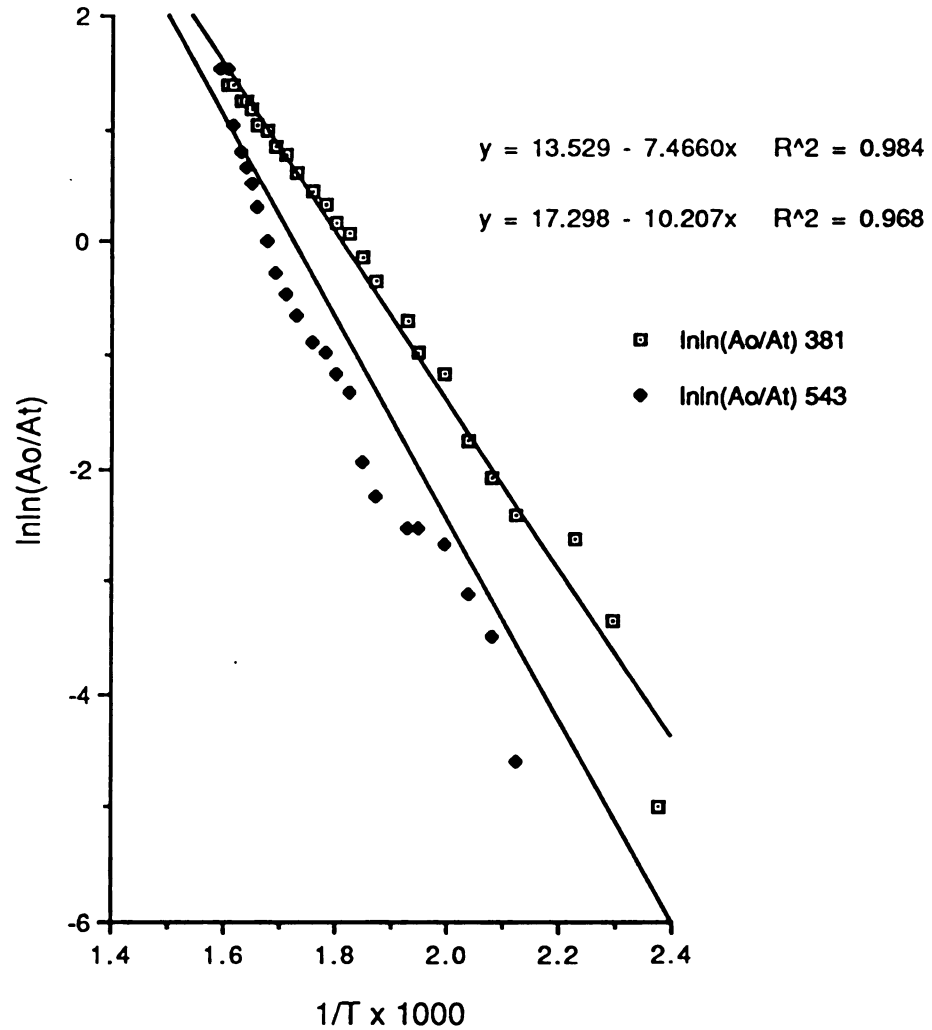

Figure A36. Arrhenius plot of ln(ln(Ao/At)) vs. 1/T for the $[M]K^+$ ions of melezitose (m/z 543) and sucrose (m/z 381). Ea(543) = 20 kcal/mol and Ea(381) = 15 kcal/mol.

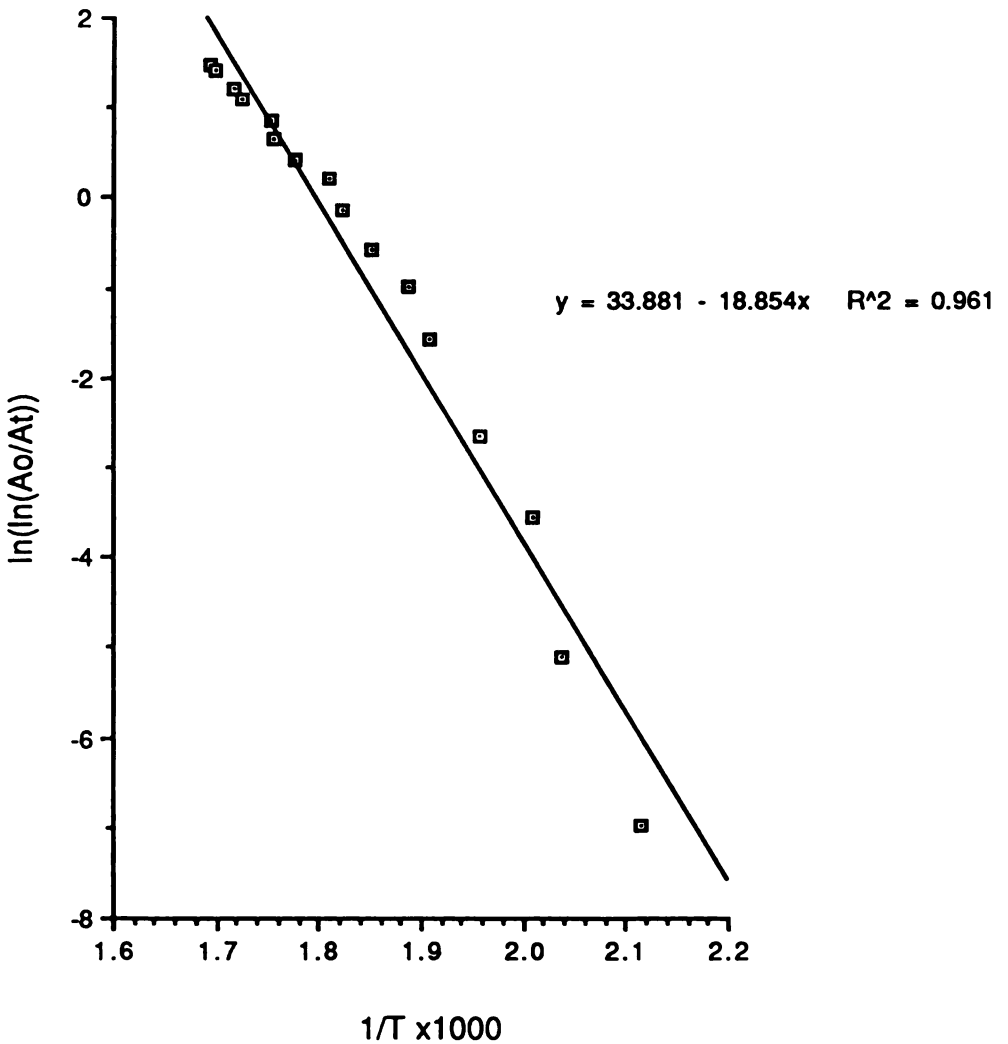

Figure A37. Arrhenius plot of ln(ln(Ao/At)) vs. 1/T for the m/z 392 fragment adduct ion of met-enkephalin. Ea calculated = 37kcal/mol

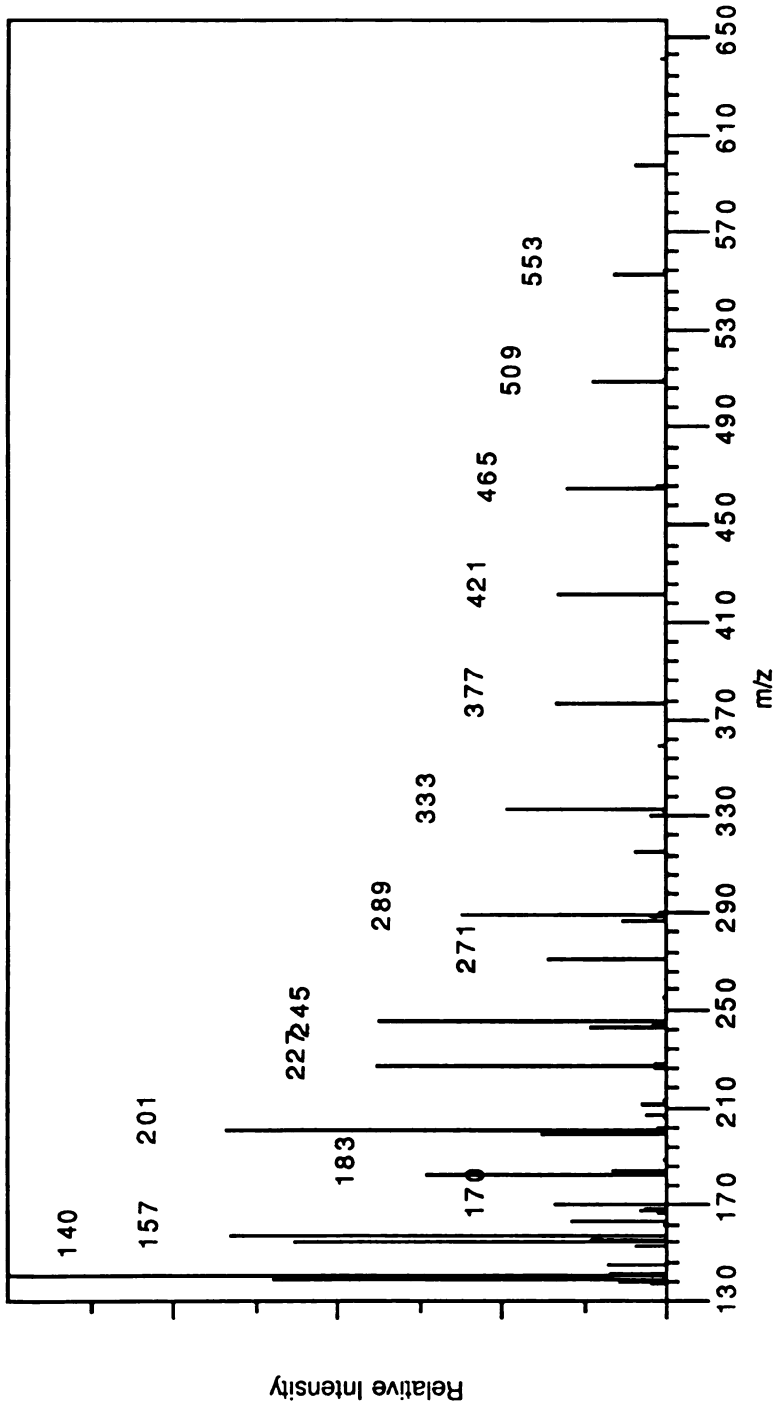

Figure A38. Li^+ IDS mass spectrum of polyethylene glycol 600 averaged over scans 30-55.

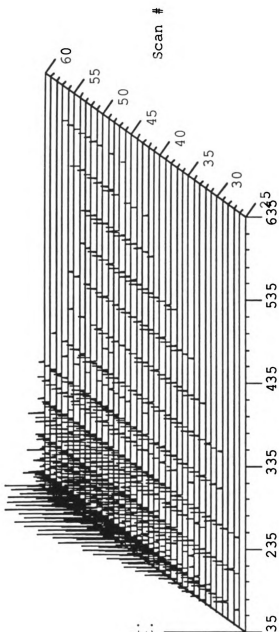

Figure A39. Plot of the Li^+IDS mass spectra of polyethylene glycol 600 vs. scan number.

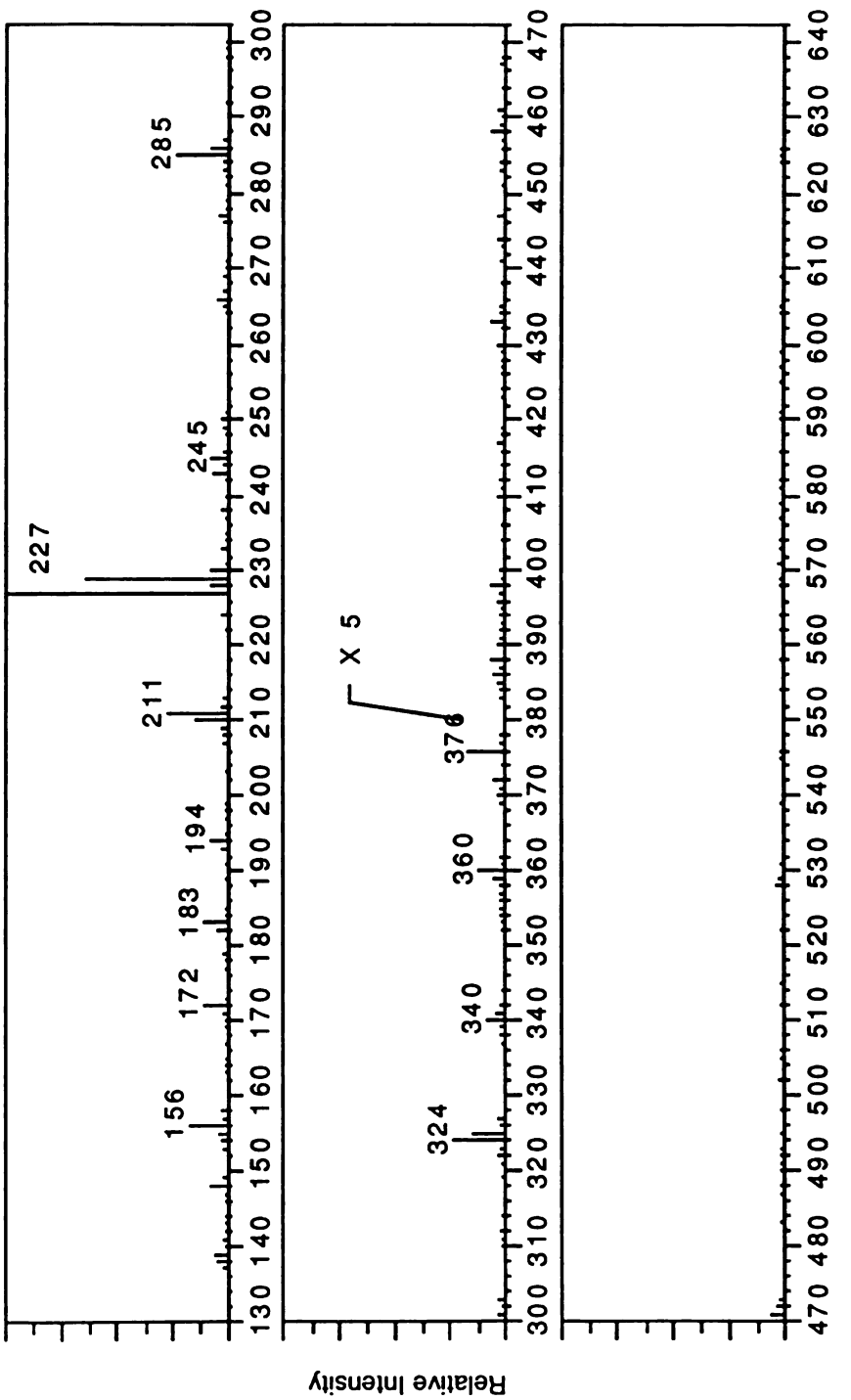

Figure A40. Li^+ IDS mass spectrum of methionine-enkephalin.

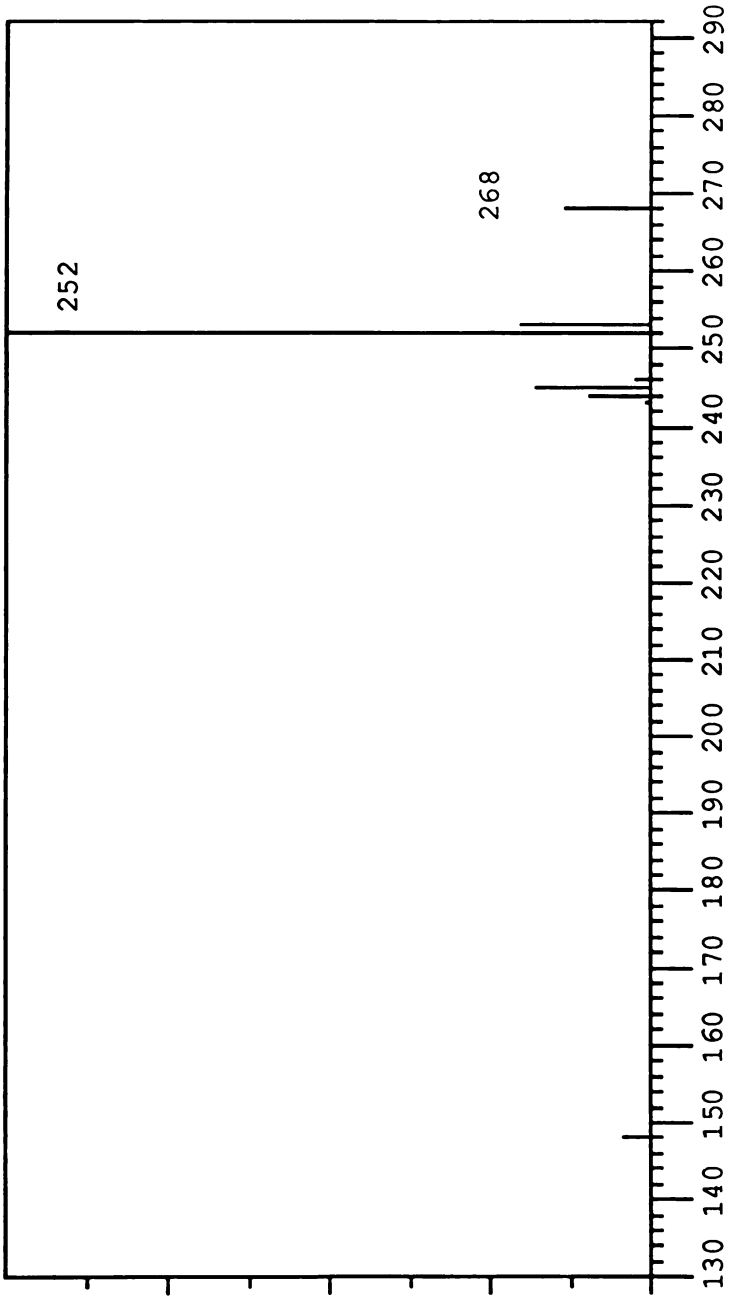

Figure A41. Li^+IDS mass spectrum of triphenylamine.

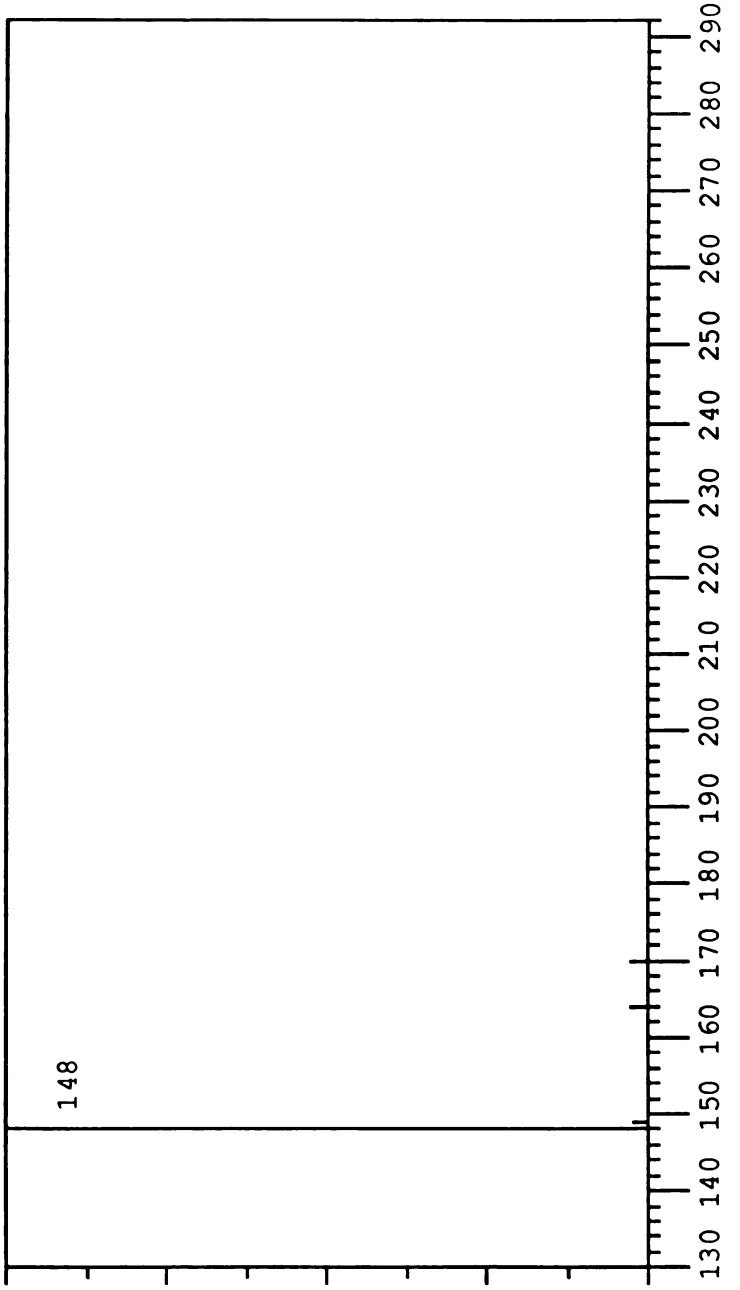

Figure A42. Li^+IDS mass spectrum of violuric acid.

APPENDIX B

BIOMEDICAL AND ENVIRONMENTAL MASS SPECTROMETRY, VOL. 18, 177–184 (1989)

Mass Spectrometric Analysis of Cardiac Glycosides by the Desorption/Ionization Technique Potassium Ion Ionization of Desorbed Species

Karen J. Light, Daniel B. Kassel and John Allison*
Department of Chemistry, Michigan State University, East Lansing, Michigan 48824, USA

The analysis of cardiac glycosides by the desorption/ionization (D/I) mass spectrometric technique potassium ion ionization of desorbed species (K^+IDS) is presented. K^+IDS mass spectra of digitoxin, digoxin, digoxigenin, digitoxin and ouabain are discussed to demonstrate the capabilities of this D/I method. The K^+IDS analysis consists of two steps: thermal desorption of neutral molecules representative of the analyte, followed by gas-phase addition of K^+ ions to these species. Structural and molecular weight information of the cardiac glycosides is obtained with the K^+IDS technique. The most intense peak in the K^+IDS mass spectrum of an analyte, M, is frequently the $[M]K^+$ ion. Interpretation of the K^+IDS mass spectra is simple, since one thermal degradation mechanism dominates. This mechanism is a 1,2-elimination process. A variation of the original K^+IDS technique, performed by changing the ionizing metal from K^+ to Na^+ (i.e. Na^+IDS), is presented for the analysis of digoxin. The Na^+IDS mass spectrum of digoxin contains more structural information than the K^+IDS mass spectrum of that compound. This may lead to a means of controlling the types of information obtainable with this D/I technique by varying the cation that is thermionically generated. K^+IDS analyses can be performed rapidly, no sample derivatization is necessary, no matrix is required and little instrument modification is necessary.

INTRODUCTION

The cardiac glycosides are an important class of cardenolide-type compounds, some of which are used as therapeutic agents for the treatment of congestive heart failure and certain heart arrythmias.[1] Their primary effect is to increase the efficiency and contractility of the heart muscle. One concern in using these compounds as therapeutic agents is the very narrow range of concentrations over which their effects are therapeutic (e.g., for digoxin, this range is 0.5–2.5 ng/ml in serum). Concentrations above 3.0 ng/ml are considered as toxic.[2] As a result, methods for identifying and accurately measuring the relative concentrations of these drugs are needed. Mass spectrometry offers one such method for accurately detecting low levels of these compounds.

The analyses of cardiac glycosides, using a wide variety of mass spectrometric approaches, have been reported. These include electron ionization (EI),[3] chemical ionization (CI),[4] desorption chemical ionization (DCI),[5] field ionization (FI),[6] field desorption (FD),[7] fast atom bombardment (FAB),[8] liquid chromatography/mass spectrometry (LC/MS)[9] and laser desorption (LD).[10] Extensive comparisons of these mass spectrometric ionization techniques for cardiac glycoside evaluation have been presented in the literature.[10a] Recently the desorption/ionization (D/I) technique, K^+ ionization of desorbed species (K^+IDS), was reported for the analysis of thermally labile compounds by mass spectrometry.[11] Presented here are the results of K^+IDS analyses of several cardiac glycosides, to allow for evaluation of the method in the context of other D/I techniques. The results show the strength of K^+IDS for the analysis of cardiac glycosides. Extensive comparisons to other techniques are limited here, to avoid redundancy with recently published review articles.[10a]

The D/I technique K^+IDS utilizes a thermionic emitter which produces a high flux of alkali ions in the gas phase when heated to temperatures in excess of 800 °C.[12] When a thermally labile compound is deposited onto the surface of such an emitter, which is then rapidly heated, K^+ adduct ions of desorbing neutrals are formed in the gas phase.[11] K^+IDS mass spectra of most thermally labile compounds frequently contain K^+ adducts of the intact molecule (M), $[M]K^+$, and of various thermal decomposition products (D_i), $[D_i]K^+$. The extent to which desorption and/or decomposition of M occurs is dependent on the heating rate and the final temperature achieved, and, of course, on the molecule M. Beuhler and coworkers have proposed that the rapid heating of a sample to a high temperature can access conditions at which the rate of vaporization of a thermally labile compound may exceed the rate of decomposition.[13]

In reviewing the literature for mass spectrometric analyses of cardiac glycosides, we found a number of approaches used to identify fragment ions produced by the various D/I mass spectrometric techniques. Many designation schemes were sufficiently vague that the reader must calculate the exact composition of the ion. Others were more complex than necessary for determining the sequence of carbohydrates. Therefore we developed a scheme for our needs that will be used here and in subsequent publications. Details are provided in the Appendix. We have found it to be useful for discussion

0887-6134/89/030177-08 $05.00

Received 25 May 1988
Revised 6 September 1988

of ionic and neutral species derived from saccharides and saccharide-containing compounds.

EXPERIMENTAL

The cardiac glycosides were obtained commercially and used without further purification or derivatization. The digitonin was obtained from Merck & Co. Inc., Rahway, New Jersey. The digoxin, digitoxin, ouabain and digoxigenin samples were obtained from the Sigma Chemical Co., St Louis, Missouri. The samples were suspended or dissolved in acetone to allow transfer of 1–2 μg of sample onto the tip of the probe. The solvent was then evaporated before inserting the probe into the mass spectrometer.

All mass spectrometric analyses were performed on an unmodified HP5985 GC/MS/DS quadrupole mass spectrometer with a mass range of 10–1000 u, equipped with a direct insertion probe (DIP) inlet. The mass spectrometer ion source was operated in the EI 'open' source configuration. The construction of the K^+IDS probe has been described previously.[11] The thermionic emitter is an alkali aluminosilicate mixture ($1K_2O:1Al_2O_3:2SiO_2$).[12]

In the early stages of the K^+IDS probe design, analyte was deposited directly onto the K^+ bead.[11] Desorption of analyte from the bead surface occurred rapidly when the K^+ emitter was resistively heated to high temperatures (>800 °C) while the onset of K^+ emission occurred after 5–6 s. Formation of adduct ions requires a sufficient temporal overlap of the alkali emission and analyte desorption.[14] In order to improve the temporal overlap between the emission of K^+ ions from the thermionic emitter and the desorption of analyte neutrals, a modification of the original probe design was made. This new design incorporates a separate 'filament', on which the sample is deposited.[15] The second filament is not directly heated, but is in close proximity to the bead and is therefore radiatively heated. Initial results using this two-filament design have shown an approximate 40-fold enhancement in sensitivity. This new probe design is currently under detailed study for further optimization and characterization.

RESULTS AND DISCUSSION

The K^+IDS mass spectra of the simplest sugars glucose and sucrose have been reported.[11] Abundant molecular adduct ions as well as K^+ adducts of thermal degradation products can be formed. For sucrose, a disaccharide, ions are observed at *m/z* 201 and 219 which are formed by a 1,2-elimination about the glycosidic linkage (Scheme 1).

Cleavage of one bond (a glycosidic bond) followed by an H-shift (to the glycosidic oxygen) occurs to produce two stable neutral species in a low-energy process. This mechanism is dominant for most types of molecules because little energy is required. For example, consider a simple molecule such as methyl ethyl ether. While cleavage of the C—O bond to yield two radicals, reaction (1), requires 318 kJ/mol, only 67 kJ/mol is required for a 1,2-elimination, i.e. C—O cleavage with an accompanying H-shift, reaction (2).

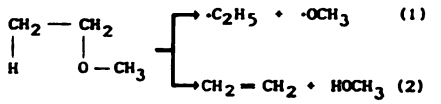

This mechanism is dominant in the thermal degradation of saccharide-containing molecules analyzed by K^+IDS. Degradation occurs in the condensed phase in a K^+IDS analysis; both neutrals from this process can desorb into the gas phase and undergo K^+ attachment to produce $[D_i]K^+$ adducts. Such 1,2-elimination reactions dominate thermal degradation processes at high temperatures and short times, and can be used to explain most of the $[D_i]K^+$ ions formed in K^+IDS analyses. Dehydration is another low-energy thermal degradation pathway, again a 1,2-elimination. Both the parent molecule, M, and decomposition products, D_i, can undergo dehydration reactions (when hydroxy groups are present) and desorb, leading to ions such as $[M - H_2O]K^+$ and $[D_i - H_2O]K^+$.

The first cardiac glycoside that will be discussed is digitonin ($C_{56}H_{92}O_{29}$, mol.wt = 1228, structure I; Fig. A1). The complete K^+IDS mass spectrum of digitonin cannot be presented here since the instrument used has

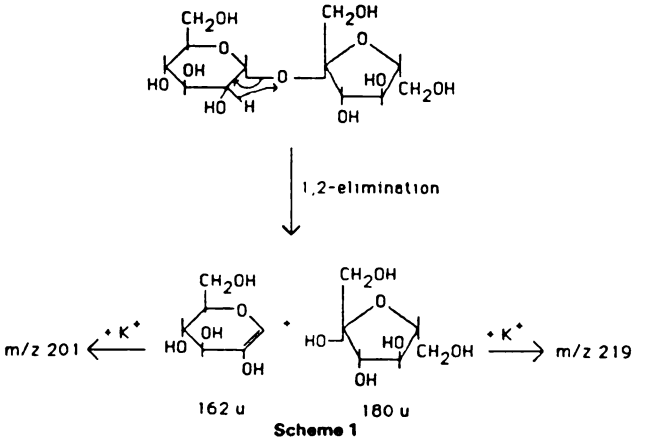

Scheme 1

a limited mass range (10–1000 u). The molecular adduct ion, $[M]K^+$, would be at *m/z* 1267. Despite this drawback we begin our discussion with digitonin since it is the most complex of the cardiac glycosides studied. The ions observed will serve as a framework for discussing the nomenclature scheme that we use and the relationship between the ions observed and the structure of the analyte. It is assumed that the 1,2-elimination mechanism, which dominates the thermal degradation of many other types of molecules, is operative for cardiac glycosides. This will be the basis for the assignments of the observed ions, and is reasonable as the following discussion will show. Unfortunately K^+IDS mass spectra are short-lived, and the quadrupole instrument currently being used cannot perform exact mass measurements, but the consistent observation of the 1,2-elimination degradation products allows these assignments to be made with some confidence.

Using the nomenclature presented in the Appendix, the digitonin molecule is designated as $AOS_1OS_2(OT_3)OS_3OS_4$ (or as M, see structure I in Appendix). The ions observed below *m/z* 1000 are listed in Table 1. Based on the mechanism observed for other compounds, especially sucrose, it is postulated that the glycosidic bonds will be the site of thermal degradation. For example, if the O—S_4 bond is cleaved, the fragment designated as S_4 has a mass of 163 u. A K^+ adduct is observed at *m/z* 201, which is the alkali ion attached to a neutral of mass 162 u, indicating that an H has shifted off of the sugar (via a 1,2-elimination). The other neutral product of this degradation reaction, $[M - (S_4^{-H})]$ has a mass of 934 u. The vaporization of this latter molecule followed by K^+ attachment leads to an ion at *m/z* 973. The observation of both ions in the K^+IDS mass spectrum further supports the proposed elimination of S_4^{-H}. In this way, the remaining ions in the mass spectrum are easily related to the structure of the molecule, as indicated in Table 1. It should be stressed again that the large number of molecules studied to date strongly support this mechanism, making interpretation simple.

Table 1. Assignment of the ions in the K^+IDS mass spectrum of digitonin

m/z	Assignment
1267[a]	$[M]K^+ = [AOS_1OS_2(OT_3)OS_3OS_4]K^+$
973	$[AOS_1OS_2(O^{+H})OS_3O^{+H}]K^+$
943	$[M - (S_4OS_3^{+H})]K^+$
927	$[M - (S_4OS_3O^{+H})]K^+$
811	$[AOS_1OS_2(O^{+H})O^{+H}]K^+$
795	impurity[b] $= [A'OS_1OS_2(O^{+H})O^{+H}]K^+$
633	$[AOS_3^{+H}]K^+$
649	$[AOS_3O^{+H}]K^+$
495	$[M - (AOS_1OS_2(O^{+H})O^{+H})]K^+$
487	$[AO^{+H}]K^+$
471	impurity[b] $= [A'O^{+H}]K^+$
363	$[S_4OS_3^{+H}]K^+$
201	$[S_4^{+H}]K^+$
171	$[T_3^{+H}]K^+$

[a] Ion not observed, since it exceeds the mass limit of the mass spectrometer used in this study.
[b] The designation A' indicates that the impurity contains an aglycone structure that differs from that in digitonin, as suggested in Ref. 16.

The thermal conversion of one molecule into two stable molecules, by this 1,2-elimination mechanism, is thermodynamically the most favored process.

Even though the mass limit of the instrument used in this study prohibited the detection of the $[M]K^+$ ion at *m/z* 1267, it has been observed by another researcher on a higher-mass instrument.[16] In this case the $[M]K^+$ ion was not the base peak in the mass spectrum, but it was the only important ion above *m/z* 1000.

There were a few peaks that did not easily correlate with the structure of digitonin but did correlate with a common impurity of digitonin that has been identified by others[17] and observed by an FAB analysis performed in this laboratory. The impurity corresponded to a deoxy version of the genin of digitonin, and the impurity ions were 16 u less than major ions of digitonin. Therefore the assignment of these ions as impurities logically followed.

Another reason for beginning this discussion with digitonin is to show the time dependence of the spectra obtained with the K^+IDS technique, unlike other D/I techniques such as FAB. A three-dimensional plot depicting the mass spectra collected v. scan number (time) for the entire K^+IDS analysis of digitonin is shown in Fig. 1. The scan rate was 1 s/scan and the analyte signal typically lasted for approximately 30 s. Early in the run, low-mass ion formation was favored, while at intermediate times the higher-mass ions became prevalent. Late in the run, both intermediate and low-mass ions were observed. Activation energies for the formation of specific decomposition products may differ and would explain the observed temperature/time dependence.[13] Thus it may be possible to extract information about specific decomposition pathways (i.e. the relative activation energies for the formation of the products) from the temperature or time at which they are formed during a K^+IDS analysis, and relate these to structural features.

The emphasis of this paper, however, is to demonstrate the wealth of information concerning the structure and carbohydrate sequence of cardiac glycosides that can be obtained with the K^+IDS technique, and the simplicity of K^+IDS mass spectra. The remaining K^+IDS mass spectra that will be shown are generated by averaging spectra from all of the scans over the entire desorption profile (approximately 30 s in duration).

DIGOXIN

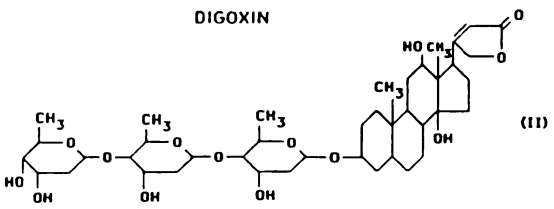

(II)

Digoxin ($C_{41}H_{64}O_{14}$, mol.wt = 780, structure II), a commonly used therapeutic agent, is a three-sugar cardiac glycoside. Molecular weight as well as abundant structural information can be obtained for digoxin using the K^+IDS technique. The averaged K^+IDS mass spectrum of digoxin is shown in Fig. 2 and assignments

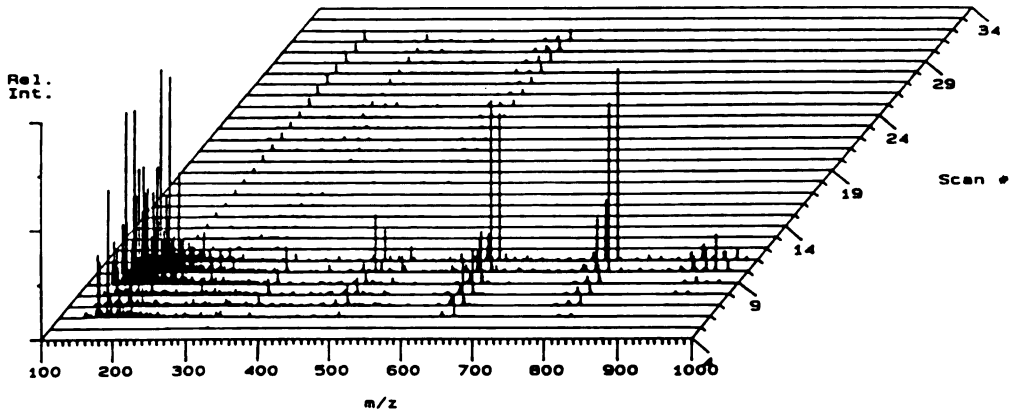

Figure 1. Time dependence of the K⁺IDS mass spectra of digitonin (structure I, mol.wt = 1228).

for the observed ions are summarized in Table 2. The base peak for digoxin is the $[M]K^+$ ion at m/z 819. All of the major cleavages at the glycosidic linkages produce two neutral species that undergo K^+ addition. These bond cleavages follow the 1,2-elimination mechanism as described for digitonin and sucrose. The low-mass ion series will be addressed shortly.

DIGITOXIN

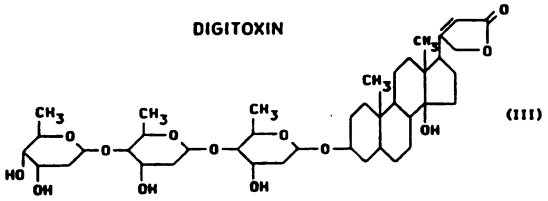

(III)

Digitoxin ($C_{41}H_{64}O_{13}$, mol.wt = 764, structure III), is a cardiac glycoside that differs from digoxin by the absence of the hydroxy group on the C(12) position of the genin portion of the molecule and thus has a molecular weight 16 u below digoxin. The K⁺IDS mass spectrum of digitoxin is very similar to that of digoxin. The K^+ adduct ions observed and their assignments are given in Table 2. All of the ions containing the genin portion are shifted 16 u lower in the digitoxin mass

Table 2. Assignment of ions in the K⁺IDS mass spectra of digoxin, digitoxin, ouabain and digoxigenin

	m/z	Assignment
Digoxin	819	$[M]K^+ = [AOS_1OS_2OS_3]K^+$
	801	$[M-H_2O]K^+$
	689	$[AOS_1OS_2O^{+H}]K^+$
	559	$[AOS_1O^{+H}]K^+$
	429	$[AO^{+H}]K^+$
		$[M-(AO^{+H})]K^+$
	299	$[S_3OS_2^{+H}]K^+$
Digitoxin	803	$[M]K^+ = [AOS_1OS_2OS_3]K^+$
	785	$[M-H_2O]K^+$
	673	$[AOS_1OS_2O^{+H}]K^+$
	543	$[AOS_1O^{+H}]K^+$
	413	$[AO^{+H}]K^+$
	429	$[M-(AO^{+H})]K^+$
	299	$[S_3OS_2^{+H}]K^+$
Ouabain	623	$[M]K^+ = [AOS_1]K^+$
	605	$[M-H_2O]K^+$
	477	$[AO^{+H}]K^+$
	459	$[A^{-H}]K^+$
Digoxigenin	429	$[M]K^+$
	411	$[M-H_2O]K^+$
	393	$[M-2H_2O]K^+$

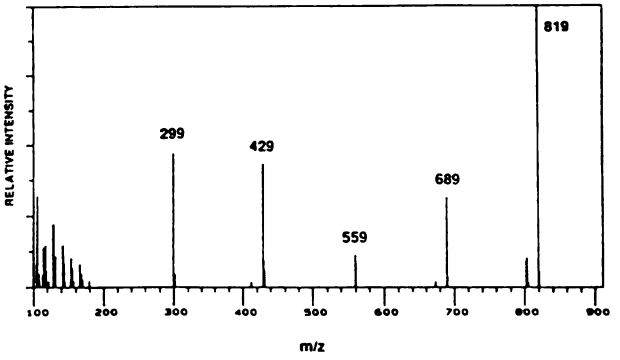

Figure 2. K⁺IDS mass spectrum of digoxin (structure II, mol.wt = 780).

spectrum relative to those formed from digoxin. For digoxin, two structures are assigned for *m/z* 429, but only one contains the aglycone portion of the molecule. For digitoxin, there is still an *m/z* 429, and the product containing the aglycone is now 16 u lower at *m/z* 413. This suggests that, for digoxin, the ion current at *m/z* 429 represents both structures as indicated in Table 2.

OUABAIN

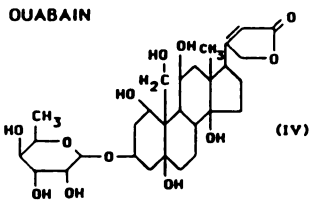

(IV)

Another cardiac glycoside, ouabain ($C_{29}H_{44}O_{12}$, mol.wt = 584, structure IV), is well characterized by its K^+IDS mass spectrum. The averaged mass spectrum of a K^+IDS analysis of ouabain is shown in Fig. 3. This glycoside contains only one sugar and a slightly different steroid moiety. The ion of highest *m/z* in the spectrum, which is also the base peak, provides the molecular weight information, since it is the $[M]K^+$ ion at *m/z* 623. Structural information is also available. The ion at *m/z* 477 is the K^+ adduct of the aglycone portion and is formed in a manner identical to that described for structural ions observed for digitonin. Table 2 gives the assignments of the major ions in this mass spectrum. Interestingly, the same low-mass ion series between *m/z* 105 and 215 u that was observed for digoxin is present in the K^+IDS mass spectrum of ouabain. These ions are separated by 12, 13 and 14 u, which suggests an aromatic system. Either the sugars or the aglycone portion could be thermally degrading to an aromatic species. Ouabain and digoxin have different numbers of sugar groups in the molecule. Therefore it seems that this low-mass ion series might be from the aglycone, upon conversion to a highly reduced form. If this low-mass ion series proves useful for indicating the presence of a steroid group, this would offer an advantage of K^+IDS over FAB in which this low-mass ion series would be lost in the chemical noise associated with that technique.

To investigate the origin of this low-mass ion series digoxigenin was studied, which is not a cardiac glycoside but rather the genin, or steroid portion, of digoxin. The K^+IDS mass spectrum of digoxigenin ($C_{23}H_{34}O_5$, mol.wt = 390, structure V) is shown in Fig. 4. Once

DIGOXIGENIN

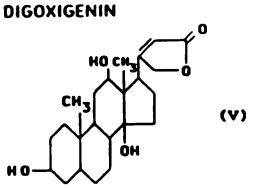

(V)

again, the base peak is the $[M]K^+$ ion at *m/z* 429. The same low-mass ion series, between *m/z* 105 and 215, does appear which shows that they arise from the steroid portion of the molecule. The prominent low-mass ions are tabulated in Table 3 along with proposed assignments. The justification for the proposed assignments is as follows. These ions are not typical of those observed in K^+IDS analyses of compounds containing only C, H and O since they appear at both odd and even *m/z* values. The mechanism that is consistently operative in K^+IDS should only form even mass neutral products for these molecules which then appear as odd mass ions following K^+ (*m/z* 39) attachment. The mass differences between the ions might suggest that they are derived from aromatic species. It is suggested that these low-mass ions are products of surface ionization of the reduced aglycone moiety ($C_{17}H_{12}$, mol.wt = 216, structure VI) (or its precursors) for two reasons. First, surface ionization of molecules with low

REDUCED AGLYCONE

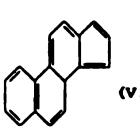

(VI)

ionization energies has been observed on these emitters.[18] Second, the ionization energy, I.E., for multicyclic hydrocarbons decreases as the size of the molecule increases and the extent of unsaturation

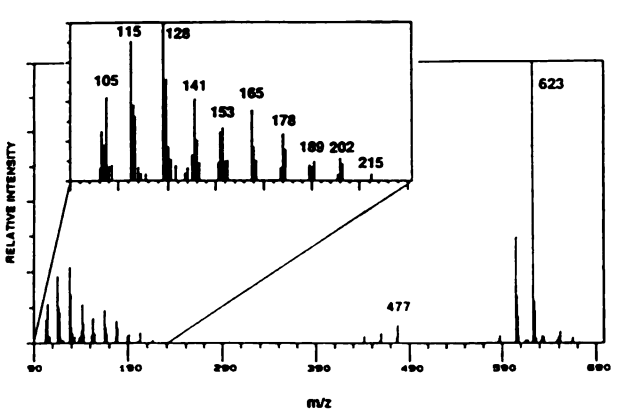

Figure 3. K^+IDS mass spectrum of ouabain (structure IV, mol.wt = 584).

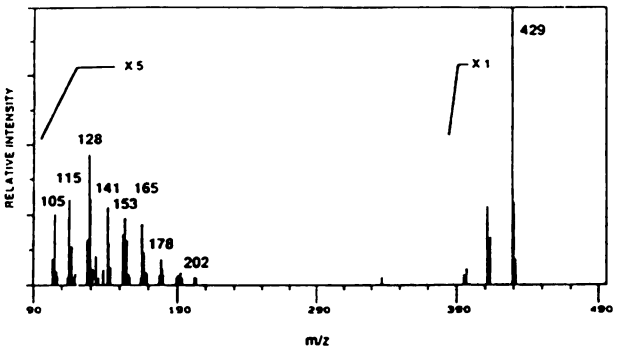

Figure 4. K⁺IDS mass spectrum of digoxigenin (structure V, mol.wt = 390).

Table 3. Low-mass ion series observed in the K⁺IDS mass spectra of ouabain, digoxin and digoxigenin

m/z	Assignment	m/z	Assignment
105	$[C_8H_9]^+$	165	$[C_{13}H_9]^+$
115	$[C_9H_7]^+$	178	$[C_{14}H_{10}]^+$
128	$[C_{10}H_8]^+$	189	$[C_{15}H_9]^+$
141	$[C_{11}H_9]^+$	202	$[C_{16}H_{10}]^+$
153	$[C_{12}H_9]^+$	215	$[C_{17}H_{11}]^+$

increases (e.g. I.E.(benzene) = 9.25 eV, I.E.(naphthalene) = 8.12 eV, I.E.(anthracene) = 7.5 eV).[19] This would also explain why the same low-mass ions are observed for cardiac glycosides with aglycones that contain different functional groups. Work is still in progress to determine whether this proposed origin of these low-mass ions is valid. However, in the final analysis, these ions are very characteristic of a steroid structure, both in terms of the mass range at which they appear, and *when* they appear during the K⁺IDS analysis.

In addition to K⁺IDS, analyses have been performed using an Na^+ emitter. The Na^+IDS mass spectrum of digoxin is shown in Fig. 5. There are several noticeable differences in the Na^+IDS mass spectrum of digoxin to that obtained utilizing K⁺IDS (Fig. 2). The $[M]Na^+$ ion is not the base peak of the spectrum in Fig. 5. The lower-mass ion peaks from cleavage of each glycosidic bond (observed as Na^+ adducts) are relatively more intense than in the K⁺IDS mass spectrum. Also the loss of H_2O from each of the major fragments is observed, providing additional structural information. This suggests that Na^+ may promote fragmentation (when K^+ does not) upon adduct formation in the gas phase, such as reaction (3).

$$Na^+ + D_i \rightarrow \{D_i + Na^+\}^* \rightarrow [D_i - H_2O]K^+ + H_2O \quad (3)$$

Thus, the metal ion used for ionization in this process is a variable that can be selected to obtain different information about the analyte. It has been shown that Li^+ is more reactive in the gas phase[20] than Na^+ or K^+, and would be more likely to undergo reactions such as (3).

CONCLUSIONS

K⁺IDS has been demonstrated as a useful ionization technique for the mass spectrometric analysis of cardiac glycosides, and the mass spectra obtained are comparable to those obtained from other desorption/ionization techniques that are currently used in mass spectrometry. The K⁺IDS mass spectra are obtained very rapidly, within 1 min, and are relatively clean. Thermal processes occurring at these short times can produce intact desorbed molecules, even though these compounds are considered to be 'thermally labile'. Also, the operative

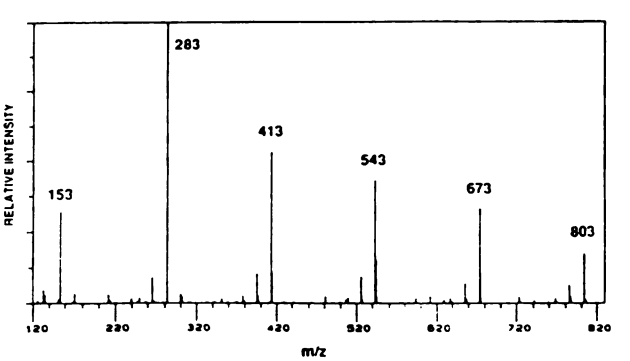

Figure 5. Na⁺IDS mass spectrum of digoxin (structure II, mol.wt = 780).

mechanisms under these conditions appear to be simple 1,2-eliminations, thus thermal degradation products can be *easily* related to the parent compound. K^+ ions appear to have a sufficient affinity for organic molecules such that adduct formation can occur. However, the energy released on complexation is insufficient to induce fragmentation, so the K^+ ions simply 'sample' the desorbed species. For molecules which only desorb intact, with no decomposition at temperatures used in K^+IDS, only the $[M]K^+$ ion is observed. However, the same type of analysis with another thermionically generated cation, such as Na^+ or Li^+, may provide some structural information via gas-phase reactions. Thus by changing the metal ion used in the analysis, it may be possible to obtain different types of information about the analyte. We are currently adapting this technique to a JEOL HX-110 mass spectrometer, for studies of higher molecular weight compounds, and to perform *B/E* linked-scanning analyses of specific ions.

Acknowledgements

The authors wish to thank T. Brody for providing the cardiac glycoside samples. This work was made possible through the financial support of: the Analytical Labs of the Dow Chemical Company; the United States Department of Agriculture (grant no. USDA-ARS-59-32U4-7-107, administered by the MSU Center for Environmental Toxicology); and the National Institutes of Health (NIH grant no. RR00480-16).

REFERENCES

1. T. W. Smith, *Digitalis Glycosides*, Grune & Stratton, Orlando (1986).
2. A. Goth, *Medical Pharmocology*, 11th edn, p. 431. Mosby, St Louis (1984).
3. (a) F. C. Falkner, J. Frolich and J. T. Watson, *Org. Mass Spectrom.* **7**, 141 (1973); (b) P. Brown, F. Bruschweiler and G. R. Pettit, *Helv. Chim. Acta* **55**, 531 (1972).
4. J. Vine, L. Brown, J. Boutagy, R. Thomas and D. Nelson, *Biomed. Mass Spectrom.* **6**, 415 (1979).
5. (a) A. Kappeler and U. Richli, *Advances in Mass Spectrometry. Part B. 10th Int. Mass Spectrom. Conf.*, p. 1497. Wiley, New York (1985); (b) A. P. Bruins, *Int. J. Mass Spectrom. Ion Proc.* **48**, 185 (1983); (c) A. P. Bruins, *Anal. Chem.* **52**, 605 (1980).
6. (a) P. Brown, F. Bruschweiler and G. R. Pettit, *Org. Mass Spectrom.* **5**, 573 (1971); (b) P. Brown, F. Bruschweiler, G. R. Pettit and T. Reichstein, *J. Am. Chem. Soc.* **92**, 4470 (1970).
7. (a) T. Komori, T. Kawasaki and H. R. Schulten, *Mass Spectrom. Rev.* **4**, 255 (1985); (b) H. R. Schulten, T. Komori, T. Nohara, R. Higuchi and T. Kawasaki, *Tetrahedron* **34**, 1003 (1978); (c) H. R. Schulten and D. E. Games, *Biomed. Mass Spectrom.* **1**, 120 (1974).
8. (a) J. R. J. Pare, P. Lafontaine, J. Belanger, W. W. Sy, N. Jordan and J. C. K. Loo, *J. Pharm. Biomed. Anal.* **5**, 131 (1987); (b) R. Isobe, T. Komori, F. Abe and T. Yamauchi, *Biomed. Environ. Mass Spectrom.* **13**, 585 (1986).
9. D. E. Games, M. A. McDowall, K. Levsen, K. H. Schafer, P. Dobberstein and D. L. Gower, *Biomed. Mass Spectrom.* **11**, 87 (1984).
10. (a) R. E. Shomo II, A. Chandrasekaran, A. G. Marshall, R. H. Reuning and L. W. Robertson, *Biomed. Environ. Mass Spectrom.* **15**, 295 (1988); (b) J. C. Tabet and R. J. Cotter, *Anal. Chem.* **56**, 1662 (1984); (c) M. A. Posthumus, P. G. Kistemaker, H. L. C. Meuzelaar and M. C. Ten Noever de Brauw, *Anal. Chem.* **50**, 985 (1978).
11. D. D. Bombick and J. Allison, *Anal. Chem.* **59**, 458 (1987).
12. J. P. Blewett and E. J. Jones, *J. Phys. Rev.* **50**, 464 (1936).
13. R. J. Beuhler, E. Flanigan, L. J. Greene and L. Friedman, *J. Am. Chem. Soc.* **96**, 3990 (1974).
14. D. B. Bombick and J. Allison, *Anal. Chim. Acta* **208**, 99 (1988).
15. D. B. Kassel and J. Allison, *Biomed. Env. Mass Spectrom.*, **17**, 221 (1988).
16. W. J. Simonsick, E. I. du Pont de Nemours & Co., Philadelphia, personal communication (1988).
17. Y. M. Yang, H. A. Lloyd, L. K. Pannell, H. M. Fales, R. D. Macfarlane, C. J. McNeal and Y. Ito, *Biomed. Env. Mass Spectrom.* **13**, 439 (1986).
18. D. Bombick, J. D. Pinkston and J. Allison, *Anal. Chem.* **56**, 396 (1984).
19. J. L. Franklin, J. G. Dillard, H. M. Rosenstock, J. T. Herron, K. Draxl and F. H. Field, *Nat. Stand. Ref. Data Ser., Nat. Bur. Stand. (US)* **26**, 289 (1969).
20. J. Allison and D. P. Ridge, *J. Am. Chem. Soc.* **101**, 4998 (1979).

APPENDIX

Analyzing the K^+IDS mass spectra of the cardiac glycosides required the aid of a labeling scheme to accurately identify the fragments observed as K^+ adduct ions. Such a scheme was not found in the literature that would show the exact designation, including the H-shifts observed, and would simply relate the fragments to the intact molecule. Therefore a scheme was designed for use in this paper as well as subsequent works utilizing K^+IDS and FAB from our laboratory on saccharide-containing compounds. This scheme was patterned after one proposed by Pettit and Brown in 1971.[6]

Digitonin (structure I; Fig. A1) will be used as an example for explaining this naming scheme since it is the most complex compound discussed in this paper. The non-sugar or steroid portion of the molecule is labeled A for aglycone. The numbering of the sugars in this molecule is similar to that used for designating the position of C atoms in alkanes. The sugars in the main (longest) chain are labeled as S_n, where n is the index for the position of that sugar along the chain, in this case the distance from the aglycone. The sugars in the branch are labelled T_n. The glycosidic oxygens between sugars are explicitly designated in the naming scheme. Therefore, we designate the molecule in a linear shorthand form as $AOS_1OS_2(OT_3)OS_3OS_4$. The branched sugars have an index number that identifies their distance from the aglycone.

With the designation of the parent molecule completed, the identification of cleavage products can be addressed. As discussed in the paper, the $O{-}S_4$ bond is broken with a concurrent H-shift to the genin portion. This H-shift is designated by '$-$H' and '$+$H' superscripts; thus the two neutrals would be labeled as $[S_4^{-H}]$ and $[AOS_1OS_2(OT_3)OS_3^{+H}]$. The later fragment could also be labeled as $[M-(S_4^{-H})]$, with the selection

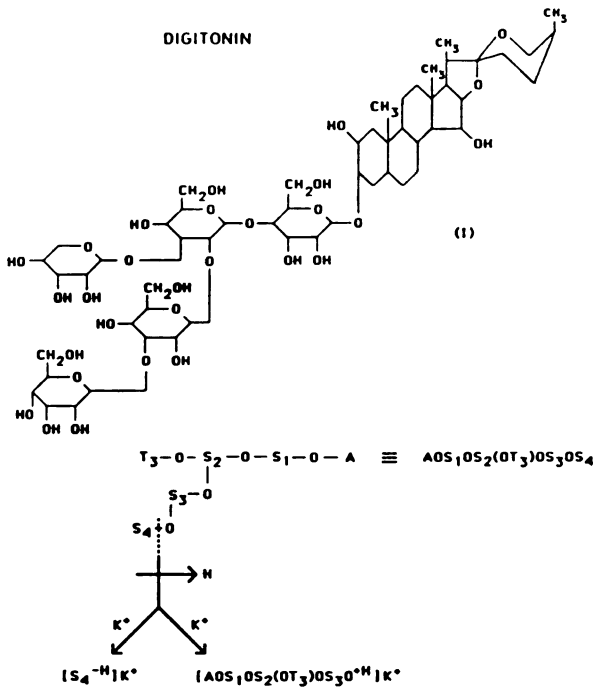

Figure A1. The structure of digitonin is shown, and its relationship to the shorthand designation scheme. The use of the designation scheme for labeling 'fragment ions' is shown here for the ions observed at *m/z* 201 and 973.

between the two possible names depending on the emphasis of the discussion and/or convenience. The ions observed with the K^+IDS technique are K^+ adducts of these neutral fragments, so they are represented as [ ]K^+. This naming scheme allows for designation of multiple cleavages, such as those observed in the analysis of digitonin. For example, two 1,2-eliminations of the digitonin molecule lead to the formation of the ion appearing at *m/z* 811 which is designated $[AOS_1OS_2(O^{+H})O^{+H}]K^+$. The $O-S_3$ and $O-T_3$ bonds are broken and the S_2 portion retained both glycosidic oxygens and gained the H's from the H-shifts.

APPENDIX C

Mechanistic Considerations of the Protonation and Fragmentation of Highly Functionalized Molecules in Fast Atom Bombardment: High Resolution Mass Spectrometry and Tandem Mass Spectrometry Analysis of the Ions Formed by Fast Atom Bombardment of Digoxin and Related Cardiac Glycosides

Karen J. Light and John Allison
Department of Chemistry, Michigan State University, East Lansing, Michigan, USA

High resolution mass spectrometry and tandem mass spectrometry analyses of the major ions of digoxin formed by fast atom bombardment are presented and discussed to investigate the mechanisms through which fragment ions are formed. Similar cardiac glycosides are also analyzed to provide support for the proposed fragment assignments. Remote site fragmentation with the charge localized on the aglycone portion of the molecule may provide an explanation for the fragment ions observed in these studies because the majority of these ions contain the aglycone portion of the molecule. The results obtained parallel previously reported results from an ammonia chemical ionization mass spectral study of cardiac glycosides. *(J Am Soc Mass Spectrom 1990, 1, 455–472)*

THE cornerstone of mass spectrometry, on which its power for structure elucidation is built, is the understanding of the mechanisms by which molecular ions fragment in the gas phase. For the ionization technique used most often in mass spectrometry, electron ionization (EI), fragmentation mechanisms have been well characterized and utilized to understand the relationship between the m/z values and relative abundances of the ions formed and the structure of the compound under study [1]. When EI is utilized, the relative abundance of a fragment ion in a mass spectrum, as well as its m/z value, gives some information on the structure of the ion, the environment in the molecule from which it is formed, and the type of mechanism involved in its formation [1]. However, mass spectrometry has moved away from EI-based techniques toward a variety of desorption ionization techniques that can be applied to the analysis of larger, more highly functionalized molecules. While the number of ionization methods available for mass spectrometry is now substantial, the mechanisms through which fragment ions are formed via these methods are not well understood, and their establishment has not been extensively pursued to date. Frequently there is little discussion of fragmentation mechanisms in the mass spectrometry analysis of large molecules, and those mechanisms that are proposed and utilized usually have not been substantiated. Often the interpretation relies only on the presence/absence of ion current at a particular m/z value, with abundance information being of relatively little utility.

The understanding of fragmentation mechanisms not only facilitates the interpretation of mass spectra of unknown compounds, but is vital when known compounds are under study in which an isotopic label has been incorporated, and the position and extent of the label incorporation must be ascertained. This has become important for larger molecules in the study of metabolic pathways [2] in which a labeled compound is introduced into a system and its fate is followed with mass spectrometry, by monitoring label incorporation into metabolites. Thus, mechanistic aspects of fragmentation for larger molecules should be considered when ionization methods other than EI are used. As it is somewhat impractical to expect that extensive labeling studies be performed on large molecules, we evaluate here the use of the tools that are available on a conventional double-focusing sector instrument—high resolution mass spectrometry (peak matching)

Address reprint requests to John Allison, Department of Chemistry, Michigan State University, East Lansing, MI 48824.

1044-0305/90/$3.50

Received February 27, 1990
Accepted May 10, 1990

and collisionally activated dissociation (CAD) methodology—for providing insights into the ions produced by fast atom bombardment (FAB). In particular, we focus on the FAB mass spectra of cardiac glycosides, and further focus on the molecule digoxin. We have chosen a case where the protonated molecule and many fragment ions are observed in the FAB mass spectrum. The CAD spectra obtained from linked scanning at constant B/E for the ions observed, and the results of accurate mass measurements, will be presented and discussed. We will assume that for this type of analyte molecule the dominant mode of ionization is essentially glycerol chemical ionization in which protonated glycerol (or some fragment ion derived from glycerol) protonates the desorbed neutral molecule in the gas phase, and fragmentation follows protonation [3].

The data will be evaluated in the context of basic questions concerning the site of protonation and fragmentation mechanisms for these highly functionalized molecules, typical of those studied by FAB and liquid secondary ion mass spectrometry (LSIMS).

Experimental

The cardiac glycosides were obtained from Sigma Chemical Co., St. Louis, MO, and were used without further purification. Acetyldigitoxin was purchased from ICN K&K Laboratories, Cleveland, OH. The samples were dissolved in methanol to concentrations of approximately $1\mu g\ \mu L^{-1}$. Two microliters were transferred to the FAB probe tip and mixed with the glycerol matrix. All FAB analyses were performed on a JEOL HX-110 double-focusing mass spectrometer (JEOL, Ltd., Tokyo, Japan) of forward geometry with an accelerating voltage of 10 kV and a FAB gun voltage of 6 kV with xenon FAB gas. Peak matching was performed with a resolving power of 7,000 or more, using glycerol cluster ions as reference ions.

All CAD experiments were performed by linked scanning (at constant B/E) controlled with the JEOL JMA-DA5000 software and using helium as the collision gas. The ability to compare CAD spectra in terms of the daughter ions observed was important for their utility in the mechanistic considerations addressed in this article. This suggested the need for performing these CAD experiments under single collision conditions, as opposed to multiple collision conditions where CAD of CAD products could be observed. Therefore all CAD experiments were performed by introducing helium into the collision cell so that the signal for the parent ion was attenuated by 10%, which produced single collision conditions [4]. In our initial studies we were intrigued that low mass ions at m/z 113 and m/z 131 were dominant ions in the FAB spectrum of digoxin, but were not observed as CAD daughter ions of the $[M]H^+$ ion of digoxin. This was particularly distressing in light of a previously reported CAD mass spectrum of digoxin in which these two low mass ions were observed [5]. Our preliminary CAD data were collected with no instrumental changes from that used in the FAB mode and with a tuning file that contained ions from m/z 39 to m/z 984 (from a mixture of KI and CsI). However, the B/E linked scanning software program used with the JEOL HX-110 double-focusing mass spectrometer to perform these CAD experiments requires a good magnetic field calibration table. A relation between the calibration table lowest mass number (m*), the linked scan parent ion mass number (m_1), and the lowest observable daughter ion (m_2) is suggested in the JEOL instruction manual by the following formula [6]: $m^* = (m_2)^2/(m_1)$. Therefore a different calibration compound, Ultramark 1621, from PCR Inc., Gainesville, FL, was selected to allow for the construction of a tuning file that contained many low mass ions, with m/z 1 being the lowest mass ion included. In addition to this change of calibration compound, performing CAD experiments on the JEOL HX-110 requires repositioning the conversion dynode and opening the slit between the electric sector and the magnetic sector to enhance detection of low mass fragment ions that have lower kinetic energies than their parent ions [7]. These modifications allowed us to observe the expected low mass daughter ions at m/z 113 and m/z 131 from the protonated digoxin molecule.

In some cases, where the parent ion was within approximately 5 u of a mass spectral peak derived from glycerol alone, interference from the glycerol matrix appeared in the CAD spectra and made it necessary to use an alternative matrix, thioglycerol. Another form of glycerol interference occurred when the parent ion selected for CAD analysis had a low relative abundance compared to the glycerol adduct ions. In this case, a cluster of ions 90, 92, 94, and 96 u lower than the nominal mass of the parent ion, with successive losses of 90, 92, 94, and 96 u, appeared in the linked scan spectrum. These "92" losses were not observed when the matrix was thioglycerol, but were observed with glycerol alone. Therefore, it was determined that these ions originated from the glycerol matrix. The artifact peaks clustered 92 u below the parent ion are denoted by T in the B/E mass spectra that are presented.

Results

The fast atom bombardment mass spectrum of digoxin – exact mass measurements and fragment ion assignments: The fragmentation pathways operative in the FAB analysis of digoxin are the subject of this article and thus discussion will begin by presenting the data obtained for digoxin. Initial assignments for the fragment ions are proposed to provide a basis for discussing the possible mechanism(s) of fragmentation. This creates a difficult situation because the identities of the frag-

J Am Soc Mass Spectrom 1990, 1, 455-472

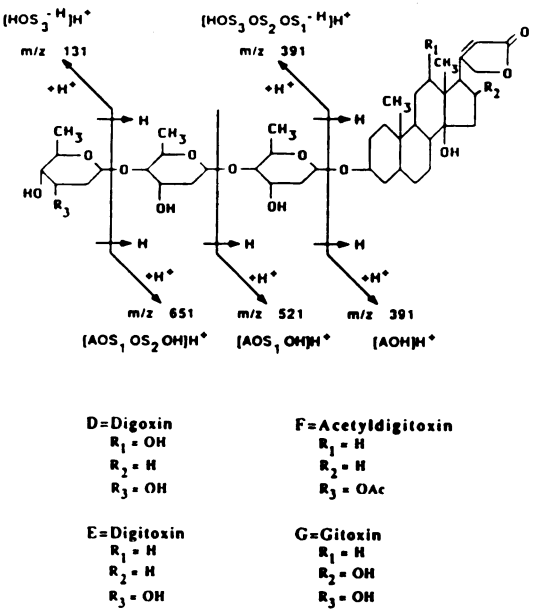

Figure 1. Structures of the cardiac glycosides. The m/z values of the fragment ions labeled on the figure are for digoxin.

ments are necessary for determining the fragmentation mechanism(s) and likewise the fragmentation mechanism is required to know the exact structure of the fragments that we wish to describe in the ionic assignments. Whereas mechanistic possibilities are being evaluated throughout this article, the nomenclature used to identify different fragments is the Light/Kassel/Allison scheme, which has previously been described [8]. The Light/Kassel/Allison scheme is designed as a precise shorthand for discussing both ionic and neutral variants of the types of molecules addressed in this article. This nomenclature allows for more mechanistic detail than the more common Domon/Costello nomenclature [9], which is mechanistically neutral. Where appropriate, reference is made to the Domon/Costello scheme to provide additional clarity for those readers more familiar with this latter system.

The structure of digoxin is shown in Figure 1 (case D). Also shown in Figure 1 are the proposed fragment ions for digoxin. The FAB mass spectrum of digoxin is shown in Figure 2a, and the linked scan spectrum of the $[M]H^+$ ion of digoxin (where M is the intact molecule), m/z 781, is shown in Figure 2b. The FAB mass spectrum contains peaks representative of the protonated digoxin molecule $[M]H^+$ at m/z 781, fragment ions derived from the analyte digoxin, and the glycerol matrix adduct ions, $[(glycerol)_n]H^+$ (denoted by *). All of the fragment ions appear at odd m/z values and are thus even electron ions. There are a few types of ions that suggest patterns of fragmentation. The first of these is represented by the ion current at m/z 651. The terminal glycosidic bond is cleaved such that the glycosidic oxygen remains on the fragment containing the aglycone. Although the actual fragmentation follows protonation, to demonstrate how the nomenclature scheme is used, consider the neutral digoxin molecule, designated as $[AOS_1OS_2OS_3OH]$. If the C—O bond of the terminal glycosidic linkage were cleaved as shown in Figure 1, two radical fragments would be formed with masses of 131 and 649 u. This bond cleavage appears to be accompanied by an H-shift toward the glycosidic oxygen, producing two neutral species with masses of 130 and 650 u that are designated by the Light/Kassel/Allison shorthand notation as $[HOS_3^{-H}]$ and $[AOS_1OS_2OH]$, respectively. Both of these neutral species are observed in protonated form in the FAB mass spectrum at m/z values of 131 and 651, respectively (see Figure 2a). These ions are labeled as $[HOS_3^{-H}]H^+$ and $[AOS_1OS_2OH]H^+$ and are confirmed by exact mass measurements as shown in Table 1. In the designation scheme of Domon and Costello [9], these ions correspond to the B_1 and Y_2 fragments, respectively.

The tentative structural assignments of the fragment ions observed in the FAB mass spectrum of digoxin using the Light/Kassel/Allison scheme are presented in Table 1, in addition to the designations based on the Domon/Costello nomenclature. Peak matching results, and the relative errors between the proposed structure exact mass calculations and the experimentally determined exact mass, are also given in Table 1. All uncertainties are within 2 mmu and thus adequately support the elemental compositions of these fragment ions as listed. There is more than one way that the fragment ions can be labeled using the Light/Kassel/Allison designation scheme. For example, the ion labeled $[HOS_3^{-H}]H^+$ could also be labeled $[HOS_3^+]$; both designations have the same chemical formula but carry different implications in terms of the process by which the ion is actually formed (as will be discussed below). The structural assignments given in Table 1 for the fragment ions observed provide a starting point for discussing fragmentation pathways and may, of course, be altered as mechanistic information is obtained. Similar to the terminal glycosidic bond cleavage that leads to the ion at m/z 651, fragmentation occurs about the other two glycosidic bonds of digoxin followed by H-shifts to produce Y ions at m/z 521, $[AOS_1OH]H^+$, and m/z 391, $[AOH]H^+$. The ion at m/z 391 may also be $[HOS_3OS_2OS_1^{-H}]H^+$. These assignments for the fragment ions based on the low resolution FAB mass spectral data are confirmed by peak matching results, as presented in Table 1. The two assignments for the ion current at m/z 391 will be discussed below.

Another type of ion formed in this experiment is represented by the ion at m/z 633. This ion could be formed by cleavage of the z bond instead of the y bond in the terminal glycosidic bond, as designated in (I) to

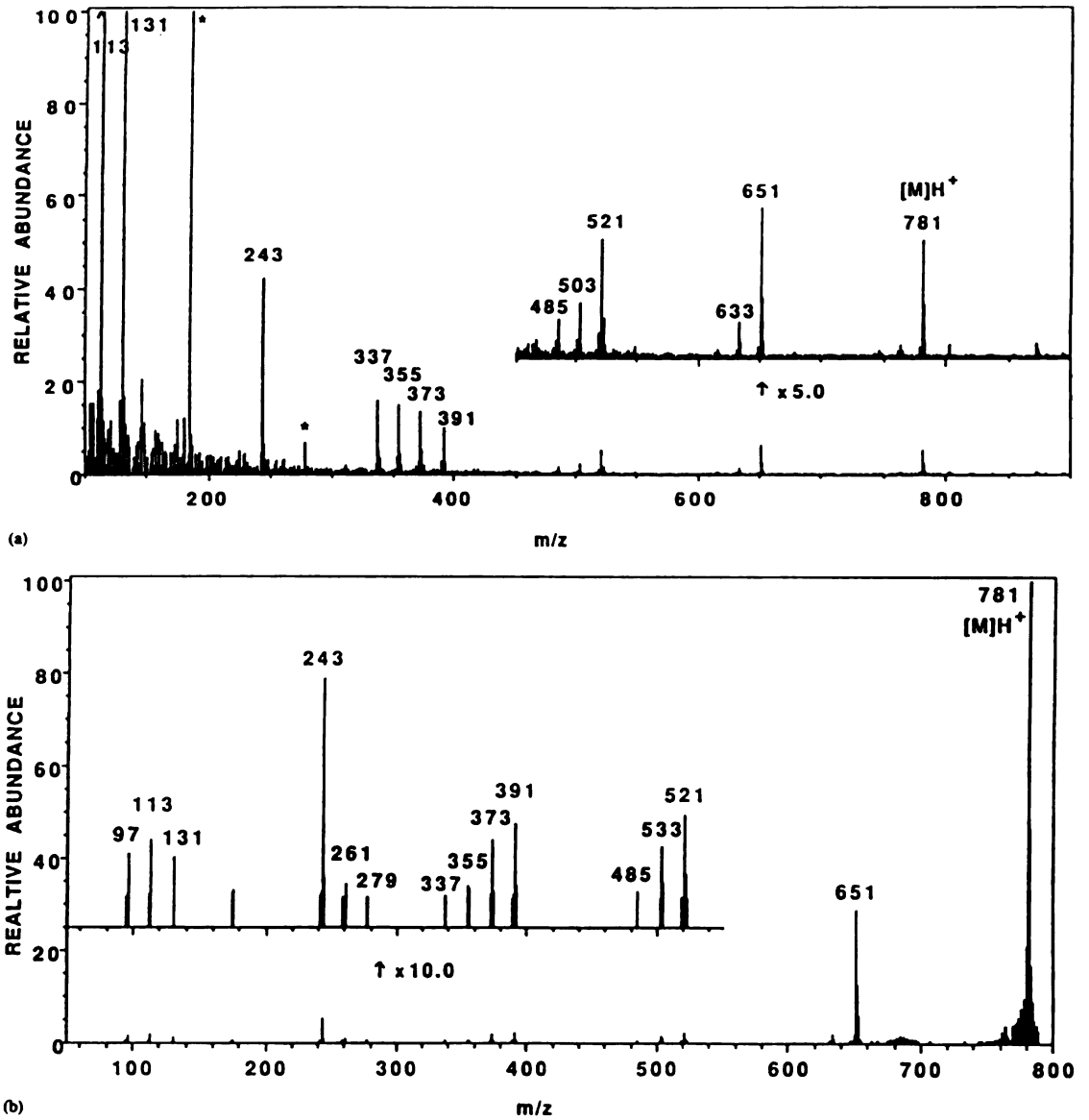

Figure 2. (a) The FAB mass spectrom of digoxin in glycerol. The glycerol adduct ions are labeled as *. (b) The linked scan CAD spectrum of the digoxin parent ion $[M]H^+$ at *m/z* 781.

produce a Z_2 ion [9]. In this case the glycosidic oxygen remains with the nonreducing terminal sugar. This cleavage would produce two fragments with masses of

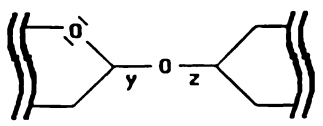

(I)

147 and 633 u. An H-shift toward the glycosidic oxygen would produce two neutral species of masses 148 and 632 u, respectively. Only one of these species is observed, in a protonated form, at *m/z* 633, which may suggest that this ion is formed by loss of H_2O from the ion at *m/z* 651 instead of involving an uncommon cleavage about the z glycosidic bond [10]. (The two C—O bonds in glycosidic linkages are chemically distinct; they tend to fragment more readily at the nonreducing end of the bond for typical glycosides, such as is seen for the cardiac glycosides upon acid catalyzed

J Am Soc Mass Spectrom 1990, 1, 455-472

Table 1. Digoxin fragment ions: possible assignments and peak matching results

m/z	Assignment	LKA[a] designation	DC[b] designation	Δmmu[c]
781	$C_{41}H_{65}O_{14}^{+}$	$[AOS_1OS_2OS_3OH]H^+$; $[M]H^+$	$[M+H]^+$	−0.2
651	$C_{35}H_{55}O_{11}^{+}$	$[AOS_1OS_2OH]H^+$	Y_2	+1.0
633	$C_{35}H_{53}O_{10}^{+}$	$[AOS_1OS_2OH-H_2O]H^+$	Z_2	−0.7
521	$C_{29}H_{45}O_{8}^{+}$	$[AOS_1OH]H^+$	Y_1	−0.2
503	$C_{29}H_{43}O_{7}^{+}$	$[AOS_1OH-H_2O]H^+$	Z_1	+1.6
391	$C_{23}H_{35}O_{5}^{+}$ (81)[d]	$[AOH]H^+$	Y_0	−1.6
	$C_{18}H_{31}O_{9}^{+}$ (19)	$[HOS_3OS_2OS_1^{-H}]H^+$	B_3	0.0
373	$C_{23}H_{33}O_{4}^{+}$ (59)	$[AOH-H_2O]H^+$	Z_0	−1.0
	$C_{18}H_{29}O_{8}^{+}$ (41)	$[HOS_3OS_2OS_1^{-H}-H_2O]H^+$	B_3-H_2O	−0.6
355	$C_{23}H_{31}O_{3}^{+}$ (82)	$[AOH-2H_2O]H^+$	Z_0-H_2O	−1.5
	$C_{18}H_{27}O_{7}^{+}$ (18)	$[HOS_3OS_2OS_1^{-H}-2H_2O]H^+$	B_3-2H_2O	e
337	$C_{23}H_{29}O_{2}^{+}$ (76)	$[AOH-3H_2O]H^+$	Z_0-2H_2O	−1.0
	$C_{18}H_{25}O_{6}^{+}$ (24)	$[HOS_3OS_2OS_1^{-H}-3H_2O]H^+$	B_3-3H_2O	+0.9
243	$C_{12}H_{19}O_{5}^{+}$	$[HOS_3OS_2^{-H}-H_2O]H^+$	B_2-H_2O	+2.2
131	$C_6H_{11}O_{3}^{+}$	$[HOS_3^{-H}]H^+$	B_1	−0.6
113	$C_6H_9O_{2}^{+}$	$[HOS_3^{-H}-H_2O]H^+$	B_1-H_2O	−0.2
97	$C_6H_9O^+$	$[S-H_2O]H^+$	?	+0.3

[a] Light/Kassel/Allison scheme presented in ref 5.
[b] Domon/Costello scheme presented in ref 9.
[c] Δmmu = measured mass−calculated mass.
[d] Percent contributions of each component based on normalized peak heights averaged for three high resolution scans. These indicate that major contributions to ion currents in the *m/z* 337-391 region are aglycone-containing fragments.
[e] Ion intensity is too low for accurate peak match; see text.

hydrolysis. See, for example, ref 10.) This presents a question as to how to designate the ion at *m/z* 633 until the mechanism is determined. It could be labeled as $[AOS_1OS_2{}^{-H}]H^+$ or $[AOS_1OS_2OH-H_2O]H^+$. The first designation suggests its formation via a one step process; by cleavage of the z bond, whereas the second notation carries no implication concerning the site of H_2O loss, but does connote a two-step process. Obviously, information on the fragmentation pathway is required to determine which of these two designations is most appropriate. However, most fragment ions observed in the spectra of glycosides appear to be formed by cleavage of the y glycosidic bond with retention of the glycosidic oxygen on the reducing portion of the molecule (containing the aglycone), accompanied by an H-shift toward this glycosidic oxygen [9]. If this cleavage (to produce Y ions) is most prevalent for digoxin, then the ion at *m/z* 633 is most probably formed by the loss of H_2O from either the aglycone or one of the sugars in the ion observed at *m/z* 651.

The final type of ions is in the 300 u range that begins with *m/z* 391, with a series of ions 18 u lower, at *m/z* 373, 355, and 337, which do not simply correlate with primary fragments of the molecule (as in the discussion above), and must be the result of multiple dehydration steps. The ion at *m/z* 391 has two possible identities due to the nearly symmetric nature of this molecule (in terms of mass). Cleavage of the $AO\text{-}S_1$ glycosidic bond in the neutral digoxin molecule followed by an H-shift toward the aglycone would produce two neutral species, each with a mass of 390, both of which could appear in the mass spectrum in the protonated form at *m/z* 391. Peak matching results are vital for this group of ions that can each have two possible origins. Without knowing the exact composition of this mass spectral peak with a nominal mass of 391, it would be impossible to discuss the fragmentation mechanism(s) involved. The exact masses of the aglycone structure and sugar portion differ by approximately 50 mmu, and thus peak matching and/or high resolution scanning can be used to determine the contribution to each peak from the aglycone portion and the contribution from the sugar portion of the molecule. Peak matching results are presented in Table 1 and the deviations of experimentally obtained exact masses from calculated exact mass determinations are all within 2 mmu. These results indicate that the ions in the 300 u range each have two components, one from each end of the molecule. The contribution to the peak at *m/z* 355 from the sugar portion could be detected, but that signal is too weak to allow an accurate mass measurement. The relative contributions, from the aglycone portion and the sugar portion of the molecule, within these doublet peaks, do vary throughout the series of 300 u-range ions. High resolution scanning is used to determine the relative contributions of each component to the ion current of each nominal mass. The results of three experiments of high resolution scanning for the ions at *m/z* 391, *m/z* 373, *m/z* 355, and *m/z* 337 were

Table 2. Relative intensity data from the CAD mass spectra of digoxin fragment ions

	Parent ions (nominal mass)*											
	781	651	633	521	503	391	373	355	337	243	131	113
Daughter ions (nominal mass)												
763	3.9											
651	28.9											
633	1.9	2.8										
615		0.6	4.3									
521	2.4	6.8	23.7									
503	1.8	1.4	12.2	5.3								
485	0.8	1.6	2.8	2.4	7.8							
467		0.4		0.7	2.6							
391	2.2	3.3	5.1	4.4	31.2							
373	1.9	2.3	2.9	5.4	6.9	8.0						
355	0.9	1.3	2.0	3.5	6.0	5.9	19.3					
337	0.7	0.5		1.0	1.7	0.8	5.8	23.6				
319								0.6	2.2			
279						0.6						
261	1.0					0.6	0.4	0.5				
243	5.4	3.1	9.4			0.6	1.3	0.6	1.0			
225			1.3			0.2	0.4	0.5		1.0		
149						0.2				0.9		
131	1.5	1.5	2.0	1.8	1.2	0.3	0.4			0.7		
113	1.9	1.4	2.4	1.2	2.3	0.3	0.4			0.3	4.9	
97	1.6	0.8	1.2			0.3	10.5	0.3		9.3		0.1
95	0.7					0.2						2.0
85												0.4
83											0.1	0.2
69											0.6	0.5
Σ	59	28	69	26	60	18	39	26	3	12	6	3

* Parent ions are the $[M]H^+$ and the fragment ions observed in the FAB mass spectrum of digoxin.

averaged and the percent contribution of each component is presented in Table 1. These ratios vary somewhat with experimental conditions, such as ion source pressure, which may suggest that some fragmentation occurs as CAD within the ion source. In most cases, the contribution to each doublet peak is greater from the aglycone portion of the molecule than from the sugar portion. The peak at m/z 373 contains the largest contribution to the ion current from the sugar portion of the molecule than any of the other 300 u-range ions.

One case where low resolution mass spectrometry and peak matching capabilities are insufficient to suggest, unambiguously, a relationship between the m/z value of a fragment ion and some substructural feature of the original molecule is the ion at m/z 243. Based on the nominal mass assignments and peak matching, it is determined that this ion is from the sugar portion of the molecule but could have one of two assignments: $[HOS_3OS_2{}^{-H}-H_2O]H^+$ or $[{}^{H}-S_2OS_1{}^{-H}]H^+$. This ion also appears as a daughter ion from CAD analyses of all of the fragment ions that contain at least two sugars. In an attempt to differentiate between these two assignments, the FAB spectrum of a similar compound was obtained. Acetyldigitoxin (structure F, Figure 1) was chosen for study because of its similarity to digoxin with two exceptions: the aglycone contains one less OH group (like digitoxin) and, more important, the terminal sugar contains an acetyl group. The ion observed at m/z 243 in the FAB mass spectrum of digoxin does shift to m/z 285 for acetyldigitoxin and suggests that this ion contains the terminal sugar where the acetyl group is located. Therefore, we will assume that the assignment for m/z 243, $[HOS_3OS_2{}^{-H}-H_2O]H^+$, is correct and is included in Table 1.

Linked scan mass spectral data on ions formed from digoxin in the fast atom bombardment mass spectrum. In addition to the peak matching information, the linked scan CAD mass spectra of the parent ion $[M]H^+$ and the major fragment ions of digoxin were obtained to provide additional information that may aid in the elucidation of fragmentation mechanisms. The results from these CAD experiments are presented in Table 2.

One difficulty with the B/E linked scan technique performed on a forward geometry double-focusing mass spectrometer is that the resolution of the parent ion selection is low [11]. In practice, the acceptance window for the parent ion selection is approximately 5 u wide. Therefore, the CAD spectra of the doublet

J Am Soc Mass Spectrom 1990, 1, 455-472

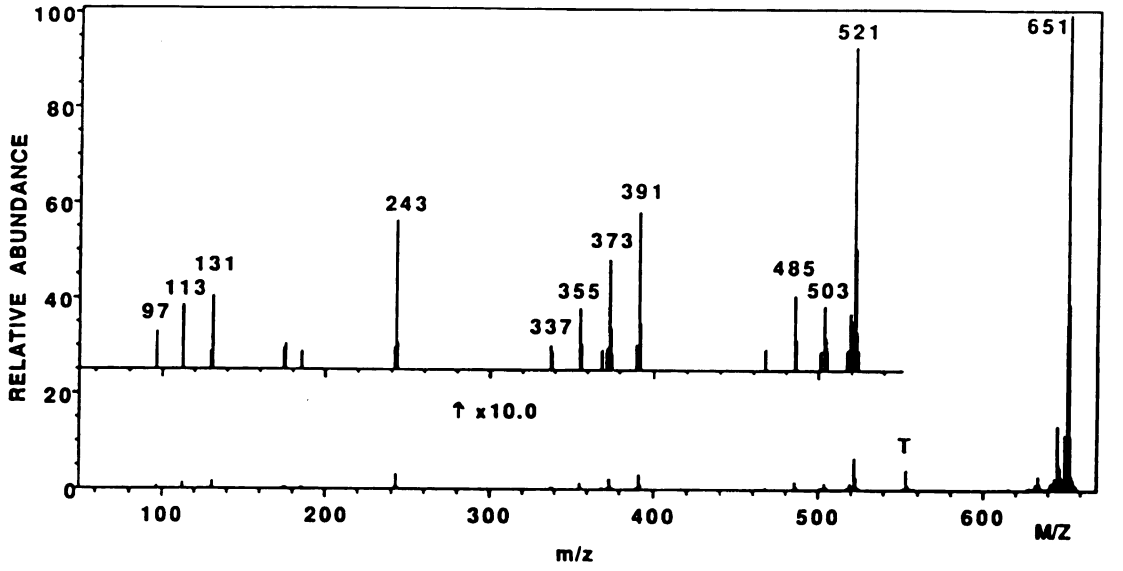

Figure 3. The linked scan CAD spectrum of the digoxin fragment ion at *m/z* 651. The peaks labeled T are glycerol interferents that are present due to the glycerol cluster ion 6 u from the parent ion at *m/z* 651 (see text).

ions, such as those at *m/z* 373, will contain a mixture of daughter ions from both of the isomass species. Also, this wide parent ion selection window can lead to artifact peaks from glycerol cluster ions (if glycerol is the matrix) when the *m/z* value of the desired parent ion is within approximately 5 u of a glycerol cluster ion.

The CAD mass spectrum of the $[M]H^+$ ion is presented in Figure 2b and that for the fragment ion at *m/z* 651 is shown in Figure 3 as an example of the linked scan spectra obtained for the major fragment ions of digoxin. The two spectra in Figures 2b and 3 are very similar in appearance and content even though the two parent ions differ by one sugar. To obtain these linked scan data, the helium collision gas pressure was set to produce a 10% attenuation of the $[M]H^+$ ion and was maintained at this same pressure to obtain the CAD linked scan spectra of the major fragment ions of digoxin. The results of these CAD experiments, the daughter ion *m/z* values and relative abundances, for all of the major fragment ions of digoxin are listed in Table 2. These relative abundances are from the normalization of the fragment ion currents to that of the parent ion. Therefore, the absence or presence of the daughter ions and their relative abundances can be compared within each B/E linked scan, but the abundances between linked scans for different parent ions should not be compared directly. The last row in Table 2 contains the sum of the relative abundances of all fragment ions produced from each selected parent ion (the sum of the columns) and gives some measure of the relative extent of fragmentation that occurs upon CAD of each species.

One ion not listed in this table is that at *m/z* 175. This fragment ion is not observed as a daughter ion in the majority of the linked scan spectra collected. This ion is believed to originate from a ring fragmentation of the middle sugar, referred to as an A_3 cleavage, using the Domon/Costello nomenclature. According to Domon and Costello [9], this ring cleavage is not common in the FAB analysis of saccharide-containing compounds in the positive ion mode. This ion at *m/z* 175 is the only ring cleavage product observed in these studies.

Discussion

Before evaluating the data in search of clues to the fragmentation mechanisms that may be operative for protonated digoxin, a discussion of some of the likely mechanistic possibilities will be presented. When considering mechanisms, one can certainly benefit from the approach used by McLafferty [1] in the context of fragment ions formed by EI. One should first consider the description of the ionized molecule (where are the charge/radical sites?), then propose possible fragmentations based on established mechanisms and chemical intuition. In the case of a protonated molecule, an even electron ion, the literature on chemical ionization (CI) mass spectrometry [12] certainly provides a useful framework. Thus, we first ask the question concerning the nature of the protonated molecule produced by FAB. Where is it protonated [13]? (We note that much work has been done to investigate the site of protonation in molecules that contain more than one basic site. See, for example, ref 13.) It is difficult to an-

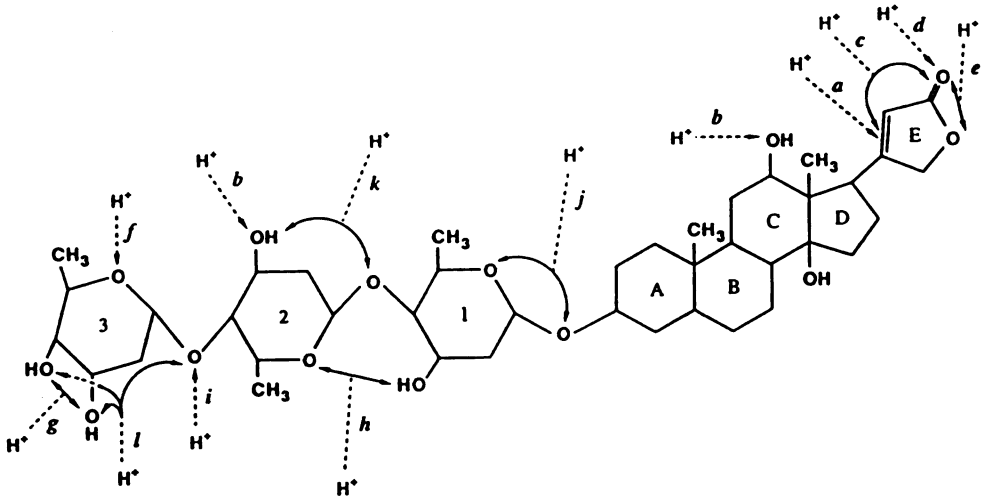

Figure 4. Extended structure of digoxin based on crystallographic data with possible sites of protonation labeled *a* through *l*.

swer this question for many reasons. We do not know how the molecule is protonated. It presumably occurs by gas phase proton transfer [3] from protonated glycerol and/or some fragment ion derived from glycerol such as m/z 45. It is probable that protonation of any of the heteroatoms in the molecule could occur because the proton transfer is probably from an oxygen-containing Lewis base to one of the oxygen atoms in the cardiac glycoside. There are many different types of sites on the digoxin molecule with different proton affinities. An extended structure of digoxin, based on the crystallographic analysis of the molecule [14], is presented in Figure 4 with possible protonation sites indicated. We have estimated the proton affinities of these sites, labeled *a* through *l* in Figure 4, and these values are presented in Figure 5. The proton affinities of the different sites on digoxin are approximated based on smaller compounds, resembling these sites, whose proton affinities are known [15]. In those cases where there are multiple interactions, estimates for the increase in proton affinity (PA) due to secondary interactions have been made and are discussed in Appendix 1. Based on the estimates in Figure 5, it appears that many of the possible sites of protonation of the digoxin molecule lie in the PA range of 190–200 kcal/mol. Also shown in Figure 5 are possible protonating species derived from glycerol. Candidates as protonating reagent ions are selected based on the FAB mass spectrum of glycerol reported by Sunner et al. [3], which includes the protonated glycerol molecule and lower mass glycerol fragments. Note that all of the glycerol fragments have proton affinities lower than that of glycerol, 209 kcal/mol [3]. If the PA values in Figure 5 are correct, proton transfer from protonated glycerol to most of the labeled sites of digoxin would be endothermic, however, proton transfer from the fragment ions of glycerol is possible. The most basic sites in the molecule appear to be the glycosidic linkages, which are further enhanced by additional interactions. It has been shown that protonated molecules containing two functional groups can show intramolecular hydrogen bonding, even when the two groups are separated by many methylene groups. Frequently, 10–20 kcal/mol can be introduced by such secondary interactions [16]. We propose that the site of highest

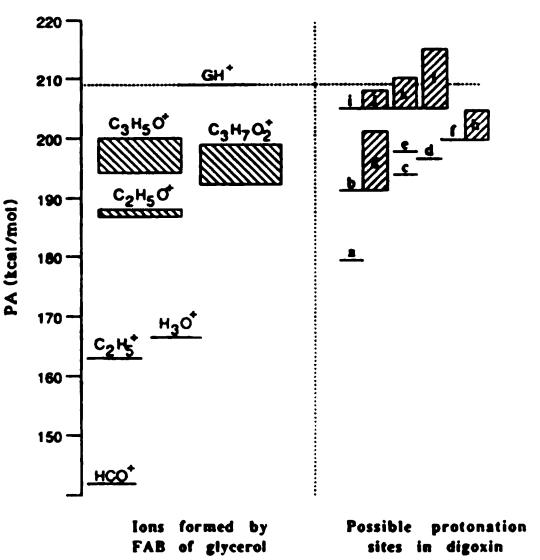

Figure 5. Estimates of the proton affinities of the basic sites labeled on the digoxin structure in the figure and estimates of the proton affinities of possible protonating agents from glycerol and glycerol fragments.

J Am Soc Mass Spectrom 1990, 1, 455–472

PA is the terminal sugar unit. The basic site formed by the two —OH groups plus the —OR group, all three being on the same side of the ring, resembles the interactions described by Winkler and McLafferty [17] for a protonated cyclohexanetriol. In digoxin (solid), the ring oxygen of sugar 2 is in close proximity to the OH group in the 3 position on sugar 1, making site *h* a possible site for a multiple interaction. Our conclusion is that any part of the molecule may be protonated in the FAB experiment with a glycerol matrix, although not necessarily by the most abundant of the possible candidates from glycerol, $[glycerol]H^+$.

How, then, should we consider the protonated molecule in the context of the fragmentation that will follow protonation? In this regard, two extremes have been discussed in the literature. In the simplest approach, the molecule is protonated and fragmentation follows directly, occurring at that protonation site [18]. For example, it has been proposed that protonated bradykinin, formed by field desorption, fragments at the site of protonation and the proton does not migrate freely about the molecule [19]. The other extreme is a dynamic model that suggests that the initial site of protonation would be, in this case, irrelevant—the proton rapidly moves from heteroatom to heteroatom, with the possibility of fragmentation occurring at every site while the proton resides at that site [20]. We believe that the latter is more likely in this case, and will assume that our starting point will be a protonated molecule that has a mobile proton.

What possible fragmentation mechanisms may be operative for this even electron ion? Mechanisms that have been proposed include inductive cleavage processes, fragmentation involving multiple bond cleavages (1,2-elimination reactions and ring cleavage processes), and remote site fragmentations.

Inductive Cleavage

Domon and Costello [9] have proposed a scheme for naming fragment ions from carbohydrates, and the process that they have proposed leading to what they call B_i ions is shown in reaction 1 for two digitoxose sugars.

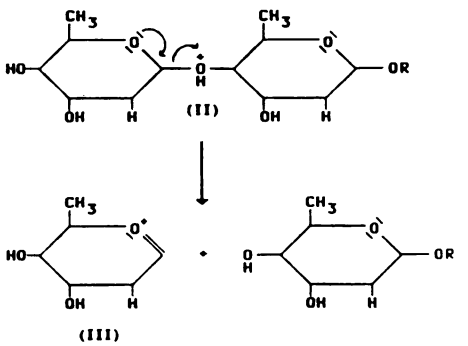

(1)

Inductive effects lead to cleavage of the glycosidic bond at the site of protonation in (II), forming the charge migration product (III). It has certainly been documented that inductive processes involving oxygen do readily occur [1], and such a mechanism is reasonable for this even-electron ion (II).

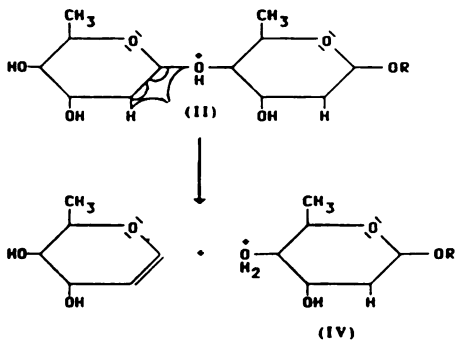

(2)

Multiple Bond Cleavage Processes

We will not discuss ring cleavage reactions because only one has, possibly, been observed in this study (at *m/z* 175). However, it is apparent that H-shifts do occur, and accompany glycosidic C—O cleavages. For example, reaction 2 has been proposed by Domon and Costello [9] to yield Y_i ions, of the type (IV). The mechanism suggests a 1,2-elimination to leave a double bond in the neutral sugar fragment, although H shifts from other sites within the molecule cannot be ruled out [21]. (H-shifts in peptides as 1,2-eliminations have been proposed in refs 19 and 21a. H-shifts in peptides as 1,3-eliminations have been proposed in ref 21b. H-shifts via 7 and 8-membered rings have been discussed in ref 21c.) Thus, the fragment ions (III) and (IV) are proposed to come from a common intermediate, (II), via two different mechanisms. It is also possible that the fragment ions (III) and (IV) are formed through another common intermediate and a single mechanistic step. This is shown in reaction 3. The starting point is an ion of the type (II), protonated on a glycosidic oxygen. The charge site stimulates a 1,2-elimination reaction to form the proton-bound adduct shown as (V), which can then dissociate to form either (VI) and/or (VII), depending on which fragment retains the proton. (This mechanism is similar to that suggested by Stevenson's rule [1] in EI, in which separating fragments compete for the charge; here the competition is for the proton. This protic analogy to Stevenson's rule has not been established to date, although it has been alluded to by Bowen et al [22].) Thus, the ions of that type labeled (III) and (VI) are the same, except that (VI) is formed via an H-shift. It is difficult to decide on a designation for such ions. In our nomenclature scheme, the two different mechanisms would suggest that an ion such as that shown as (VI) could be labeled as $HOS_3OS_2^+$ or $[HOS_3OS_2^{-H}]H^+$, and we have ten-

J Am Soc Mass Spectrom 1990, 1, 455-472

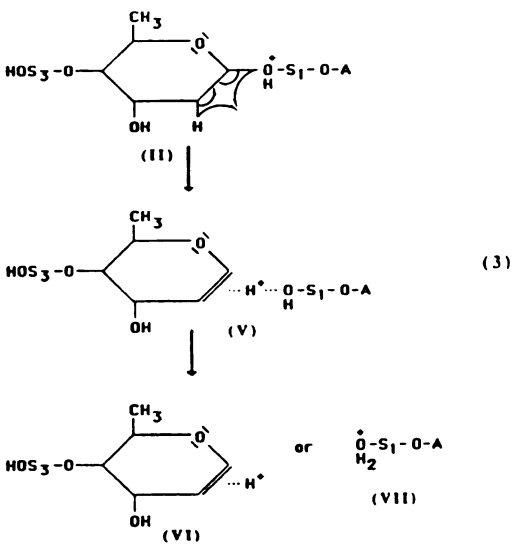

(3)

tatively chosen the latter. It is also interesting to note that while Domon and Costello [9] have proposed reaction 2, they write the product not as (IV) but as (VIII), in which the proton in this fragment ion has moved from its initial site on the terminal hydroxy group in (IV) to another glycosidic linkage; presumably this was done to suggest that the proton is mobile following protonation.

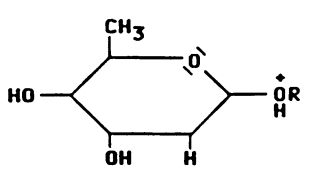

(VIII)

Remote Site Fragmentation

Jensen et al. [23], Adams [24], and Wysocki et al. [25] discussed the remote site mechanism in ions for which the charge and/or radical site are apparently far from the site of fragmentation. Such mechanisms certainly seem reasonable when a C—C bond is broken in a long alkyl chain of an ion containing a single functional group, and difficult to prove for multifunctional molecules. This mechanism would suggest that protonation can occur at any part of the molecule, and fragmentation need not be local to the site of protonation. Vine et al. [26] discussed the possibility of remote site fragmentation occurring in the ammonia CI mass spectra of cardiac glycosides. They suggest that the ammonium ion may complex with the aglycone portion of the molecule and 1,2-eliminations about the glycosidic linkage may occur far from this site, as

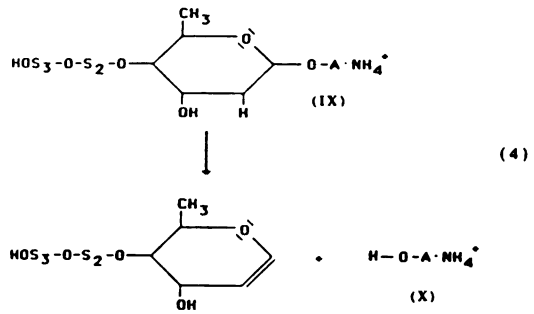

(4)

shown in reaction 4. It is interesting to note that in a recent article on the mass spectrometry of peptides by Johnson et al. [21a], it was proposed that much of the fragmentation observed for peptides may occur via remote site processes.

Adams and Gross [27] have discussed the analogy of remote site fragmentations to thermolytic processes. Energy is imparted into the molecular ion, which fragments as it would if energy were added to the corresponding neutral molecule. In this context, we have reported the K^+IDS mass spectrometric analysis of cardiac glycosides [8]. K^+IDS, K^+ ionization of desorbed species, is a technique that combines rapid thermal processes, thermal degradation, and vaporization, with gas phase K^+ attachment. We note that when digoxin is rapidly heated, 1,2-eliminations appear to readily occur about the glycosidic bonds, yielding K^+ adducts that are very similar to those seen here in protonated form. In K^+IDS, decomposition occurs before K^+ attachment (K^+ attachment does not induce much fragmentation), while in FAB protonation presumably precedes decomposition and often induces fragmentation. Even with these differences in fragmentation processes, preceding ionization in K^+IDS and following ionization in FAB, most of the same fragmentation processes are observed in both mass spectra. The correlation between the FAB and K^+IDS spectra could be fortuitous, but may support remote site processes that are not initiated by the charge site but rather by energy deposition in general.

Mechanistic discussions of FAB presented here are based on the assumption that protonation of the intact molecule precedes fragmentation. However, it is possible that direct fragment ion formation from the matrix upon bombardment can occur. Many of the fragment ions of digoxin contain the aglycone. However, there are some ions in the low mass range that are from the sugar portion of the molecule. Two such ions are at m/z 113 and 131 from the terminal sugar (Table 1) and are the most abundant fragment ions in the FAB mass spectrum (Figure 2a) of the digoxin sample. Additional experiments were performed to investigate the origin of these two abundant low mass ions. The FAB mass spectra of digoxin in glycerol were collected and monitored for a period of thirty minutes.

J Am Soc Mass Spectrom 1990, 1, 455-472

During this time the ions at m/z 113 and m/z 131 remained dominant, even when only a trace of glycerol remained and the $[M]H^+$ ion of digoxin was no longer observed. These two low mass ions seem to be formed, at least to some extent, in a different manner than the $[M]H^+$ ion. It is possible, based on the observations of this extended FAB experiment, that these two low mass sugar ions may be formed directly from the liquid target upon bombardment and are not only the result of fragmentation of the $[M]H^+$ ion. If this is the case, then the decomposition of the $[M]H^+$ ion of digoxin produces predominantly daughter ions that contain the aglycone. The ions from the sugar portion that do not contain the aglycone may be formed by other ionization/fragmentation processes.

The mechanisms discussed here must be evaluated with experimental data in order to determine the most probable fragmentation pathways. We now turn to the peak matching and linked scan data to determine whether these results support any of the mechanisms discussed, or suggest others.

Discussion of Collisionally Activated Dissociation Data

Analysis of the CAD data should provide some insights into the fragment ion structures and, from these, insights into the mechanisms through which they are formed. The mechanisms proposed above that are based on a localized site of protonation in the molecule, leading to fragmentation at the site of protonation, would be substantiated by a CAD mass spectrum of a fragment ion with very few daughter ions produced. If the site of protonation is also the site of fragmentation and the charge site does not migrate, then the primary fragment [with a structure such as (IV)] might be expected to only undergo H_2O losses with no extensive fragmentation upon CAD. Other types of fragmentation mechanisms, where the charge is mobile throughout the molecule or is localized followed by remote fragmentation, may produce more extensive fragmentation of the parent species upon CAD. Substructure-specific daughter ions may be formed, and this concept will be used here. Suppose an ion is observed 18 u below another fragment ion due to a water loss, for example, the ion at m/z 633, 18 u below the major fragment ion at m/z 651. From where was the water lost? The ion at m/z 651, $[AOS_1OS_2OH]H^+$, could eliminate water from the terminal sugar (S_2), the interior sugar (S_1), or from the aglycone (A). If there is a daughter ion present in the CAD mass spectrum of m/z 633 that represents the loss of an intact sugar, a neutral loss of 130, $[HOS_2{}^{-H}]$, then the water elimination cannot be from the terminal sugar. However, if a neutral loss of 112, $[HOS_2{}^{-H}-H_2O]$, is observed in the absence of a 130 loss, this would suggest that the terminal sugar in m/z 651 was the site of H_2O loss. This neutral loss prediction is shown in Figure 6 and is

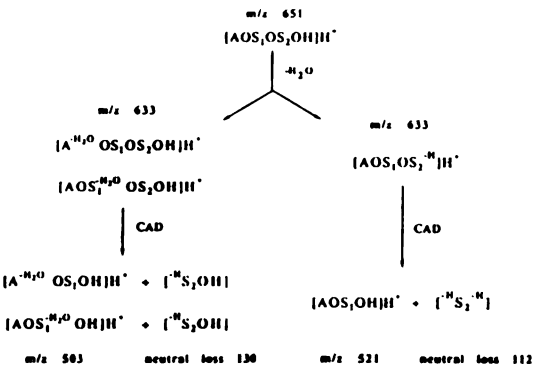

Figure 6. Schematic diagram of the H_2O losses from m/z 651 that can occur to produce the ion at m/z 633. Neutral losses observed from the CAD of m/z 633 can help determine the structure of the ions at m/z 633.

explained in more detail in the discussion of the CAD results for the ion at m/z 633. In a similar fashion, one could search for ions indicative of the intact aglycone, which would indicate that the H_2O loss is not from that portion of the selected parent ion. These types of observations and conclusions are presented here for the CAD data obtained for the fragment ions formed in the FAB analysis of digoxin.

Collisionally activated dissociation of m/z 781. The discussion of the data begins with the $[M]H^+$ ion of digoxin at m/z 781. The daughter ions of the protonated molecule are very similar to those observed in the FAB mass spectrum of digoxin except for some relative abundance variations of the fragment ions. The same fragment ions appear in both the FAB mass spectrum of digoxin (Figure 2a) and the CAD mass spectrum of the protonated molecule (Figure 2b). This observation is consistent with the desorption ionization mechanism that is assumed to be operative here, that is, the fragment ions observed in the FAB spectrum of this neutral analyte are from unimolecular decomposition of the protonated, intact, molecule as opposed to being fragments that are emerging directly from the target upon FAB. There are some differences between these two spectra, notably that the FAB mass spectrum shows a more abundant $[M-H_2O]H^+$ ion than the B/E mass spectrum. Also, the dominant ions from the FAB analysis of digoxin are at m/z 113 and m/z 131 and are less abundant in the linked scan mass spectrum of the $[M]H^+$ ion. An explanation is suggested from the data in Figure 5. There exists in the selvedge region of the FAB experiment a collection of reagent ions available for proton transfer in the m/z range 19-93. Of these, the most abundant is protonated glycerol at m/z 93, which may only be able to protonate the most basic site (*l*), on the terminal sugar, leading to prompt formation of m/z 131 and m/z 113, and a large abundance

J Am Soc Mass Spectrom 1990, 1, 455-472

of these ions. The lower mass reagent ions protonate other parts of the digoxin molecule, and many of these $[M]H^+$ ions are sufficiently long lived to be observed in the FAB mass spectrum at m/z 781. These latter ions are the ones chosen for CAD analysis.

Collisionally activated dissociation of m/z 651. A major fragment ion of digoxin is observed at m/z 651 in the FAB mass spectrum. It is also the most abundant daughter ion of $[M]H^+$, as shown in Figure 2b. From the peak matching results it is proposed that the structure of this ion corresponds to a protonated cardiac glycoside containing only two sugars (see Table 1). The daughter spectrum of m/z 651, shown in Figure 3, closely resembles that of the $[M]H^+$ species of digoxin, shown in Figure 2b. If the mechanism of fragmentation to produce the ion at m/z 651 were charge initiated as shown in reaction 2, then the CAD mass spectrum of m/z 651 should be very simple with daughter ions at m/z [651-18]. Instead, the CAD mass spectrum closely resembles that of the $[M]H^+$ ion and is what would be expected for a CAD mass spectrum of a protonated cardiac glycoside containing two sugars, $[AOS_1OS_2OH]H^+$. If the mechanism of reaction 2 is operative, the proton must be mobile and not localized in the product. This requirement of proton mobility to explain the extensive subsequent fragmentation of primary fragments undergoing CAD was presumably recognized by Domon and Costello [9] when they chose the specific designation shown as structure (VIII), with the proton moving within the ion following fragmentation. The neutral loss of 130 from the parent ion at m/z 651 yielding m/z 521 further supports the structural assignment of m/z 651, as this requires that the terminal sugar must be intact, without any H_2O losses. One fragment ion of m/z 651, at m/z 467, is not observed in the linked scan mass spectrum of the $[M]H^+$ ion. A possible explanation for the presence of this daughter ion in the CAD mass spectrum of m/z 651 is as follows. Both parent species at m/z 781 and m/z 651 can form the daughter ion at m/z 521, which is $[AOS_1OH]H^+$. In the CAD of m/z 781, the fragment at m/z 521 loses one and two H_2Os to yield ions at m/z 503 and m/z 485. In the B/E spectrum of m/z 651, the fragment at m/z 521 is formed to a greater extent, and therefore may allow for the observation of up to three H_2O losses, at m/z 503, m/z 485, and m/z 467. The sugar component of m/z 521 can only lose two of these water molecules as there are only two —OH groups on the sugar, and likewise for the aglycone portion, which has only two —OH groups. Therefore, these multiple H_2O eliminations from m/z 521 must occur throughout the $[AOS_1OH]H^+$ ion and not from one isolated part. The similarities of the CAD results for m/z 651 and m/z 781 would be consistent with a remote site mechanism in which the site of protonation is either the aglycone or is mobile and does not directly induce the fragmentations observed.

Collisionally activated dissociation of m/z 633. Another fragment ion of interest is observed at m/z 633 and could have several origins. First, this ion could be a primary fragment following protonation produced by cleavage of the z glycosidic C—O bond on the terminal sugar to produce what Domon and Costello [9] refer to as the Z_2 ion. This ion at m/z 633 could also be a secondary fragment, as suggested by the abundance ratio of m/z 651 to m/z 633 in the FAB mass spectrum and in the CAD daughter ion spectra of m/z 651. If m/z 633 is produced by a loss of H_2O from m/z 651, the H_2O could be from either of the two sugars retained in the ion, or from the aglycone. If the ion at m/z 651, $[AOS_1OS_2OH]H^+$, loses a water molecule from the terminal S_2 sugar, then a daughter ion corresponding to the neutral loss of 130, due to loss of an intact sugar molecule, should not be observed in the B/E mass spectrum of m/z 633. Instead, a daughter ion corresponding to the neutral loss of 112 should be observed, as discussed in Figure 6. Both of these neutral losses are observed yielding daughter ions at m/z 503 and m/z 521. Therefore, at least some of the water loss is from the terminal sugar, as evidenced by the large abundance at m/z 521 (which requires an intact aglycone and internal sugar). It is also possible that some of the $[AOS_1{}^{-H_2O}OS_2OH]H^+$ species is present as this would fragment upon CAD to produce daughter ions at m/z 243 (from the two sugars), m/z 391 (from the intact aglycone), and m/z 503 (from the loss of the terminal S_2 sugar), all of which are observed in the CAD spectrum of m/z 633. The third possible identity of m/z 633 is $[A^{-H_2O}OS_1OS_2OH]H^+$. This species should (and does) fragment upon CAD to produce m/z 373 (from the dehydrated aglycone) and m/z 503 (from the y glycosidic cleavage). This species could also form m/z 243 in the same manner that m/z 781 does, as the two sugars from this species resemble the sugar portion of the ion at m/z 781. Therefore, H_2O losses are not specific as they do not come from any one substructural group. There are no daughter ions, present or absent, that can be used to make definitive structural assignments for the species at m/z 633.

Collisionally activated dissociation of m/z 521. The fragment ion observed at m/z 521 is also a prominent daughter ion of protonated digoxin and is identified as being structurally equivalent to a protonated cardiac glycoside containing only one sugar (see Table 1). The daughter ion mass spectrum of m/z 521 shows that substantial further fragmentation occurs. Again, the CAD results are consistent with a remote-site mechanism and/or a mobile proton. The parent ion at m/z 521 does not yield a daughter ion at m/z 243, which is present in the CAD spectra of the ions at m/z 781, m/z 651, and m/z 633. This ion at m/z 243 is indicative of the presence of two sugars, as noted in Table 1, and therefore is not expected as a daughter ion of m/z 521, which contains only one sugar. This is consistent with,

J Am Soc Mass Spectrom 1990, 1, 455-472

and further supports, the assignments suggested by the peak matching results. The CAD of m/z 521 shows cleavage of the AO—S_1 bond to produce the daughter ion at m/z 391, which is also observed in the FAB mass spectrum, and is given the assignment $[AOH]H^+$ based on peak matching results. Also observed are the subsequent eliminations of three H_2O molecules from the species at m/z 391. These water losses must be coming from the two —OH groups on the aglycone and the —OH group formed upon fragmentation (from the glycosidic oxygen with the H-shift). Though the relative abundances are slightly different, this same series of ions, m/z 391, 373, 355, and 337, is present in the CAD spectra of m/z 781, 655, and 633. These 300–400 dalton-series fragment ions will be discussed in more detail shortly.

Collisionally activated dissociation of m/z 503. The fragment ion at m/z 503 is structurally similar to the ion at m/z 633 in that these are both secondary fragments formed by a glycosidic bond cleavage and a water loss. The relative abundance ratio of m/z 521/503 is similar to that for the m/z 651/633 pair. This ion fragments upon CAD to give daughter ions at m/z 391, m/z 373, m/z 355, and m/z 337. The m/z 503 ion also loses one and two waters to form daughter ions at m/z 485 and m/z 467. The fragment ions at m/z 391 and m/z 373 are from neutral losses of 112 and 130, as was observed for the CAD of m/z 633. Once again the ion current at m/z 503 is probably a mixture of species with water loss from the aglycone portion of m/z 521 (which would show a neutral loss of 130 upon CAD), water loss from the sugar (which would show a neutral loss of 112), and possibly some primary fragment from m/z 781 (cleavage at the z glycosidic bond). The abundant daughter ion at m/z 391, which corresponds to a neutral loss of 112, suggests that a large percentage of m/z 503 contains a sugar that is monodehydrated and that this species readily fragments at the glycosidic bond to produce the protonated aglycone species $[AOH]H^+$ at m/z 391.

Collisionally activated dissociation of m/z 391, m/z 373, m/z 355, and m/z 337. There are four ions in the 300–400 u range that have two structural assignments for each nominal mass, as shown in Table 1. Peak matching with a resolution of 1/7000 or better is used to distinguish between the two peaks with the same nominal mass but of different origin. The ion current observed at m/z 391 has two possible origins, the aglycone end and the saccharide end of digoxin. Both of these species are capable of losing up to three H_2O molecules upon CAD. Thus the other three ions observed in this mass range, at m/z 373, m/z 355, and m/z 337, can be, and are, formed by H_2O losses from both species contributing to the ion current at m/z 391. The peak matching and high resolution scanning results show that the largest contributor to the ion current for each of these four m/z values is from the aglycone portion of the molecule. This follows with the previous observation that the majority of the types of fragment ions observed do contain the aglycone. The ion at m/z 373 has the strongest contribution from the sugar but this contribution still accounts for less than half of the total ion current at m/z 373 (see relative contributions in parentheses in Table 1). Unlike the other 300 series ions, the CAD analysis of m/z 373 does show some fragments indicative of the sugars. The daughter ions from sugars are observed at m/z 243, which represents a species containing two sugars, and at m/z 131 and m/z 113, which are derived from one sugar of the molecule, as identified in Table 1. The CAD results for the other three ions at m/z 391, m/z 355, and m/z 337 support the conclusion that they primarily contain the aglycone, since only H_2O losses upon CAD are observed (no fragmentation of the steroid ring structure is observed). The relative abundances of the ions representative of these water losses increase as the parent ion becomes more unsaturated. For example, the loss of H_2O from m/z 391 to form m/z 373 is not as prominent as the loss of H_2O from the parent at m/z 373 upon CAD to form m/z 355. This is supported by the data presented in Table 2. This suggests that once one OH group is lost in the form of H_2O, subsequent dehydrations are more facile. It is expected, as observed, that dehydration of the aglycone would occur before demethylation or dehydrogenation. Consideration of the decomposition of substituted cyclohexanes can be used as a model to understand the energetics of H_2O elimination versus CH_4 elimination versus loss of H_2 from the aglycone structure. The dehydration of cyclohexanol to form cyclohexene requires +10.4 kcal/mole [28]. (Thermochemical estimates are based on data contained in ref 28.) In contrast, +18.1 kcal/mole is required to eliminate methane from methylcyclohexanol, and +28.4 kcal/mole is required to induce the dehydrogenation of cyclohexane. Therefore, energetic considerations suggest that water losses are expected before loss of CH_4 or H_2 from a cyclic system such as the aglycone of digoxin.

The recognition that the second H_2O loss occurs more readily than the first is also observed for other ions, such as the pairs m/z 651/633 and m/z 521/503. The monodehydrated species in each pair (lower mass) loses another H_2O more readily (upon CAD) than the nondehydrated species, as seen in Table 2. It is possible that, once a double bond is formed (upon H_2O loss), the second loss is more facile.

Collisionally activated dissociation of m/z 243. The ion at m/z 243 is a prominent fragment ion in both the FAB mass spectrum of digoxin and the linked scan mass spectrum of protonated digoxin. This ion is unique in that it is isolated from any other peaks and is not associated with other ions 18 u higher or lower in mass.

Most other major fragment ions observed in the FAB mass spectrum have an ion 18 u below them due to H_2O loss. This ion at m/z 243 is observed as a daughter ion from m/z 781, m/z 651, m/z 633, m/z 391, and m/z 373. These are the only species that should be able to produce the fragment ion at m/z 243 by CAD if the assignment for this ion is correct as given in Table 1. The species at m/z 355 and m/z 337 have already lost too many H_2Os to form the ion at m/z 243. The assignment proposed in Table 1 for this ion at m/z 243 is the same, minus one sugar, as that given to the ion at m/z 373 for the sugar portion of that doublet. These two ions may be formed by the same fragmentation mechanism that may differ from the mechanism that forms the ions containing the aglycone. The fact that the ion at m/z 243 does not lose H_2O suggests that the sugars do not as readily lose H_2O as does the aglycone. Further support for the proposed assignment of m/z 243 is from the linked scan mass spectrum of this ion. The appearance of a daughter ion at m/z 149 proves that m/z 243 contains an intact terminal sugar. The ion at m/z 149 is from the terminal sugar with retention of the glycosidic oxygen, $[HOS_3OH]H^+$.

The most abundant daughter ion observed by the CAD of m/z 243 is m/z 97. It is also observed in the FAB mass spectrum of digoxin. The chemical formula of this ion is determined to be $C_6H_9O^+$ by peak matching (Table 1). From Table 2, it can be seen that this daughter ion is present to a minor extent in many of the B/E spectra collected, but is only a significant daughter ion of the parent ions at m/z 373 and m/z 243. These two species contain a partially dehydrated sugar that leads to the possibility that the structure of m/z 97 is a completely dehydrated digitoxose (sugar) unit in the protonated form, structure (XI). This ion is designated as $[S-H_2O]H^+$ in Table 1. It is unclear whether this ion comes from the terminal sugar, in which case it would be labeled as $[HOS_3{}^{-H}-H_2O_2]H^+$, or from an internal sugar, $[{}^{+H}S_2{}^{-H}-H_2O]H^+$ or $[{}^{+H}S_1{}^{-H}-H_2O]H^+$. However, structure (XI) is supported by the results of the CAD of m/z 97. This B/E mass spectrum of m/z 97 contained fragment ions corresponding to the loss of CH_4 and CO, which would be expected from this proposed structure, consistent with the presence of a methyl group and the ring oxygen atom.

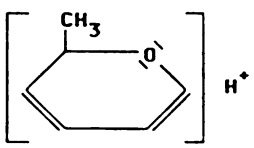

(XI)

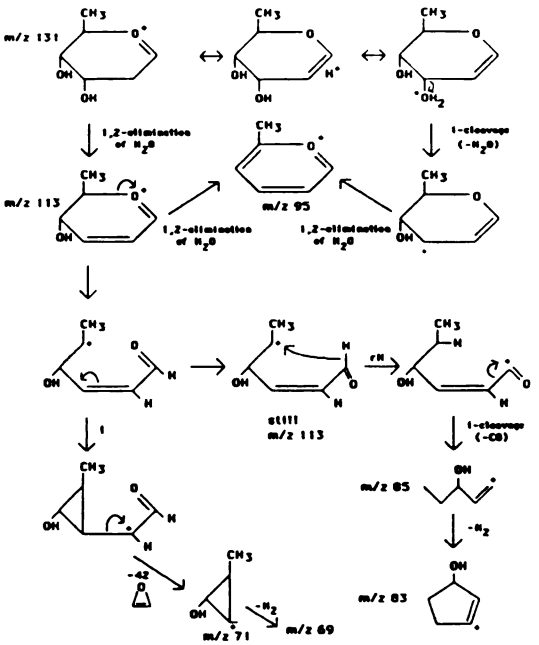

Figure 7. Possible mechanisms for the fragmentation of the parent ion at m/z 131 upon CAD to produce the ions observed in the linked scan (see Table 2).

Collisionally activated dissociation of m/z 131 and m/z 113. The two low mass fragment ions at m/z 131 and m/z 113 are very abundant in the FAB mass spectrum of digoxin and appear to be terminal sugar fragments. This is supported by the results of peak matching data presented in Table 1. The m/z 131 ion fragments upon CAD to give some interesting low mass ions. At the low collision gas pressure used for most of this study, the main fragment ion observed from m/z 131 is at m/z 113 due to loss of H_2O. If the collision gas pressure is increased, to attenuate m/z 131 by more than 10%, more fragmentation results to give all the low mass fragments listed in Table 2 (between m/z 69 and m/z 113). Possible mechanisms for the CAD of the primary ions at m/z 131 and m/z 113 to produce the low mass daughter ions observed in a B/E linked scan are outlined in Figure 7. Inductive cleavages of rearrangement species and 1,2-eliminations are used to explain the fragmentation of m/z 131 and m/z 113. The daughter ion at m/z 97 is of low relative abundance compared to the other daughter ions from the CAD of m/z 131 and m/z 113. It is possible that this fragment is formed by the loss of H_2O_2 from the species at m/z 131 to give the structure proposed. However, due to the low relative abundance of this daughter ion and the uncertainty in the fragmentation pathway, m/z 97 is not included in the fragmentation scheme of m/z 131 and m/z 113 shown in Figure 7.

J Am Soc Mass Spectrom 1990, 1, 455-472

Relevant results from the fast atom bombardment mass spectra of other cardiac glycosides. The effects of small structural changes in the analyte molecule on the FAB mass spectra and the B/E linked scan mass spectra of the $[M]H^+$ ions were investigated. Two cardiac glycosides, digitoxin and gitoxin, were chosen for study because of their differences in the aglycone portion of the molecule from digoxin. The structures of these two compounds are shown in Figure 1 where digitoxin is structure E and gitoxin is structure G. Digitoxin has one less OH group on the aglycone than digoxin, and gitoxin has the same molecular formula but with different positioning of one of the OH groups on the aglycone ring structure (C-12 on digoxin and C-16 on gitoxin). Another compound, acetyldigitoxin (structure F) was chosen for its modification to the sugar portion of the compound. The aglycone of acetyldigitoxin is identical to that of digitoxin, but the terminal sugar contains an acetyl group. The FAB mass spectra and the B/E spectra of the $[M]H^+$ ions of digitoxin, gitoxin, and acetyldigitoxin were obtained and compared with the corresponding spectra of digoxin in order to determine whether changes in the aglycone portion or the sugar portion of digoxin have more effect on the types and relative abundances of the fragment ions observed. The mass spectra of these related compounds all contained relatively the same protonated fragments (and parent ions) as observed for digoxin, with some of the m/z values shifted due to the introduced modifications from digoxin. For example, with the compound digitoxin, the ions in the m/z 337 to m/z 391 range that were given two assignments for digoxin (from the aglycone end and from the sugar portion of the molecule for the same m/z value) were split into two series, separated by 16 u, due to the change in the mass of the aglycone portion of digitoxin. This further supports the double assignments given to these fragment ions of digoxin in Table 1. The relative abundances of the daughter ions in the B/E linked scan mass spectra of the $[M]H^+$ ions of the two compounds with aglycone modifications (digitoxin and gitoxin) are different from digoxin. The most notable changes are that the $[M-H_2O]H^+$ ions are more abundant in the B/E mass spectra of these two modified aglycone compounds than for digoxin. This observation is probably a result of the differences in locations, and hence reactivity, of the —OH groups on the aglycone portions of these compounds. The modifications to the sugar portion of the compound digitoxin do not produce any noticeable differences in the FAB mass spectrum or the B/E spectrum of the $[M]H^+$ ion of acetyldigitoxin from the corresponding spectra of digoxin with respect to the protonated species observed and their relative abundances. One exception is the shift in mass of the ions containing the terminal sugar with the added acetyl group. Therefore, small changes in the aglycone portion of these cardiac glycosides result in more dramatic mass spectral changes than do modifications to the sugar portion of the molecules. The differences in the FAB and B/E linked scan mass spectra produced by slight alterations in the aglycone suggest that the aglycone does play a major role in controlling the fragmentation mechanism(s) and may possibly be the site of charge localization. A possible explanation for the importance of this aglycone on the mechanisms of fragmentation could be related to energetics and the proton affinities of specific sites on the aglycone. However, there is no obvious site where the charge resides on the aglycone of digoxin. The modifications in the aglycone of these cardiac glycosides may affect the energy that the $[M]H^+$ ion contains as it fragments via remote site processes and therefore may affect the relative abundances of the fragment ions observed.

Conclusions

The data presented from the FAB mass spectrum and the MS/MS analyses of all the major fragment ions of digoxin show that over half of the different types of fragment ions formed contain the aglycone portion of the molecule and that many different bonds are cleaved. The results we obtained from the FAB mass spectrum of digoxin can be closely compared with the reported NH_3 CI spectrum of digoxin [26]. All of the fragments, including those due to multiple H_2O losses, that are observed in protonated form in the FAB mass spectrum are observed in the NH_3 CI spectrum as NH_4^+ adducts. This suggests that very similar fragmentation mechanisms are occurring with these two techniques and that the difference between protonation by glycerol and NH_4^+ adduct formation does not affect the fragmentation mechanism(s) significantly. If the fragment ions formed in the NH_3 CI experiment evolve from $[M]NH_4^+$, as they appear to, the charge resides on the ammonium ion and not on some part of the digoxin molecule itself. This rules out reaction 1 as a possible pathway of fragmentation because it requires that the charge reside on the oxygen of the glycosidic bond in order to induce fragmentation of this bond. Reactions 2 and 3 are possible fragmentation pathways for NH_3 CI, as well as protonation by glycerol fragment ions because the charge site is not required to be on the oxygen atom, as in reaction 1. However, further fragmentation of the primary fragments would be unlikely following reaction 2 because charge migration through the molecule is required for the formation of the secondary fragmentations observed. If the charge site in the adduct ion formed in NH_3 CI is localized on the NH_4^+ ion, then charge migration throughout the molecule would not be possible. Therefore, reaction 3 would not predict the production of the same fragment ions in the decomposition of protonated molecules and NH_4^+ adducts. A remote site mechanism, reaction 4, provides the best explanation for the similarities in the fragmentations of digoxin observed with FAB/MS and

NH_3 CI. In this case the charge site can be localized on the aglycone and induce fragmentation at remote sites throughout the molecule. As the charge is not directly involved in the fragmentation and no charge migration is required, it is expected, by reaction 4, that the protonated ion and NH_4^+ adduct ion would produce the same fragmentation products, as observed, as long as the charge can be localized on the aglycone in both cases.

The data presented here from the mass spectrometry and MS/MS analysis of digoxin lend further support to the role of the remote site mechanism in the formation of the fragment ions observed. Reaction 1 can explain only a limited number of the types of fragmentations of digoxin observed. For instance, the ion at *m/z* 131 can be easily explained via reaction 1 by protonation of the oxygen atom of the terminal glycosidic bond, inducing fragmentation to produce the species at *m/z* 131. By this same mechanism, other fragment ions at *m/z* 261 and *m/z* 391 should be formed from protonation and fragmentation of the other two glycosidic bonds. However, the ion current at *m/z* 391 is primarily from the aglycone portion of the molecule (see Tables 1 and 2) and no ion is observed at *m/z* 261, in contradiction to what would be expected by reaction 1. Therefore, reaction 1 fails to provide a consistent explanation of the fragmentation pathways for the decomposition of digoxin and is only a possible mechanism for the formation of a few fragment ions observed.

Reactions 2 and 3, based on charge-induced fragmentation, can explain the majority of the primary fragments observed in the FAB analysis of digoxin. It is possible that these mechanisms can provide pathways for the extensive fragmentation of the primary fragments as reported in Table 2. The charge site must be able to migrate throughout the molecule following primary fragmentation in order to explain all of the ions observed in the MS/MS spectra, which may be possible with the protonated species. Based on reaction 3, competition for the charge should be determined by the relative basicity of the two competing sites. This holds true for the formation of *m/z* 651 and *m/z* 521 where fragmentation about the glycosidic bond, following reaction 3, results in the charge site residing on the nonreducing end of the sugar that contains the aglycone portion of the molecule. This nonreducing end of the sugar contains a more basic site, due to the close proximity of two —OH groups, than does the reducing end of the terminal sugar, which has only a ring oxygen and double bond in close proximity. However, this mechanism does not hold true for the formation of the fragment ion at *m/z* 391. This species is primarily composed of the aglycone portion of the molecule, even though the aglycone has no —OH group or other functional group near the site of protonation/fragmentation to increase the basicity, whereas the sugar moiety has a ring oxygen and double bond near the competing site. In this case the aglycone end is not more basic than the sugar end and therefore should not effectively compete for the H^+. Therefore, some other fragmentation mechanism is required to explain the production of *m/z* 391.

The remote site fragmentation mechanism can explain a high proportion of the fragment ions containing the aglycone and the occurrence of the majority of the ions observed if the charge site is localized on the aglycone. This requires that a basic site or stable cation be formed for the charge to remain localized on the aglycone throughout the extensive fragmentation observed. There is no obvious basic site in the digoxin molecule on the aglycone that has a higher proton affinity than parts of the sugars, as can be seen in Figure 5. However, the five-membered ring of the aglycone provides a very plausible site for charge localization. Protonation of the oxygen atom in this strained five-membered ring could induce ring cleavage followed by H migration to produce a tertiary cation. This is shown in reaction 5. The formation of the tertiary cation provides a charge site that hinders free migration of the charge back onto the sugars. This is one possible way that charge localization can occur on the aglycone to allow for remote site fragmentation to produce the majority of the ions observed. The modifications in the aglycone that were investigated with digitoxin and gitoxin would not prevent this charge localization and therefore would still allow for the remote site fragmentation mechanism to occur.

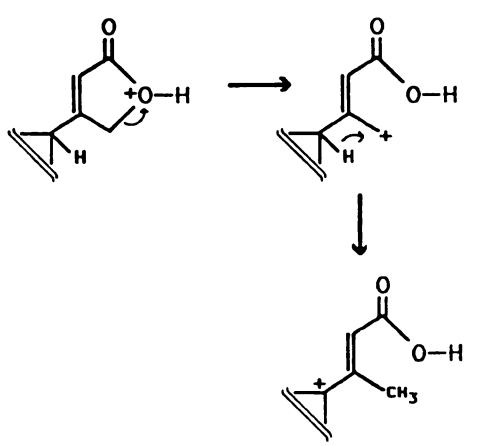

(5)

Thermodynamic considerations of these fragmentation processes support remote site fragmentation mechanisms. Consider the case of the $[M]H^+$ ion of a multifunctional compound containing at least two —OH groups, where one is protonated. If the ion is formed with excess energy, fragmentation can occur. In such a situation, ionic pathways are not necessarily

more energetically favored than neutral (remote site) processes. These pathways are shown in reaction 6. For example, pathway B, elimination of water due to an inductive cleavage, yielding a carbocation, requires approximately 23 kcal/mol [28]. In contrast, pathway A, a remote site fragmentation to form a double bond and H_2O, only requires 12 kcal/mol [28]. Thus, there is no thermodynamic basis for excluding remote site eliminations because they should be competitive with ionic fragmentation mechanisms.

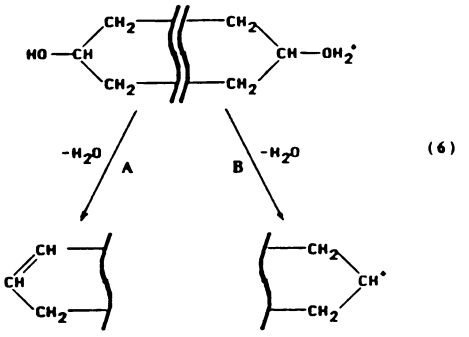

(6)

This remote site mechanism, however, does not explain the large ion currents at m/z 131 and m/z 113 that are present in the FAB analysis of digoxin. It is possible that reaction 1 or 3 is the primary pathway for producing these two ions. According to Figure 5 the site with the highest proton affinity is on the terminal sugar. This could allow for charge-induced fragmentation via reaction 1 or 3 to produce these two abundant low mass fragment ions at m/z 113 and m/z 131.

It is highly probable that more than one mechanism is involved in forming all of the fragment ions observed in this FAB mass spectrometric study of digoxin. A combination of these mechanisms can explain the results obtained satisfactorily. More extensive studies on similar compounds need to be performed to determine the exact fragmentation pathways involved in the formation of each fragment ion observed by both primary and secondary fragmentation.

We have attempted to take a fundamental approach to the interpretation of the mass spectra obtained in the FAB and CAD experiments of digoxin and other related cardiac glycosides. The extensive fragmentation observed for these compounds is certainly not uncommon in FAB analyses of such highly functionalized compounds. It is possible that the extensive fragmentation observed for these types of complex compounds may occur for different reasons and that fragmentation patterns may not be transferable to different types of compounds. However, the information presented here may provide a starting point for similar detailed analyses of the mechanisms of fragmentation of protonated molecules from other highly functionalized compounds by FAB.

Acknowledgments

This work was supported by a grant from the Biotechnology Research Program of the Division of Research Resources of NIH (RR-00480-20). We thank Gary A. Schultz for early discussions and CAD experiments that led to the development of this project, and John T. Stults for conversations concerning the B/E linked scanning technique.

References

1. McLafferty, F. W. *Interpretation of Mass Spectra*, 3rd ed.; University Science: Mill Valley, CA, 1980.
2. Kassel, D. B.; Glerum, M.; Robinson, B. H.; Sweeley, C. C. *Anal. Biochem.* **1989**, *176*, 382.
3. Sunner, J. A.; Kulatunga, R.; Kebarle, P.; *Anal. Chem.* **1986**, *58*, 1312.
4. Holmes, J. L.; *Org. Mass Spectrom.* **1985**, *20*, 169.
5. Crow, F. W.; Tomer, K. B.; Looker, J. H.; Gross, M. L. *Anal. Biochem.* **1986**, *155*, 286.
6. Instruction Manual for MS-LN09/08/11, Linked Neutral Loss Scan Program, JEOL, Ltd., Tokyo, Japan, No. IMS-LNS, p. 10. Sato, K.; Asada, T.; Ishihara, M.; Kunihiro, F.; Kammei, Y.; Kubota, E.; Costello, C. E.; Martin, S. A.; Scoble, H. A.; Biemann, K. *Anal. Chem.* **1987**, *59*, 1652.
7. Holmes, J. L.; Szulejko, J. E. *Org. Mass Spectrom.* **1983**, *18*, 273.
8. Light, K. J.; Kassel, D. B.; Allison, J.; *Biomed. Environ. Mass Spectrom.* **1989**, *18*, 177.
9. Domon, B.; Costello, C. E. *Glycoconjugate J.* **1988**, *5*, 397.
10. Bochkov, A. F.; Zaikov, G. E. *Chemistry of the O-Glycosidic Bond: Formation and Cleavage;* Pergamon: Oxford, 1979; pp 179-181.
11. Busch, K. L.; Glish, G. L.; McLuckey, S. A. *Mass Spectrometry / Mass Spectrometry: Techniques and Applications of Tandem Mass Spectrometry;* VCH: New York, 1988.
12. (a) Field, F. H. In *MTP International Review of Science Mass Spectrometry Series One;* Maccoll, A., Ed.; Butterworths, 1972. (b) McLafferty, F. W. *Org. Mass Spectrom.* **1980**, *15*, 114.
13. (a) Ichikawa, H.; Harrison, A. G. *Org. Mass Spectrom.* **1978**, *13*, 389. (b) Martinsen, D. P.; Buttrill, S. E., Jr. *Org. Mass Spectrom.* **1976**, *11*, 762. (c) Pesheck, C. V., Buttrill, S. E., Jr. *J. Amer. Chem. Soc.* **1974**, *96*, 6027. (d) Pollack, S. K.; Devlin, J. L. III; Summerhays, K. D.; Taft, R. W.; Hehre, W. J. *J. Amer. Chem. Soc.* **1977**, *99*, 4583.
14. Go, K.; Kartha, G.; Chen, J. P. *Acta Cryst.* **1980**, *B36*, 1811.
15. Lias, S. G.; Liebman, J. F., Levin, R. D. *J. Phys. Chem. Ref. Data* **1984**, *13*, 695.
16. (a) Aue, D. H.; Webb, H. M.; Bowers, M. T.; *J. Amer. Chem. Soc.* **1973**, *95*, 2699. (b) Yamdagni, R.; Kebarle, P. *J. Amer. Chem. Soc.* **1973**, *95*, 3504. (c) Longevialle, P.; Milne, G. W. A.; Fales, H. M. *J. Amer. Chem. Soc.* **1973**, *95*, 6666. (d) Houriet, R.; Rufenacht, H.; Carrupt, P. A.; Vogel, P.; Tichy, M. *J. Amer. Chem. Soc.* **1983**, *105*, 3417. (e) Davis, D. V.; Cooks, R. G. *Org. Mass Spectrom.* **1981**, *16*, 176. (f) Houriet, R.; Rufenacht, H.; Stahl, D.; Tichy, M.; Longevialle, P. *Org. Mass Spectrom.* **1985**, *20*, 300. (g) Nacson, S.; Harrison, A. G.; Davidson, W. R. *Org. Mass Spectrom.* **1986**, *21*, 317. (h) Longevialle, P.; Girard, J.-P.; Rossi, J.-C.; Tichy, M. *Org. Mass Spectrom.* **1979**, *14*, 414. (i) McMahon, A. W.; Chadikun, F.; Harrison, A. G.; March, R. E. *Int. J. Mass Spectrom. Ion Process.* **1989**, *87*, 275.
17. Winkler, J.; McLafferty, F. W. *Tetrahedron* **1974**, *30*, 2971.

18. Michnowicz, J.; Munson, B. *Org. Mass Spectrom.* **1972**, *6*, 283.
19. Neumann, G. M.; Derrick, P. J. *Aust. J. Chem.* **1984**, *37*, 2261.
20. (a) Tsang, C. W.; Harrison, A. G. *J. Amer. Chem. Soc.* **1976**, *98*, 1301. (b) Mandelbaum, A.; Biemann, K. *J. Amer. Chem. Soc.* **1968**, *90*, 2975.
21. (a) Johnson, R. S.; Martin, S. A.; Biemann, K. *Int. J. Mass Spectrom. Ion Process.* **1988**, *86*, 137. (b) Kiryushkin, A. A.; Fales, H. M.; Axenrod, T.; Gilbert, E. J.; Milne, G. W. A. *Org. Mass Spectrom.* **1971**, *5*, 19. (c) Winnik, M. A. *Org. Mass Spectrom.* **1974**, *9*, 920.
22. Bowen, R. D.; Stapelton, B. J.; Williams, D. H. *J. Chem. Soc. Chem. Commun.* **1978**, *24*.
23. Jensen, N. J.; Tomer, K. B.; Gross, M. L. *J. Amer. Chem. Soc.* **1985**, *107*, 1863.
24. Adams, J. *Mass Spectrom. Rev.* **1990**, *9*, 141.
25. Wysocki, V. H.; Bier, M. E.; Cooks, R. G. *Org. Mass Spectrom.* **1988**, *23*, 627.
26. Vine, J.; Brown, L.; Boutagy, J.; Thomas, R.; Nelson, D. *Biomed. Mass Spectrom.* **1979**, *6*, 415.
27. Adams, J.; Gross, M. L. *J. Amer. Chem. Soc.* **1989**, *111*, 435.
28. Lias, S. G.; Bartmess, J. E.; Liebman, J. F.; Holmes, J. L.; Levin, R. D.; Mallard, W. G. *J. Phys. Chem. Ref. Data* **1988**, *17*, Suppl. 1.

Appendix

The proton affinities listed in Figure 5 for the various sites in digoxin, as indicated in Figure 4, are estimated as follows. Three types of protonation sites are present. First, we consider simple functional groups such as double bonds (site *a*), —OH groups (site *b*), keto-oxygens (site *d*), ring (ether) oxygens (site *f*), and glycosidic (ether) oxygens (site *i*). In these cases, small, simple molecules containing such functional groups are used as models. Thus, the proton affinities of these sites are based on the PA of the following molecules: site *a*: 2-butene; site *b*: isopropanol; site *d*: acetone; site *f*: tetrahydropyran; and site *i*: isopropyl ether. The second type of protonation site is represented by compounds containing more complex functional groups or multiple functional groups. For example, site *e* is represented by an ester, which has a PA different from that of an ether or a ketone. The PA of site *e* is estimated based on the PA of methyl acetate. In a similar way, site *c* is considered to be similar to that found in the propenal molecule.

The third type of protonation site involves multiple interactions from heteroatoms/functional groups that are in close proximity. Many studies reported an increase in the stability of the protonated species with the addition of functional groups, such as —OH, to the molecule [16]. This is believed to be due to intramolecular H-bonding with these functional groups upon protonation. For example, butanol has a PA of 191 kcal/mol [15] compared to 1,2,4-butanetriol, which has a PA of 216 kcal/mol [3]. This increase in PA of 25 kcal/mol can be attributed to the two extra —OH groups, which allow for multiple H-bonding interactions that increase the stability of the protonated species. Following this pattern, the PA of propanol, 190 kcal/mol [15] can be compared to the PA of glycerol, which is 209 kcal/mol [3]. In this case, the addition of two —OH groups leads to an increase in the PA of the molecule of approximately 19 kcal/mol. Therefore, we propose that similar H-bonding interactions with a corresponding increase in PA occur with the molecule digoxin when functional groups such as —OH groups, ring oxygens, and glycoside oxygens are in close proximity to each other, due to the stereochemistry of the molecule. We have conservatively proposed, based on the above PA values for linear mono and triols, that the interaction of a single —OH group with an —OR group (such as the glycosidic oxygen site on digoxin) results in an increase in PA of the more basic site of approximately 5 kcal/mol. For instance, site *l* has two —OH groups near the —OR (glycosidic O), all of which are on the same side of the ring and have the potential for H-bonding. If the presence of each —OH group increases the PA of this site by at least 5 kcal/mol, then site *l* would have a PA of at least 10 kcal/mol above the PA of the glycosidic oxygen (site *i*) alone. This is represented in Figure 5 as a shaded region above the value for site *i*, due to the uncertainty of these estimates and interactions. In a similar way, it has been estimated that the presence of a ring oxygen near a glycosidic oxygen (site *j*) may increase the PA of that site by at least 3 kcal/mol. These estimates for the proton affinities for the possible sites of protonation on digoxin, based on similar organic molecules and the possible multifunctional interactions that have been shown to occur for other molecules, are presented in Figure 5.

REFERENCES

1. F. W. McLafferty, Interpretation of Mass Spectra, 3rd. Ed., University Science Books, Mill Valley, CA, 1980.

2. M. S. B. Munson and F. H. Field, *J. Amer. Chem. Soc.*, **88**, 2621 (1966).

3. H. D. Beckey, *Int. J. Mass Spectrom. Ion Phys.*, **2**, 500 (1969).

4. D. F. Torgerson, R. P. Showronski, and R. D. Macfarlane, *Biochem. Biophys. Res. Commun.*, **60**, 616 (1974).

5. M. A. Posthumas, P. G. Kistemaker, H. L. C. Meuzelaar, and M. C. Ten Noever de Brauw, *Anal. Chem.*, **50**, 985 (1978).

6. M. Barber, R. S. Bordoli, R. D. Sedgwick, and A. N. Tyler, *J. Chem. Soc. Chem. Commun.*, 325 (1981).

7. A. Benninghoven, *Int. J. Mass Spectrom. Ion Phys.*, **46**, 459 (1983).

8. A. Dell, D. H. Williams, H. R. Morris, G. A. Smith, J. Feeney, and G. C. K. Roberts, *J. Amer. Chem. Soc.*, **97**, 2497 (1975).

9. M. A. Baldwin, and F. W. McLafferty, *Org. Mass Spectrom.*, **7**, 1353 (1973).

10. M. L. Vestel, *Mass Spectrom. Rev.*, **2**, 447 (1983).

11. R. M. Caprioli, T. Fan, and J. S. Cottrell, *Anal. Chem.*, **58**, 2949 (1986); L. J. Deterding, M. A. Moseley, K. B. Tomer, and J. W. Jorgenson, *Anal. Chem.*, **61**, 2504 (1989).

12. F. W. McLafferty, Ed., Tandem Mass Spectrometry, Wiley, New York (1983).

13. R. J. Cotter, *Biomed. Environ. Mass Spectrom.*, **18**, 513 (1989).

14. L. M. Mallis and D. H. Russell, *Anal. Chem.*, **58**, 1076 (1986).

15. R. L. Cerny, K. B. Tomer, and M. L. Gross, *Org. Mass Spectrom.*, **21**, 655 (1986); Z. Zhou, S. Ogden, and J. A. Leary, Proc. 38th ASMS Conf. Mass Spectrom. Allied Topics, 1990, 974.

16. L. M. Teesch and J. Adams, Proc. 38th ASMS Conf. Mass Spectrom. Allied Topics, 1990, 457; R. P. Reese, R. Cerny, and M. L. Gross, *J. Amer. Chem. Soc.*, **111**, 2835 (1989); D. Renner and G. Spiteller, *Biomed. Environ. Mass Spectrom.*, **15**, 75 (1988); X. Tang, W. Ens, K. G. Standing, and J. B. Westmore, *Anal. Chem.*, **60**, 179 (1988).

17. F. W. Rollgen and H. R. Schulten, *Z. Naturforsch.*, **30a**, 1685 (1975); F. Borchers, U. Giessmann and F. W. Rollgen, *Org. Mass Spectrom.*, **12**, 539 (1977).

18. R. Stoll and F. W. Rollgen, *Z. Naturforsch.*, **37a**, 9 (1982).

19. G. Schmelzeisen-Redeker, U. Giessmann and F. W. Rollgen, *Org. Mass Spectrom.*, **20**, 305 (1985).

20. G. J. Q. van der Peyl, K. Isa, J. Haverkamp, and P. G. Kistemaker, *Org. Mass Spectrom.*, **16**, 416 (1981).

21. J. B. Fenn, M. Mann, C. K. Meng, S. F. Wong, and C. M. Whitehouse, *Science*, **246**, 64 (1989).

22. M. Karas and F. Hillenkamp, *Anal. Chem.*, **60**, 2299 (1988); M. Karas, U. Bahr, A. Ingendoh, and F. Hillenkamp, *Angew. Chem.*, **101**, 805 (1989).

23. M. Mann, C. K. Meng, and J. B. Fenn, *Anal. Chem.*, **61**, 1702 (1989); J. A. Loo, H. R. Udseth, and R. D. Smith, *Anal. Biochem.*, **179**, 404 (1989).

24. M. Dole, L. L. Mack, R. L. Hines, R. C. Mobley, L. D. Ferguson, and M. B. Alice, *J. Chem. Phys.*, **49**, 2240 (1968); L. L. Mack, P. Kralik, A. Rheude, and M. Dole, *J. Chem. Phys.*, **52**, 4977 (1970).

25. M. Yamashita and J. B. Fenn, *J. Phys. Chem.*, **88**, 4451 (1984).

26. C. K. Meng, M. Mann, and J. B. Fenn, *Z. Phys. D.*, **10**, 361 (1988).

27. D. Bombick, J. D. Pinkston, and J. Allison, *Anal. Chem.*, **56**, 396 (1984); D. Bombick and J. Allison, *Anal. Chem.*, **59**, 458 (1987).

28. J. P. Blewett and E. J. Jones, *J. Phys. Rev.*, **50**, 464 (1936).

29. D. Bombick, *Doctoral Dissertation*, Michigan State University, 1986.

30. R. J. Beuhler, E. Flanigan, L. J. Greene and L. Friedman, *J. Amer. Chem. Soc.*, **96**, 3990 (1974).

31. R. L. Woodin and J. L. Beauchamp, *Chem. Phys.*, **41**, 1 (1979).

32. See, for example B. C. Guo, B. J. Conklin, and A. W. Castleman, Jr., *J. Amer. Chem. Soc.*, **111**, 6506 (1989).

33. T. A. Lehman and M. M. Bursey, Ion Cyclotron Resonance Spectrometry, J. Wiley & Sons, New York (1976).

34. R. J. Beuhler, E. Flanigan, L. J. Greene, and L. Friedman, Biochem. *Biophys. Res. Commun.*, **46**, 1082 (1972).

35. V. N. Reinhold and S. A. Carr, *Anal. Chem.*, **54**, 499 (1982).

36. D. I. Carroll, J. G. Nowlin, R. N. Stillwell, adn E. C. Horning, *Anal. Chem.*, **53**, 2007 (1981); W. Lange, M. Jirikowsky, and A. Benninghoven, *Surf. Sci.*, **136**, 419 (1984).

37. R. J. Cotter, *Anal. Chem.*, **51**, 317 (1979).

38. G. P. Johnson, A. B. Hedin, P. L. Hakansson, B. U. R. Sundqvist, B. G. S. Save, P. F. Nielson, P. Roepstorff, K. E. Johansson, I. Kamensky, and M. S. L. Lindberg, *Anal. Chem.*, **58**, 1084 (1986).

39. J. P. Thenot, J. Nowlin, D. I. Carroll, F. E. Montgomery, and E. C. Horning, *Anal. Chem.*, **51**, 1101 (1979).

40. B. W. Williams, A. P. Irsa, H. Zmora, and R. J. Beuhler, *J. Phys. Chem.*, **87**, 2185 (1983).

41. D. B., Kassell, *Doctoral Dissertation*, Michigan State University, 1988.

42. CRC Handbook of Chemistry and Physics, 63rd Ed., CRC Press, Inc., Boca Raton, FL, 1982.

43. D. Bombick and J. Allison, *Anal. Chim. Acta.*, **208**, 99 (1988).

44. D. B. Kassel and J. Allison, *Biomed. Environ. Mass Spectrom.*, **17**, 221 (1988).

45. See, for example: R. E. Shomo, II, A. Chandrasekaran, A. G. Marshall, R. H. Reuning, and L. W. Robertson, *Biomed. Environ. Mass Spectrom.*, **15**, 295 (1988).

46. V. N. Reinhold and S. A. Carr, *Mass Spectrom. Rev.*, **2**, 216 (1983).

47. P. M. Holland and A. W. Castleman, Jr., *J. Amer. Chem. Soc.*, **102**, 6174 (1980).

48. J. Allison, "The Gas Phase Chemistry of Transition-Metal Ions with Organic Molecules", in Progress in Inorganic Chemistry, vol. 34, S. J. Lippard, Ed., John Wiley and Sons, Inc., 1986.

49. a) M. Lombarski and J. Allison, *Int. J. Mass Spectrom. Ion Phys.*, **49**, 281 (1981); b) M. Lombarski and J. Allison, *Int. J. Mass Spectrom. Ion Phys.*, **65**, 31 (1985).

50. J. Volkening and K. G. Huemann, 10th Int. Conf. Mass Spectrom. Advances in Mass Spectrometry, 1985, Part B, John Wiley & Sons, 1059.

51. See, for example: J. Allison and D. P. Ridge, *J. Amer. Chem. Soc.*, **101**, 4998 (1979); M. L. Larrivee and J. Allison ?????

52. J. Allison and D. P. Ridge, *J. Amer. Chem. Soc.*, **101**, 4998 (1979).

53. S. G. Lias, J. E. Bartmess, J. F. Liebman, J. L. Holmes, R. D. Levin, and W. G. Mallard, J. Phys Chem. Ref. Data, **17** (1988).

54. R. E. Weber and L. I. Cordes, *Rev. Sci. Instrum.*, **37**, 112 (1966).

55. R. J. Cotter, *Anal. Chem.*, **52**, 1589A (1980).

56. J. C. Rouse, K. J. Light, and J. Allison, Proc. 38th ASMS Conf. Mass Spectrom. Allied Topics, 1990, 455.

57. J. R. Pare, P. Lafontaine, J. Belanger, W. W. Sy, N. Jordan, and J. C. K. Loo, *J. Pharm. Biomed. Anal.*, **5**, 131 (1987).